YCRETS 2021

CEMENT & CONCRETE SA

PROCEEDINGS OF THE

YOUNG CONCRETE RESEARCHERS, ENGINEERS & TECHNOLOGIST SYMPOSIUM (YCRETS)

13 – 14 JULY 2021

Young Concrete Researchers,
Engineers and Technologist Symposium (YCRETS)
Proceedings

July, 2021

Edited by:
Janina Kanjee

Published by:
Cement & Concrete SA
Tel: 270 113 150 300
Website: https://www.cemcon-sa.org.za/
Info: info@cemcon-sa.org.za

ISBN: 978-0-9922176-3-1

PREFACE

These proceedings contain papers presented at the Young Concrete Researchers, Engineers and Technologist Symposium (YCRETS) held virtually from the 13th to 14th of July, 2021. The purpose of the symposium was to provide a platform for young researchers to discuss recent developments and applications in concrete and cement-based materials in South Africa, and Southern Africa at large. A wide range of themes were covered including new generation of construction materials, durability, monitoring and repair of reinforced concrete structures, challenges in the design and management of structures, sustainability and structural analysis.

Only selected papers were accepted for presentation at the Symposium. All the papers published in the proceedings with ISBN 978-0-9922176-3-1 were subjected to independent peer review by at least two members of the scientific committee before being accepted. A summary of the technical paper contributions by the participating institutions were as follows: University of Cape Town = 12.50%; University of the Witwatersrand, Johannesburg = 33.33%; University of Pretoria = 8.33%; University of KwaZulu-Natal = 4.17%; Joint South African Institutions = 12.50%; International institutions = 29.17%.

In addition to the selected technical paper presentations, two guest lectures were also presented at the Symposium. The first lecture, titled "Concrete and research: a mutually compatible duo", was presented by Emeritus Professor Mark Alexander from the University of Cape Town. The second lecture, titled "Locating research and scholarship in frameworks of understanding in the discipline", was presented by Professor Yunus Ballim from the University of the Witwatersrand.

Sincere thanks to the following individuals who contributed to the success of the Symposium: Mark Alexander, Yunus Ballim, Sunday Nwaubani, Mike Otieno, Billy Boshhoff, Elsabe Kearsley, George Fanourakis, Philemon Arito, Emmanuel Leo, Hans Beushausen, Gideon Van Zijl, Wibke De Villiers, Rakesh Gopinath, Patrick Bukenya, Manu Santhanam, Prabha Mohandoss, Bryan Perrie, Bolanle Ikotun, Walied A. Elsaigh, Inès Ngassam and Wolfram Schmidt for reviewing and ensuring a high quality of papers; Hanlie Turner and Natasja Pols for help in planning and organising the symposium. Special thanks go to Cement and Concrete SA, the custodians of this event.

A special acknowledgement is also extended to the authors and presenters who contributed to the proceedings and the success of the Symposium.

Ms. Janina Kanjee
Conference Chair
Lecturer, School of Civil and Environmental Engineering
University of the Witwatersrand, Johannesburg, SOUTH AFRICA

FOREWORD

The idea of gathering young researchers together, to be in conversation with each other on a technical subject of mutual interest is unquestionably centred on the need to acculturate and develop the next generation of intellectuals - in this case, in the field of cement and concrete materials science and technology. The motive force of the YCRETS Symposium idea is to be found, using Joseph Conrad's words, in that *"… which binds together all humanity – the dead to the living and the living to the unborn"*. But there is also another reason: it is the social duty of young people to be disruptive, to question the handed-down *"wisdom"* that they receive and to stand on the shoulders of their elders so as to better see further horizons. The student must do better than the teacher – for the teacher to be successful.

In the foreseeable future, cement-based materials will continue to be of dominant use in infrastructure construction. However, this does not mean that these materials can continue to be used in the same manner, mainly because of their significant negative environmental impacts. The subjects and the papers presented at this YCRETS Symposium reflect the responses of the young research community, not only to an acknowledgement of the challenges but also to a willingness to develop the evidence base that will guide future practice and policy in more sustainable use of infrastructure materials. It is also about young researchers showing optimism in the possibility of a more environmentally sensitive and a more sustainable future world.

This symposium is being held in a time of tyranny by viruses, with serious hardship visited on homes and countries by the Covid-19 epidemic. Nevertheless, online platforms allow the global flow of ideas to continue, ignoring national and identity boundaries – even if as a second-best option to physical meetings. In this environment, it is important that researchers from a range of countries have chosen to participate in this symposium. The challenges to cement and concrete engineering are global in character and the answers are best to be found in shared conversations across the globe.

The researchers participating in this 2021 YCRETS Symposium will find their ideas tested and contested – in the best tradition of the growth of knowledge and ideas – and all will leave with a better understanding of their own work and the location of their research activities in the broad landscape of current research in cement and concrete materials. Such symposium discussions are important if we are to ensure sensible and sensitive use of cement-based materials into the future.

Professor Yunus Ballim, July 2021

TABLE OF CONTENTS

INVESTIGATING THE USE OF ISOTHERMAL CALORIMETRY FOR PREDICTING PHYSICAL PROPERTIES OF CEMENTS

Refiloe Mokoena [(1)], Tshepo Motau [(2)] and Georges Mturi [(1)]

(1) Smart Mobility, Council for Scientific and Industrial Research (CSIR)

(2) PPC Cement SA (Pty) Ltd

ABSTRACT

Isothermal calorimetry is a useful technique for studying the cement hydration process that measures the heat flow of cement paste during hydration. Standard cement properties, such as compressive strength, setting times and compatibility can be derived from calorimetry investigation. This becomes relevant in assisting with monitoring the strength development during construction activities and studying the thermal related behaviour of concrete structures. During this study, the heat generated from the cement hydration reactions was investigated of four different cement types, namely CEM II/B-V 32.5N, CEM II/B-V 42.5N, CEM II/A-M (S-V) 42.5R and CEM I 52.5N. Correlations between the calorimeter results and the (i) initial setting time and final setting time; (ii) 28 day compressive strength and; (iii) fineness, were established for the cement types investigated. With the exception of early-day strength, the results indicated strong correlations between the investigated parameters and the cement hydration curves. This was particularly the case for the setting time of the cements with an R^2 value of 0.82 and 0.89 for the initial and final setting times respectively.

Keywords: isothermal calorimetry, cement hydration, cement setting time, cement fineness, cement strength.

1. INTRODUCTION

Setting and strength development of concrete mixes are important variables in the construction program of concrete structures. The constructability of concrete structures can be highly dependent on the fresh properties of the concrete mix used, as this will inform various on-site activities such as formwork removal and surface texturing. In this paper, the initial and final setting times, early and 28-day compressive strengths and fineness of four South African cements will be assessed in relation to their respective heat of hydration curves from an isothermal calorimeter.

Establishing the cement setting time and monitoring the early phase of strength development is valuable during the placement of concrete as it provides an indication of the optimum time for activities such as saw-cutting. Depending on the ambient climatic conditions, this can be between 4 – 18 hours after placement but it is typically recommended to be completed within 24 hours [1].

Currently, the South African standard test method for determining the setting time requires the use of a Vicat apparatus and makes a mechanical determination of the initial and final set

for a given cement paste SANS 50196-3 [7]. There has been extensive research done to explain the heat rate evolution in relation to the setting time of cement pastes [2, 3, 4]. However, empirical test methods such as the Vicat test remain standardized for determining the setting times as a measure of a cement paste's consistency.

Development of internal heat stresses within concrete structures is also dependent on the cement hydration and it has the potential to cause excessive cracking when not properly managed. One of the contributing factors of the concrete's heat evolution is the cement's fineness, with fineness being a measure of the cement's overall surface area and therefore indicative of the cement's reactivity. This relationship has been shown by researchers such as Goodwin [5] who reported that the smaller cement particle sizes, i.e. less than 10 -15 μm are in fact, the most active. In addition, Goodwin [5] found typical ranges of fineness values for Ordinary Portland Cement (OPC) and rapid hardening Portland cement to be 3000 - 3500 cm^2/g and 4000 - 4500 cm^2/g respectively, indicating that rapid hardening cements have higher fineness values compared to OPC.

The 28 day compressive strength of concrete is one of the primary mechanical properties used for engineering design and is determined in accordance with SANS 5863 [7]. Cement strength is determined using an appropriate press for mortar specimens as per the national test method SANS 50196-1 [6] for measuring the early (2 or 7 day) and 28 day compressive. These are widely accepted methods for concrete and cement strength determination but it is still debated whether such laboratory tests are truly representative of the *in-situ* concrete properties. Researchers such as Indelicato [9] have argued that even cubes cast from the same batch of concrete do not necessarily represent the *in-situ* concrete strength due to reasons such as the differences in specimen size, geometry, compaction and curing conditions; compared to the concrete structure being represented. Although Indelicato [9] did acknowledge that the strength values obtained from testing laboratory cube specimens can coincide with *in-situ* strength values from time to time. The findings prompted non-destructive test (NDT) methods for condition assessments of concrete structures as well as concrete pavement rehabilitations as demonstrated by Al-Abbasi & Shalaby [10].

The above cement properties are all reliant on the cementitious hydration reactions and can therefore be inferred using analytical techniques that quantify these reactions. This paper presents an investigation carried out using an isothermal calorimeter for determining the relationships between the heat output from cement reactions and the three cement properties indicated above, namely, setting time, fineness and strength.

2. BACKGROUND

Differential Thermal Analysis (DTA) is described as a testing technique that is used to measure the phase changes of materials by means of temperature measurements as a sample is subjected to constant heating or cooling [11]. The technique is therefore useful in studying and understanding the physical and chemical changes in materials due to changes in temperature. The output graphs from DTA analyses can be used to distinguish between endothermic and exothermic relationships.

The use of DTA techniques can be dated back to Le Chatelier [12] who set up an experiment to automatically record the heating curve of the clays on a photographic plate in order to investigate the material's phase change relationship. This was followed by other scientists who modified different aspects of how the temperature measurements were recorded from the

sample and reference material such as Boersma [13], which subsequently led to the development of the Differential Scanning Calorimetry (DSC) which measures the heat flux output as opposed to temperature.

Isothermal (conduction) calorimetry is used to monitor the heat development of hydrating cements and is considered to be the most accurate method for cement pastes and mortar samples in comparison to adiabatic and semi-adiabatic calorimeters which are usually used for concrete samples [14]. Research on the use of calorimetry for cement and concrete applications began between 1923 and 1939 when Carlson [15] used a conduction calorimeter to investigate the heat development of cement. This sparked further research to gain a better understanding on the quantitative and qualitative effects of various cement constituents and additives on the heat of hydration [16, 17].

Aschan [18] found that the hydration reactions that characterize the hardening process is a better method in establishing the setting time of cement paste, mortar and concrete in comparison to popular mechanical methods. During the study, a copper-lead electrode was used to establish the setting time through distinct increases of potential difference when the copper surface was oxidized.

The cement industry saw significant developments in conduction calorimetry with the introduction of the Wexham calorimeter in 1970 by J.A. Forrester and then the Setaram heat flux calorimeter in 1990 which allowed the *in-situ* mixing of cements and recording of initial reactions. Subsequently, other researchers have investigated the heat of hydration using calorimetry techniques for their unique investigation.

A report by Acker [19] on the contribution of the physical and mechanical properties of concrete on its mechanical behavior found that the two major influencing processes were (i) the heat of hydration resulting from the cementitious reactions and (ii) the natural drying of concrete elements. This given that these two phenomena caused major mechanical effects related to the internal stresses and strains on various structural elements.

According to Lootens & Bentz [20], previous research has demonstrated the linear relationship between the compressive strengths of mortar specimens from 1-day and beyond. The research explored this relationship through the use of ultrasonic reflection and calorimetry on specimens for up to 3 days. From the investigation, it was found that ultrasonic reflection and calorimetry can be used to monitor the early (up to 8 hours) strength development of mortar and concrete.

It is well accepted that the heat of hydration of cement pastes can be related to certain physical properties particularly, setting time and strength development during the early stages of hydration. However, little research has been conducted on the correlation of the different phases within the hydration process to the physical properties of the cement paste and concrete specimens. This paper presents a study that investigated the correlations between the heat of hydration, setting times and compressive strengths of four South African cements.

2.1 Cement heat evolution

The four major compounds of OPC, namely C_3S, C_2S, C_3A and C_4AF combine with water during hydration to form the various cementitious products. The cement hydration process and can be described as consisting of five stages as shown in Figure 1. The first stage is initiated when the cement is mixed with water. During the second/dormant stage, the paste is plastic and workable. The transition between dormant and setting stages is defined as the initial set. During the setting stage, the paste is typically stiff and unworkable. The transition between setting and

hardening stages is defined as the final set, after which, the paste is a rigid solid that gains strength with time [3].

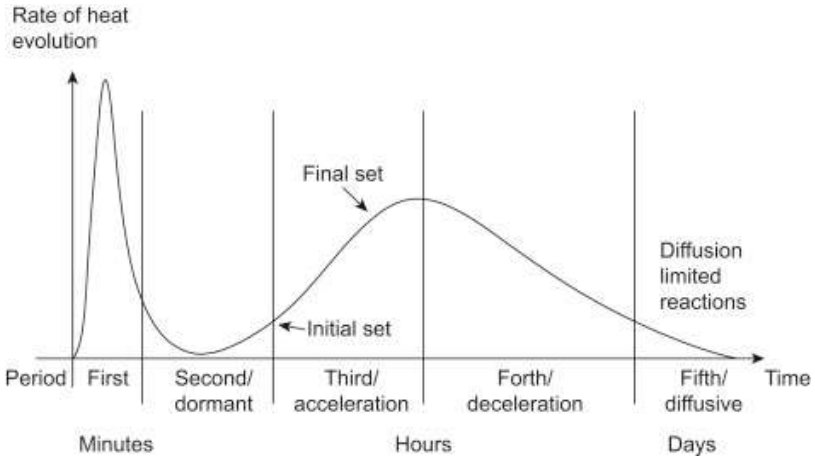

Figure 1: Phases of cement heat of hydration [4]

South African standards do not require testing for the heat of hydration of cements unless the cement is identified as a Low Heat Common Cements (LH). The solution calorimetry method or the semi-adiabatic method can be used to determine the heat of hydration which needs to be below a specified threshold of 270 J/g. Low heat cements are ideal for large mass pour applications. In these applications, the generation of excessive heat that can cause large amounts of thermal cracking is avoided.

Typically, isothermal calorimeters are used for cement testing while adiabatic/semi-adiabatic calorimeters are used for testing concrete specimens. The equipment used and methodology followed for the laboratory investigation presented in this paper is described below.

3 METHODOLOGY

Four different cements were tested using an isothermal calorimeter namely (i) CEM II/B-V 32.5N, (ii) CEM II/B-V 42.5N, (iii) CEM II/A-M (S-V) 42.5R and, (iv) CEM I 52.5N. Approximately 3 g of each cement was mixed with approximately 2 ml of distilled water in a 20 ml disposable glass ampoule for about 1 minute to produce a paste of uniform consistency, where an electronic syringe was used for mixing the cement paste. The ampoule was then placed in the isothermal calorimeter, connected to a computer for data capturing and securely insulated to prevent any heat loss where a constant temperature of approximately 20 ˚C was maintained.

A reference ampoule containing water to balance the heat capacity of the sample ampoule was used in order to reduce the noise of the signal. The sample and reference ampoules were loaded at the same time to minimize the time to reach thermal equilibrium. The heat generated by the paste sample, in the isothermal calorimeter is sent as electric signals by a sensitive thermopile to the computer for recording and calibration. The heat of hydration generated for 8 days from the start of the test was progressively recorded to obtain the total heat generated. The test was performed in accordance with ASTM C1679 [21].

4 RESULTS

4.1 Heat of hydration results

The plots showing the heat flux and the recorded heat of hydration during the test are shown in Figure 2 and Figure 3 respectively for the four cements used in this study.

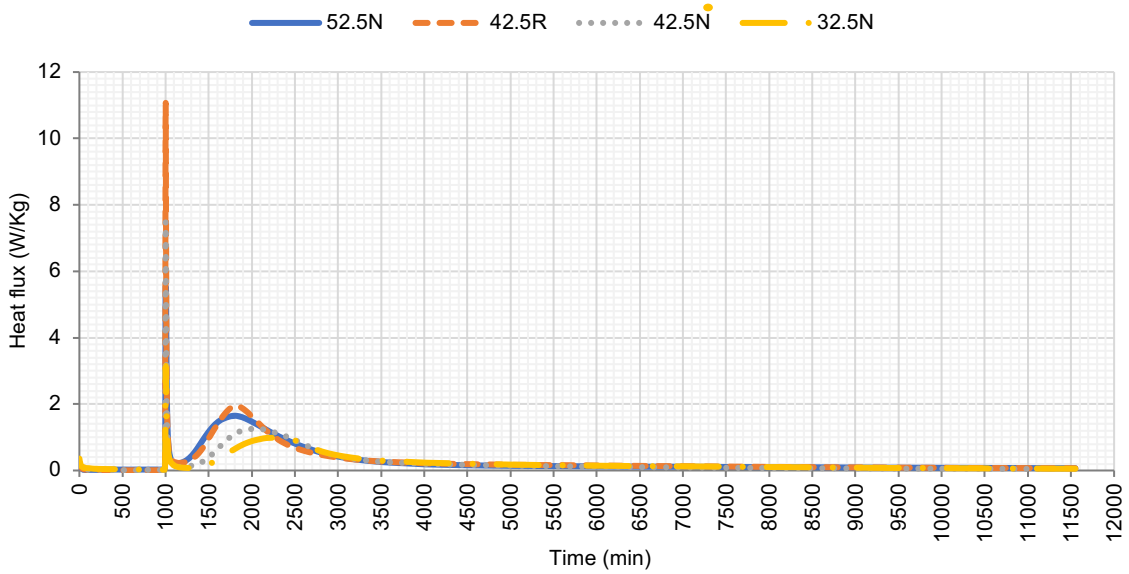

Figure 2: Heat flux plot

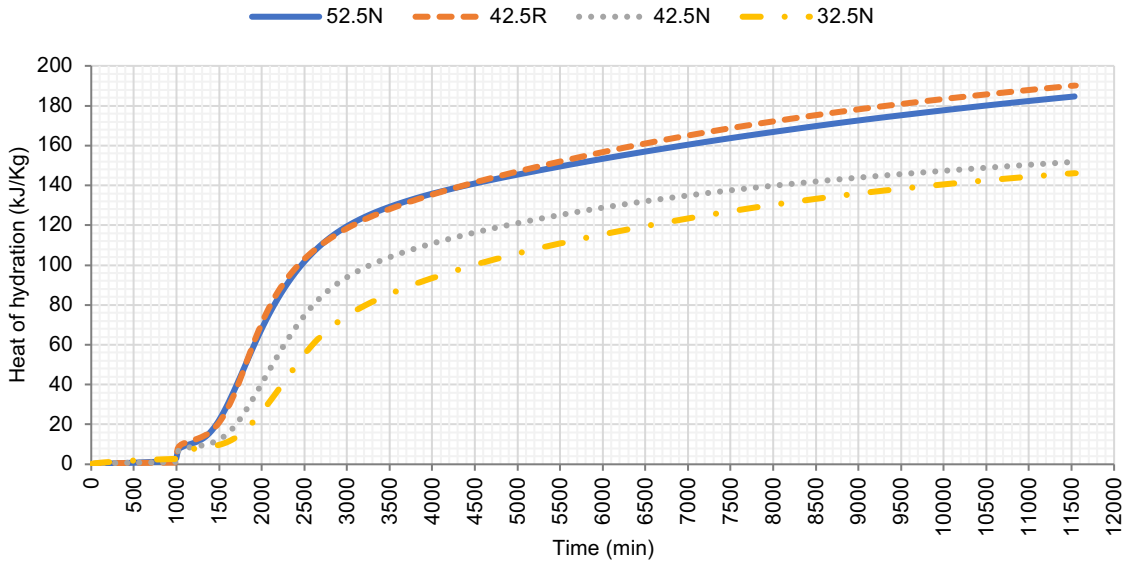

Figure 3: Heat of hydration plot

As illustrated earlier in Figure 1, the first heat flux peak occurs during Phase 1 of the cement hydration which is also known as the pre-induction period associated with the rapid release of Ca^{2+} and OH^- ions into solution Ramachandran *et. al.*, [22]. The second peak occurs at the end of Phase 3 and is associated with the final set according to Vazquez & Pique [4], this is

described as when the rapid crystallization of CH and CSH occurs. For the purpose of this paper, the second heat flux peak is analysed and discussed.

It is also observed how the heat flux corresponds to the heat of hydration output shown in Figure 3, where the two major gradients are related to each of the heat flux peaks. While the heat flux presented in Figure 2, shows no significant activity after the second peak, the heat of hydration was still observed to increase, albeit at a much lower rate, for all the cements until the end of the test period at 8 days as seen in Figure 3.

CEM II 42.5R showed the highest reactivity of all the tested cements with a total heat output of 190 kJ/kg at the end of the 8-day experiment. While this outcome was expected in comparison with the lower strength cements, this is also justified by the "R" classification used to indicate a faster strength gain usually associated with precast concrete elements. The time at which the second heat flux peak occurred is presented in Table 1, for each cement, as well as corresponding values for heat flux and heat of hydration. The last column is included to show the total heat of hydration at the end of the eight day experiment.

Table 1: Summary of peak values and corresponding times

Cement	Heat flux (W/kg)	Time (min)	Heat of hydration (kJ/kg)	8 Day Heat of hydration (kJ/kg)
II 32.5N	1.00	2250	40.63	146
II 42.5N	1.20	2045	43.91	152
II 42.5R	1.90	1815	50.52	190
I 52.5N	1.60	1800	49.03	185

With the exception of CEM II 42,5R, the heat flux peak was observed to reduce with an increase in cement strength. CEM I 52.5N reached the second peak fastest at 1800 minutes, and 15 minutes later cement type CEM II 42.5R reached its second peak. Almost 4 hours later, CEM II 42.5N reached its second peak, this was then followed by CEM II 32.5N, approximately 3.4 hours later, which is also the lowest strength cement.

4.2 Results of other cement properties

Additional information of the respective cements was also provided from the cement manufacturer. This included test results of (i) initial setting time; (ii) final setting time; (iii) fineness; (iv) early day compressive strength; and (v) 28 day compressive strength. The results for each parameters are shown below in Figure 4 to Figure 6.

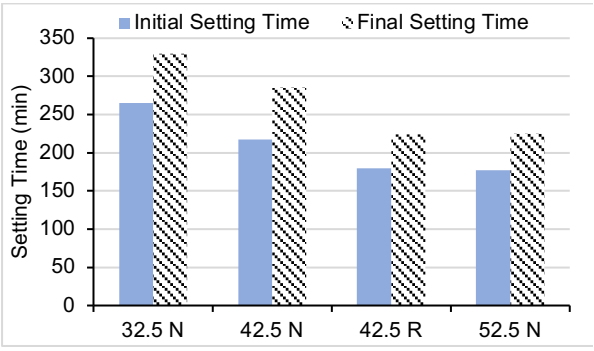

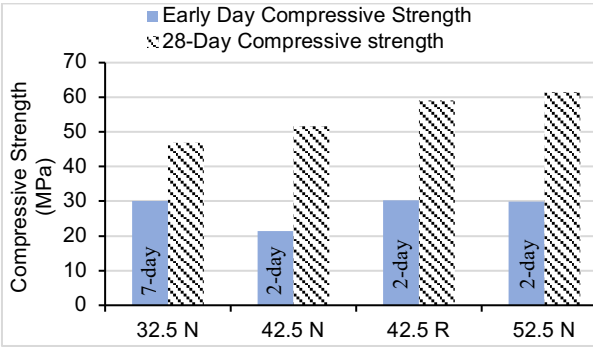

Figure 4: Plot of setting time based on average results

Figure 5: Plot of compressive strength based on average results

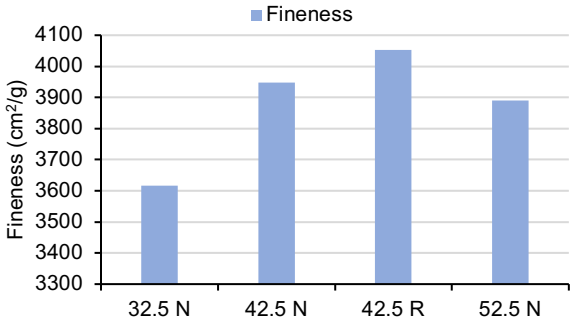

Figure 6: Plot of fineness based on average results

The average setting time plot in Figure 4 shows a decrease in initial and final setting time based on the results as expected. The results also show that the setting times for CEM II 42.5R and CEM I 52.5N are similar with only 2.5 minutes between the two initial setting times and 1.25 minutes between the two final setting times.

As expected, the 28-day compressive strength results exhibit an increase with an increase in cement strength class as seen in Figure 5. A similar trend is observed for the 2-day strength for CEM II 42.5N, CEM II 42.5R and CEM I 52.5N. Due to the low compressive strength gain at 2 days, the 7-day strength is reported for CEM II 32.5N instead of 2-day compressive strength results.

The fineness results in Figure 6 show the increase in fineness as the cement classification increases except for the CEM I 52.5N which has the second lowest fineness value out of the investigated cements.

4.3 Relationship between heat of hydration and other cement parameters

In order to understand the relationship between the heat flux peak and the setting times, the correlation plots between the second heat flux peak and the parameters obtained from the manufacturer are also shown from Figure 7 to Figure 11. The averaged values used to develop the relationships were extracted from the raw data of all four cement properties and are summarised in Table 2.

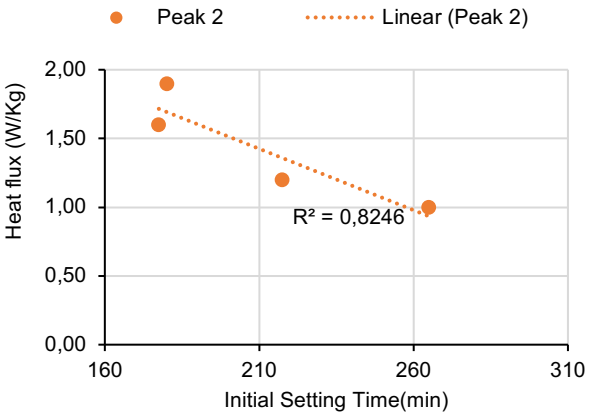

Figure 7: Correlation plot between heat flux peak and initial setting time

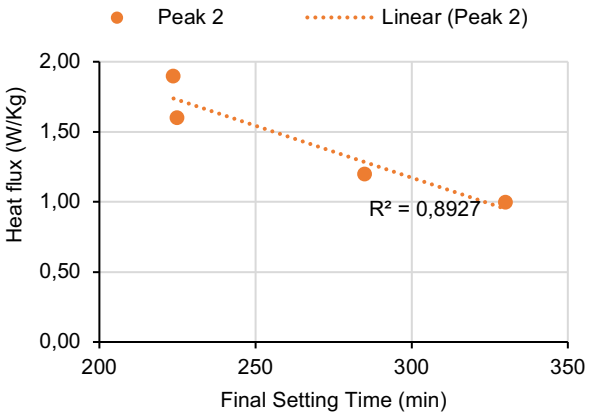

Figure 8: Correlation plot between heat flux peak and final setting time

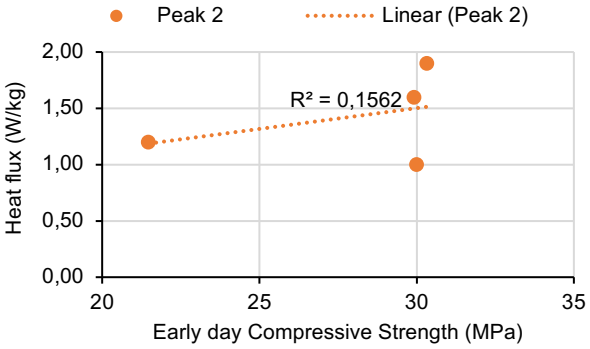

Figure 9: Correlation plot between heat flux peak and early day compressive strength

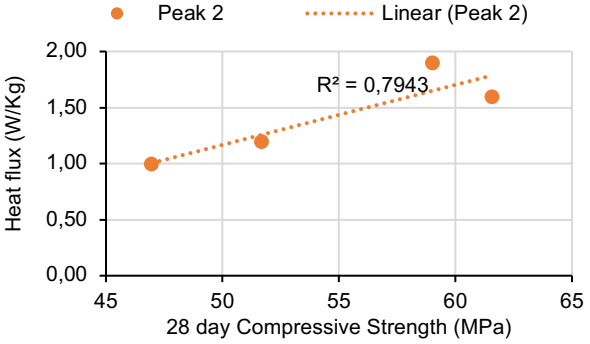

Figure 10: Correlation plot between heat flux peak and 28 day compressive strength

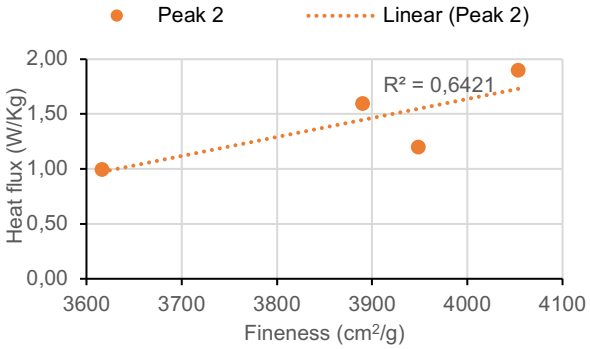

Figure 11: Correlation plot between heat flux peak and fineness

Table 2: Cement properties

Cement Type	Average Initial Setting Time (min)	Average Final Setting Time (min)	Average early day compressive strength (MPa)	Average 28 Day compressive strength (MPa)	Average Fineness (cm^2/g)
II 32.5N	265	330	30 (7day)	47	3616
II 42.5N	218	285	22 (2day)	52	3949
II 42.5R	180	224	30 (2day)	59	4054
I 52.5N	178	225	30 (2day)	62	3890

The relationship between the setting times and time of the second heat flux peak is shown below in Figure 12 and Figure 13 where a strong correlation is observed for both initial and final set.

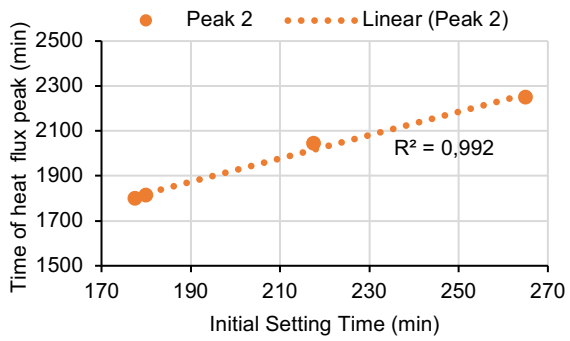

Figure 12: Correlation plot between time of heat flux peak and initial set

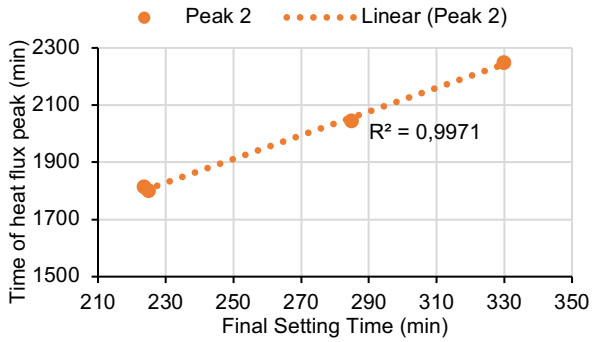

Figure 13: Correlation plot between time of heat flux peak and final set

4.4 Discussion of results

With the exception of fineness (R^2 = 0.87), the first peak did not reveal much about the cement properties. Table 3 shows the summarised R^2 values for the second heat flux peak and the investigated properties.

Table 3: Linear regression values for the different cement parameters

Parameter	R^2
Initial set	0.82
Final set	0.89
Early day compressive strength	0.16
28-day compressive strength	0.79
Fineness	0.64

It is observed from the results that there is strong correlation between the heat flux peak, setting times and 28-day compressive strength. Lower correlation was observed for fineness and no correlation observed for early day strength. The parameter with high correlation are noteworthy because it shows that the 28-day compressive strength can in fact be inferred during the early stages of hydration. Even though there is a strong correlation between the second heat flux peak and the investigated properties, with the exception of early day strength and fineness,

stronger correlation exists between the time at which the second heat flux peak occurs and the corresponding setting times as shown in Figure 12 and Figure 13, as opposed to the heat flux (W/kg). Given the strong correlation (where $R^2 > 0.99$), this demonstrates how the setting times can be determined by assessing the heat output curves from a calorimeter.

5. CONCLUSIONS

An isothermal calorimeter was used in this study to investigate the relationship between five different cement properties and the heat evolution of four types of South African cements. The properties investigated were:

- Initial and final setting time;
- Early day (2 day or 7 day) and 28-day compressive strength and;
- Cement fineness.

Understandably, current standardized test methods use different equipment and specimens to measure each of the above properties as per the relevant test method. In this study it has been shown how these properties can also be inferred with the use of a single equipment, i.e. an isothermal calorimeter for cement, through analysis of the heat development during cement hydration.

In fact, thermal analysis techniques have been shown useful for many types of cement and concrete studies, particularly to quantify the heat relationships that cause thermally induced cracking and also to assist engineers in making decisions related to material handling and construction activities that are dependent on the setting times and strength development of concrete.

The following relationships were identified during this study:

i. Strong correlation was found between the second heat flux peak (W/kg) and (a) setting times and (b) 28-day compressive strength for all the cements investigated. The highest R^2 value (0.89) was that for final setting time. The heat flux peak was observed to decrease with an longer cement setting times and increase with higher cement strengths.
ii. The strongest correlation found in this study was that for final setting time and the time at which the second heat flux peak occurred as opposed to the heat flux peak in point (i) above. This is in line with other researchers' findings such as Ramachandran *et. al*. [22], Soroka [3] and Vazquez & Pique [4].
iii. Given the strong correlation (i.e. $R^2 > 0.99$) of both initial and final set, this demonstrates how the heat output curves from a calorimeter can be used to determine setting times.
iv. CEM II 42.5R exhibited the highest reactivity of all cements through analysis of the calorimetry output curves. The cement consistently showed the highest values at each of the heat flux peaks as well as overall heat output within the 8 day duration of the experiment.
v. Early day cement strength showed no significant correlation with any of the heat flux peaks.
vi. The value of the second heat flux peak reduced with an increase in cement strength.

According to this study, three out of the five cement properties investigated can be inferred through analysis of its heat flux peak, namely initial, final setting time and 28-day compressive strength.

REFERENCES

[1] Perrie, B. & Rossman, D., 2009. *Concrete Road Construction.* MIdrand: Cement & Concrete Institute.

[2] Czernin, W., 1980. *Cement Chemistry and Physics for Civil Engineers.* 2nd ed. Michigan: Bauverlag.

[3] Soroka, I., 1979. Setting and Hardening . In: *Portland Cement Paste and Concrete.* London: Palgrave. https://doi.org/10.1007/978-1-349-03994-4_2, pp. 28-45.

[4] Vazquez, A. & Pique, T. M., 2016. Biotech admixtures for enhancing portland cement hydration. In: F. Pacheco-Torgal, V. Ivanov, N. Karak & H. Jonkers, eds. *Biopolymers and Biotech Admixtures for Eco-Efficient Construction Materials.* s.l.:Woodhead Publishing, pp. 81-96. https://doi.org/10.1016/B978-0-08-100214-8.00005-1.

[5] Goodwin, R. W., 2014. Chapter 6 - Utilization Methodology - MWC Residues. In: R. W. Goodwin, ed. *Combustion Ash Residue Management: An Engineering Perspective.* s.l.:William Andrew Publishing, pp. 77-96.

[6] SANS 50196-1:2006, 2006. *South African National Standard. Methods of testing cement. Part 1: Determination of strength,* Pretoria: South African Bureau of Standdards (SABS).

[7] SANS 5863:2006, 2006. *South African National Standard. Concrete tests - Compressive strength of hardened concrete.,* Pretoria: South African Bureau of Standdards (SABS).

[8] SANS 50196-3:2006, 2006. *South African National Standard. Methods of testing cement. Part 3: Determination of setting times and soundness,* Pretoria: South African Bureau of Standdards (SABS).

[9] Indelicato, F., 1997. Estimate of concrete cube strength by means of different diameter cores: A statistical approach. *Materials and Structures/Materiaux et Constructions,* Volume 30, pp.131-138.

[10] Al-Abbasi, A. & Shalaby, A., 2018. *Non-Destructive Testing for Optimizing Concrete Pavement Rehabilitation.* Saskatoon, Proceedings of Innovations in Pavement Management, Engineering and Technologies Session.

[11] Vold, M. J., 1949. Differential Thermal Analysis. *Analytical Chemistry,* 21(6), pp. 683-688.

[12] Le Châtelier, H., 1887. Compt. Rend. Hebd. Séanc. Acad. Sci. Paris, 104:1443.

[13] Boersma, S. M., 1955. A Theory of Differential Thermal Analysis and New Methods of Measurement and Interpretation. *Journal of the American Ceramic Society,* 38(8), pp. 281-284.

[14] Wadsö, L., 1995. *Evaluation of isothermal calorimetry for characterization of very early and early cement reactions: A critical literature review. Report TVBM, Intern 7000-rapport, Vol. 7094,* Lund: Division of Building Materials, LTH, Lund University.

[15] Carlson, R. W., 1934. The Vane Calorimeter. *Proceedings- American Society for Testing and Materials,* 34(2), pp. 322-328.

[16] Lerch, W. & Bogue, R. H., 1934. Heat of hydration of Portland Cement pastes. *Part of Bureau of Standards Journal of Research,* Volume 12, pp. 645-664.

[17] Rastrup, E.,1954. Heat of Hydration in Concrete. *Magazine of Concrete Research,* 6(17), pp.79-92.

[18] Aschan, N., 1966. Determining the setting time of cement paste, mortar and concrete with a copper-lead electrode. *Magazine of Concrete Research,* 18(56), pp. 156-160.

[19] Acker, P., 1988. Mechanical behaviour of concrete: contribution of the physical and chemical approach. *Rapport de Recherche LPC (Laboratoire Central des Ponts et Chaussees),* Issue 152.

[20] Lootens, D. & Bentz, D. P., 2016. On the Relation of Setting and Early-Age Strength Development to Porosity and Hydration in Cement-Based Materials. *Cement and Concrete Composites,* Volume 68, pp. 9-14.

[21] ASTM C1679-09, Standard Practice for Measuring Hydration Kinetics of Hydraulic Cementitious Mixtures Using Isothermal Calorimetry, ASTM International, West Conshohocken, PA, 2009.

[22] Ramachandran, V. S., Paroli, R. M., Beaudoin, J. J. & Delgado, A. H., 2002. *Handbook of Thermal Analysis of Construction Materials.* New York: Noyes Publications / William Andrew Publishing.

POTENTIAL FOR CARBON DIOXIDE SEQUESTRATION IN WET CONCRETE MIXES

Ivy I. Milanova [(1)] and Elsabe Kearsley [(1)]

(1) Department of Civil Engineering, University of Pretoria

ABSTRACT

The novel concept of CO_2 sequestration in wet concrete mixes relies on permanent capture and storage of CO_2 in the form of solid limestone within the concrete matrix. This technology is designed to alleviate a portion of the carbon footprint while ensuring that the strength and integrity of the concrete is not impaired. Sequestration occurs when CO_2 is introduced into the freshly hydrating cement paste where it reacts with the main calcium silicate phases, forming calcite and silicate hydrate gel. In this study, CO_2 was added to fresh concrete and mortar mixes during mixing. Two forms of CO_2 addition were utilised: the first comprised carbonating the mix water and the second, CO_2 within its solid state, commonly referred to as dry ice. The effects of CO_2 absorption of mixes were physically and chemically investigated during a series of comparative tests. Results indicate a strong potential for concrete mixes treated with dry ice to reach acceptable flexural and compressive strengths after 28 days, suggesting that carbonation continues within the cementitious matrix past early age strength.

Keywords: concrete, carbon dioxide, carbonation

1. INTRODUCTION

The anthropogenic CO_2 load is an increasingly problematic secondary effect of the modern world. Cement production alone is responsible for nearly 7% of global CO_2 emissions [14]. In an attempt to combat this, Carbon Capture and Storage (CCS) has become a popular field of study in recent years [5]. As concrete is the most universal building material, storage of CO_2 within it offers massive promise, offering a 'greener' solution to current industrial practices. During the production of cement, a calcination process occurs wherein calcite ($CaCO_3$) is transformed into calcium oxide (CaO) as indicated in Equation 1.

$$CaCO_3 \rightarrow CaO + CO_2 \qquad \textbf{Equation (1)}$$

This reaction, along with the energy necessary to run the cement kiln, together comprise the CO_2 released into the atmosphere. The chemical makeup of concrete has a direct effect upon its strength and durability. During the carbonation of freshly hydrating cement paste, the main calcium silicate phases present in the cement and the added CO_2 react together to form calcite as well as silicate hydrate gel as shown in Equation 2 and 3 respectively.

$$3CaO{\cdot}SiO_2 + 3CO_2 + XH_2O \rightarrow SiO_3{\cdot}XH_2O + 3CaCO_3 \qquad \textbf{Equation (2)}$$

$$2CaO{\cdot}SiO_2 + 2CO_2 + XH_2O \rightarrow SiO_3{\cdot}XH_2O + 2CaCO_3 \qquad \textbf{Equation (3)}$$

This reaction begins during the hydration of the cementitious phases with the added CO_2. The products formed during these hydration reactions are calcium ions (Ca^{+}) and carbonate ions

(CO_3^{-2}) respectively. When these ions bond together, they undergo an exothermic carbonation reaction in which calcite is produced as seen in Equation 4. This carbonation reaction is diffusion limited when it takes place in cement, responding with CaO individually as well as in the C-S-H phase [5].

$$Ca^{+2} + CO_3^{-2} \rightarrow CaCO_3 \quad \textbf{Equation (4)}$$

Various experimentation with CCS in concrete have been undertaken, with adjustments made in the means and methods of CO_2 sequestration. From these, it was concluded that introducing CO_2 to wet concrete during the mixing stage would utilize CCS on a larger scale, as opposed to it being exposed to mature concrete. The addition of CO_2 to the concrete mix thus eventually accounts for the formation of calcite within the hardened concrete matrix. Moreover, the fresh properties of the mix are also said to experience an impact, such as accelerated drying times and decreased alkalinity. Further experiments [5] saw increased early-age compressive strengths of concrete cubes treated with varying concentrations of solid CO_2 during the mixing phase. This strength increase is attributed to the formation of calcite within the hardened concrete. When carbonation takes place within a concrete matrix, carbonic acid is formed during the reaction shown in Equation 5:

$$CO_2 + H_2O \rightarrow H_2CO_3 \quad \textbf{Equation (5)}$$

The creation of this acid results in a pH drop of the pore solution which is originally of a high alkalinity, usually a pH reading of above 12.5. Carbonation of hydrated Portland cement paste can reduce this value to as low as 8.3, which may be deemed problematic as the depassivation threshold of reinforcing steel is approximately 9.5 [7], thus potentially resulting in accelerated corrosion of reinforcement. However, this is said to be a possibility only when CO_2 is exposed to mature concrete and its hydration phases [6]. Furthermore, the porosity of carbonated cement paste may change. This change can be manifested as a decrease in the case of Portland cement and an increase in the case of blended cement paste [4]. The chemical changes arising in cement paste when it is carbonated can be analysed using X-ray powder diffraction (XRD) and Thermogravimetric analysis (TGA). XRD is a reliable method to use to identify the phases present in the cement, as well as trends in the production and consumption of secondary hydration products like portlandite and ettringite [2]. TGA portrays the change of mass of a material sample as a function of time over a temperature heating rate.

2. EXPERIMENTAL WORK

2.1 Preparation of Mortar

The mortar mix allowed for a comparative, small scale representation of the concrete mix which could be chemically analysed while disregarding chemically inert aggregates. The mix design for one batch of mortar consisting of a set of three prismatic specimens comprised of 450 g of CEM II with a 20 % fly ash content, 1350 g of ISO standard sand and 225 g of water and possessed a 0.5 water:binder ratio. Each prismatic specimen had dimensions of 40 mm x 40 mm x 160 mm. As the ultimate goal of this experiment was to test the structural suitability of a greener and more environmentally friendly building material, CEM II was chosen as it already contains fly ash as an admixture.

Originally, three test mixes were created: the reference mix (Mix T) with the standard mix design, Mix A wherein one litre of mix water was carbonated using approximately 3.3 litres of CO_2 and Mix B wherein one litre of mix water was carbonated using approximately 6 litres of

CO_2. Mix water was carbonated one litre at a time using commercially available home carbonation equipment. Subsequently, it was decided to include two more mortar mixes, to which CO_2 was introduced during the mixing stage in the form of dry ice in additions of 200 g and 300 g respectively per litre of mix water.

Specimens from Mixes T, A and B were prepared for curing ages 1, 3, 7 and 14 days, while specimens from Mixes C and D were prepared for curing ages 1, 3, 7, 14 and 28 days. Directly following the mixing stage, the wet mortar from each mix was tested for its pH using an electronic pH probe and subsequently for its workability using the flow table test (ASTM C230). Mortar specimens were left to set for 24 hours in a humidity and temperature controlled room, whereafter they remained in a water bath until their respective curing ages were reached.

Flexural strength testing followed by compressive strength testing were performed on the mortar specimens at the stipulated curing ages (EN 196-1). Thermogravimetric analyses were performed on mortar samples at their various curing ages. Pieces from the mortar specimens were stored in an oven at 60 ˚C for a duration of 24 hours to expel any remaining water, and thereafter ground into powder and stored in sealed, clearly marked packets to be used during TGA. During the test, the sample was covered by the TGA furnace and heated to a temperature of 800 ˚C at a rate of 20 ˚C/min in the presence of Nitrogen gas to induce chemical decomposition of the material. XRD analysis was performed on samples from each of the five mortar mixes at a curing age of 14 days.

2.2 Preparation of Concrete

A simple concrete mix design, with a water:binder ratio of 0.5 was chosen. The mix design per cubic meter comprised of 400 kg CEM II (containing 20 % fly ash), 200 kg of water, 900 kg of dolomite sand and 900 kg of 10 mm dolomite aggregate. A reference mix (Mix 1) and a CO_2 treated mix (Mix 2) were produced in order to run comparative tests. The CO_2 for Mix 2 was added in the form of carbonated mix water, with approximately 3.3 litres of CO_2 used per litre of mix water. Directly following the mixing stage, both concrete mixes were tested for their pH level using an electronic pH probe. Thereafter slump tests were performed for each mix (SANS 5862-1) in the attempt to observe potential relationships between the added CO_2 and the resulting workability of the mix. Concrete specimens were cast into the required moulds and left to set for 24 hours in a humidity and temperature controlled room, whereafter they remained in a water bath until their respective curing ages were reached.

The CO_2 treated concrete was examined in order to determine whether its transformed chemical composition would impact its durability in any way. Test specimens comprised of circular disks, approximately 70 mm in diameter and 30 mm in thickness, cored and cut from previously cast cubes. Specimens were left in an oven for 7 days at a temperature of 50 ˚C in order to remove an excess moisture within the sample. The same set of specimens were used first in the oxygen permeability test, and later in the water sorptivity test.

An investigation of the impact of carbonation on the concrete's pH level was conducted through an experiment in which 300 mm x 300 mm x 200 mm concrete specimens were cast from Mix 1 and Mix 2 and reinforcing was positioned within each specimen such as to create a voltaic cell. Sodium Chloride (NaCl) solution was periodically poured on the top surface of each specimen so as to accelerate the natural rusting process by inducing cyclic wetting and drying of the concrete. This corrosion experiment continued for 28 days, after which both specimens were broken in half and the exposed inner surface sprayed with a phenolphthalein solution to give an indication of the concrete's pH level. Thereafter, the reinforcement bars were cleaned from rust and weighed to determine the degree of corrosion suffered.

3. ANALYSIS OF RESULTS

3.1 Mortar Results

Analysis of the mortar results suggest a higher rate of CO_2 sequestration taking place in Mix C and Mix D. This is indicated in Table 1 by lower pH values and workability as well as greater amounts of calcite within the samples as predicted.

Table 1: Summary of mortar results

	Mix T	Mix A	Mix B	Mix C	Mix D
pH value	12.96	12.53	12.50	11.35	11.02
Flow (%)	183	186	195	138	115
Weight of calcite within sample at 14 days (%)	1.48	1.79	1.84	1.99	2.38

Flexural and compressive strength of the prismatic specimens from each mix are portrayed in Figure 1 and Figure 2 respectively. Prisms from the reference mix appear to have the highest strengths, followed by those from Mix A and Mix B, which increase in relative flexural and compressive strength with time. Mixes C and D indicate an even smaller retention of the reference mix's flexural and compressive strength at early age. The general decline in strengths between prism of the reference mix and those of Mixes A, B, C and D can be attributed to the previous exposure to CO_2. However, their steady increase in percentage flexural and compressive strength of the reference mix suggests the possibility of minimal strength differences between these mixes and the reference mix at later ages.

Results thus imply that the addition of solid CO_2 offers a more efficient sequestration method compared to the carbonation of mix water.

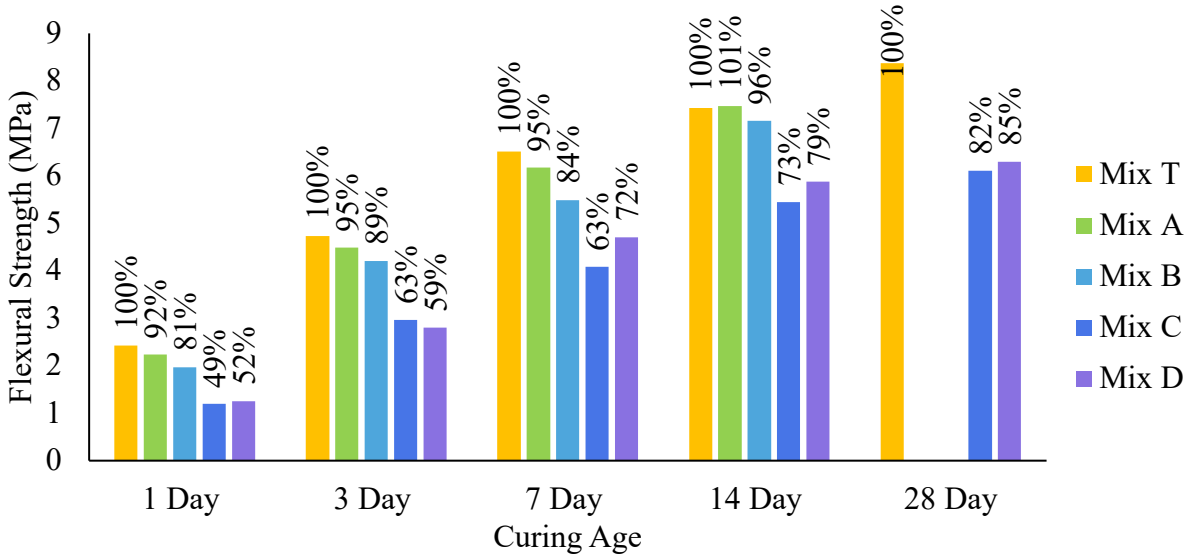

Figure 1: Flexural strength of mortar prisms

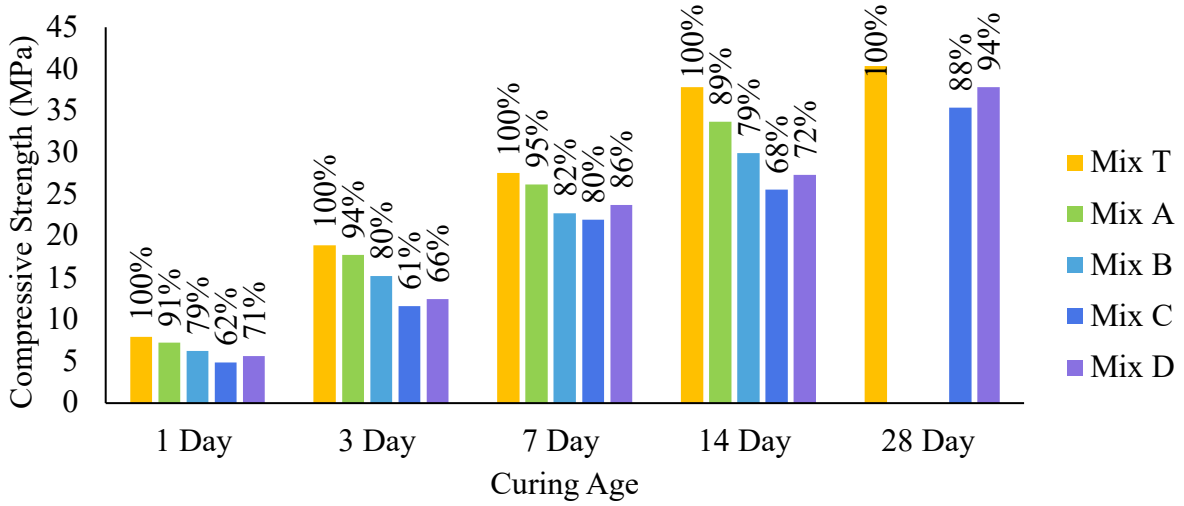

Figure 2: Compressive strength of mortar prisms

TGA curves relating percentage weight loss of the five samples at 14 days curing age as a function of temperature are indicated in Figure 3. A distinct dip is visible in every curve between 600 ˚C and 800 ˚C, indicating the temperature region of calcite decomposition (decarbonation). The varying amounts of calcite within the mortar, most prominent in the case of Mix C and Mix D, within the mortar allude to the fact that CO_2 has been captured inside the mortar as anticipated. The percentage mass loss due to decarbonation can be further deduced as a result of this.

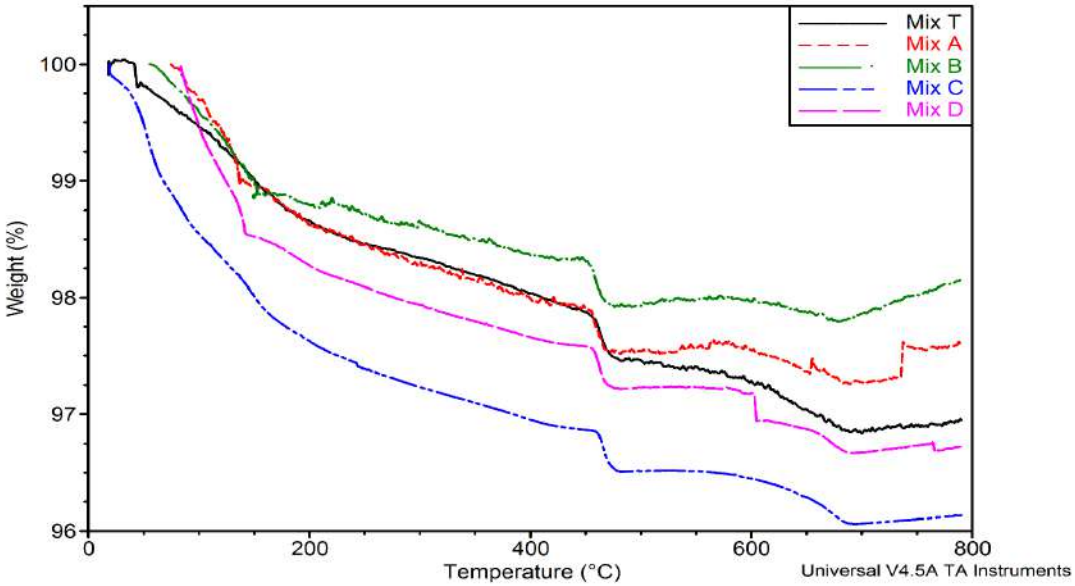

Figure 3: Fourteen-day TGA of mortar samples

3.2 Concrete Results

Comparison of the concrete results revealed a certain difference in performance between the CO_2 treated mix and the reference one. The pH readings for Mix 1 and Mix 2 were 13.30 and 12.68 respectively. This discrepancy in values indicate a change in original concrete alkalinity which can only be attributed to the CO_2 addition. While the lower value remains higher than the depassivation threshold of reinforcing, problems may arise when the concrete sets and hardens as the drop in alkalinity may potentially continue as a result of the hydration of products inside the concrete matrix. The slump was determined as an indication of the workability of the fresh concrete. The slump was measured as 90 mm for Mix 1 and 105 mm for Mix 2. The CO_2 addition in Mix 2 thus increased the workability with more than 15 %. This may be attributed to improved lubrication of the mix as a result of the entrained air present from carbonation of the mix water. The results for oxygen permeability and water sorptivity testing are summarised in Table 2. General observation of these values indicates good durability characteristics in both mixes. The permeability of concrete defines its ability to resist flow of a fluid within its hardened matrix. Permeability of Mixes 1 and 2 appears to be practically equivalent, with no significant variance which may be linked to the CO_2 addition.

Table 2: Summary of results from oxygen permeability and water sorptivity testing

	Mix 1	Mix 2
Oxygen Permeability Index	10.53	10.50
Water Sorptivity Index ($mm/hr^{0.5}$)	8.68	9.95
Porosity (%)	9.49	10.62

Considering the data, sorptivity and porosity are depicted to be higher in the case of Mix 2. This behaviour is in line with the findings of [4], which states that carbonation may induce an increase in the pore structure of concrete produced with blended cements. While a rise in sorptivity and porosity in concrete are not ideal, the results of Mix 2 are still within the limits of good practice. However, care should be taken in cases where reinforcement is present or higher CO_2 dosages are desired in the mix design.During the wetting-dry cycles of the accelerated corrosion test, qualitative changes were observed as a rust stain on the surface of the Mix 2 specimen (significantly larger than that on the surface of the Mix 1 specimen) began to appear. Figure 4 depicts, the specimens when they were halved and sprayed with phenolphthalein solution.

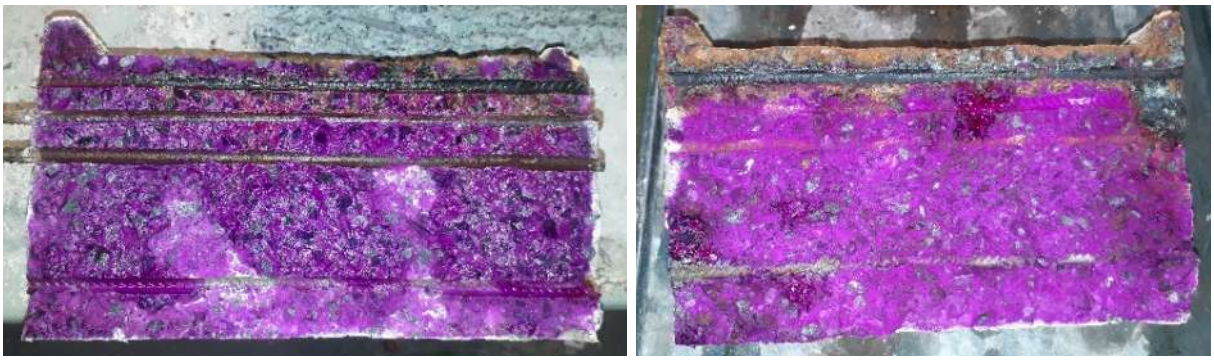

Figure 4: Inner surface of Mix 1 (left) and Mix 2 (right) specimens

Considering the specimen of Mix 1, there is a very fine colourless strip at the top right-hand surface which signifies a small reduction in pH in this region. A pH drop was only experienced near the top of the specimen, and any potential corrosion of reinforcement is limited to that region. The previously CO_2 treated specimen of Mix 2, in contrast, displays an acidic region of substantial size near the top of its cross-section, entirely surrounding the first reinforcement bar. The drop in alkalinity caused by the extraction of sodium chloride ions within the NaCl solution into the concrete, further resulted in corrosion induced mass loss of the fixed reinforcement bars. The top reinforcement bar of Mix 1 experienced a mass loss of 2.07 % as opposed to that of Mix 2 which experienced a 6.41 % mass loss. Acidity was thus able to diffuse through a greater distance from the top surface of the Mix 2 specimen, similarly affecting the rest of the reinforcement bars, albeit to a lesser degree. This creates cause for concern as any reinforcing within CO_2 treated cement is at a greater risk for corrosion.

4. CONCLUSIONS

Treating mortar and concrete with CO_2 during mixing results in carbonation of the cement and alters the chemical composition of the mix on an elemental level. TGA results exhibited a considerable mass percentage of the anticipated calcite within samples of mortar mixed with dry ice during decarbonation of the sample. From XRD analyses calcite was found to exist in the least amounts within the reference mix, with increasing dosages present in Mixes A to D, correlating to the sequestration method used and difference in carbon content. Better CO_2 sequestration appears to have taken place in Mixes C and D where it was added as dry ice.

The strengths of mortar prisms from Mixes C and D showed substantially weaker results for early-age strength gain, however, a prominent increase in strength was noticed toward the 28-day mark. This shows potential when considering strength development at later ages. In terms of durability aspects, it was found that sorptivity and porosity increased in the case of the CO_2 treated concrete mix, suggesting potential problems in the long-term durability of the concrete. This was further supported when results showed corrosion occurred at a faster rate in the CO_2 treated mix due to decreased alkalinity within it. Outcomes of the investigation prove that it is possible to sequestrate CO_2 into mortar and concrete during mixing without significant negative consequences on the material properties, especially in their later age. This, however, is only true on condition that no steel reinforcement is present in CO_2 sequestrated concrete.

REFERENCES

[1] ASTM C230 (2014), Standard specification for flow table for use in tests of hydraulic cement
[2] Du Toit, G. 2018. Chemical and mechanical activation of hybrid fly ash cement. PhD thesis. University of Pretoria.
[3] EN 196-1 (2005), Methods of testing cement Part 1: Determination of strength
[4] G. Rimmelé, V. Barlet-Gouédard, O. Porcherie, B. Goffé, F. Brunet. 2008. Heterogeneous porosity distribution in Portland cement exposed to CO2-rich fluids. *Cement and Constrution Research*, Vol 38, No 8, pp1038–1048.
[5] Monkman, S. Macdonald, M. 2016. Carbon upcycling into industrially produced concrete blocks. *Construction and Building Materials,* Vol 124.
[6] Papadakis, V. Fardis, M. Vayenas, C. 1992. Effect of composition, environmental factors and cement-lime mortar coating on concrete carbonation. Materials and Structures, Vol 25, No 5, pp 293-304.
[7] Sajiva, B. Lukovic, M. 2016. Carbonation of cement paste: Understanding, challenges and opportunities. Construction and Building Materials, Vol 117.
[8] SANS 50196-1 (2006): Methods of testing cement - Part 1: Determination of strength
[9] SANS 5861-1 (2006), Concrete tests – Part 1: Mixing fresh concrete in the laboratory
[10] SANS 5861-2 (2006), Concrete tests – Part 2: Sampling of freshly mixed concrete
[11] SANS 5861-3 (2006), Concrete tests – Part 3: Making and curing of test specimens
[12] SANS 5862-1 (2006), Concrete tests – Part 1: Consistence of freshly mixed concrete – slump test
[13] SANS 5863 (2006), Concrete tests – Compressive strength of hardened concrete
[14] Shi, C. Jimenez, AF. Palomo, A. 2011. New cements for the 21st century: The pursuit of an alternative to Portland cement. *Cement and Concrete Research,* Vol 41, No 7, pp750-763.

MANAGEMENT OF CONCRETE AND CEMENTITIOUS WASTE: AN ASSESSMENT OF PRACTICES AND STRATEGIES IN SOUTH AFRICA

Frieda M. Mogodi [(1)] and Mike Otieno [(1)]

(1) School of Civil and Environmental Engineering, University of the Witwatersrand, Johannesburg

ABSTRACT

The construction industry is among the top three waste producers in South Africa. There is limited literature on the contribution of concrete and cementitious material to waste generated in the Construction and Demolition (C&D) category. The government outlines waste management strategies in the State of Waste Report (SoWR) which aim to minimise waste production levels and landfill issues; however, there is a poor understanding of the link between these strategies and practices in the industry. This study assesses the practices and strategies for the waste management of concrete and cementitious material on construction sites based in Braamfontein, Midrand, Rosebank, Menlyn and Johannesburg Central Business District. The results indicate that there is limited published literature on the management of concrete and cementitious waste produced in construction projects; also, that there is a partial practice of the Reduce, Re-use and Recycle strategies. There is poor adherence to the recent waste hierarchy model stated in the SoWR because practitioners are unfamiliar with the report. The study contributes to sustainable development practice in South Africa and recommends that the private and public sector should actively participate in transferring knowledge to practitioners, thus encouraging them to consciously practice sustainable waste management in the SoWR.

Keywords: concrete, construction and demolition, project life cycle, waste management hierarchy, landfill.

1 INTRODUCTION

In 2018, the South African Department of Environmental Affairs (DEA) published a State of Waste Report (SoWR) which contained waste management legislations from 1989 to 2018 [1]. These legislations inform the management of waste produced in South Africa including construction and demolition (C&D) waste, organic waste and municipal waste, among others. The SoWR, issued in 2018, [1] indicated that C&D waste contributed the third largest (13%) proportion of the total waste produced in the country. C&D waste can comprise a variety of materials including concrete, ceramics, glass, timber, and metals. However, the report does not provide this breakdown. Therefore, the proportion of concrete and other cementitious material waste in the lump sum C&D figures in the DEA report is potentially unknown.

In South Africa, a large proportion of all the wastes produced end up in landfills. This strategy is common even in the disposal of C&D waste from the construction industry and poses several environmental challenges. To overcome this challenge, the DEA legislation encourages practitioners to have proper Waste Management Plans (WMP) that are environmentally friendly [2].

2 SIGNIFICANCE AND SCOPE OF THE STUDY

The study reported in this paper focused on the management of concrete and cementitious waste which is part of C&D waste considering that concrete is one of the most used materials in the construction industry and the second most used material in the world [3]. Although there are studies that have been conducted on C&D waste in South Africa [2], there is limited published literature on the management of concrete and cementitious waste specifically. One of the envisaged outcomes of the study is to create awareness of the current practices and strategies for waste management of concrete and cementitious waste in South Africa, and thus presenting a case for the need for improved approaches to managing concrete and cementitious waste. The findings of the study also contribute to the promotion of sustainable practices, thereby supporting the National Development goals of South Africa which call for the urgent implementation of the Nationally Appropriate Mitigation Action (NAMA) [4].

This study critically reviewed the current management practices and strategies for concrete and cementitious waste generated by construction projects in South Africa, China, Australia, Germany and Kenya. Due to time and cost constraints, the study was carried out on selected construction projects in South Africa's Gauteng province.

3 LITERATURE REVIEW

Between 2011 and 2017, South Africa reported a relatively small per capita decline of 0.19 in the total waste produced in the country [1]. This period also coincided with the introduction of waste management policies as reported in the SoWR which can lead to the conclusion that the policies contributed to the decline. However, it is difficult to apportion how much of the decline can be apportioned first, to C&D waste, and second, to concrete and cementitious waste. There is a gap for studies focusing on classified waste such as concrete, glass, wood, etc.

When a concrete structure is demolished, the rubble material can be either be disposed of in a landfill or re-used or recycled on site. Disposal in a landfill is the last phase and least preferred option in the life cycle of a concrete structure [5]. Barnes [6] reported that in South Africa most concrete and cementitious materials waste is transported to a landfill but there are no records of exactly how much of the waste is disposed of. Abel [7] reported that there is a problem of illegal dumping of concrete waste in South Africa; this can be attributed to the country's potential shortage of technology for processing waste material and limited published literature on the waste produced in construction sites.

Strategies should be put in place to encourage the practice of re-using and/or recycling of the materials, and disposal on landfill last when managing concrete and cementitious waste. This is a grave-to-cradle approach that has been shown to have the capacity to decrease the quantities of concrete dumped in landfills [8]. Further studies are required to understand the capacity and limits on the utilisation of recycled concrete and other cementitious materials, and the perception of contractors on the utilisation of recycled concrete and other cementitious materials.

4 METHOD

A qualitative approach was adopted for the study which was conducted in 2019. According to Minchiello [9], this method focuses on understanding human behaviour from the informant's perspective and assumes a dynamic and negotiated reality. The data is collected through participant observation and interviews. In the method, data analysis is carried out through themes informed by the informants' descriptions. This approach allowed for the exploration of an untapped area of study for C&D waste management in South Africa. Sinaga [10] reports that the advantage of the qualitative method is that it enables the researcher to "identify new and untouched phenomena; provide a deeper understanding of mechanisms; provide verbal information that may sometimes be converted to numerical form and reveal information that would not be identified through pre-determined survey questions". However, the disadvantage with qualitative method is that it can restrict the researcher as the results are "general to the population, easily applied in statistical methods, and easily assessed in relations between characteristics" [10].

Construction practitioners formed the target population, with non-probability and purposive sampling methods being used to select the samples. According to Showkat & Parveen [11], non-probability sampling is characterised using; non-randomised methods to select the sample and judgement, convenience and access to the sample. It is less expensive, less complicated, and easier to apply. The results lack generalization of the sample to an entire population and generate valuable insight on an existing phenomenon or developing a new one. The sampling techniques include Convenience Sampling, Purposive Sampling, Quota Sampling and Snowball Sampling.

In addition to the critical review of literature, case studies were carried out on five selected construction sites located in Braamfontein, Midrand, Rosebank, Menlyn and Johannesburg's Central Business District (CBD), all in South Africa's Gauteng province – see **Table 1**. The five construction sites comprised of one small, two medium and two large projects, as per the project classification criteria presented in **Table 2** [12].

A survey questionnaire (available online at https://bit.ly/39GTFEv) was developed to source information from the target population. The development of the questionnaires was guided by the aim and objectives of the study, as well as a review of available literature. Ethics clearance was obtained from the University before commencing the study to facilitate the collection of data. A response rate of 22% was received on the questionnaires. The questionnaire feedback was the primary data for analysing the findings in conjunction with the interviews held on site. The [informal] interviews were conducted with the construction practitioners on site during the site visits and while distributing the questionnaires. The [informal] interviews were essential in the understanding and interpretation of the data collected. An inductive method was used to code the data, a process that facilitated a holistic view of the results to enable the generalization of the outcomes of the study albeit with the limitations mentioned earlier.

The respondents in the study comprised civil engineers, site managers, safety officers, site agents, forepersons, managing directors and general workers. Also, they had varying site and professional experiences ranging from interns, junior workers to senior personnel. In terms of site experience, and considering all the respondents, 27%, 37%, 18% and 18% had 0–1, 1–3, 10–15 and over 15 years of working experience.

Table 1: Construction sites sampled as Case studies

Case study No.	Location	Type of construction	Project size
1	Braamfontein, Johannesburg	Multi-storey accommodation	Medium
2	Midrand, Johannesburg	Multi-storey hotel with office space	Medium to large
3	Rosebank, Johannesburg	Multi-storey office	Medium
4	Menlyn, Pretoria	Multi-story office, apartment and shopping centre	Large
5	Johannesburg Central Business District (CBD)	Multi-story residential	Small

Table 2: Project sizing criteria of Case studies based on the guidelines by Wilson [12]

Project aspect considered	Construction site														
	Case study 1			Case study 2			Case study 3			Case study 4			Case study 5		
	S	M	L	S	M	L	S	M	L	S	M	L	S	M	L
Size of project team (full-time equivalent)	–	–	–	–	–	–	–	–	–	–	–	–	–	–	–
Completion time	☐	☒	☐	☐	☐	☒	☐	☒	☐	☐	☐	☒	☐	☒	☐
Timeframe	☐	☒	☐	☐	☐	☒	☐	☒	☐	☐	☐	☒	☒	☐	☐
Complexity	☒	☐	☐	☐	☐	☒	☐	☒	☐	☐	☐	☒	☒	☐	☐
Strategic importance	☐	☐	☒	☐	☒	☐	*	*	*	☐	☐	☒	☒	☐	☐
Reputation importance	☐	☒	☐	☐	☒	☐	☐	☒	☐	☐	☒	☐	☒	☐	☐
Total cost	☐	☐	☒	*	*	*	*	*	*	☐	☐	☒	*	*	*
Level of change	☐	☒	☐	☐	☐	☒	☒	☐	☐	☐	☒	☐	☒	☐	☐
Dependencies and inter-related projects	☒	☐	☐	☐	☒	☐	☐	☒	☐	☐	☐	☒	☒	☐	☐
Overall project size	Medium			Medium-to-large			Medium			Large			Small		

S: Small-sized project
M: Medium-sized project
L: Large-sized project
*: Information confidential
'–': Information not available/provided

As indicated in Table 2, none of the construction sites provided information on the sizes of the project teams. Table 2 can be interpreted as follows [12]:

(i) Completion time takes less than six months, six to twelve months and more than 12 months for, respectively, small projects, medium projects and large projects.
(ii) The complexity levels of small projects are manageable, the problem is easily understood, and the solution is readily achievable. In medium projects, the problem is either difficult to understand or the solution is unclear or difficult to achieve while in large projects, both the problem and the solution is difficult to define or understand and the solution difficult to achieve.
(iii) Strategic importance in small projects is of internal interests only and thus have no reputation implications. In medium projects, there could be some direct impact on a low priority initiative with some reputation implications. Large projects affect core university service delivery and/or directly relates to key initiatives in a strategic plan and there are major reputation implications.
(iv) In small projects the total costs are less than USD 25K, medium projects range from USD 25K to USD 200K and in large projects the costs are more than USD 200K.

(v) Small projects have no major dependencies as their changes impact a single area. Medium projects have some low-risk dependencies and changes could impact several areas. Large projects have high-risk dependencies, and the changes could impact the entire project.

5 RESULTS

From the data collected, 46% of the respondents indicated that there was a designated strategy for the management of concrete and cementitious waste on site while 27% indicated that there was no strategy. The remaining 27% of the respondents were not sure if there were designated strategies for concrete and cementitious waste management. Amongst the respondents who indicated the presence of waste management strategies on site, "reduce, reuse and recycle" were the most cited strategies for managing concrete and cementitious waste – see **Table 3**. Based on the observations made during the site visits, there were waste management plans in all construction sites. It was therefore clear, from the responses received, that all the site workers were not familiar with the [formal] site waste management plans in place. Possible reasons for this may include (i) poor communication of the waste management strategies on the construction sites, or (ii) poor inculcation of a waste management culture in the organisation and on site.

50% of the respondents in Table 3 indicated that backfilling is the primary form of re-use strategy for managing concrete and cementitious waste. 'Reuse' is one of the preferred methods of waste management in the SoWR. 39% of the respondents indicated that 'Disposal' is the next most used strategy after re-use. According to the respondents interviewed on site, the waste is collected from the site by formal waste management collectors for disposal in landfills. These findings corroborate the findings of previous studies [6] that South Africa faces excessive amounts of waste disposed of in landfills. The survey results indicate that ´selling´ (or exchange of waste for money) is not utilized by any of the construction sites as a waste management strategy. The insufficient use of the exchange for money strategy suggests that there exists an opportunity to develop incentives that will encourage practitioners to sell waste as a form of managing the waste.

Case study 1 (a medium multi-storey accommodation construction site) indicated that their construction project produced an estimate of 0.07 cubic meters of concrete and cementitious waste per day. Case studies 2, 3, 4 and 5 did not have an estimate and records of quantities of concrete and cementitious waste material produced on their construction projects. Due to minimal information provided by other sites, results from case study 1 cannot be generalized. These findings demonstrate why there is limited [published] literature on the amounts of concrete and cementitious waste generated in construction sites. Construction practitioners should be encouraged and incentivised to document the type and quantity of waste generated in their projects.

The survey results in

Table 4 indicate that up to 73% of the respondents support the notion that the management of waste concrete and cementitious material is necessary and important. However, the implementation of this seems to be poor based on the response rate of 64% indicating a non-committal (neutral) stance. Nevertheless, these results present an optimistic perception of advancing the waste management of concrete and cementitious waste because the practitioners understand the underlying value.

Table 3: Waste management methods on the construction sites

Waste management method	Response rate
Re-use	50%
Disposal	39%
Recycling	11%
Selling (exchange for money)	0%

Table 4: Responses on practices and strategies for managing concrete and cementitious waste

Statement	Strongly disagree	Disagree	Neutral	Agree	Strongly agree
The management of waste concrete and cementitious material is a necessary practice in the South African industry	0%	0%	18%	73%	9%
The use of a waste management plan for waste concrete and cementitious material is well adapted in the South African construction industry	0%	0%	64%	36%	0%

6 CONCLUSIONS

The study focused on current practices and strategies for waste management of concrete and cement-based materials in the South African construction sector. A desktop study (critical literature review) and a qualitative approach were used in the study in which questionnaires and informal oral interviews were used to collect data in five selected construction sites in Gauteng province, South Africa. The target population was site construction practitioners.

The results showed that practitioners are generally aware of the traditional waste management hierarchy (i.e., reduce, re-use and recycle) and how it is implemented. However, they are unaware of the current waste management hierarchy in the State of Waste Report (SoWR). Nevertheless, the SoWR is a useful tool that construction practitioners should not only familiarise themselves with but also put in place systems in construction sites to implement. Given that construction sites are the primary sources of waste, accurate data on the type and quantity of waste generated, and how it is managed can be obtained therein. There is a need for the government to encourage and incentivise construction practitioners to collect and share this data.

The waste hierarchy outlined in the SoWR should be implemented in construction sites. Practitioners should, in particular, be encouraged to put in place systems that aim at waste avoidance and reduction. The policies and legislation need to encourage practitioners to quantify the different types of waste produced in construction sites. This will improve the data available in South Africa and enable an objective up-to-date analysis to be carried out. Stakeholders involved in construction need to be educated on the importance of waste management. Stakeholders that need to be educated on waste management include construction practitioners, and in particular the Environment, Health and Safety (EHS) practitioners. This can be done through workshops, awareness campaigns and by creating website groups (including social media). The government should ensure that EHS practitioners are aware of the latest policies and legislations in the SoWR.

The responses received did not indicate 'avoidance' and/or 'reduction' of concrete and cementitious waste material. If practitioners are educated on these practices, there will be a reduction in the amount of waste disposed of in landfills. According to the findings of this study, practitioners acknowledge that the management of concrete and cementitious waste is

necessary; therefore, both the private and public sectors should work together to incentivise construction practitioners to pro-actively consider recycling concrete and cementitious waste before resorting to disposal of the same in landfills. None of the construction sites sampled in this study indicated using recycled concrete; it will be beneficial to conduct studies to obtain the views of construction practitioners on the use of recycled concrete. Concrete and cementitious waste can be disposed of by sending the material to recycling plants to be crushed or recovered for reuse (e.g., aggregate or blocks) through waste management collectors. For recycling, the concrete and cementitious waste can be sent, through waste management collectors, to cement and concrete manufacturing plants and/or other similar plants that recycle the waste material.

The scope of this study did not extend to investigating the role of the construction sector in self-regulating and developing organisational cultures that promote responsible generation and management of concrete and cementitious waste within the industry. Future studies are recommended to find out how the industry, and contractors, in particular, view self-regulation and development of cultures that promote responsible generation and management of concrete and cementitious waste.

ACKNOWLEDGEMENTS

The authors express their gratitude to the construction project owners who gave access to the construction sites and all the respondents who voluntarily participated in the study. The support of The Concrete Institute, The National Research Foundation, AfriSam and the Department of Environment is greatly acknowledged.

REFERENCES

[1] Department of Environmental Affairs (DEA), ′South Africa State of Waste. A report on the state of the environment′, (First draft report, South Africa, 2018).
[2] Van Wyk, L., 'Towards Net-Zero Construction and Demolition Waste', 59, (2008) 1–7.
[3] WBCSD, ′The Cement Sustainability Initiative. Recycling concrete′, (Executive Summary, North America Office, 2009).
[4] DEA, ′Climate Change and Air Quality', in South Africa's Intended Nationally Contribution (INDC), to the United Nations Framework Convention on Climate Change: Discussion Document′, (2015) 1-13.
[5] ICCA, ′How to know If and When it's time to Commission a Life Cycle Assessment an Executive Guide′, (2010).
[6] Barnes, K., ′Builders' rubble: opportunities in processing and application′, (Cape Town, 2016).
[7] Abel, D. J., ′Perceptions on illegal dumping in the eThekwini municipality′, (University of Free State, 2009).
[8] Muigai, R., Alexander, M. G. and Moyo, P., ′Cradle-to-gate environmental impacts of the concrete industry in South Africa′, (Journal of the South African Institution of Civil Engineering, South Africa, 2013).
[9] Minchiello, V. et al., ′In-Depth Interviewing: Researching People′, (Reprint, Melbourne: Longman, Cheshire. Reprint. Longman Cheshire, 1990).
[10] Sinaga, A., ′Difference between Qualitative and Quantitative Analysis and How it should be Applied in our Research′, (2014) 1–7.
[11] Showkat, N. and Parveen, H., 'Non-Probability and Probability Sampling', (2017) pp. 1–9.
[12] Wilson, E., ′Project sizing guidelines′, (2014).

CHARACTERIZATION OF MAHOGANY BARK ASH FOR ITS USE AS SUPPLEMENTARY CEMENTITIOUS MATERIAL AND ITS BEHAVIOR IN A CEMENT PASTE AT ITS EARLIER AGE.

Inés Ngassam [(1)], Mohamed Walda [(1)], David Dodoo-Arhin [(2)], Hans-Carstern Kühne [(1)], and Wolfram Schmidt [(1)]

(1) Technology of Construction Materials Department, Bundesanstalt für Materialforschung und -prüfung (BAM), Berlin, Germany

(2) Department of Materials Science and Engineering, School of Engineering Sciences, University of Ghana, Accra, Ghana

ABSTRACT

The cement demand is constantly increasing in Africa while the production of clinker is still not the most environmentally friendly process. Besides, the agriculture is this the backbone of the economy many African countries. Based on these two observations, more studies are now focused on the use of waste from agriculture in concrete technology. In this framework, the ashes of the bark of Mahogany tree were studied to be used as a supplementary cementitious material (SCM). This article presents the characterization of ashes produced by different process and the behaviour of Mahogany bark ash in a cement paste. The results show that the calcination of Mahogany bark induces ashes with a high content of calcium oxide. The composition of the ashes is not affected by the calcination mode. Moreover, the substitution of cement with the Mahogany bark ash increases the heat of hydration of the cement paste and this also affects the rheology of the modified cement paste.

Keywords: Mahogany bark ash, SCM, characterization, calcination temperature, cement paste

1. INTRODUCTION

The demand of cement is in constant increase all over the globe but mainly in developing countries. This is due to the economic growth in these countries that lead to the development of infrastructures. This is the case for almost all the sub-Saharan African countries. Besides, it is in this region that the cost of the cement is still high compared to the rest of the continent. Moreover, it is clearly known that the production of clinker is not the most environmentally friendly technology in construction field, even though concrete is one of the most used materials on the earth. Indeed, the cement industry highly pollutes the environment since it produces 900 kg of CO2 per ton of cement [1].

In the case of African sub-Saharan regions, this observation is more blatant since this region hardly produces cement replacement like GGBFS or fly ash, and not even concrete chemical admixtures. Moreover, most of the sub-Saharan country economies are still based mainly on the agriculture. Indeed, this region is known for its extreme diverse agricultural products. Therefore, it is easy to imagine the huge amount of agricultural waste which is most of the time

not used. Though some agro-waste materials have already started to be used in the formulation of cements, such as rice husk ash and cassava peels [1], the majority remains unexploited.

The Adaptation of systemic infrastructural concrete structures to environmental challenges and risks (INFRACOST) project aims to develop adequate materials for infrastructure rehabilitations in Sub-Saharan region and to promote more waste materials by using them in concrete technology. It was in the framework that some agro-waste were selected based on their availability to their possibility to be used as supplementary cementitious materials (SCMs). This was the case for the Mahogany bark. Mahogany is ranked as one of the best-known and most valuable tropical timbers on the international market [4]. Mahoganies are distributed across Africa in Benin, Ghana, Ivory Coast, Sudan, Togo, D.R Congo and Uganda. 327,119 m3 of Mahogany wood were exported from Ghana alone from 2000 to 2015 [4], not including locally used wood. This shows that the waste from the Mahogany wood production is abundant enough for it to a good source of economical SCMs.

This article focuses on the calcination of the Mahogany bark to obtain ashes and on the impact of Mahogany ash on a cement paste. The ashes were produced at different calcination temperatures, then they were characterized to select the one with the highest potential alkali-reactivity. The ash with the highest potential alkali-reactivity was used to substitute the cement and the properties of the modified cement paste was analysed.

2. MATERIALS AND TECHNIQUES

2.1 Calcination

To determine the optimal calcination temperature, a part of the Mahogany bark powder was calcinated at the following temperatures: 600, 700, 800, 900 and 1000 °C for an hour with a pre-firing of 20 min in an open flame to burn the organic phase that induces smoke. These calcinations were done in platinum crucibles. After the selection of the optimum temperature, the remaining Mahogany bark powder was calcinated in an electric furnace for 12 hours at this temperature. These second calcinations were done in ceramic crucibles.

2.2 X-ray diffraction (XRD)

X-ray diffraction was done on all ash samples from the initial burning process and the final burning process. All samples were grinded and compacted in the holder to ensure accuracy. The device used was made by Rigaku incorporating the Ultima IV X-ray diffraction (XRD) systems. The program used for XRD results analysis was Match! 3 version 3.8.3.151 64-bit. The reference database was Crystallography Open Database (COD).

2.3 Chemical analysis and loss of ignition

The chemical analysis and the loss of ignition of the ashes were realised in accordance to the European standard EN 196 [5].

2.4 Consistency

The device used for this test was a CT3 Texture Analyzer made by Bookfield. The program used to collect the data was TexturePro CT V1.9 Build 35. The machine was set up to use a spherical probe of 12.7 mm of diameter that was lowered at a rate 1mm/s into the cement mix sample. The device measures the resistance exerted by the cement mix during the lowering of the probe. The samples were prepared in cylinder containers with the height of 32mm and a

diameter of 34mm. The samples were measured at 6 different time intervals after mixing: 0, 0.5, 1, 1.5, 2 and 3h.

2.5 Heat of hydration test

The evolution of heat during hydration was measured for the control mix and all the mixes. A Thermometric TAM Air calorimeter was used to measure all the samples. The calorimeter was calibrated for 3g samples at 20°C. The samples were prepared in accordance with EN 196-11 [5].

3 RESULTS

3.1 Influence of the temperature on the calcination yield and on the composition of the Mahogany bark ashes

The Table 1 shows that the loss of the matter increased with the calcination temperature. At 600°C, only 13% of the bark ash was collected at the end of the calcination, while it was remaining only 7% of the matter at the end of the calcination at 1000°C. however, this yield seems to become constant from 900°C. These results are similar the one obtained with the rice husk that are also calcinated to be used as SCMs [2, 3, 6].

Table 1: Lost yield after the calcination of Mahogany bark at different temperatures

Temperature	600°C	700°C	800°C	900°C	1000°C
Lost yield	86.80%	87.40%	81.60%	93.24%	93.82%

The composition of each of these ashes was found with the combination of their X-ray spectrum (Figure 2), and results of their chemical analysis (Table 2). The major observation is the presence of calcium carbonate ($CaCO_3$) between 600°C and 800°C, which is transform into calcium oxide (CaO) above 800°C (1).

$$CaCO_3 \rightarrow CaO + CO_2 \qquad \textbf{Equation (1)}$$

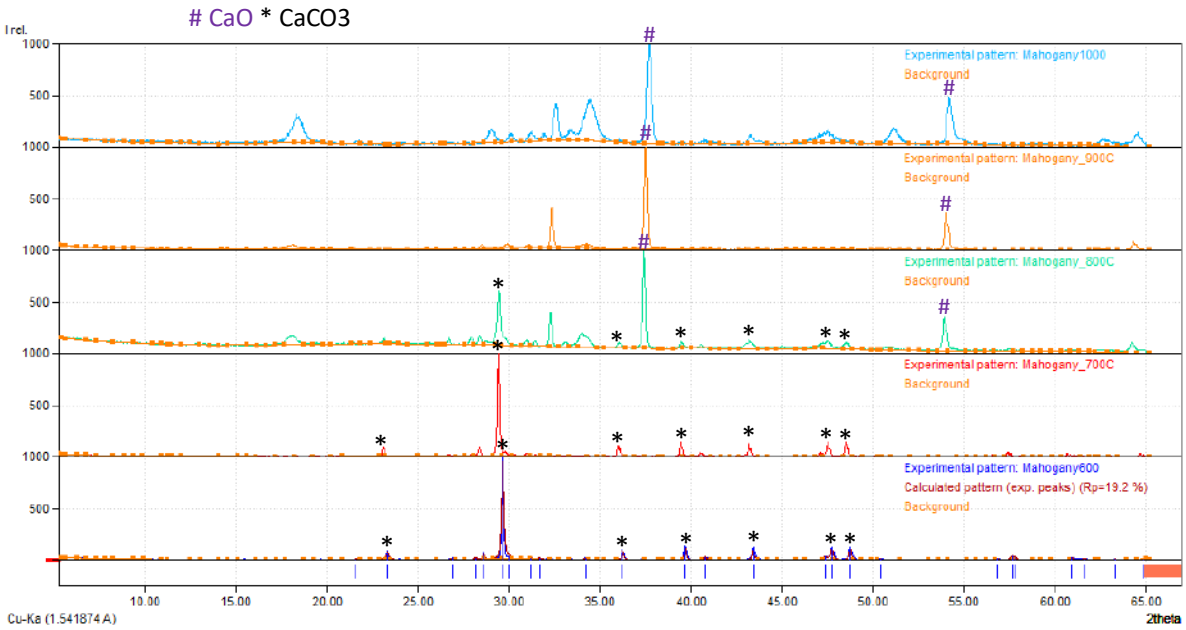

Figure 1: X-Ray spectra of Mahogany bark ashes

The other minerals found during the chemical analysis appeared on a very low amount (lower than 5%), except for the phosphor oxide that has a percentage of around 7% before 800°C and around 4% from 800°C. Therefore, the choice for the optimum calcination temperature was made based only on the amounts of silica and calcium oxide. Thus, the optimum temperature was 900°C, since the calcium oxide is at its highest percentage (58,99%) and the percentage of silica is similar the one at 800°C (13,35%).

Table 2: Composition of the Mahogany bark ashes

%		T 600	T 700	T800	T 900	T 1000
Silicium	**SiO_2**	12.02	12.51	13.22	13.05	17.69
Aluminium	**Al_2O_3**	0.08	0.10	0.14	0.45	0.18
Iron	**Fe_2O_3**	0.07	0.07	0.22	0.20	0.22
Titan	**TiO_2**	0.01	0.02	0.01	0.02	0.02
Calcium	**CaO**	2.76	4.12	32.55	58.99	2.26
Magnesium	**MgO**	0.29	0.37	1.42	3.15	0.17
Natriumoxid	**Na_2O**	0.20	0.33	0.13	0.11	0.30
Kaliumoxid	**K_2O**	7.02	7.42	4.02	5.12	4.50
Sulfat	**SO_3**	3.76	3.50	1.49	2.86	4.71
Phosphat	**P_2O_5**	1.14	1.11	0.33	1.00	1.57
Rest		72.65	70.45	46.47	15.05	68.38

3.2 Substitution of cement with Mahogany bark ash on a cement paste

3.2.1 Evolution of the hydration

The Figure 2 presents the evolution of the heat of hydration in function of the percentage of substitution of the cement by of the Mahogany bark ash. This heat increases and appears earlier with the increase of the substitution rate. This is due to the rapid and exothermic reaction of calcium oxide with water (2).

$CaO + H_2O \rightarrow Ca(OH)_2$ **Equation (2)**

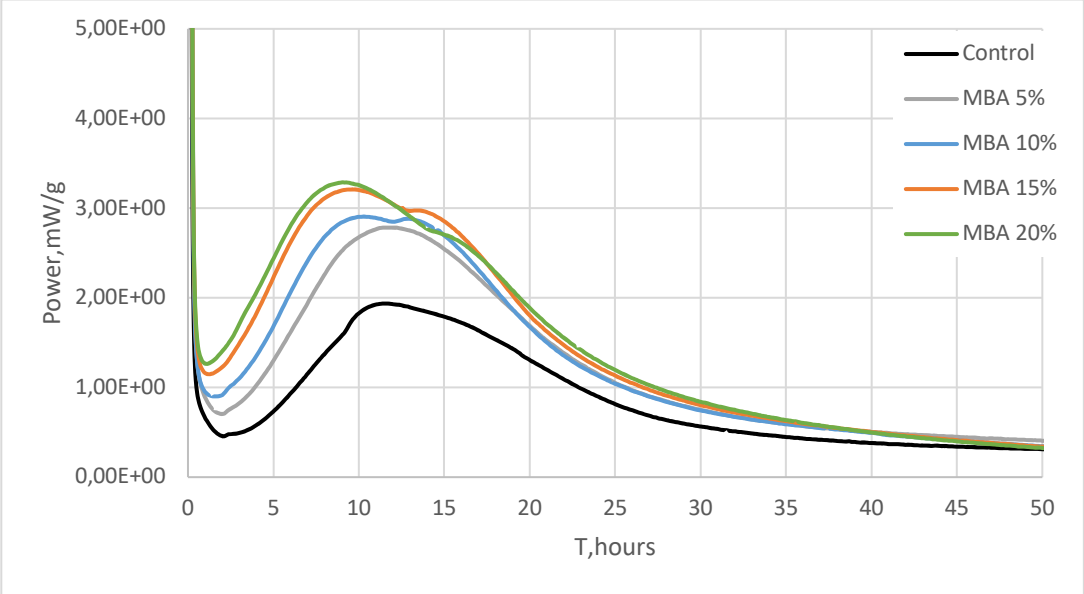

Figure 2: Heat of hydration of cement pastes modified with Mahogany bark ash

This acceleration of the hydration induced by the Mahogany bark ash may be an asset for the cement paste in the case of the elaboration cementitious materials that aim to set quickly. However, this acceleration can also play against the durability of cementitious materials by creating extra-internal heat that can lead to microcracking [7]. Furthermore, the rapid hydration of the CaO can reduce water in the system, available for the cement hydration.

3.2.2 Evolution of the hydration in presence of superplasticizer

The Figure 3 shows that the use of a superplasticizer in a cement paste modified with the Mahoganybark ash did not efficiently affect the hydration of the cement paste.

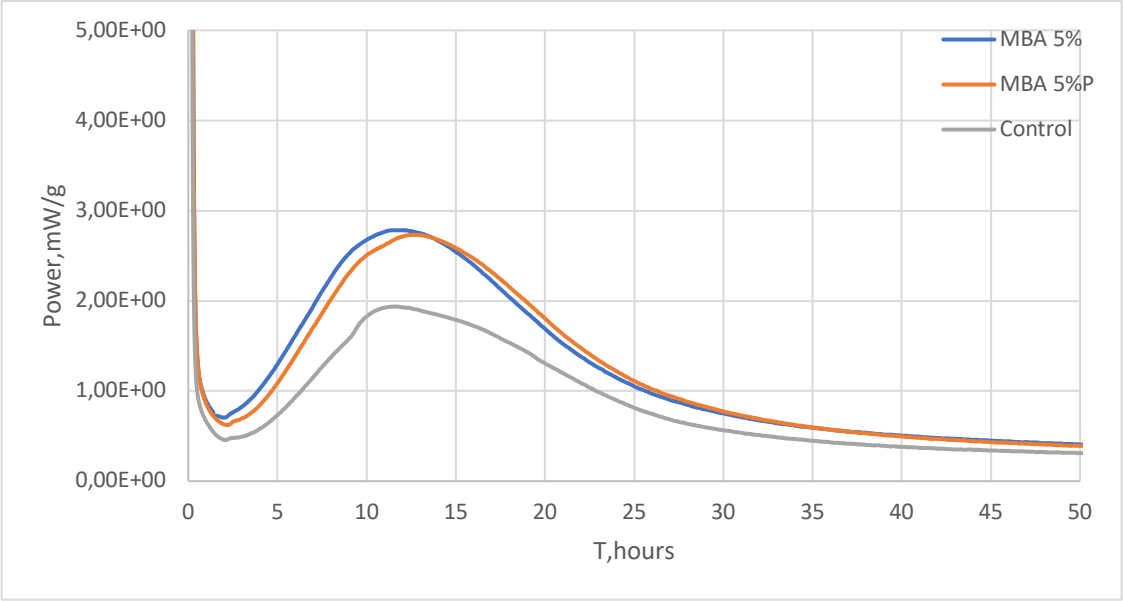

Figure 3: Evolution of the heat of hydration of cement pastes modified with Mahogany bark ash with a superplasticizer

3.2.3 Effect on the paste consistency

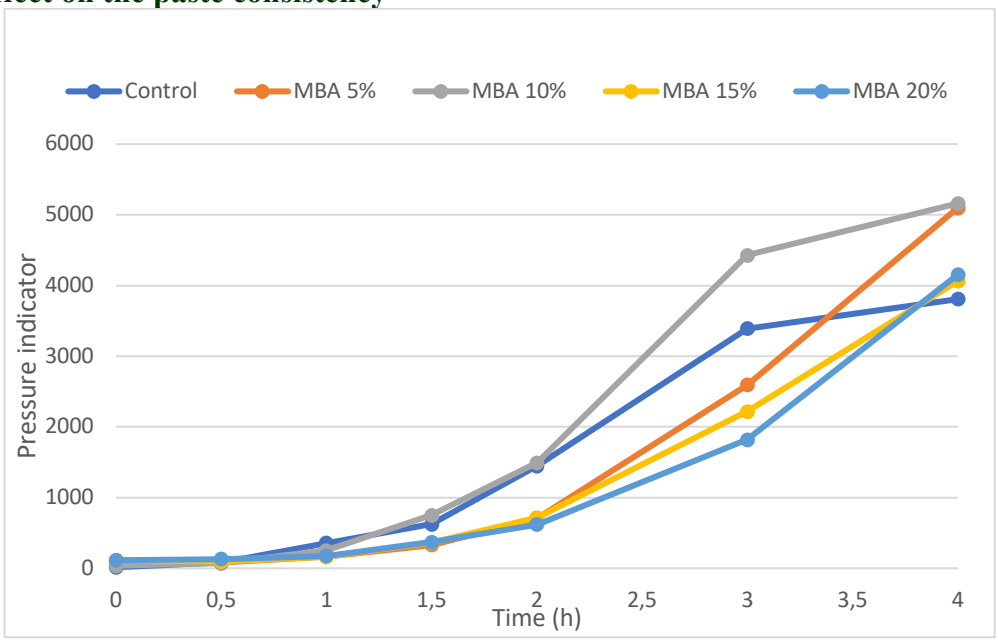

Figure 4: Consistency of the cement pastes modified with Mahogany bark ash

The results of the evolution of the consistency were presented on the Figure 4. Globally, the pressure applied on the samples started to increase after an hour, and the differences of pressure clearly appeared after 1,5h. Between 1h and 3h, the pressures of the cement paste without ash (control) and the one with 10% (MBA 10%) of ash were the highest, meaning they were the paste with the fastest setting. On the same period, the pressure of the three other modified cement pastes (MBA 5%, MBA 15%, and MBA 20%) were decreasing with the increase of the

amount of ash. After 4h, the unmodified cement paste and the one with 15 and 20% of Mahogany bark ash were presenting the lowest pressures, while the one with 5 and 10% one had the highest pressures.

3.2.4 Effect on the paste consistency in presence of superplasticizer

The Figure 5 shows that the cement paste that contains both the ash and the superplasticizer (MBA 5%P) had the lowest pressure between 0,5h and 3h, while the unmodified cement paste had the highest pressure on that same interval. But at 4h, the modified pastes had similar pressures and higher than for the control one. According to these results, the superplasticizer tends to slow the settling of the modified cement paste.

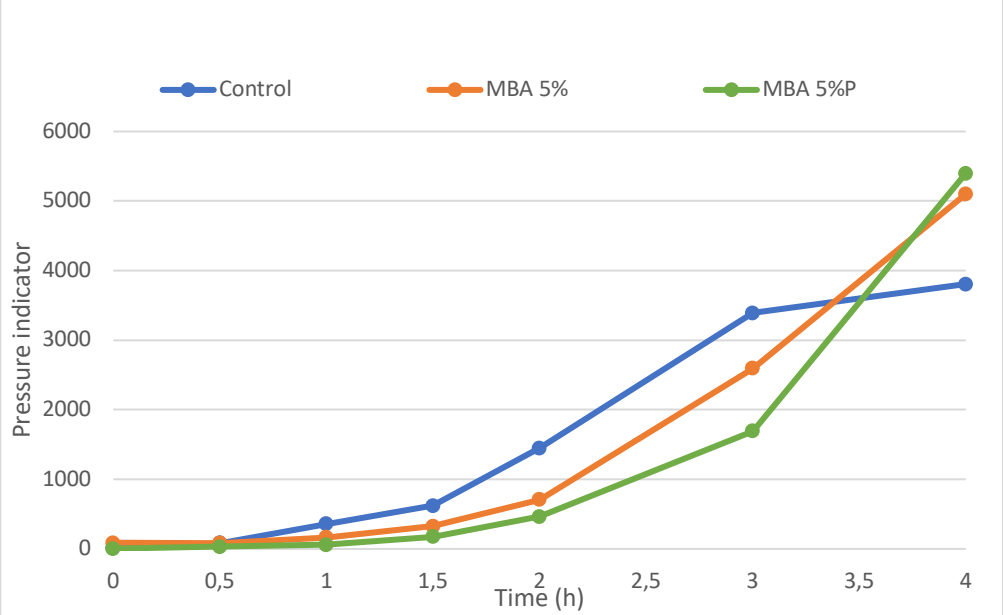

Figure 5: Consistency of a cement paste modified with Mahogany bark ash with a superplasticizer

4 DISCUSSION

Regarding the composition of the Mahogany bark ashes in function of the calcination temperature, the XRD spectra showed that there were some pics that were not able to be identified. This observation is aligned with the chemical analysis results. Indeed, for almost all the calcination more than the half of the samples could not be identified by this method. These results can be explained by the fact that the measurement methods used for the characterization of this bio-ash are the same commonly used for classic cementitious materials. Indeed, there was a limitation in the type of elements that can be analysed with the chemical analysis, for instance the carbon that could not be analysed. Therefore, these results could be questionable, and they should be confirmed by other methods of characterisation, more appropriate to bio-based materials.

In the same line, the outcomes on the consistency can also be doubtful. Indeed, it was showed that the almost all the cement pastes modified with the Mahogany bark ash slowly settled, compared to the unmodified cement paste. However, the Mahogany bark ash contained in

majority the calcium oxide, according to the results of their characterization. This was also illustrated with the increase of the temperature and the heat of the hydration observed with the calorimetry measurements because of the hydration of the calcium oxide. Therefore, it was expected that the modified pastes settle faster than the unmodified paste.

Finally, there was no difference in the results when a superplasticizer was added to the modified cement paste.

5 CONCLUSION

This article deals with the influence of the temperature on the composition of the Mahogany bark ashes and their potential to be used as a SCM. The characterisation of these ashes showed that the classic methods and techniques used for the characterisation of cementitious materials might not be the most adequate for this bio-waste materials. Indeed, there was a huge part of the samples which could not be identified. Moreover, the behaviour of cement pastes, in which a percentage of cement was substituted with the Mahogany bark ash, tended to delay the settling. This result was not expected since the ash contained a high amount of calcium oxide which hardens rapidly with water. To sum up, it will be interesting to look for adequate methods and techniques for the bio-waste materials.

REFERENCES

[1] U.S. Geological Survey, Mineral Commodity Summaries, February 2019

[2] Fapohunda Christopher, Akinbile Bolatitob, Shittu Ahmed, Structure and properties of mortar and concrete with rice husk ash partial replacement of ordinary Portland cement – A review, International Journal of Sustainable Built Environment, 2017

[3] T. Ofuyatan, A. Ede, S. O. Oyebisi, O. Olofinnade, 'Assessment of strength properties of Cassava peel ash-concrete', January 2018

[4] T. L Stephen., E. Appiah-Kubi, C. Essien, E. Opuni-Frimpong, J. Korang, S. Pentsil, F. W. Owusu, Wood and Lumber Quality of Plantation Grown Khaya ivorensis, ITTO, 2015

[5] EN 196 - Methods of testing cement, 2016

[6] R. P. Jaya, Z. A. Ahmad, Z. M. Amin, 'Properties of Mortar Containing Rice Husk Ash at Different Temperature and exposed to aggressive Environment', Advanced Materials Research, 620 , 2013, 87-93

[7] F. O. Slate, K. C. Hover, 'Microcracking in concrete', in 'Fracture mechanics of concrete: Material characterization and testing', 3, 1984

ENGINEERING PERFORMANCE OF CONCRETE WITH PAPER MILL WASTE ASH – TOWARDS SUSTAINABLE RIGID PAVEMENT CONSTRUCTION

Deveshan L. Pillay [(1)], Oladimeji B. Olalusi [(1)] and Mohamed M.H. Mostafa [(1)]
(1) Department of Civil Engineering, University of KwaZulu-Natal

ABSTRACT

The drastic surge in urbanisation and the constantly changing human lifestyle are the main contributory factors to the increased demand for concrete construction-related activities. Concrete is widely utilised for various structural applications, including rigid pavement construction, due to its superior mechanical and durability performance. However, the cement production process releases harmful greenhouse gases, leads to the depletion of calcareous materials and consumes significant quantities of energy. Therefore, there is an increased need for sustainable pavement designs that maintain a high level of service. In the case of rigid pavement applications, this can be achieved by incorporating alternate binder systems, such as paper mill ash (PMA). This experimental study aims to investigate the engineering performance of concrete manufactured with PMA. This was achieved by assessing the workability, mechanical and durability properties of concrete specimens containing 0%, 5%, 10%, 15% and 20% of PMA as a supplementary cementitious material (w/b = 0.64). Based on the favourable flexural and tensile strength results that were obtained, coupled with the negligible CO_{2e} emission value, it can be concluded that PMA is a viable alternate binder system for enhancing the serviceability and sustainability states of rigid pavements.

Keywords: supplementary cementitious materials; rigid pavements; sustainability; paper mill ash

1. INTRODUCTION

Concrete pavements, also known as rigid pavements, are mainly used in roadways and various alternate transportation applications such as parking lots, airport aprons, toll stations, ports and military facilities [1, 2]. It has also been documented that concrete pavements achieve an improved service life and reduced maintenance costs when suitable design guidelines and precise construction processes are implemented [3, 4]. However, large amounts of Portland Cement (PC) and aggregates are used when constructing rigid pavements [5]. Furthermore, the cement production process has an increased carbon footprint and leads to the rapid depletion of calcareous materials [6, 7]. Therefore, the sustainability characteristics of rigid pavements can be enhanced by adopting a pavement design that integrates sustainable construction materials and achieves a consistent service level. Furthermore, there is a higher demand for alternate binder systems to address concerns surrounding the CO_2 emissions resulting from the cement manufacturing industry [8-12]. The amount of cement produced for concrete construction purposes can be reduced by incorporating supplementary cementitious materials like paper mill ash (PMA) [5]. This experimental study aims to investigate the engineering properties (fresh state, mechanical strength, durability and frictional resistance), sustainability (CO_{2e}) performance and economic characteristics (material and construction costs) of concrete containing PMA. The overall goal is towards sustainable rigid pavement construction.

2. MATERIALS AND METHODOLOGY

2.1. Methodology: Assessment of the feasibility of PMA as an alternate binder system for rigid pavements

The experimental research approach includes a critical analysis of paper mill ash-based concrete's engineering performance, used to assess its viability for rigid pavement applications. The research approach consists of an experimental investigation of the fresh state, mechanical (compressive, flexural and tensile splitting strengths), durability and frictional resistance properties of concrete incorporating paper mill ash as supplementary cementitious material. A construction cost analysis and an assessment of the equivalent carbon dioxide (CO_{2e}) levels were also used to provide a definitive answer to the feasibility of concrete containing paper mill ash for real-world applications.

2.2. Methodology: Assessment of the economic feasibility of PMA as an alternate binder system for rigid pavements

The economic feasibility of PMA as an alternate binder material for rigid pavements was assessed by performing a construction cost analysis for a typical rigid pavement scenario in South Africa. This cost analysis was based on the concrete platform or bullpen at the OneLogix Vehicle Distribution Facility situated in the Umlaas Road area (north-west of Durban). The bullpen area at the OneLogix Umlaas Road Vehicle Distribution Facility comprises of a 170 mm thick unreinforced concrete surface bed with an average slope of 1:100. The surface bed area (including the entrance area) is estimated to be 13 500 m^2. The main traffic movement within this area is predominantly focused on a 9 m wide access loop used by car carriers. The 9 m wide section, which has an approximate length of 500 m, shows signs of premature failure.

2.3. Materials

Portland-Slag cement and PMA were the binding agents used for the experimental investigations in this research study. The cement (CEM II/B-S 42.5N Plus) satisfied the strength and quality requirements that have been outlined in SANS 50197-1. The PMA used in this research study was obtained from the Mondi Merebank Mill in Durban, South Africa. Based on the chemical composition results documented in Table 1, it can be concluded that the waste ash from Mondi Merebank is pozzolanic, as the summation of the percentage of the three main oxide constituents (SiO_2, Al_2O_3 and Fe_2O_3) is greater than 50% [13]. In accordance with SANS 5844, the relative density of the PMA was determined to be 2.25, which is significantly lower than the relative density of the cement (3.1).

Table 1: Chemical composition of paper mill waste ash sample from Mondi Merebank [14]

Oxide Compound	Percentage (by weight)
CaO	32.58
SiO_2	35.83
Al_2O_3	22.41
Fe_2O_3	1.11
MgO	1.55
SO_2	4.93
K_2O	0.43
TiO_2	1.16

The fine aggregate selected for this research study was Umgeni River Sand (in accordance with SANS 1083), which had a fineness modulus of 2.39. Coedmore Quartz Stone (nominal size = 19 mm) was used as the coarse aggregate in this study. The quartzite stone was pre-graded and conformed with the requirements in SANS 1083. Potable water (in compliance with the specifications outlined in SANS 51008) was added to the dry ingredients during the experimental study's mixing and curing phases.

2.4. Concrete mix design

The experimental investigations were performed by using concrete mix designs containing 0%, 5%, 10%, 15% and 20% of PMA as a partial replacement (by volume) for Portland-Slag cement. In accordance with Everitt [15], the Cement & Concrete Institute (C&CI) concrete mix design method was followed, and the proportions of each mix have been summarised in Table 2.

Table 2: Proportions of the concrete mixes used for this research study

Designation	w/b	Water (l)	Sand (kg)	Stone (kg)	Binder	
					PC (kg)	PMA (kg)
0% PMA	0.64	40.6	137.7	212.7	63.4	0
5% PMA	0.64	40.6	137.7	212.7	60.3	2.3
10% PMA	0.64	40.6	137.7	212.7	57.1	4.6
15% PMA	0.64	29.3	99.3	153.4	38.9	5
20% PMA	0.64	29.3	99.3	153.4	36.6	6.6

2.5. Casting and curing of laboratory samples

The concrete samples used in the experimental study were cast and cured in accordance with SANS 5861-3. The dry materials, i.e., sand, stone, cement and PMA, were first mixed in a revolving drum tilting mixer for one minute. Water was then added, and the mixing process continued until the concrete achieved an even consistency, texture and colour. The cube (100 x 100 x 100 mm & 150 x 150 x 150 mm), beam (100 x 100 x 500 mm), cylinder (Ø150 x 300 mm) and slab (600 x 300 x 50 mm) moulds were then filled. A vibrating table was used to compact the concrete, while a trowel was used to finish the concrete surface. In order to determine the skid resistance properties of PMA concrete, a broom was used to add surface texturing (longitudinal and transverse) to the two slabs. The concrete samples were demoulded twenty-four hours later and cured under normal conditions until the 7-day strength tests. After the 7-day period had elapsed, the specimens were removed from the curing bath and air cured. Alternatively, the two concrete slabs were air cured after they were demoulded.

2.6. Testing procedures

In accordance with SANS 5862-1, the slump test was used to quantify the fresh concrete's workability properties. As outlined in SANS 5860, 5861-2, 5861-3 and 5863, the compressive strength was determined by crushing three concrete cube specimens with a hydraulic press equipped with two platens. In accordance with SANS 5864, the flexural strength performance was measured by crushing concrete beam specimens between two plates with two rollers that apply vertical point loads along the beam's entire length. As described in SANS 6253, the laboratory test used to quantify the tensile strength properties consists of subjecting a concrete cylindrical specimen to compressive forces acting along diametrically opposed lines [16].

The durability of concrete containing PMA as a partial cement replacement was assessed with concrete durability index tests (oxygen permeability, water sorptivity and chloride conductivity). In accordance with TMH 6, the skid resistance and sand patch tests were used to assess the resistance to skidding of concrete slabs containing PMA. A desktop study was the selected method for analysing the equivalent carbon dioxide (CO_{2e}) of a hypothetical 1 m^3 concrete mix. The average emission values documented in Table 3 were used in this study. A material cost analysis and construction cost analysis were used to evaluate the economic feasibility of PMA concrete for use in industry. Both cost assessments utilized market rates (Table 4) provided by local suppliers and the main contractor.

Table 3: Average CO_{2e} emission values for various concrete constituents [11, 16]

Material Type	Notation	Avg. emission values (kg CO_{2e}/ton)
Portland-Slag Cement	CEM II B-S	730
Aggregates	–	5
Water	–	1
Paper Mill Ash	PMA	0

Table 4: Undelivered rates for the various constituent materials used to produce concrete containing PMA

Material	Rate	Supplier/Source
CEM II B-S	R 92 per 50 kg bag	Just Build
Umgeni River Sand	R 550 per m^3	Umlaas Road Cartage
Coedmore Quartz Stone (19mm)	R 650 per m^3	Umlaas Road Cartage
Water	R 36.52 per kL	eThekwini Municipality
PMA	R 0 per kg	Mondi Merebank

3. RESULTS AND DISCUSSION

3.1. Workability

From the results documented in Table 5, it was noted that the addition of PMA as a supplementary cementitious material resulted in a reduced slump and workability performance. This is in agreement with the results obtained in past year research studies. The reduced workability of the fresh concrete can be attributed to the high-water demand needed by the PMA (which is finer than PC) for the formation of the hydration products [17]. The PMA

produced by Mondi Merebank contains high percentages of CaO, SiO_2 and Al_2O_3. In combination with the presence of metakaolin in PMA, the high oxide content will accelerate the hydration of C_3S, thus decreasing the setting time and reducing the workability performance of the fresh concrete [18].

In accordance with the target slump ranges specified in SAPEM [19], it was determined that all PMA concrete mixes were suitable for fixed form paving operations, while the 20% PMA replacement level was the optimum concrete mix for slipform paving. It is also worth mentioning that concrete used for rigid pavement construction not only requires sufficient workability but should also retain sufficient rigidity to resist flow on roads with steep cross falls and gradients [20].

Table 5: Results obtained from the slump test, equivalent carbon dioxide (CO_{2e}) and material cost analysis

PMA Content (%)	Slump (mm)	CO_{2e} (kg CO_{2e})	Cost (R/m^3)
0% PMA	84	284.35	R 1222.27
5% PMA	70	270.7	R 1222.27
10% PMA	65	256.98	R 1130.27
15% PMA	60	243.32	R 1130.27
20% PMA	35	229.6	R 1038.27

3.2. Mechanical strength

From the results achieved in Table 6, it was determined that the addition of PMA as a supplementary cementitious material improved the concrete's compressive, flexural and tensile splitting strength compared with the results obtained for conventional concrete. This can be attributed to the higher concentrations of CaO, SiO_2 and Al_2O_3 found in the PMA sample used in this study. The increased oxide percentages coupled with the presence of metakaolin will have a direct correlation with the PC-PMA hydration process, which results in the formation of additional C-S-H gel and improved strength properties [18]. The 5% PMA and 10% PMA concrete mixes achieved the highest 7- and 28-day compressive strength respectively, with reduced strength readings noted for subsequent PMA replacement levels. Likewise, the 10% PMA concrete samples achieving the highest 7- and 28-day flexural and tensile splitting strength readings.

The reduced strength readings noted for the PMA replacement levels after the optimum content can be associated with the higher PMA concentrations in these samples, which results in reduced pozzolanic reactivity and strength development [21]. The experimental results show that all concrete mixes containing PMA have satisfied the minimum 28-day characteristic compressive strength of concrete pavements (30 MPa) specified in SAPEM [20]. Likewise, all PMA concrete mixes have achieved the 28-day flexural strength target of 4 MPa for rigid pavements in South Africa [20].

Table 6: Results obtained from the compressive, flexural and tensile splitting strength tests

PMA Content (%)	Compressive Strength (MPa)		Flexural Strength (MPa)		Tensile Splitting Strength (MPa)	
	7 day	28 day	7 day	28 day	7 day	28 day
0% PMA	18.17	25.42	3.05	3.96	1.53	1.98
5% PMA	23.79	31.81	3.94	4.86	1.61	2.26
10% PMA	22.53	32.17	4.48	5.67	1.89	2.68
15% PMA	21.13	31.29	4.06	4.91	1.79	2.56
20% PMA	20.12	30.84	3.91	4.24	1.76	2.44

3.3. Durability

From the durability index test results documented in Table 7, it was determined that there was no discernible trend between the oxygen permeability value and PMA content. The test results also displayed that the 20% PMA concrete samples achieved the highest oxygen permeability value and was classified accordingly. The water sorptivity results shows that all the concrete mixes exhibited excellent durability performance; however, there was no distinct relationship evident between the water sorptivity index value and the PMA replacement level. Likewise, the chloride conductivity results also indicated that all the concrete specimens achieved excellent durability performance. On closer inspection, there was no distinct trend between the chloride conductivity value and the PMA content. This contradicts with the initial observations made by Pillay et al. [5], where the durability performance was expected to improve as the PMA content increased.

As described by Pillay et al. [5], the strengthening of the aggregate paste bond characteristics resulting from the incorporation of PMA will decrease the occurrence of localised impact stresses and cavitation of concrete pavements. Furthermore, the densified concrete microstructure of PMA concrete will also be an ideal design characteristic for combatting chloride attack and salt crystallisation in concrete pavements located in coastal/marine environments. However, additional tests are needed to clarify the inconsistent experimental results noted.

Table 7: Results obtained from the durability index tests

PMA Content (%)	Oxygen Permeability		Water Sorptivity		Chloride Conductivity	
	OPI (log value)	Durability Class	WS ($mmh^{-0.5}$)	Durability Class	CC (mS/cm)	Durability Class
0% PMA	9.84	Good	4.66	Excellent	0.23	Excellent
5% PMA	9.48	Poor	4.09	Excellent	0.20	Excellent
10% PMA	9.52	Good	3.95	Excellent	0.25	Excellent
15% PMA	9.20	Poor	4.20	Excellent	0.24	Excellent
20% PMA	10.09	Excellent	4.29	Excellent	0.25	Excellent

3.4. Frictional resistance

The results documented in Table 8 noted that there was no discernible trend between the average skid resistance value (SRV), average texture depth (TD) and PMA replacement level. Aggregate texture, road gradation, pavement finishing technique, pavement age, and wear significantly influence rigid pavements' overall surface texture characteristics [22]. Therefore,

the abovementioned trend was expected as PMA and CEM II/B-S have a fine material texture, while the type and quantity of aggregate material remained constant across all mix designs. Hence, it was concluded that incorporating PMA as an alternate binder material in rigid pavements has a minimal effect on the skid resistance performance.

Table 8: Results obtained from the skid resistance and sand patch tests

PMA Content (%)	Surface Texturing	Average SRV	Average TD
0% PMA	Broom (longitudinal)	74	1.03
	Broom (transverse)	77	1.05
5% PMA	Broom (longitudinal)	73.2	1.02
	Broom (transverse)	77.4	1.06
10% PMA	Broom (longitudinal)	74.8	1.04
	Broom (transverse)	77.8	1.07
15% PMA	Broom (longitudinal)	73.8	1.02
	Broom (transverse)	76.6	1.03
20% PMA	Broom (longitudinal)	73.6	1.02
	Broom (transverse)	77.2	1.06

3.5. Sustainability – Equivalent Carbon Dioxide (CO_{2e})

It was determined that the CO_{2e} of the concrete mixes decreased as the PMA content increased (Table 5). This trend was anticipated as the average CO_{2e} emission value for PMA was zero. It is also worth noting that Mondi Merebank produces PMA by incinerating paper mill sludge, classified as a waste product, for energy recovery purposes. Improper disposal of the PMA can have a detrimental environmental impact. Therefore, utilising PMA as an alternate binder material for rigid pavement applications will reduce the PMA disposal process's environmental impacts and simultaneously decrease the carbon footprint related to the cement manufacturing industry.

3.6. Material cost analysis

From the results shown in Table 5, it was noted that the cost per m^3 decreased as the PMA content increased. This relationship was expected as the PMA was provided free of charge by Mondi Merebank. It is also worth mentioning that the 0% and 5% PMA concrete mixes had the same material cost, which is due to the fact that the cement and PMA were the only quantities that were changing per mix design. The cement quantities were measured per 50 kg bag; therefore the variation in the amount of cement used will not be detected in the material cost analysis. The same trend was also documented for the 10% and 15% PMA concrete mixes.

3.7. Construction cost analysis

The results documented in Table 9 indicate that the total cost of the construction work decreased as the PMA replacement level increased. The PMA had no material cost as it was obtained for free from Mondi Merebank. The transportation cost was the only cost variable associated with the PMA; however, it was also noted that in general the material costs were considerably higher than the transports costs. Therefore, the increased transport costs for each PMA replacement level will have a minimal effect in counteracting the corresponding decrease in material cost, which led to the documented reduced overall cost. From the favourable

construction cost analysis results that were achieved in this study, it was concluded that concrete incorporating PMA as supplementary cementitious material is economically feasible construction material for use in rigid pavement applications.

Table 9: Results obtained from the construction cost analysis

PMA Content (%)	Material Costs	Transport Costs	Plant Costs	Labour Costs	TOTAL
0% PMA	R456 865.38	R99 738.90	R177 934.00	R276 006.00	**R1 010 544.28**
5% PMA	R451 345.38	R101 238.90	R177 934.00	R276 006.00	**R1 006 524.28**
10% PMA	R445 825.38	R102 382.20	R177 934.00	R276 006.00	**R1 002 147.58**
15% PMA	R440 305.38	R102 382.20	R177 934.00	R276 006.00	**R996 627.58**
20% PMA	R434 785.38	R103 525.50	R177 934.00	R276 006.00	**R992 250.88**

4. CONCLUSION

This research study's aims, and objectives primarily focused on identifying the benefits of utilising PMA concrete as a construction material for rigid pavements. The reduced workability performance and the improved mechanical strength performance proved that concrete containing PMA successfully meets the minimum strength requirements for rigid pavements in South Africa. The favourable strength and durability performance of PMA concrete also highlights the fact that it should not be restricted to concrete pavements only and can also be implemented for use in a wide variety of structural applications within the civil engineering industry. Furthermore, the positive findings that were documented from the equivalent carbon dioxide assessment, material cost analysis and construction cost analysis also indicate the benefits of utilising PMA based concrete as a construction material for concrete pavements. Therefore, it can be concluded that the research work undertaken in this study proves that concrete incorporating PMA as an alternate binder material is a feasible option for improving the sustainability and serviceability states of rigid pavements in South Africa.

ACKNOWLEDGEMENTS

The authors would like to express their sincere thanks to Mondi Merebank for providing the PMA that was used in this study and Contest – Concrete Technology Services for their assistance with conducting the durability index tests.

REFERENCES

[1] Plati, C. (2019). Sustainability factors in pavement materials, design, and preservation strategies: A literature review. *Construction and Building Materials*, 211, pp.539-555.

[2] Poongodi, K., Murthi, P., Awoyera, P. O., Gobinath, R., & Olalusi, O. B. (2020). Durability properties of self-compacting concrete made with recycled aggregate. *Silicon*, 1-9.

[3] Pandey, A., & Kumar, B. (2020). A comprehensive investigation on application of microsilica and rice straw ash in rigid pavement. *Construction and Building Materials*, 252, 119053.

[4] South African Pavement Engineering Manual (SAPEM). (2013). Chapter 2: Pavement Composition and Behaviour. South African National Roads Agency Ltd (SANRAL).

[5] Pillay, D.L., Olalusi, O.B. and Mostafa, M.M. (2020). A review of the engineering properties of concrete with paper mill waste ash—towards sustainable rigid pavement construction. *Silicon*, pp.1-17 . https://doi.org/10.1007/s12633-020-00664-2

[6] Murthi P., Poongodi K., Awoyera P.O., Gobinath R., Raja K.T., Olalusi O.B. (2020) Fresh properties of self-compacting concrete incorporating electric arc furnace oxidising slag (EAFOS) as coarse aggregate. SN Applied Sciences 2(4):1–8.
[7] Thangapandi K., Anuradha R., Awoyera P.O., Gobinath R., Archana N., Berlin M., Oladimeji O.B. (2020) Durability phenomenon in manufactured sand concrete: effects of zinc oxide and Alcofine on behaviour. Silicon.
[8] Schneider, M. (2019). The cement industry on the way to a low-carbon future. *Cement and Concrete Research*, 124, 105792.
[9] Doudart de la Grée, G. C. H., Yu, Q. L., & Brouwers, H. J. H. (2018). Upgrading and evaluation of waste paper sludge ash in eco-lightweight cement composites. *Journal of Materials in Civil Engineering*, 30(3), 04018021.
[10] Singh, N. B., & Middendorf, B. (2020). Geopolymers as an alternative to Portland cement: An overview. *Construction and Building Materials*, 237, 117455.
[11] Pandey, A., & Kumar, B. (2020). A comprehensive investigation on application of microsilica and rice straw ash in rigid pavement. *Construction and Building Materials*, 252, 119053.
[12] Kumar, K. R., Shyamala, G., Awoyera, P. O., Vedhasakthi, K., & Olalusi, O. B. (2020). Cleaner production of self-compacting concrete with selected industrial rejects-an overview. *Silicon*, 1-12.
[13] ASTM. (2008). Standard specification for coal fly ash and raw or calcined natural pozzolan for use in concrete. *C618*, West Conshohocken, PA.
[14] Byiringiro, A. (2014). *Effect of Paper Mill Ash on Properties of Expansive Soils*. Master of Engineering. Stellenbosch University.
[15] Everitt, P.R. (2016). Practical Number 3: Concrete Mix Design. *ENCV2MTH1, Civil Engineering Materials*. Civil Engineering Programme, School of Civil Engineering, Surveying and Construction, University of KwaZulu-Natal.
[16] Owens, G. (2013). *Fundamentals of concrete*. 3rd ed. Midrand, South Africa: The Concrete Institute.
[17] Mavroulidou, M., Boulouki, G. and Unsworth, C. (2013). Incorporating waste paper sludge ash as partial cement replacement in concrete. In: *13th International Conference of Environmental Science and Technology*.
[18] Vegas, I., Urreta, J., Frías, M., Rodríguez, O., Ferreiro, S., Nebreda, B., García, R. and Vigil, R. (2009). Engineering Properties of Cement Mortars Containing Thermally Activated Paper Sludge. In: *7th International Conference on Sustainable Management of Waste and Recycled Materials in Construction*, pp.225-232.
[19] South African Pavement Engineering Manual (SAPEM). (2013). Chapter 4: Standards. South African National Roads Agency Ltd (SANRAL).
[20] South African Pavement Engineering Manual (SAPEM). (2013). Chapter 9: Materials Utilisation and Design. South African National Roads Agency Ltd (SANRAL).
[21] Sharipudin, S. and Ridzuan, A.R.M. (2012). Influence of Waste Paper Sludge Ash (WPSA) and Fine Recycled Concrete Aggregate (FRCA) on the Compressive Strength Characteristic of Foamed Concrete. *Advanced Materials Research*, 626, pp.376-380.
[22] Federal Highway Administration. (2019). *Concrete Pavement Texturing.*

CHARACTERIZATION OF TERNARY BLENDED SELF COMPACTING CONCRETE EXPOSED TO SULPHATE ENVIRONMENT

Deep Tripathi [(1)], Rakesh Kumar [(1)] and Pradeep K. Mehta [(1)]

(1) Department of Civil Engineering, Motilal Nehru National Institute of Technology Allahabad, Prayagraj, Uttar Pradesh, India

ABSTRACT

A ternary blend comprising of 43 grade Ordinary Portland Cement (OPC), Fly Ash (FA) and Metakaolin (MK) was prepared for use in Self Compacting Concrete (SCC), and its optimum composition was determined, with respect to the compressive strength. Different SCC mixes were tested for workability parameters, as recommended by EFNARC and Bureau of Indian Standards (BIS) viz., Slump flow, T-50 time flow, V-funnel, L-box, U-box and J-ring. The concrete cubes of size 100mm were cast for all the mixes, and cured in Tap-water for determination of compressive strength and micro-structural changes at different ages. The compressive strength and micro-structural changes of ternary blended SCC (TBSCC) were compared with a referral SCC mix (RSCC) i.e., SCC containing only OPC. The optimum TBSCC and RSCC were exposed to Ammonium Sulphate solution (4% and 16%) for different periods, after 28 days of water curing, and its compressive strength and micro-level changes were compared. The micro-structural changes due to FA and MK inclusion were observed by X-Ray Diffraction (XRD), Scanning Electron Microscope (SEM) and Energy Dispersive Spectroscopy (EDS).

Keywords: self-compacting concrete, ordinary portland cement, ternary blend

1. INTRODUCTION

Durability is the main concern for concrete because it is highly susceptible to aggressive environments viz., acid and sulphate attacks. It is a serious issue due to the speed of damage of concrete structures worldwide. Ettringite is a very expansive compound which creates an internal pressure on the surrounding concrete. This leads to the formation of cracks, resulting in the loss of its mechanical properties. The sulphate ion responds to the hydrating cement, when the concrete specimens are exposed to its solutions, and generates expansive products that cause spalling and cracking [1, 2]. It is reported that a partial replacement of fly ash by metakaolin improves the mechanical properties, optimizes the microstructure, and reduces the level of damage due to sulphate attack [3].

The behaviour of every material is related to its microstructure. The micro-structural analysis is the best way to find the reason(s) behind the performance of concrete because it controls the properties and behaviour of concrete. The mineral data obtained from micro-structural study helps in interpreting the unique behaviour of concrete, and in finding the presence of other minor compound in the hardened concrete. MK mixed concrete showed improved micro-structural properties [4]. The SEM and EDS analyses of the specimens

provide the details of the additional compounds formed. The bond between particles/constituents is improved with the curing time because of the formation of additional C-S-H gel due to pozzolanic activity [5]. Nehdi et al. reported that SCCs incorporating binary, ternary and quaternary mineral admixtures showed improved resistance to Ammonium Sulphate exposure; the formation of ettringite was identified by SEM and EDS analysis [6]. The XRD and SEM analysis confirms the formation of hydrated phases such as gismondine [$CaAl_2 Si_2O_8$ .4(H_2O)] and C–S–H in SCC for higher FA and MK contents. It is reported that formation of gismondine, due to dissolution of Si and Al present in MK and FA, may have contributed to the increased compressive strength of SCC because of addition of hydrated lime [7]. Paul Brown et al. reported that the micro-structural evidence supports the hypothesis that ettringite formation precedes that of thaumasite. Associated cracking due to expansion provides a means for ingress of carbon dioxide which supports thaumasite formation [8]. The incorporation of mineral admixtures stabilizes the concrete and makes it more durable due to improved pore structure [9, 10].

2. EXPERIMENTAL INVESTIGATION

2.1 Materials and their properties

For this research, a 43 grade OPC (Brand-MP Birla), conforming to IS: 8112-1989, was used. Rounded Natural Sand (NS) falling in Zone II of IS: 383-1970 was used. The other important properties of the NS are: Specific gravity- 2.65; Fineness modulus- 2.7; Bulk density- 1680 kg/m^3. The properties of 10 and 20 mm coarse aggregates are as follows: Specific gravity- 2.66 and 2.7; Water absorption- 1.0 and 0.9%; Fineness modulus- 6.7 and 7.2; Bulk density- 1590 and 1560 kg/m^3. The above values satisfy the requirements of IS: 383-1970. The FA (Class-F; Colour- grey; Specific gravity- 2.13), satisfying the requirements of IS: 3812-2000, was purchased from NTPC-Unchahar (UP). MK (Off-white colour) was procured from Kaolin Techniques Pvt. Ltd, Bhuj, Kutch, Gujarat. The specific gravity and bulk density of MK as reported by manufacturer are 2.5 and 0.9 gm/mm^2, respectively. A Naphthalene Sulphonate Based High Range Water Reducer (HRWR)/ Superplasticizer (Master Rheobuild @875) was used for maintaining the fresh properties as per the requirements. Table 1 presents the constituents of OPC and mineral admixtures.

Table 1: Chemical properties of OPC and mineral admixtures

Chemical Composition (%)	OPC	FA	MK
Silicon dioxide (SiO_2)	20.05	59.51	51.46
Calcium oxide (CaO)	62.95	5.0	36.05
Aluminum oxide (Al_2O_3)	5.28	20.34	2.21
Iron oxide (Fe_2O_3)	4.01	5.89	0.81
Magnesium oxide (MgO)	1.5	1.5	0.18
Potassium oxide (K_2O)	0.95	1.92	0.28
Sodium oxide (Na_2O)	0.24	0.61	0.74
Loss of ignition	3.12	0.35	0.96

2.2 Mix proportioning

The SCC mix of M25 grade was prepared using w/b ratio of 0.44, and the total binder content was kept constant (450 Kg/m^3). The quantity of fine aggregate, coarse aggregate and dosage of superplastisizer were 890 Kg/m^3, 750 Kg/m^3 and 4.95 Kg/m^3, respectively. The final mix proportion was 1: 1.98: 1.66 (Binder: Fine aggregate: Coarse aggregate).

2.3 Test procedure

For the experiments, 100 mm cubes of different mixes were prepared. The RSCC and TBSCC specimens were cured for 28 days in tap water. Thereafter, these were exposed to 4 and 16% Ammonium Sulphate solution for 180 days to study the durability and micro-structural properties.

The compressive strength of specimens, at different ages, was determined in accordance with IS: 516- 1959. To determine the change in weight, one specimen from each mix category was weighed before exposure to Ammonium Sulphate solution and tap-water. After the required exposure, the mass of specimens was found. The weight change of specimens at specified time intervals was calculated. The micro-structural analyses were conducted by using XRD, SEM and EDS.

3. RESULTS AND DISCUSSION

3.1 Preparation of TBSCC

For the optimization of doses of FA and MK, 25 different mixes were prepared for different replacement levels of OPC by FA, MK, and FA+MK. The replacement levels of OPC with FA was- 5, 10, 15 and 20%, by mass. The replacement level of OPC with MK was- 5, 10, 15 and 20%, by mass. For each replacement level of OPC with FA, replacement level of MK was also varied from 0-20%, at an interval of 5%. Total 150 cubes were cast and cured in tap water for 28 days and their compressive strengths was determined at 7 and 28 days. The optimum dose of FA and MK was found as 15 and 10%, respectively, with respect to the compressive strength. The TBSCC was prepared by using 75%OPC+15%FA+10%MK, as per the findings of Deep et. al [11].

3.2 Fresh and hardened properties

3.2.1 Fresh properties

The workability parameters of SCCs were found by performing different tests, and are included in Table 2. It was found that the workability of TBSCC improved in comparison to RSCC.

Table 2: Workability parameters of SCCs

Tests	Results	
	RSCC	**TBSCC**
Slump flow	670 mm	690 mm
T_{50} time	4.5 sec	3.0 sec
V- funnel	11.5 sec	10 sec
L-box (h_2/h_1)	0.85	0.94
U-box (h_2-h_1)	29 mm	20 mm
J-ring	9.5 mm	6 mm

3.2.2 Hardened properties

The compressive strength of all mixes, exposed to different concentrations of Ammonium sulphate solution and tap water, were found at different intervals, and the results are represented in Table 3.

Table 3: Compressive strength (N/mm^2) of RSCC and TBSCC in different exposure conditions

Period (Days)	Exposure Condition					
	Tap water		4% $(NH_4)_2SO_4$ Solution		16%$(NH_4)_2SO_4$ Solution	
	RSCC	TBSCC	RSCC	TBSCC	RSCC	TBSCC
7	24.67	27.00	--	--	--	--
28	36.00	42.33	--	--	--	--
56	36.67	43.67	35.67	42.67	35.00	41.67
90	37.33	45.33	36.00	44.00	35.33	43.00
180	38.00	46.33	36.33	44.33	35.67	43.67

3.3 Durability properties and microstructural analysis

3.3.1 Compressive strength

The loss in RSCC's compressive strength after exposure to Ammonium Sulphate solution (4 and 16%) at 56, 90 and 180 days is 2.53%, 2.96%, 4.25% and 4.53%, 6.01%, 7.43%, respectively, with respect to those cured in tap water; while the respective improvements in TBSCC are 2.42%, 2.76%, 4.13% and 4.25%, 5.33%, 6.53%. Pera et al. [9] and Roy et al. [10] have also reported a similar pattern. The loss in compressive strength of both the SCCs are presented in Fig1.

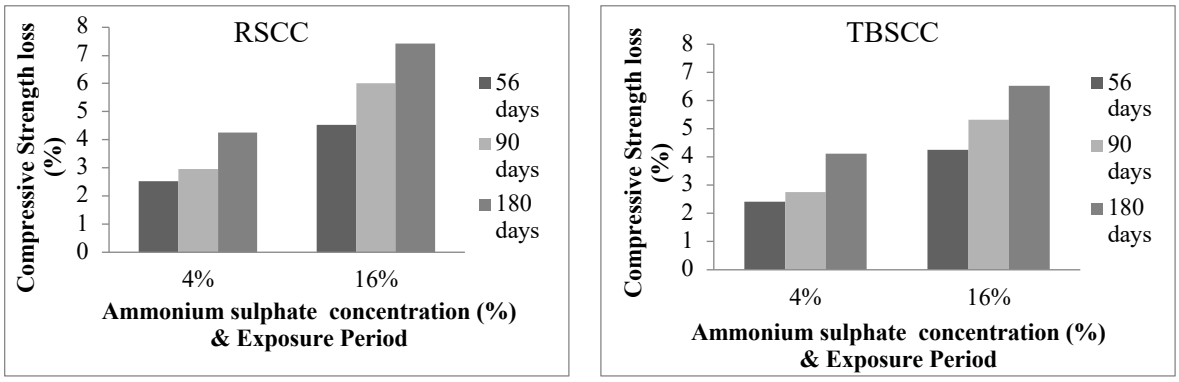

Figure 1: Compressive Strength loss of SCCs

3.3.2 Weight change

Figure 2 shows the variation in weight change of, RSCC and TBSCC samples in Ammonium Sulphate solution (4 and 16%) with age. Maximum weight change was found at 90 days, thereafter a decrement was observed. Most specimens underwent a continual increase in mass followed by a decreasing trend at advanced stages of the test. The former might be due to absorption and deposition of reaction products within the surface of specimens, while the latter might be linked to loss of surface and leaching to the surrounding solution. This result is similar to the findings of Roy et al. [10].

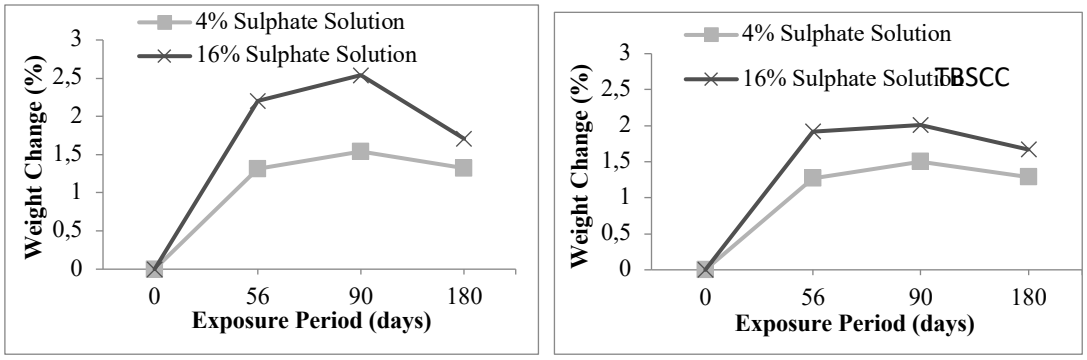

Figure 2: Weight change of SCCs

3.3.3 XRD, SEM and EDS Analysis

An XRD analysis of both the RSCC and TBSCC samples was conducted at 56 and 180 days, cured separately in Tap-water and Ammonium Sulphate solution (4 and 16%). Figures 3, 4 and 5 present the standard XRD results. Some of the significant crystalline phases identified are Quartz, Calcium Silicate Hydrate (C-S-H), Calcium Hydroxide (CH), Aluminum Sulphate, Monosulphate, Stratlingite, Potassium Aluminum sulphate hydrate and Ettringite. It is found that the TBSCC specimen exposed to the Sulphate solution have lower gypsum, ettringite and brucite intensity, which are mainly responsible for expansion and cracking cracking of the concrete. In contrast to the TBSCC, higher peaks of ettringite are observed in RSCC after exposure to the Sulphate solution.

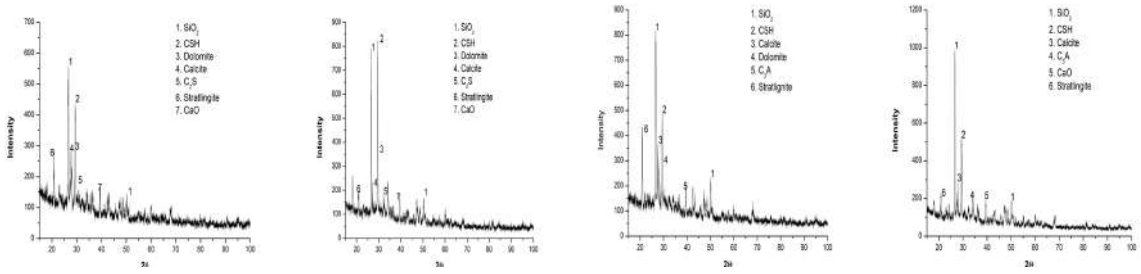

(a) RSCC and TBSCC at 56 days (b) RSCC and TBSCC at 180 days

Figure 3: XRD traces of RSCC and TBSCC at 56 and 180 days tap water

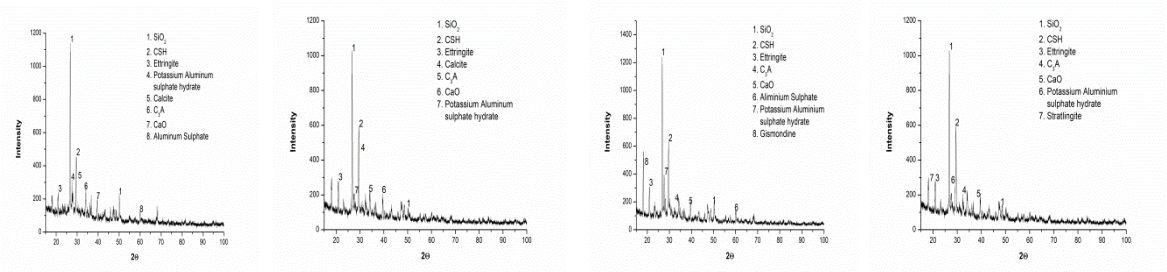

(a) RSCC and TBSCC at 56 days (b) RSCC and TBSCC at 180 days

Figure 4: XRD traces of RSCC and TBSCC at 56 and 180 days Sulphate solution (4%)

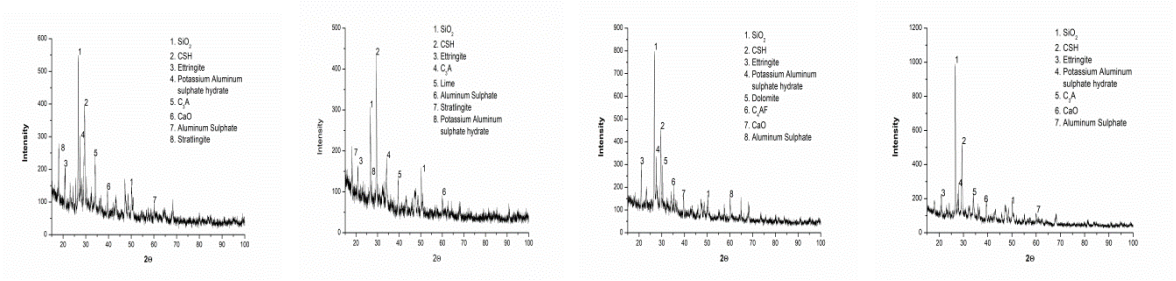

(a) RSCC and TBSCC at 56 days (b) RSCC and TBSCC at 180 days

Figure 5: XRD traces of RSCC and TBSCC at 56 and 180 days Sulphate solution (16%)

In order to validate the internal microstructure obtained by XRD, SEM, the EDS study on both the RSCC and TBSCC was performed. The morphological changes in the specimens after curing in Tap-water for 56 and 180 days are presented in Fig 6; while, the similar changes for the specimens exposed to the Ammonium Sulphate solution (4 and 16%) for 56 and 180 days are included in Figs 7 and 8. The corresponding EDS spectrum also verifies the formation of ettringite and Aluminum sulphate in the specimens exposed to Sulphate solution. In TBSCC specimen, the needle like crystals of ettringite were rarely seen; however, in RSCC specimen, these are clearly visible.

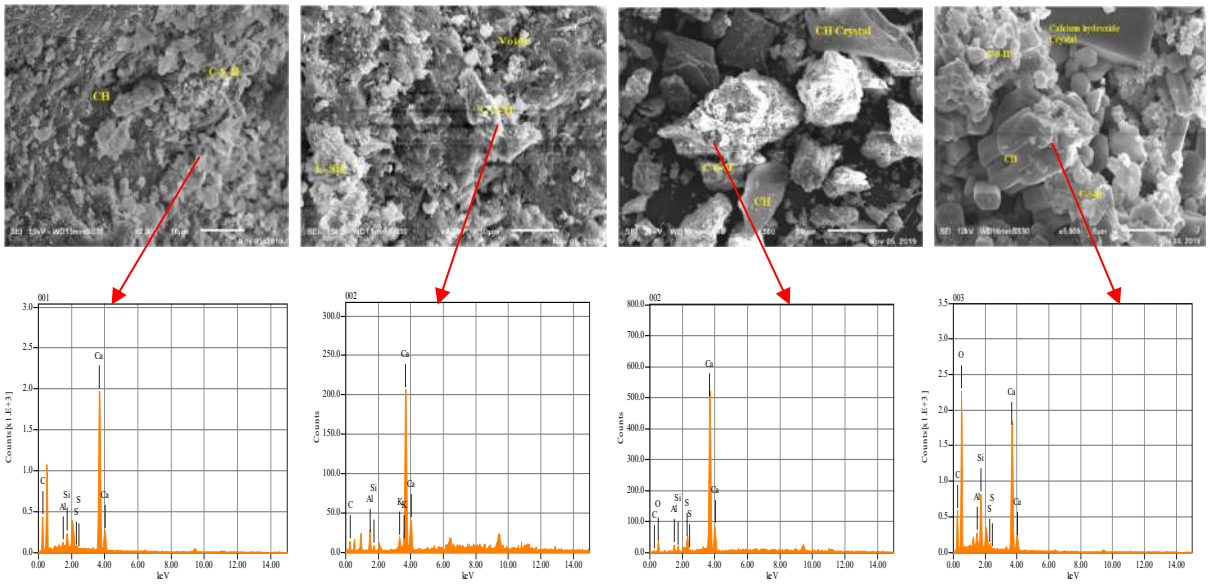

(a) RSCC and TBSCC at 56 days (b) RSCC and TBSCC at 180 days

Figure 6: SEM and EDS of RSCC and TBSCC at 56 and 180 days tap water

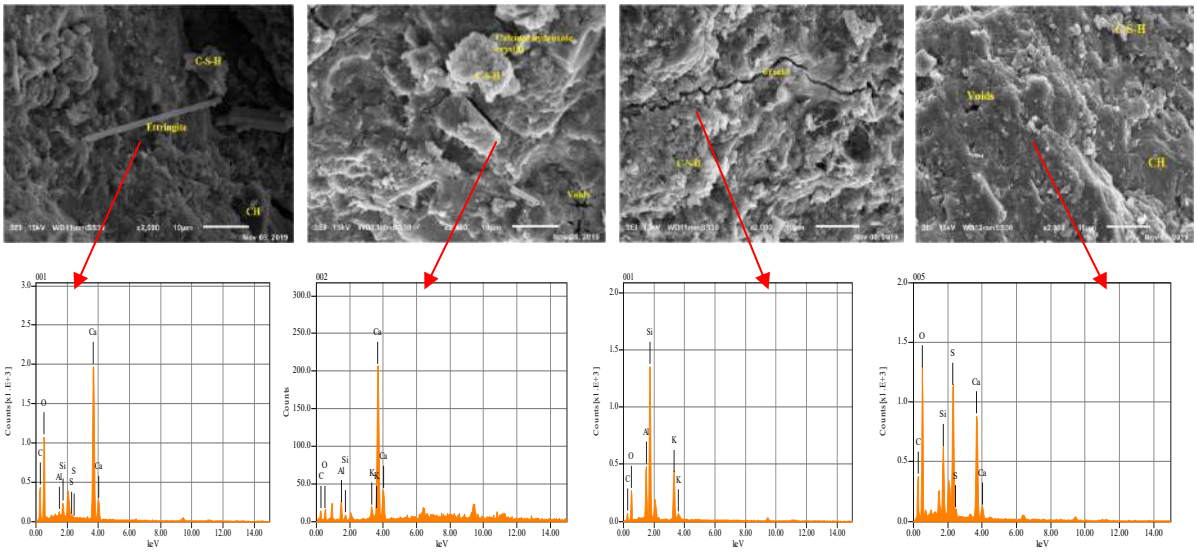

(a) RSCC and TBSCC at 56 days (b) RSCC and TBSCC at 180 days

Figure 7: SEM and EDS of RSCC and TBSCC at 56 and 180 days Sulphate solution (4%)

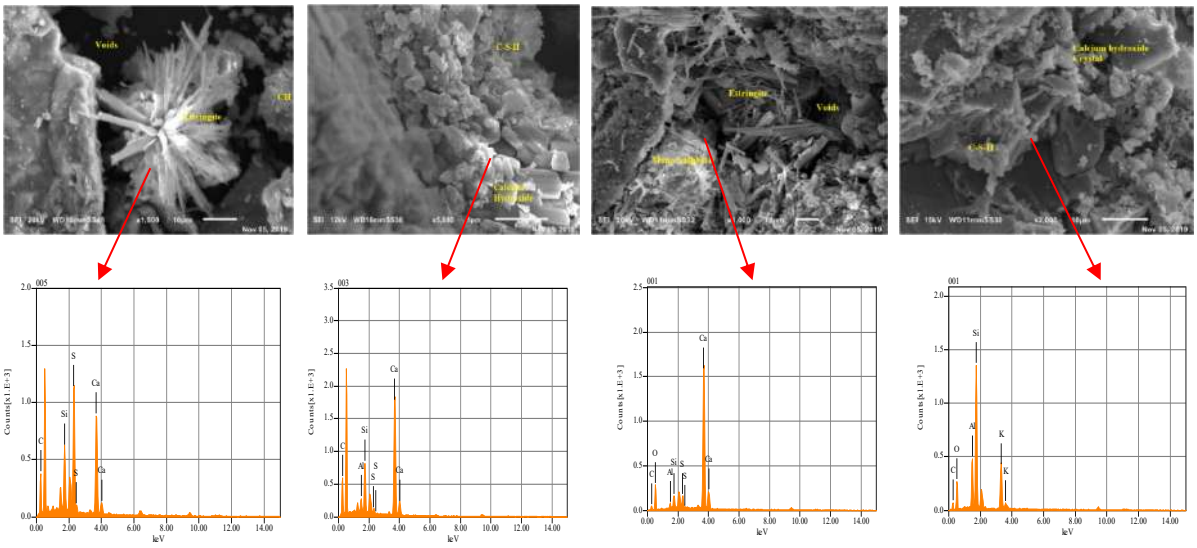

(a) RSCC and TBSCC at 56 days (b) RSCC and TBSCC at 180 days

Figure 8: SEM and EDS of RSCC and TBSCC at 56 and 180 days Sulphate solution (16%)

4. CONCLUSIONS

Followings are concluded from the present study,

- The workability of ternary blended SCC is improved in comparison to referral SCC.
- The loss in compressive strength of RSCC is more in comparison to the TBSCC and increases with the exposure period and strength of the Sulphate solution.
- The weight of SCCs increases up to 90 days, and then it decreases.
- XRD analysis reveals that Ettringite, Aluminum sulphate and Potassium Aluminum sulphate hydrate are formed in the specimens exposed to the Sulphate solution and these are more dominant in RSCC than TBSCC.
- SEM and EDS show the morphological and elemental composition of compounds formed and confirms the XRD results.

REFERENCES

[1] Neville, 'The confused world of sulphate attack on concrete' (2004). *Cem. Concr. Res.* 34 (8), 1275-1296.

[2] Q.K. Nie, C.J. Zhou, H.W. Li X. Shu, H.R. Gong, B.S. Huang (2015). Numerical simulation of fly ash concrete under sulphate attack, *Constr. Build. Mater*, 84, 261-268.

[3] Ping Duana, ChunjieYana, Wei Zhoua, Influence of partial replacement of fly ash by metakaolin on mechanical properties and microstructure of fly ash geopolymer paste exposed to sulphate attack, Ceramics International, 42 (2016), pp. 3504–3517.

[4] Kavitha O. R., Shanthi V.M., Arulraj G.P., and Sivakumar P. (2015). Fresh, micro-and macro level studies of metakaolin blended self-compacting concrete, *Applied Clay Science*, 114, 370-374.

[5] Ann Mary Mathew (2016). Microstructural Development in Fly Ash-Lime-Metakaolin Mix, *International Journal of Scientific & Engineering Research*, 7 (8).

[6] M. T. Bassuoni, M. L. Nehdi (2012). Resistance of self-consolidating concrete to ammonium sulphate attack, *Materials and Structures*, 45, 977–994.

[7] Marcos A.S. Anjos a,e, Aires Cam~oes b, Pedro Campos b, Givanildo A. Azeredo c, Ruan L. S. Ferreira d, Effect of high volume fly ash and metakaolin with and without hydrated lime on the properties of self-compacting concrete, Journal of Building Engineering 27 (2020) 100985

[8] Paul Brown, R.D. Hooton, Boyd Clark, Microstructural changes in concretes with sulfate exposure, Cement & Concrete Composites 26 (2004) 993–999.

[9] Mbessa M, Pera J. (2001). Durability of high-strength concrete in ammonium sulfate solution, *Cem Concr Res*, 31(8), 1227–123.

[10] Roy D.M, Arjunan P, Silsbee N.R. (2001). Effect of Silica Fume, Metakaoline and Low calcium fly ash on Chemical resistance of Concrete, 31(12), 1809-1813.

[11] Deep Tripathi, Rakesh Kumar, P.K. Mehta, Amrendra Singh (2019). Optimum Dose of Binary Admixture in Self Compacting Concrete, *International Journal of Innovative and Exploring Engineering*, 9 (1), 103-108.

THE VIABILITY OF RUBBERISED CONCRETE IN THE SOUTH AFRICAN CONSTRUCTION INDUSTRY

Matthew Jonck [(1)], Dawid J. M. Vuuren [(1)] and Sunday Nwaubani [(1)]
(1) School of Civil and Environmental Engineering, University of the Witwatersrand, Johannesburg

ABSTRACT

This paper describes the results of an investigation to determine the viability of using waste rubber chips as a substitute for natural aggregate in producing structural concrete. The rubber chips used were obtained from shredded scrap tyres, which are costly to discard at landfill sites and often constitute undesirable environmental and health risks. A major focus of the investigation was to identify whether treatment of the rubber chips before batching would result in an improved rubberised concrete to be used in structural applications. Concrete mixes consisting of 0% rubber chips, were compared with those incorporating, 5%, 10% and 20% rubber replacement percentages for natural coarse aggregate. The water to binder ratio of 0.45 and cement content were kept constant for all mixes. The results showed no significant difference in slump values for the differing rubber replacement values. The strength test results suggest that rubberised concrete has potential for use in structural applications, provided the level of replacement is below 17.5%, for untreated and treated samples, respectively. Dynamic test results suggest that high rubber replacements could be utilised for making concrete elements that do not experience high levels of mechanical stress but rather for elements that experience high levels of fatigue and dynamic loading.

Keywords: rubberised Concrete, pre-treatment, compressive strength, dynamic loading

1. INTRODUCTION

In modern society, most importantly in the construction industry, the control and management of waste is a key facet in ensuring sustainable development. This sustainability not only should encompass environmental aspects, but also economic and social environments. Incorporating the widespread use of waste materials in the construction industry as a replacement for the current waste management act can help alleviate the stress put on the environment and landfill sites, while also creating employment opportunities. Dumping tyres in landfills requires a lot of space and acts as a breeding space for mosquitoes and other vermin. Besides this, there is economic value to be obtained through the reuse and recycling of waste tyres, creating a circular economy from cradle to cradle of tyre management [1]. Circular Economy can be seen as the process of reusing, recycling and remanufacturing products to keep them circulating within the economy [2].

The use of rubber in concrete as a replacement for aggregate has been progressing since the mid 90's. Al-Fadhli, M. [3] carried out extensive testing on the static and mechanical properties of rubberised concrete and has found that current methods do not allow for rubberised concrete

to be used as a substitute for load bearing structural elements [3]. His results indicate an indirectly proportional relationship between loss of compressive strength of concrete and increased percentages of rubber as an aggregate replacement [3]. Little to no research has been done with regards to the static and dynamic properties of rubberised concrete in a South African context. Furthermore, most research that has been done has focused on replacing the fine aggregate and not the coarse aggregate in concrete. This provides a motive to further investigate both the static and dynamic properties of concrete with rubber particles as a coarse aggregate replacement from a South African perspective. This will help to deduce the feasibility thereof in terms of methods to create a structural concrete from chipped rubber particles, whilst examining the changes in dynamic properties and durability that will arise from replacing stone content with chipped rubber.

The study reported in this paper addresses the need for greater research to be conducted within this field, to further push sustainability in civil engineering and assuage the negative effects that waste tyres have on the environment.

2. AIM

The aim of this study is to identify a working range of rubber replacement percentages that can produce structural concrete. A second aim is to investigate the effect of soaking the rubber chips in a sodium hydroxide bath and coating the chips in metakaolin as a pre-treatment method to help mitigate the inevitable loss of compressive strength in rubberised concrete. Lastly, examining the dynamic properties of a rubberised concrete in comparison with a plain concrete control sample.

3 METHODOLOGY

3.1 Mix Design

Before the mix designs were finalised, 3 trial mixes were done in accordance with the South African Concrete & Cement Institute (C&CI) design method, to determine the optimum moisture content to theoretically achieve a 75mm slump for the control mix design. Three different mix designs with water contents ranging between 225 kg/m^3; 215 kg/m^3 and 205 kg/m^3, were done using a principle of ratios. This method was used to ensure that no material was wasted, and excess water used whilst conducting three different slump tests each having different water contents. The method of ratios consisted of designing the initial mix in accordance with the C&CI method, and then performing numerous ratio calculations to determine the new quantities. The recorded slumps can be seen in Figure 1.

With reference to the C&CI method as well as the new optimum water content, the mix designs were scaled to the required volumes for each batch consisting of cubes for compressive strength tests and beams for dynamic loading tests. A constant w/c ratio of 0,45 was used throughout the seven different batches, with the batch quantities for the treated and untreated rubber staying constant. Table 1 shows the final mix designs for the four different batches.

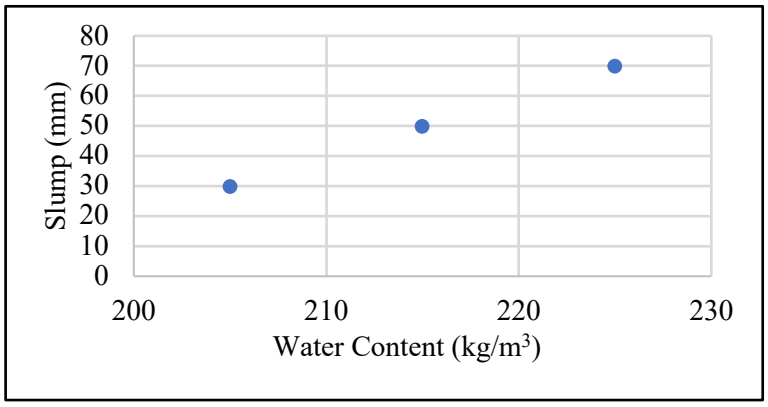

Figure 1: Trial cement mix with subsequent slump

Table 1: Finalised mix Designs

	Plain Concrete	5% Rubber	10% Rubber	20% Rubber
Water (kg/m^3)	230	230	230	230
w/c Ratio	0.45	0.45	0.45	0.45
Cement (kg/m^3)	505	505	505	505
CBD (kg/m^3)	1670	1670	1670	1670
Sand FM	3.26	3.26	3.26	3.26
Stone K	0.94	0.94	0.94	0.94
Stone (kg/m^3)	1040	985	935	830
Rubber (kg/m^3)	-	50	105	210
Sand (kg/m^3)	755	675	590	510
Density (kg/m^3)	2530	2445	2365	2285
Density (kg/m^3)	2530	2445	2365	2285

3.2 Rubber Treatment

The rubber was first rinsed in a water bath and sieved multiple times to get rid of excess nylon leftover from the shredding process and any excess dirt that may still be on the rubber. The sieving process also enabled the rubber to be sorted in a size range between 4.75 and 19 mm, rendering it in a coarse aggregate range.

After the rubber had been sufficiently sorted and cleaned, an appropriate quantity of rubber to meet the batch requirements for the treated rubber concrete was taken and soaked in a sodium hydroxide solution. The solution was a 20% sodium hydroxide diluted with water. The pH of water containing the rubber before the sodium hydroxide was recorded and found to be between 7 and 8. After adding the sodium hydroxide, the pH of the solution was again measured and recorded as 13 before the testing kit was promptly dissolved by the solution. After sitting for twenty minutes, the solution was drained, and the rubber thoroughly rinsed multiple times to bring the pH back to its original state of around 8. After the treated rubber had been air dried, the rubber was then coated in a fine metakaolin coating to assist with the binding when in the concrete matrix. Going forward, the treated rubber will be referred to as TR and the untreated rubber referred to as UR.

4 RESULTS AND ANALYSIS

4.1 Compressive Strength

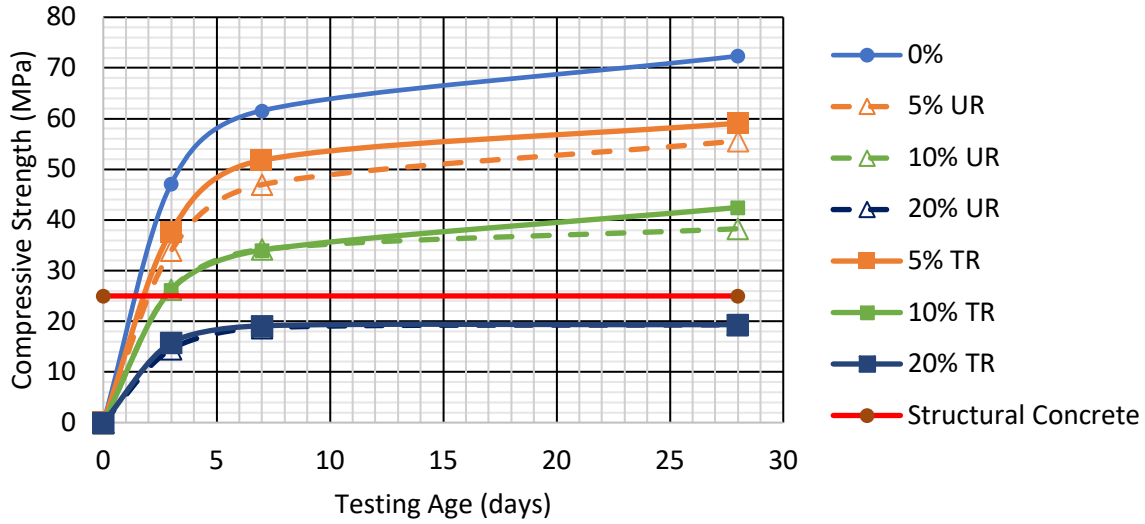

Figure 2: Compressive strength gain over 28 days

All results obtained in Figure 2 were achieved by taking an average of three cubes crushed per mix over 3, 7 and 28 days after initially being cast.

The control mix, which contained a 52.5 MPa rapid hardening cement, was designed to achieve a target strength of 59 MPa after 28 days. The control mix achieved a 28-day compressive strength of 72.4 MPa, far outperforming the expected compressive strength. This increase in strength can be possibly attributed to the use of a water to binder ratio of 0.45. A lower water content in relation to cement content is known to result in higher achievable compressive strengths in concrete.

There is a general trend that can be seen in Figure 2 that an increase in rubber replacement percentage results in a significant loss in strength. Neither of the 20% replacement mixes achieved a 28-day strength higher than the structural concrete target of 25 MPa. There was also no discernible difference in the compressive strength values of the 20% treated and untreated rubber mixes over the 3, 7 and 28-day tests. This alludes to the possibility that treating the rubber has no positive benefits to mitigating strength loss when using rubber as a coarse aggregate replacement.

The 5% and 10% rubber replacement mixes showed promising results. Both replacement values achieved 28-day compressive strength results far greater than the 25 MPa target. The 10% untreated and treated mixes reached a 28-day strength of 38.3 MPa and 42.5 MPa, respectively. Despite those strengths falling way short of the strengths witnessed by the control, reaching only 53% and 59% of the control mix's 28-day strength, we observed a significant strength increase over the treated mix when compared to the untreated mix. Treating the rubber before mixing and casting resulted in an increase of 4.2 MPa when compared to its untreated counterpart at 28-days. This increase in strength in the 10% treated mix however only occurred sometime after 7 days of curing.

At 28-days, the 5% treated and untreated mixes produced compressive strengths of 59.1 MPa and 55.6 MPa, respectively. Similar to the 10% mixes, we see a significant increase in compressive strength after treating the rubber before mixing and casting in comparison to the untreated mix. Promisingly though, the 5% treated and untreated mixes achieved 77% and 82% of the control mix's 28-day strength.

An interesting observation, as can be seen in Figure 3, was how the rubber seemed to hold the testing cubes together post crushing. The plain concrete samples exhibited the textbook hourglass failure pattern. However, the higher the rubber replacement, the less superficial the failure patterns became. It is thus assumed that the rubber within the cement matrix absorbs the tensile stress that the cubes undergo whilst being crushed. Therefore, rubberised concrete does not seem to experience the same brittle failure that plain concrete does.

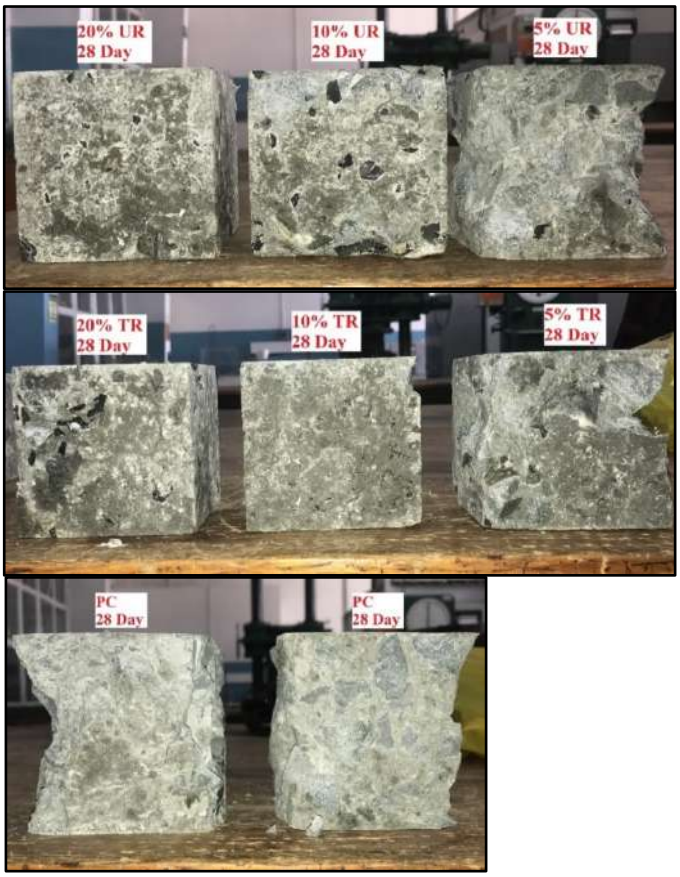

Figure 3: Post crushing failure patterns

4.2 Dynamic Analysis

Two separate methods were used to calculate the damping ratio of the beam specimens in order to assess the accuracy of the results. Three tests per beam were conducted to achieve an average damping ratio per beam specimen. It is known that plain concrete has a damping ratio of approximately 5% and that when replacing the aggregates with a percentage of rubber, this damping ratio would increase. This means that the time it takes for the load to oscillate through the structure and to be absorbed, returning to the equilibrium state would be less in a rubberised concrete than that of plain concrete. Figure 4 shows the setup of the dynamic analysis.

Figure 4: Setup of the dynamic analysis

In brief, an impact load was applied to the concrete specimens and the logarithmic decay of the amplitude of the oscillations due to the force was measured. From this, the damping ratio was then calculated and can be seen in Table 2.

Table 2: Average damping ratio using the MIT and INV methods

	Average Damping Ratio (%)	
% Rubber Replacement	INV-Method	MIT-Method
0	5.2	5.4
5	8.9	9.3
10	10.8	10

It should be noted that an average damping ratio was calculated for each of the 5% and 10% rubber replacement for treated and untreated samples. This was done as due to the mixing and batching process; we cannot confidently specify the exact percentage of rubber as a mass replacement per specimen. There is no indication to believe that the treatment of rubber would result in results different to that of an untreated rubber specimen. Therefore, by taking the average over the treated and untreated damping ratios, we aim to mitigate the variability in results due to the possibility of varying rubber replacement percentages through samples of the same replacement values.

Taking the average of the treated and untreated beam specimens results in a linear relationship. That linear relationship being an increase in rubber replacement percentage will result in a higher damping ratio in the specimen. This can be attributed to rubber having a higher damping ratio than the other constituents in the concrete matrix, therefore the scrap rubber will have an influence over the damping of the concrete. Most noteworthy is the similarity of the results between the two different methods used to calculate the damping ratio of the different beam specimens. Two methods providing similar values helps solidify the validity of the results.

The 20% rubber replacement prism results were mitigated from the results as the values produced did not match the trend produced by the 5% and 10% replacement results. The reasoning behind the rogue 20% damping ratios can be attributed to the lack of precision in ensuring exact replacement percentages were met.

4.3 Analysis of Results

The compressive strength results followed what literature had deemed to be the norm when replacing coarse aggregate with rubber. There is a clear linear relationship between increasing the percentage of rubber as a replacement and the loss of compressive strength. Along with that, there is also a linear relationship with increasing the rubber percentage and increased damping in the samples. With these two relationships, the optimum rubber replacement percentage can be calculated to still meet the minimum compressive strength requirements to meet the standard of structural concrete. Using the linear relationship developed from the treated and untreated rubber samples, the maximum rubber replacement percentage to still meet a compressive strength of 25 MPa for this particular mix design is 17.48% and 16.87% respectively.

As seen evident from the results of the compressive strength tests, treating the rubber significantly mitigates the strength lost when using rubber as a coarse aggregate replacement. By mitigating the strength, a higher rubber replacement percentage is attainable before falling below the limit of compressive strength required to be used as a structural concrete.

By increasing the rubber replacement percentage, the dynamic performance of the concrete greatly improves when compared to a plain concrete mix. The results in Table 3, using both methods and the values from the untreated rubber and treated rubber samples, the damping ratio of the specimens were all more than two and a half times that of plain concrete.

Table 3: Maximum Rubber Replacement and Resultant Damping Ratios

		INV Method	MIT Method
	Max Rubber (%)	Damping Ratio (%)	Damping Ratio (%)
UR	16.87	14.86	13.66
TR	17.48	15.2	13.94

The greatest benefit of using rubber as a coarse aggregate replacement, beyond the environmental benefits, is the increase in dynamic performance. It is thus recommended to use a rubberised concrete mix where concrete strength performance is not a paramount aspect of the project and where dynamic loading is great or occurs often. This will allow for high percentage replacements of rubber, greatly improving the dynamic properties and possibly increasing the fatigue life of the concrete.

Another benefit is the lower density of rubberised concrete in comparison to plain concrete. The lower density will result in a lower self-weight and in turn lower dead load on the concrete structure. This will allow for a higher imposed load to be added and still meet the factor of safety requirements.

Beyond the physical properties of rubberised concrete, the strongest driving factor for adopting rubberised concrete into the construction industry is that of sustainability. With the ability of recycling 100% of waste tyres on a large-scale, the construction industry will be able to significantly reduce the impact that waste tyres are creating on the environment. Just considering the lowest percentage replacement of 5%, that equates to 51.89 kg of rubber per cubic metre of concrete. That is equivalent of using six average 15-inch tyres (381 mm diameter) per cubic metre of concrete.

For a sustainable future, the onus is on large industries to lead the way forward. Sustainable engineering and construction has the potential to alleviate current environmental concerns as well as ensuring these concerns are not prevalent for future generations. Rubberised concrete

provides a viable means to tackle the issue of waste tyres and the threat they pose to the environment as well as introducing a cost-effective process to increase the dynamic properties of concrete.

It is from these results that we believe with further testing and researching, a rubberised concrete mix is not only sustainable but viable for use in the construction industry.

5. CONCLUSIONS

The results and data obtained over the various experiments conducted further reinforces what has been stated in literature beforehand. These statements being that introducing rubber into concrete as a percentage replacement for coarse aggregate will greatly reduce the compressive strength of concrete, whilst improving the dynamic properties of said concrete.

- The 5% and 10% replacement mixes registered strength greater than the minimum value of 25 MPa associated with structural concrete whereas the 20% replacement mix fell below this minimum.
- Soaking the rubber chips in sodium hydroxide and coating it with a layer of metakaolin resulted in a significantly higher 28-day compressive strength when compared to the untreated rubber mixes of equal percentage replacement.
- Replacing coarse aggregate with chipped rubber greatly increases the damping ratio of concrete, critically resulting in better performance under shock loading.
- It is recommended that rubberised concrete be utilised where strength performance is not critical and where the loads being applied are mainly dynamic in nature.
- To ensure that mix designs and percentage replacements are accurate and performance across the board is normalised, precast sections of rubberised concrete should be employed.
- Scenarios whereby rubberised concrete will have best performance include, roadside barriers, industrial warehouse flooring, platforms supporting mining machinery and railway sleepers.

REFERENCES

[1] Sebola, M., Mativenga, P. and Pretorius, J. (2018). *A Benchmark Study of Waste Tyre Recycling in South Africa to European Union Practice*. [online] ScienceDirect. Available at: https://www.sciencedirect.com/science/article/pii/S2212827117309253 [Accessed 22 Feb. 2020].

[2] Ellenmacarthurfoundation.org. (2017). *The Circular Economy In Detail*. [online] Available at: https://www.ellenmacarthurfoundation.org/explore/the-circular-economy-in-detail [Accessed 7 Mar. 2020].

[3] Al-Fadhli, M. (2017). Advantages of Concrete Mixing with Tyre Rubber. *Int. Journal of Engineering Research and Application*, [online] 7(4), pp.96-98. Available at: http://www.ijera.com/papers/Vol7_issue4/Part-6/P0704069698.pdf [Accessed 16 Feb. 2020].

STRESS-STRAIN CHARACTERISTIC OF CRUMB-RUBBER MASONRY CONCRETE PRISM COLUMN UNDER COMPRESSION

Sanni M. Yinka [(1)], Leonard N. Dugguh [(1)] and Laraiyetan E. Taiye [(2)]

(1) Department of Civil Engineering, Ahmadu Bello University, Zaria, Kaduna State, Nigeria

(2) Department of Civil Engineering, Kogi State Polytechnic, Lokoja, Kogi State, Nigeria

ABSTRACT

This paper presents an experimental study into the stress-strain behaviour of an unreinforced and un-grouted crumb-rubber modified masonry hollow concrete block prism under uniaxial monotonic compressive loading conditions. The investigation was carried out on the reference and modified masonry prism samples with varying content of crumb-rubber from end-of-life tyres partially replacing coarse aggregate (granite) by volume at 0, 5, 10, 15, 20, and 25%. Based on the results obtained, the stress-strain curves have revealed a convergent strength level deformation under compression. Furthermore, the results indicated a linear increase in the stress of the reference prism column before fracture at the maximum stress with the stress-strain curve considered as a ‘‘sharp peak’’. It was also noticed that increasing the crumb-rubber content has a significant effect on the maximum stress and strain of the prism columns. This variation reached about 74% at maximum stress with crumb-rubber content up to 25%. The result also revealed an increase of 49% and 30% in lateral and vertical (strain) respectively at maximum stress to the reference prism column and crumb-rubber content up to 25%. Thus, the increase in the plastic strain translates into an increase in the toughness with a gradual failure and high-energy absorption capability.

Keywords: concrete; masonry; crumb-rubber; specified strength; stress-strain

1. INTRODUCTION

Masonry hollow concrete blocks are widely used in many parts of the world due to their numerous relative advantages such as low cost, lightweight, high bearing capacity, and efficiency in terms of energy and acoustic performance [22]. The brittle failure behavior of hollow concrete blocks masonry in compression necessitates the utilization of alternative materials such as post-consumer tyre particles to enable it to be more ductile and also produce more sustainable concrete blocks [11]

Post-consumer tyres are always embattled with the problem of how to dispose of them. Discarded post-consumer tyre into landfills and open fields pile up and create large voids under the surface and on the surface of land as the case may be which leads to the trapping of gases such as methane. The trapped gases can ignite at any given opportunity leading to uncontrollable fire [4]; such as the recent experience reported by [2] in Sesena, Spain where an uncontrollable fire rage through a pile of millions of kilograms (millions number) of tyres unleashing and releasing a thick black cloud of toxic fumes into the air at the dumpsite covering

100,000 square meters. The blaze was said to have lasted for days before it was controlled as the fire continues to burn inside even though it has been extinguished from outside. Open-air combustion of waste tyre pollutes the air and poison the groundwater with the release of benzene and heavy metals that produce dioxins which are linked to various serious health problems [4].

[21], revealed that every year around 9 billion kilograms of end-of-life tyres are discarded everywhere throughout the world, which was likewise evaluated to associate with one billion waste tyres generated annually [6] and [9].

Based on 2018 statistics with a 15% annual generation rate, it is estimated that around 37 million waste tyres exist in Nigeria [18]. One of the most common ways of disposing of waste tyres is through open field disposal and combustion [17]. With this quantity, the large stockpile of waste tyre poses both environmental and health risks to its population.

Waste tyres in form of chips, fibers, crumbs, and particles have been successfully incorporated into asphalt mix and used as a surface layer in a flexible pavement which is dated back to the 1980s; results reveals that the modified asphalt had better resistance to skidding, reduce fatigue cracking and prolong pavement life span compared to the conventional asphalt mix [1, 7, 8, 13, 5, 12]. The application of waste tyre derived aggregate in Portland cement-based materials mixes such as structural concrete and blocks has been exploded in past years using chips, fines, shreds, slit, fibers, and crumb-rubber to replace fine aggregate. Results revealed that compressive strength decreased with an increase in rubber tyre particle content however structural concrete and blocks for both load-bearing and non-load bearing structures can be produced with partial replacement of rubber particles up to 15% [15, 12, 10].

This present study is aimed at introducing crumb-rubber aggregate in various proportion as a partial replacement for coarse aggregate in masonry concrete mix and also investigate the the unit weight specified compressive strength, and stress-strain characteristics of masonry hollow concrete blocks prism column constructed.

2. MATERIALS AND METHODOLOGY

2.1 Material

A general-purpose blended limestone Portland cement CEM II (42.5R MPa) with a specific gravity *G* of approximately 3.15 that conforms to BS EN 197-1:2000 was used in this work. The natural river quartzite sand smaller than 4.76mm but larger than 75μm with average bulk specific gravity (SSD) of 2.65 was used for both fine and medium-fine aggregate. It was graded with the appropriate zone of sieves according to BS EN 933-1:2012 to ensure that it conforms to BS EN 1260:2002+A1:2008 specification. Natural crushed (granite) with nominal maximum sizes of 9.52mm-10mm sourced from a local commercial quarry with average bulk specific gravity (SSD) of 2.66 was used. Tests were conducted on the coarse aggregate to ensure that it conforms to BS EN 1260:2002+A1:2008 specification. Crumb-rubber aggregate in Figure 1 was derived from post-consumer tyres and processed to a nominal maximum size of 4 - 9mm with average bulk specific gravity (SSD) of 1.14. The surface of the crumb-rubber was treated by soaking in a sodium hydroxide (NaOH) which enhances the hydrophilic properties of the rubber and increases the intermolecular interaction forces between rubber and calcium silicate hydrate (C-S-H) gel which enhances the strength of the composite matrix [14]. Ordinary tap water was used for all concrete mixes and curing.

Figure 1: Crumb-Rubber Aggregate Used for Concrete Mix

2.2 Mix Design and Manufacture of Hollow Concrete Block Units

The mix design for the masonry hollow concrete block adopted was based on absolute volume method according to BS EN 206-1:2000, "Method of specifying concrete mixes", A mix ratio of 1:1.5:3 and water/cement ratio of 0.42 was adopted for all the concrete mixes due to the high strength above the required minimum standard of 30N/mm^2. Water cement ratio (w/c) of 0.42 was taken as the optimum because of the moderate compacting factor of 0.84 (low) and high strength of 30.71N/mm^2 attached to it. General-purpose masonry mortar with a strength grade of 20N/mm^2 was produced with a mix ratio of 1:3 (cement: sand) and a w/c ratio of 0.6. The masonry concrete blocks (hollow) with the size 450 x 225 x 225mm were produced to the requirements given in BS 771-3(2003) with the use of a vibrating machine. Six various percentages of coarse aggregate (granite) partially substituted with crumb-rubber at 0, 5, 10, 15, 20, and 25% by volume were used.

2.3 Experimental Procedures

Tests were conducted to assess the workability of the freshly mixed concrete which includes compacting factor in accordance to BS EN 12350-4:2009 and unit weight in accordance to BS EN 12350-6:2009 while the yield was computed based on ASTM C138-09. The density and compressive strength of masonry hollow concrete block units were determined according to BS EN772 -13 (2000) and BS EN 772 -1:2000 respectively after twenty-eight (28) days of curing. Masonry prism columns were constructed following ASTM C1314, wooden pallets of suitable sizes were prepared and used as a flat base upon which the masonry prism columns stand. A total of eighteen (18) masonry prism columns (230 x 720 x 230) mm were built as shown in Figure 2 in the same manner to investigate the effect of crumb-rubber on its properties. M20 general-purpose mortar with the mixture consisting of Portland cement (CEMII) and sand in a proportion of 1:3 by volume and water/cement ratio of 0.6 was used for the mix and kept constant for all mixes. All prism columns were covered with polythene and left for 24hrs to gain an initial set before being moved to storage. The constructed columns were cured with water through sprinkling twice per day for 28 days to achieve the desired bonding strength of the mortar.

2.4 Test Set-up, Instrumentation, and Measurement

The compressive strength of the un-grouted masonry prism column was tested following ASTM C1314 after curing for 28 days. A testing rig and lateral displacement gauges (dial gauge) were used for the test.

Figure 2: Construction of Masonry Hollow Concrete Block Prism Column

A schematic description of the setup can be seen in Figure 3. Displacement gauges (dial gauge) were set up on each prism column to record the strain values during compression. Loading was applied uniformly to the top and bottom of the specimen. The load increased steadily so that failure is reached after 15 min to 30 min from the commencement of loading. The compressive load (stress) at initial cracks and final cracks i.e., the ultimate load was observed. The net cross-sectional area of the masonry unit determined following ASTM C140 was used to calculate compressive strength for the un-grouted reduced-size prisms.

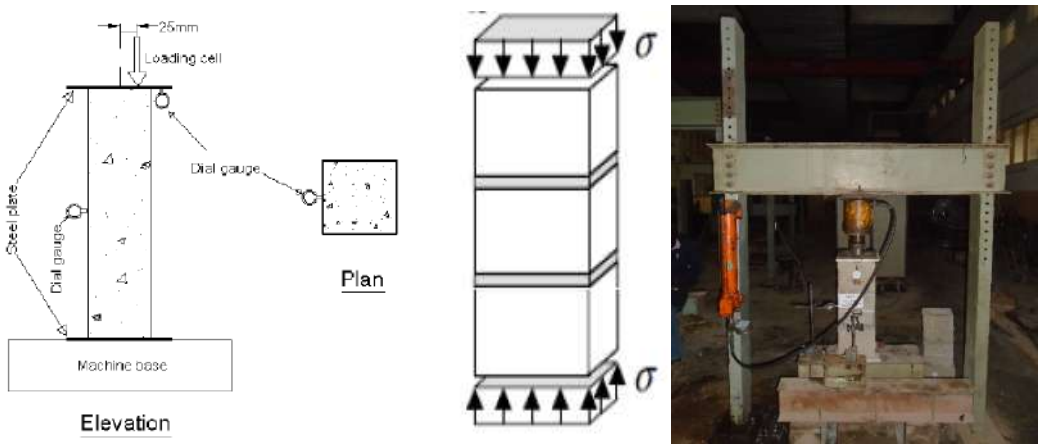

Figure 3: Schematic Description and Picture of Masonry Prism Column Test Set up

Equation 1 was used to determine the compressive strength of each prism column:

$$f_i = \frac{f_{i\max}}{A_i}(N/mm^2) \qquad \textbf{Equation (1)}$$

Where f_i is the compressive strength of an individual masonry prism column specimen, (N/mm^2); f_{imax} is the maximum load reached on an individual masonry prism column specimen, (N); A_i is the loaded cross-section of an individual specimen, (mm^2). The specified compressive strength (f_m) was determined using Equation 2:

$$f_m = f \times 1.08 \text{ (N/mm}^2\text{)} \qquad \textbf{Equation (2)}$$

Where: f =Compressive Strength (N/mm^2) and Correction factor = 1.08

3. RESULTS AND DISCUSSION

3.1 Compacting Factor, Yield, and Unit weight

The compacting factor (C.F) was observed to decrease significantly, reference masonry concrete mixes had a C.F of 0.84 (low workability) while the 25% rubberized mix had a C.F of 0.77 (very low workability) indicating an 8.3% reduction. Incorporation of crumb-rubber tyre aggregate decreased the unit weight of fresh concrete mix from 2,436Kg/m3 to 2,191Kg/m3 with crumb-rubber content up to 25% which indicates a 10.1% reduction.

3.2 Density

The density of control and rubberized masonry hollow concrete blocks samples indicates that the rubberized masonry hollow concrete blocks exhibited lower densities than the control mixes, also it can be deduced from the result that density reduces by 19%, with the reference concrete block units having an average net density of 2079 kg/m^3 while 25% modified masonry hollow concrete block units have an average of 1686 kg/m^3 which indicate a range of medium weight to normal weight.

3.3 Compressive Strength (f)

Compressive strength of rubberized masonry hollow concrete blocks results indicates a decrease in compressive strength with an increase in crumb-rubber content also a percentage loss of strength by 49% was observed with the reference units having a strength of 9.43N/mm2 while 5, 10, 15, 20 and 25% crumb-rubber modified masonry concrete block units having a strength of 8.29N/mm2, 7.20N/mm2, 7.02N/mm2, 6.61N/mm2 and 4.84N/mm2 respectively. [11] reported a non-linearly decrease in the compressive strength of masonry hollow concrete block unit. He also mentioned that increasing crumb-rubber replacement from 0 to 37% decreased the compressive strength by 77.5%. However, increasing rubber replacement from 0 to 20% decreased the compressive strength by 48.3%.

3.4 Specified Compressive Strength (f_m):

Specified compressive strength (f_m) results of rubberized masonry hollow concrete block prism column shown in Figure 4 indicates a loss of strength by 74% with the reference prism column having a strength of 5.02N/mm^2 while 5, 10, 15, 20, and 25% rubberized masonry concrete block prism column have a strength of 4.72N/mm^2, 3.31N/mm^2, 3.23N/mm^2, 2.65N/mm^2 and 1.32N/mm^2 respectively. While conducting the compression test on the prism column, it was observed that the sides of prism columns were broken and several layers from the sides of the blocks were peeled off, which showed a larger deformation without complete disintegration and remained relatively intact after failure. The crumb-rubber aggregates were responsible for bridging the gap and keeping the broken parts together as one piece. This observation suggests a gradual change from brittle to more flexible behavior by using crumb-rubber aggregates. This may be attributed to the characteristics of crumb-rubber as it has great flexibility and the ability to stretch and rotate around its axes. Hence, rubber particles inside the mix seemed to act as springs causing a delay in widening the cracks [3]. This trend was more pronounced by increasing the content of crumb-rubber aggregate. [10] reported that using

crumb-rubber generally reduced the compressive strengths of the investigated un-grouted masonry prisms with ratios ranging from 31 to 71% proportional to the rubber content. The loss in strength can be attributed to factors which include: i) The large disparity between the Modulus of Elasticity (E) for rubber particles and the cement paste ii) The high Poisson ratio (v) for rubber particles, which may encourage premature cracking under load iii) Weak bonding characteristics in the ITZ between the cement paste and crumb-rubber particles [16].

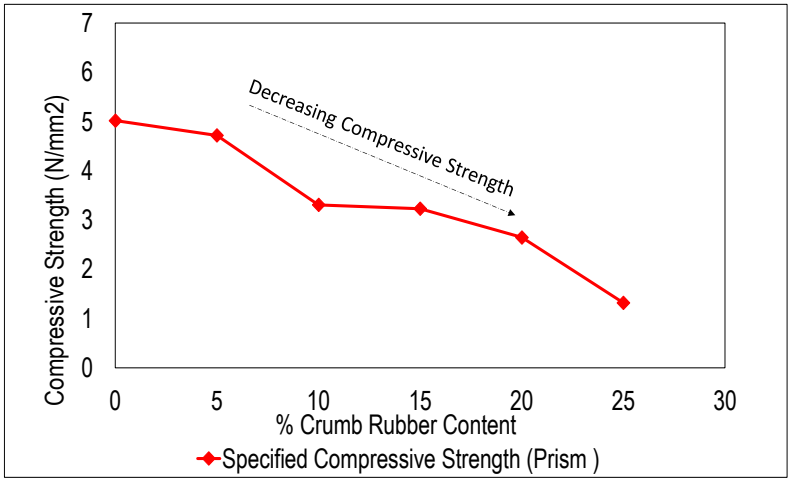

Figure 4: Specified Compressive Strength of Rubberized Masonry Hollow Concrete Block Prism Column Against % CR Content

3.5 Stress-Strain Behavior of Crumb-Rubber Masonry Concrete Block Prism Column

The stress-strain relationship of crumb-rubber masonry hollow concrete block prism column can be seen in Figure 5. The behavior indicates a convergent strength level and deformation criterion under compression loads for these concrete mixes. There was a linear increase in the stress of the reference and modified masonry hollow concrete block prism columns until reaching the maximum stress before releasing the energy by fracture. The stress-strain curves, in this case, are "sharp peaks" therefore the stress-strain relationships were considered to be quasi-linear. Furthermore, it can be noticed that increasing the crumb-rubber content has a significant effect on the maximum stress and strain of the masonry prism column. Nevertheless, a remarkable variation in the stress and deformation was observed between the reference mix and the modified mixes. This variation reached about 74% at the maximum stress with crumb-rubber content up to 25% as shown in Figure 5. The modified prism columns also revealed an increase in lateral and vertical (axial) strain up to 49% and 30% respectively at the maximum stress for the reference prism columns and crumb-rubber content up to 25%. This increase in the plastic strain translates into an increase in the toughness with a gradual failure and high-energy absorption capability [19]. The displacement-load relationship of the modified masonry concrete block prism columns as shown in Figure 6 revealed that the maximum axial loads at failure were 130.78kN for the reference prism column implying a corresponding vertical (axial) displacement of 0.00139 and lateral displacement of 0.00076. while the 5, 10, 15, 20, and 25% modified prism columns recorded maximum axial loads of 122.89kN, 85.89kN, 84.02kN, 69.13kN, and 34.28kN respectively with a corresponding ultimate displacement of 0.00180 for vertical and 0.00113 for lateral respectively with 25% crumb-rubber replacement which

indicates a percentage loss in the vertical strain of 22.8% and lateral strain of 38.7%. It can also be observed that the displacement-load relationships were quasi-linear.

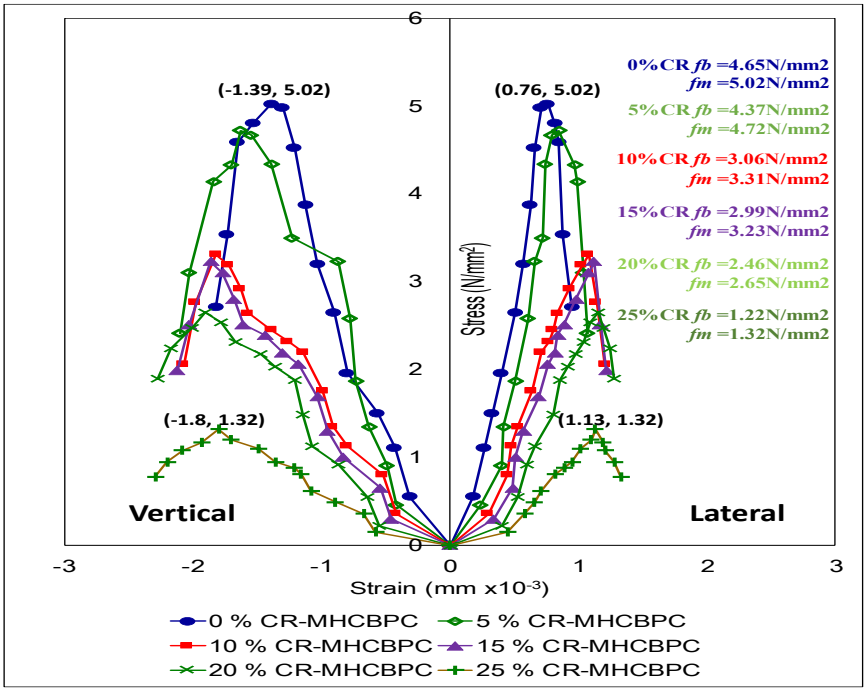

Figure 5: Stress-Strain Relationship for Masonry Concrete Prism Column

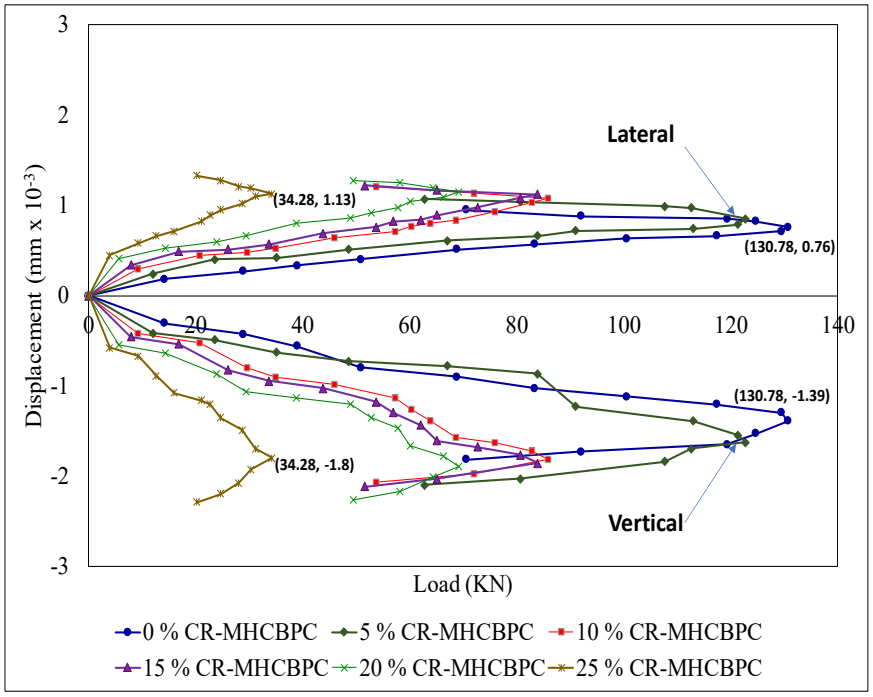

Figure 6: Displacement-Load Relationship for Concrete Prism Column

4. CONCLUSIONS

i. The compacting factor (C.F) of masonry concrete was observed to decrease significantly by 8.3%, the yield of fresh concrete mix increased slightly by 10.2%, and the density of masonry hollow concrete block unit reduced by 19% with 25% crumb-rubber content.

ii. Compressive strength of 9.43N/mm^2 was obtained for the reference mixes while the compressive strength of rubberized masonry hollow concrete block with 25% crumb-rubber content is 4.84N/mm^2 indicating a loss of strength by 49%. Despite the strength reduction, load-bearing rubberized masonry hollow concrete blocks can be produced with 15% crumb-rubber content which is above the minimum (7N/mm^2) requirement specified in BS EN 771-3. Also, Non-load bearing rubberized masonry hollow concrete blocks with strength above the minimum (>3N/mm^2) specified in BS EN 771-3 can be produced with crumb-rubber content ranging from 16% to 25% which makes the material viable for building applications.

iii. Specified compressive strength (f_m) of masonry concrete block prism column decreased in strength with increase in crumb-rubber content, a percentage loss of strength by 74% was recorded with the reference prism column having a strength of 5.02N/mm^2 while 5, 10, 15, 20 and 25% crumb-rubber modified masonry concrete block prism column recorded strength of 4.72N/mm^2, 3.31N/mm^2, 3.23N/mm^2, 2.65N/mm^2 and 1.32N/mm^2 respectively.

iv. The stress-strain relationship of crumb-rubber masonry concrete block prism column shows a quasi-linear relationship with an increase in the crumb-rubber content which has a significant effect on the maximum stress and maximum strain.

REFERENCES

[1] Adams, C., Lamborn, M., and Shuler, S. (1985). *"Asphalt-Rubber Binder Laboratory Performance".* Report FHWA/TX-8571, 347-1F, Texas Department of Public Transportation.

[2] Agence France-Press AFP (2016) www.spain4g.com/spain-tyre-dump-fire-sends-gaint-toxic-cloud-swamps-over-town-of-20000-people retried on 13/04/2016.

[3] Azmi, N. J. Mohammed, B.S and Al-Mattarneh, H.M.A. (2008). *"Engineering Properties of Concrete Containing Recycled Tire Rubber,"* ICCBT Universiti Tenaga Nasional.

[4] Dinoflex Rubber Reimagined (2012). *''Sustainable Design with Recycled Rubber Surfaces''* Online Course Materials. doi:10.1007/s11803-015-0030-5

[5] Epps, J.A. (1994). *''Uses of Recycled Rubber Tires in Highways.''* Synthesis of Highway Practice 198, Transportation Research, National Research Council, Washington, DC.

[6] Erdogan, S. O. Mohammed, L. and Umur. K. S. (2010). *"Compressive Strength Abrasion Resistance and Energy Absorption Capacity of Rubberized Concrete with and without slag".*

[7] Esch, D.C. (1984). "*Asphalt Pavement Modified with Coarse Rubber Particles*". Design, Construction and Ice Control Observations, Alaska Department of Transp and Public Facilities.

[8] Estakhri, C. (1990). "*Use, Availability and cost Effectiveness of Asphalt Rubber in Texas*". Research Report 1902-1f, Texas Transportation Institute, Texas A & M University System.

[9] Forrest M.J and Rapra. S (2014), *''Recycling and Re-use of waste Rubber''* by Smithers Rapra.

[10] Gheni A, Elgwady M and Myers J (2017) ''Cyclic Behaviour of Concrete Masonry Units Manufactured with recycled tires as an aggregate''. 13th CMS, Canada. June 4th -June 7^{th,} 2017.

[11] Gheni. A Elgwady M and Myers J (2017) ''Mechanical Characterization of Concrete Masonry Units Manufactured with Crumb Rubber Aggregate.'' ACI Materials Journal. 114 (01).

[12] Khatib, Z.K., and Bayomy, F.M. (1999). *''Rubberized Portland Cement Concrete''*, J.Mater. Civ. ENg., 10.1061/(ASCE)0899-1561(1999) 11:3(206), 206-213.
[13] Khosla, N.P., and Trogdon, J.T. (1990). "*Use of Ground Rubber in Asphalt paving mixtures*". Technical Report Department of Civil Engineering. North Carolina State University Raleigh.
[14] Mohammadi, I. (2014). *''Investigation on the Use of Crumb Rubber Concrete (CRC) for Rigid Pavements,'' the University* of Technology Sydney, Centre for Built Infrastructure Research.
[15] Mohammed, B.S., et al., ''Properties of Crumb rubber hollow concrete block.'' Journal of Cleaner Production, 2012.23(1): p.57-67.
[16] Najim, K.B. and M.R. Hall, (2010). *"A review of the fresh/hardened properties and applications for plain (PRC) and self-compacting rubberized concrete (SCRC),"* Construction and Building Materials, 24(11):2043-2051.
[17] Ocholi, A, Ejeh S.P and Sanni M.Y., (2014). ''An Investigation into the Thermal Performance of Rubber-Concrete'', Academic Journal of Interdisciplinary Studies MCSER Publishing, Rome-Italy Vol 3 No 5 July 2014 Doi:10.5901/ajis. 2014.v3n5p29.
[18] Ocholi, A, Sanni M.Y and Ejeh S.P., (2018). *''The impact resistance effect of partially replacing coarse aggregate with ground-rubber aggregate in concrete''*. Nigeria Journal of Technology (NIJOTECH) pp.330-337. http://dx.doi.org/10.4314/njt.v37i2.7.
[19] Sadek, D., (2015). *''Structural behavior of rubberized masonry walls,''* Journal of Cleaner Production 89 (2015) 174e186.
[20] Siddique, R. and Naik, T.R (2004). *"Properties of Concrete Containing Scrap Tire Rubber an Overview"* UMM CBU Report No. CBU-2002-06.
[21] Yang, Y. Chen, J., and Zhao, G. (2000). "*Technical Advance on the Pyrolysis of Used Tires in China,"* Dept. of Chem. Eng., Zhejiang University, Hangzhou, 310027, P.R. CHINA.
[22] Zhao Y, Wang FL (2015) Experimental studies on behaviour of fully grouted reinforced-concrete masonry shear walls. Earthq Eng Eng Vib 14(4):743–757.

EFFECT OF RECYCLED CRUSHED CONCRETE FINES ON DENSITY, SLUMP, STRENGTH AND ACCELERATED SHRINKAGE OF CONCRETE

Philemon A. Arito [(1)] and Fares Miri [(2)]

(1) Department of Civil and Environmental Engineering, University of Namibia

(2) Department of Civil Engineering, University of Cape Town

ABSTRACT

This paper discusses the effect of recycled crushed concrete fines (RCCF) with particle sizes less than 75 μm on concrete properties. Specifically, the effect of RCCF at 10% and 20% by mass of cement on the density, slump, compressive strength and accelerated drying shrinkage of laboratory-made concrete mixes was investigated. The mixes were cast with a fixed water:binder ratio of 0.50. The incorporation of RCCF reduced strength, density, slump and accelerated drying shrinkage. There was no statistically significant difference in the magnitude of accelerated drying shrinkage across the specimens with RCCF. Generally, the performance of the mix cast using 20% RCCF was significantly lower than the control mix. The incorporation of 10% RCCF, in comparison with the control mix, did not result in a significant reduction in density, compressive strength and accelerated shrinkage.

Keywords: recycled crushed concrete fines, construction and demolition waste, concrete, cement replacement.

1. INTRODUCTION

Notable strategies that have been used globally to mitigate the negative effects of increased cement consumption comprise the use of supplementary cementitious materials (SCMs) such as ground granulated blast furnace slag (GGBS) and fly ash (FA). SCMs produce concrete with improved durability and mechanical performance. Despite their superior performance, the declining steel production in Cape Town has resulted in fluctuations in the quantity of slag available for construction. Also, FA has become uneconomical due to high costs involved in freighting over long distances and the high carbon impact of coal combustion. It is evident, therefore, that the demand for fly ash and slag in Cape Town outstrips the supply - a situation that could potentially increase the cost of construction significantly in future. There is a need, therefore, to identify and investigate alternative cementitious materials that are affordable, readily available and in significant quantities to meet the long-term demand for construction with a minimum negative impact on the environment. Recycled crushed concrete fines (RCCF) from construction and demolition waste (C&DW) is such a material. The use of RCCF in concrete would also contribute to the efficient management of municipal solid waste [1–7].

Research on, and the use of, C&DW in concrete has been ongoing since the early 1940s [4, 5, 7–12]. Limited research, however, has been done on the use RCCF in concrete production [3, 5, 7, 12–14]. Shui et al [9], Oksri-Nelfia et al [3] and Prošek et al [6, 7] specifically report

that sub-sieve recycled concrete fractions are yet to be adopted in construction. Studies [1–3, 6, 7, 11–13, 15] have reported that the incorporation of RCCF in concrete and cement-based composites results in: reduced water demand for normal consistency, accelerated hydration of cement, negligible heat production during hydration, increased porosity and slump and reduced carbonation resistance and compressive strength. Contradictions have been reported on the effect of RCCF on slump, tensile strength and the overall fluidity of concrete [1, 3, 12, 13].

This paper presents the preliminary results from an ongoing study on the effect of RCCF on the following concrete properties: slump, density, compressive strength and accelerated drying shrinkage. The primary objective of this feasibility study is to assess the potential of RCCF as an SCM in concrete. This is one of the pioneer feasibility studies on the effect of RCCF in concrete cast using materials that are locally available in Cape Town and South Africa. The findings from this study will, therefore, inform future studies on the effect of RCCF on concrete cast using locally-available materials and the development of future guidelines on the use of RCCF in concrete.

2. METHODOLOGY

Three concrete mixes were designed and tested. The following materials were used:

i. CEM II B-M (L), 42.5 N: limestone content = 20%, clinker content = 80%, fineness = 3500 cm^2/g; density = 2790 kg/m^3.
ii. Dune sand: Fineness Modulus = 1.88, compacted bulk density = 1670 kg/m^3.
iii. Greywacke crusher sand: Fineness Modulus = 3.09, compacted bulk density = 1890 kg/m^3.
iv. 13 mm Greywacke stone: bulk density = 1500 kg/m^3, relative density = 2.71.
v. Recycled crushed concrete fines (abbreviated as RCCF hereafter): density = 2590 kg/m^3, particle size < 75 µm.

The mix designs are summarised in Table 1.

Table 1: Concrete mix designs

Mix component	Mix ID		
	Control (0% RCCF)	10% RCCF	20% RCCF
CEM II B-M(L) (kg/m^3)	450	405	360
RCCF (kg/m^3)	0	45	90
Water (l/m^3)	225	225	225
Dune sand (kg/m^3)	402.5	402.5	402.5
Greywacke crusher sand (kg/m^3)	402.5	402.5	402.5
13 mm greywacke stone (kg/m^3)	850	850	850
Water:binder ratio	0.50	0.50	0.50

Discarded laboratory-made concrete specimens of varying ages (older than 1 year) were mechanically crushed into small pieces using a hammer and a hydraulic compression machine. Utmost care was taken to minimise the inherent variability in the chemical composition of the discarded concrete by ensuring that they were from one source. The crushed concrete pieces were pulverised using a laboratory jaw crusher into fine powder. The powder extracts that

passed through the 75 µm sieve – i.e., RCCF - were collected for subsequent testing. The RCCF, dune sand and greywacke crusher sand were oven-dried at 105 ºC for 48 hours. Oven-drying was used to remove moisture. The oven-dried sands were left to cool for at least 4 hours and thereafter stored in cylindrical steel containers. The fineness modulus and grading of the dune and greywacke crusher sands was done according to ASTM C 136 [16]. The dune and greywacke crusher sands were blended at a ratio of 1:1. The density of aggregates was determined according to ASTM C 29 [17]. A water to binder (i.e., CEM II B-M(L) and RCCF) ratio – abbreviated as water:binder or w:b hereafter - of 0.50 was used. This water:binder ratio was deemed to be representative of conventional concrete. Three concrete mixes were cast: a control mix and two test mixes containing RCCF at replacement levels of 10% and 20% by mass of binder. The maximum replacement level of 20% was informed by past studies [1, 3, 9, 12, 15].

The dry materials – 13 mm greywacke stone, greywacke crusher sand, dune sand, cement and RCCF - were mass-batched and put in a 50-litre pan mixer. Thereafter, water was added to the dry mix in small increments after the mixer was switched on. The materials were mixed for five minutes. The slump of the freshly-cast concrete mixes was tested according to ASTM C 143 [18]. The test for slump was repeated thrice and the mean of three test results calculated. The slump test results are presented in Section 3.1. Test specimens were cast in standard moulds depending on the specifications for the particular test. A vibrating table was used to compact the freshly cast concrete mixes. The mixes, after compaction, were covered in a dark polythene sheet and left to harden in an undisturbed state in the laboratory (temperature = 21 ± 2 ºC; relative humidity 60 ± 5%) for 24 ± 8 hours. The hardened specimens were demoulded and water-cured in a bath maintained at 21 ± 3 ºC for 3, 7 or 28 days depending on the test. Three replicate specimens were cast and tested for each material property under investigation. Tests for density and compressive strength were done on 100 mm cube specimens while those for accelerated shrinkage were done on 100 x 100 x 200 mm prisms.

3. RESULTS AND DISCUSSIONS

3.1 Slump

The effect of RCCF on the slump of fresh concrete mixes is presented in Figure 1.

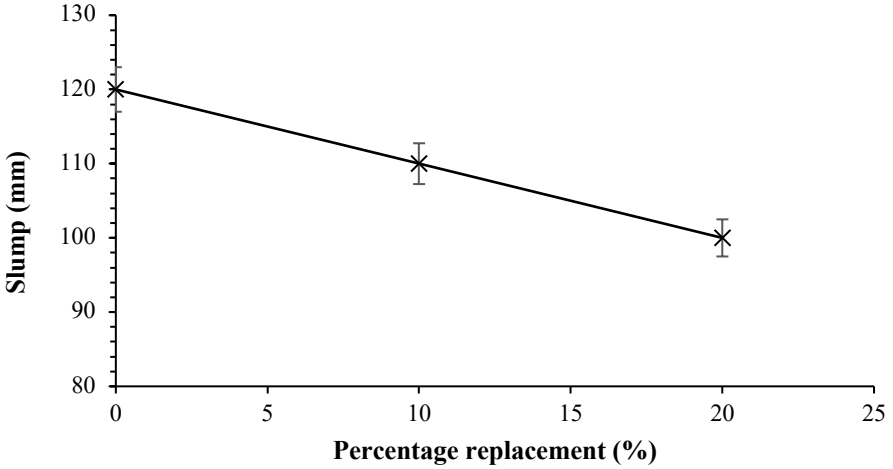

Figure 1: Slump of fresh concrete mixes

It can be observed, from Figure 1, that the incorporation of RCCF reduced slump significantly. The reduction in slump increased with an increase in RCCF content. This reduction has also been observed by other researchers [7, 12]. The observed reduction in slump could be attributed to the reduction in the volume of spherical cement particles due to their replacement with coarser RCCF particles. The coarse RCCF particles increase inter-particle friction during mixing and a corresponding reduction in slump. The reduction in slump could also be attributed to the high absorption of RCCF particles which would reduce the volume of water available for the lubrication of the concrete mix [3, 5]. Ma and Wang [1], while referring to other researchers, report that the surface of RCCF particles have pores which absorb water. The absorption of water in a mix would increase interparticle friction among the particles due to the reduction in water which acts as a lubricating agent. The increased friction would manifest as a reduction in slump. Prošek, et al [7] further attribute the reduction in slump in concrete containing RCCF to their high adhesion which results from their high specific surface area.

3.2 Density

The effect of RCCF on the density of the concrete is presented in Figure 2.

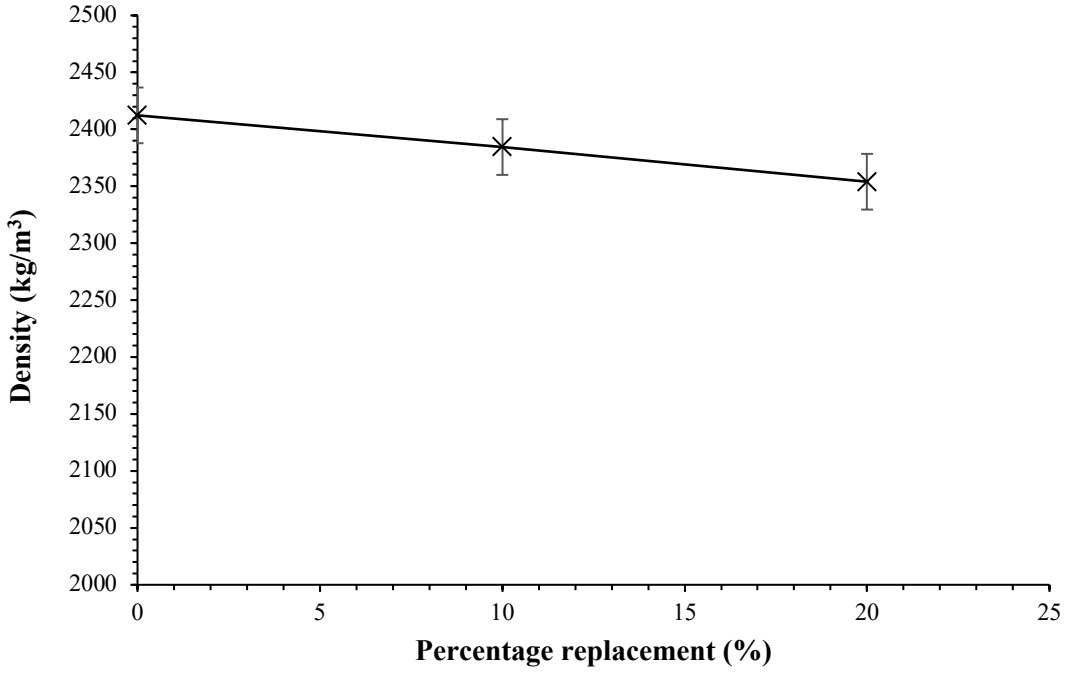

Figure 2: Density of concrete at various RCCF replacement levels

It can be observed, from Figure 2, that the incorporation of RCCF in concrete reduced its density. This observation is consistent with the findings of Lidmula et al [11]. The reduction in density, however, is not statistically significant. The observed reduction in density can be attributed to the reduction in the volume of cement paste. Cement particles were found to be denser (2790 kg/m^3) than RCCF particles (2590 kg/m^3). The partial replacement of cement with RCCF would thus result in a reduction in the density of concrete. Body et al [2, 13] and Prošek

et al [7] also report that the incorporation of RCCF increases porosity; with the porosity increasing with an increase in RCCF content. An increase in porosity due to the incorporation of RCCF would result in a reduction in density. From this result, it can be inferred that RCCF could find potential use in light-weight concrete construction.

3.3 Compressive strength

The compressive strength test results are presented in Figure 3.

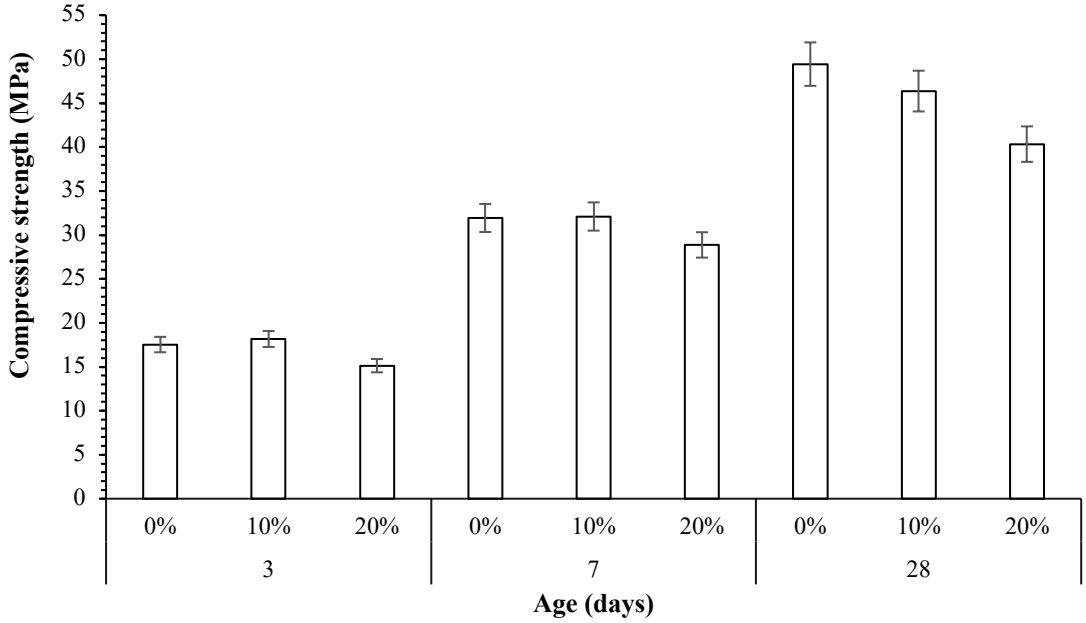

Figure 3: Compressive strength of concrete at various RCCF replacement levels

It can be observed that the replacement of cement with RCCF resulted in a reduction in compressive strength at all ages. Similar trends and observations have also been reported by other researchers [1, 3, 7, 11–13]. While studies by Prošek et al [7] and Oksri-Nelfia et al [3] report that the replacement of cement with 20-30% RCCF by mass of cement would not result in a significant change in properties; the test results from this study do not support their observations entirely. The results from this study, however, are consistent with the findings of Ma and Wang [1]. The replacement of cement with 20% RCCF reduced compressive strength significantly at all ages. However, the difference between the compressive strength of the control mix and the 10% RCCF mix at all ages was not statistically significant.

The observed reduction in strength due to the replacement of cement with RCCF could be attributed to the increased porosity of RCCF mixes [2, 6, 13], the low quantity of anhydrous cement in RCCF and the overall reduction in cement content in RCCF concrete mixes. A reduction in cement content results in a corresponding reduction in the volume of C-S-H formed during hydration [2]. A reduction in the volume of C-S-H, the main strength bearing component of concrete, results in a corresponding reduction in compressive strength. The reduction in strength, with all factors held constant, would be proportional to the reduction in cement content. Oksri-Nelfia et al [3] further report that the low anhydrous cement content in RCCF reduces the likelihood of hydraulic actions (and the formation of C-S-H) with would manifest as a reduction in strength.

3.4 Accelerated drying shrinkage

The test results for accelerated drying shrinkage are presented in Figure 4.

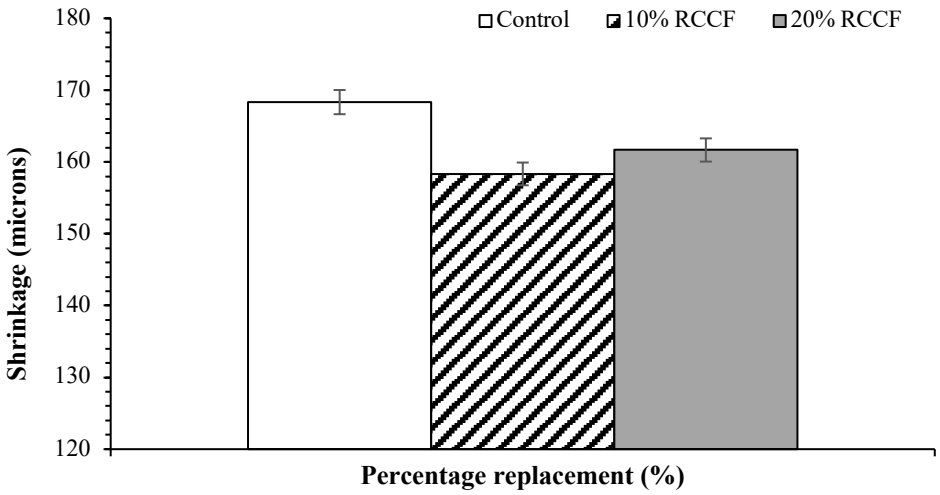

Figure 4: Accelerated drying shrinkage of concrete at varying RCCF content

From Figure 4, it can be observed that the incorporation of RCCF in concrete reduced accelerated drying shrinkage significantly in relation to the control mix. The reduction in shrinkage could be attributed to the reduction in the volume of cement paste which is usually responsible for shrinkage in concrete. Also, anhydrous and hydrated cement and crushed aggregate particles in RCCF could have provided internal restraint to the shrinkage of the paste. The recycled sand and hydrated cement particles within RCCF also act as microfillers which would reduce the porosity of interfacial transition zones [6, 7]. These microfillers would also result in a pore-blocking effect which reduces interconnectivity in the pores; and a consequent reduction in the rate of loss of moisture (i.e., shrinkage) from the concrete.

4. CONCLUSIONS

The following conclusions have been arrived at based on the test results from this study:

i. The replacement of cement with RCCF resulted in a significant reduction in slump. The reduction in slump increases with an increase in RCCF content.
ii. The replacement of cement with RCCF results in a reduction in density. This reduction, however, is not significant.
iii. The replacement of cement with 20% RCCF results in a significant reduction in compressive strength at all ages. The replacement of cement with 10% RCCF, however, does not result in a significant reduction in compressive strength at all ages.
iv. The replacement of cement with RCCF results in a significant reduction in accelerated drying shrinkage.

ACKNOWLEDGEMENTS

The authors wish to acknowledge with gratitude the following for financial support and materials for this research: Chryso SA, PPC, AfriSam, Sika (SA) Pty Ltd, and The Carnegie Corporation of New York

REFERENCES

[1] X. Ma, Z. Wang, Effect of Ground Waste Concrete Powder on Cement Properties, Adv. Mater. Sci. Eng. 2013 (2013) 1–5. https://doi.org/10.1155/2013/918294.

[2] A. Bordy, A. Younsi, B. Fiorio, S. Aggoun, Influence of drying conditions on hydration of cement pastes with substitution of Portland cement by a recycled cement paste fine., in: ICOME'16 Int. Conf. Mater. Energy, 2016: pp. 1–6.

[3] L. Oksri-Nelfia, P.-Y. Mahieux, O. Amiri, P. Turcry, J. Lux, Reuse of recycled crushed concrete fines as mineral addition in cementitious materials, Mater. Struct. 49 (2016) 3239–3251. https://doi.org/10.1617/s11527-015-0716-1.

[4] A. Pilipenko, S. Bazhenova, Usage of Crushed Concrete Fines in Decorative Concrete, in: IOP Conf. Ser. Mater. Sci. Eng., 2017: p. 032082. https://doi.org/10.1088/1757-899X/245/3/032082.

[5] A. Pilipenko, S. Bazhenova, A. Kryukova, M. Khapov, Decorative light transmitting concrete based on crushed concrete fines, in: IOP Conf. Ser. Mater. Sci. Eng., 2018: p. 032046. https://doi.org/10.1088/1757-899X/365/3/032046.

[6] Z. Prošek, V. Nežerka, R. Hlůžek, J. Trejbal, P. Tesárek, G. Karra'a, Role of lime, fly ash, and slag in cement pastes containing recycled concrete fines, Constr. Build. Mater. 201 (2019) 702–714. https://doi.org/10.1016/j.conbuildmat.2018.12.227.

[7] Z. Prošek, J. Trejbal, V. Nežerka, V. Goliáš, M. Faltus, P. Tesárek, Recovery of residual anhydrous clinker in finely ground recycled concrete, Resour. Conserv. Recycl. 155 (2020) 104640. https://doi.org/10.1016/j.resconrec.2019.104640.

[8] C. De Pauw, Reuse of building materials and disposal of structural waste material, 1994.

[9] Z. Shui, D. Xuan, H. Wan, B. Cao, Rehydration reactivity of recycled mortar from concrete waste experienced to thermal treatment, Constr. Build. Mater. 22 (2008) 1723–1729. https://doi.org/10.1016/j.conbuildmat.2007.05.012.

[10] E. Anastasiou, K. Georgiadis Filikas, M. Stefanidou, Utilization of fine recycled aggregates in concrete with fly ash and steel slag, Constr. Build. Mater. 50 (2014) 154–161. https://doi.org/10.1016/j.conbuildmat.2013.09.037.

[11] M. Lidmila, P. Tesárek, T. Plachy, Z. Rácová, P. Padevět, V. Nežerka, O. Zobal, Utilization of Recycled Fine-Ground Concrete from Railway Sleepers for Production of Cement-Based Binder, Appl. Mech. Mater. 486 (2013) 323–326. https://doi.org/10.4028/www.scientific.net/AMM.486.323.

[12] X. Kang, Y. Li, Effect of Recycled Fine Powder and Mineral Admixture on the Properties of the Cement Mortar, in: IOP Conf. Ser. Earth Environ. Sci., 2019: p. 012026. https://doi.org/10.1088/1755-1315/219/1/012026.

[13] A. Bordy, A. Younsi, S. Aggoun, B. Fiorio, Cement substitution by a recycled cement paste fine: Role of the residual anhydrous clinker, Constr. Build. Mater. 132 (2017) 1–8. https://doi.org/10.1016/j.conbuildmat.2016.11.080.

[14] L. Evangelista, J. de Brito, Durability of crushed fine recycled aggregate concrete assessed by permeability-related properties, Mag. Concr. Res. 71 (2019) 1142–1150. https://doi.org/10.1680/jmacr.18.00093.

[15] V. Letelier, E. Tarela, P. Muñoz, G. Moriconi, Combined effects of recycled hydrated cement and recycled aggregates on the mechanical properties of concrete, Constr. Build. Mater. 132 (2017) 365–375. https://doi.org/10.1016/j.conbuildmat.2016.12.010.

[16] ASTM, C 136: Standard Test Method for Sieve Analysis of Fine and Coarse Aggregates, 2006.

[17] ASTM, C29: Standard Test Method for Bulk Density ("Unit Weight") and Voids in Aggregate, 1997.

[18] ASTM, C 143: Standard test method for Slump of Hydraulic Cement Concrete, 2015.

SUSTAINABLE TREATMENT METHODS FOR RECYCLED CONCRETE AGGREGATE

Priyadharshini Perumal [(1)], Antti Korva [(1)] and Mamdouh Omran [(2)]

(1) Fibre and Particle Engineering Research Unit, University of Oulu, Finland.

(2) Process Metallurgy Research Group, University of Oulu, Finland.

ABSTRACT

For a reasonable use of recycled aggregate in concrete applications, it is important to consider methods that can enhance the quality of these aggregates. The European Union-funded (Kolartic CBC) project "DeConcrete" attempted to identify some eco-efficient technologies that can be used for reusing concrete waste in construction materials. In this regard, different treatment methods for recycled aggregates have been studied, including heat treatment through microwaving, carbonation, and pozzolanic coating. The treatment methods are carefully chosen such that minimum secondary waste is produced, and thus, maximum material is recycled. In this study, the water absorption capacity and dry density of the recycled aggregate were evaluated and compared with those of the treated aggregate. The carbonation method, which simply involved exposing the aggregate to CO_2, reduced the water absorption capacity by 10%. This method also facilitated CO_2 sequestration and made the material further sustainable and eco-efficient. Moreover, carbonation when applied after pozzolanic coating drastically boosted the interfacial transition zone of the concrete formed with recycled aggregate, which in turn increased the compressive strength. Hence, a combination of treatment methods is more effective than individual treatments. In particular, methods that do not produce any secondary waste yield the best results.

Keywords: recycled concrete aggregate, treatment, carbonation, pozzolanic coating, CO_2 sequestration

1. INTRODUCTION

In Europe, approximately 374 million tons of construction and demolition waste, excluding excavated soil, was produced in 2016 [1]. In Finland, out of the 800 metric tons of concrete recycled in earth constructions, approximately 200 metric tons is landfilled [2]. Although all the used concrete could be recycled for reuse with modern technology, approximately one-fourth of the concrete waste ended up in landfill sites, whereas the remaining was used in nonvalue-added applications. Thus, the application of effective concrete recycling on the field remains limited. One of the major reasons that hinder the recycling of concrete aggregate in the new concrete production is the decrease in the strength properties of the concrete [3,4]. Recycled concrete aggregate (RCA) incurs the major issue of adhered cement mortar from the old concrete, which is porous and increases water absorption in the concrete [5,6]. Moreover, the composition of these waste aggregates varies significantly, and their physical properties substantially influence the concrete properties [7]. According to RILEM recommendations,

only 20% of the recycled coarse aggregate can be used for new concrete production, whereas the recycled fine aggregate cannot be used for structural concrete production at all. Hence, enhancing the properties of recycled aggregates using various treatment methods is essential to extend their application range [8, 9].

The present study aims to determine the efficiencies of different treatment methods, such as abrasive action, carbonation, and microwaving, on RCA procured from the same demolition site in terms of the improvements achieved in RCA properties and the effects on the strength and water absorption capacity of the produced concrete.

2. MATERIALS AND METHODOLOGY

2.1 RCA

The recycled concrete used in this study was procured from a local Finnish building demolition site. The original material was a mixture of concrete and impurities such as metal pieces, plastic, and electric wires. Concrete pieces were carefully handpicked and crushed into 4–16-mm-diameter fractions by using a jaw crusher. Figure 1 shows the crushed RCA, which is ready to be treated.

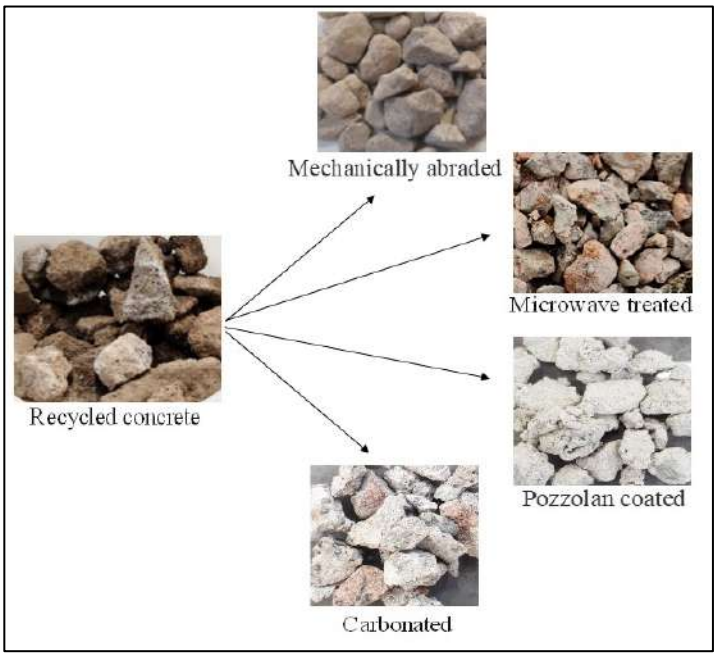

Figure 1: Treatment methods for the recycled concrete aggregate

2.2 Treatment methods

The treatment methods were designed to either remove the old mortar or to strengthen it. Removal of old mortar was facilitated through mechanical abrasion, which was performed using a bar mill (Wedag mill, 1 rpm, 300 s) without any crushing rod to avoid powdering of the recycled aggregate. The RCA was microwaved at 4 kW power and 2.45 GHz frequency for 600 s to loosen the old mortar. After the mechanical abrasion and microwave treatments, the treated RCA was sieved through a pore size of 4 mm to detach the old mortar from the parent material.

Two other treatments, pozzolanic coating and carbonation, were performed to strengthen the old mortar in the RCA. Pozzolanic coating was performed using a blast-furnace slag paste formed with a water-to-binder ratio of 2, where 1 kg of RCA was mixed with 1.2 l of the slag paste and maintained for 24 h. After this time, excess slurry was drained off and the coated RCA was sealed in a plastic bag until testing. Carbonation of RCA was performed under the conditions of 10% CO_2, 20°C temperature, and 60% relative humidity (RH) for 24 h. The RCA samples obtained from the four treatments are presented in Figure 1. In addition, a fifth treatment method was introduced, which combined pozzolanic coating with carbonation. In this treatment, the coated RCA sample obtained after 24 h was shifted to a carbonation chamber under the same conditions as those used for carbonation.

2.3 Tests conducted on RCA

The densities and water absorption capacities of the RCA samples were measured before and after the treatments. Density can be calculated as follows:

$$\rho = \frac{m}{V} \quad \textbf{Equation (1)}$$

where ρ is the density (kg/m^3), m is the mass of the RCA (kg), and V is the volume (m^3) of the container.

The water absorption capacity can be calculated as follows:

$$\text{Water absorption} = \frac{\text{wet weight} - \text{dry weight}}{\text{dry weight}} \times 100\% \quad \textbf{Equation (2)}$$

where dry weight represents the mass of RCA dried at 105°C for 24 h and wet weight indicates the mass of RCA obtained after 24-h water immersion.

2.4 Production of alkali-activated concrete

The treated and untreated RCA samples were used to produce one-part alkali-activated concrete with blast-furnace slag and sodium hydroxide, where the binder-to-aggregate ratio was fixed at 1:2. In addition, the slag-to-sodium silicate ratio in the binder was set as 9:1 based on previous studies [10, 11]. The aggregate was obtained as combination of 33% standard sand (fine aggregate) and 64% RCA (coarse aggregate). The water-to-binder ratio for different mixes was maintained constant at 0.35. Cubical specimens of dimensions 15 cm × 15 cm × 15 cm were developed to measure the compressive strength and water absorption capacity on the 7th day of curing age. The specimens were cured in a humidity chamber at 20°C and 100% RH until testing. The samples broken after the strength testing were preserved in isopropanol to be observed using a scanning electron microscope (SEM). The samples were mounted in epoxy resin and polished for SEM studies.

3. RESULTS AND DISCUSSION

3.1 Properties of RCA

The water absorption capacity of the concrete was found to be reduced with some of the treatments adopted, such as mechanical abrasion and carbonation (Figure 2). However, this was not the case for all methods, especially microwaving and pozzolanic coating. Mechanical abrasion removed some of the old mortar responsible for increased water absorption in RCA. In contrast, the microwave treatment loosened the old mortar but did not detach it from the aggregate. This can be the reason behind the increased absorption observed in microwaving. However, this contradicts the results obtained for a previous study conducted using microwave

heating of RCA, which yielded approximately 1.4% reduction in water absorption capacity and a corresponding increase in density [12]. Thus, a combination of microwaving with mechanical abrasion was expected to yield improved performance.

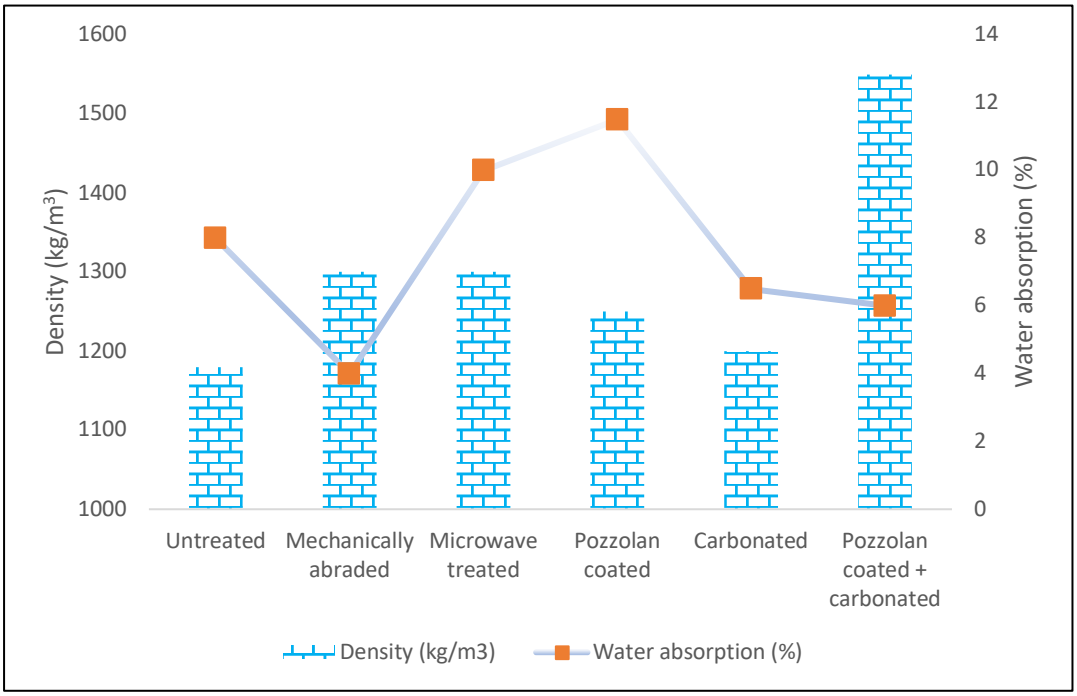

Figure 2: Properties of recycled concrete aggregate

Meanwhile, the pozzolan-coated RCA exhibited increased absorption values, which indicates that the applied pozzolan was not sufficiently hydrating and highly porous. This can be explained by the type of pozzolan used in the present study, as blast-furnace slag requires a co-binder for its activation. Hence, the coating enhanced the porosity of the aggregate, which resulted in increased water absorption. However, the density of the coated RCA was higher than that of the untreated RCA (Figure 2). Previous studies on RCA coating have shown significant improvement in concrete properties, though the properties of coated aggregate have not been reported [13, 14]. In contrast, the carbonation of RCA significantly reduces the water absorption capacity. It strengthens the old mortar by forming calcium carbonate products, which seals the porosity of the mortar [15]. Thus, the combination of pozzolanic coating and carbonation performs well in reducing the water absorption capacity, which is also reflected in the increase in density (Figure 2).

3.2 Properties of RCA

The compressive strength of the untreated and treated RCA samples is related to the aggregate properties discussed in section 3.1 (Figure 3). Mechanical abrasion improved the concrete strength by 17%, though there was no significant difference in the water absorption capacity. As expected, the microwave-treated and pozzolan-coated samples exhibited 14% and 28%, respectively, reduction in concrete strength. Although the water absorption capacity of the microwave-treated RCA increased substantially (Figure 3), this was not reflected in the

water absorption capacity of the concrete produced with them. The strength of carbonated RCA increased by 21% (34 MPa), and even 42% (40 MPa), through the combination of microwave treatment with pozzolanic coating. According to previous research, pozzolanic slurry coating improved the workability of the concrete, whereas carbonation improved its the strength and durability properties [8]. Thus, the present study emphasized that RCA should be subjected to combined treatments to yield the benefits of different mechanisms involved in the different treatment methods.

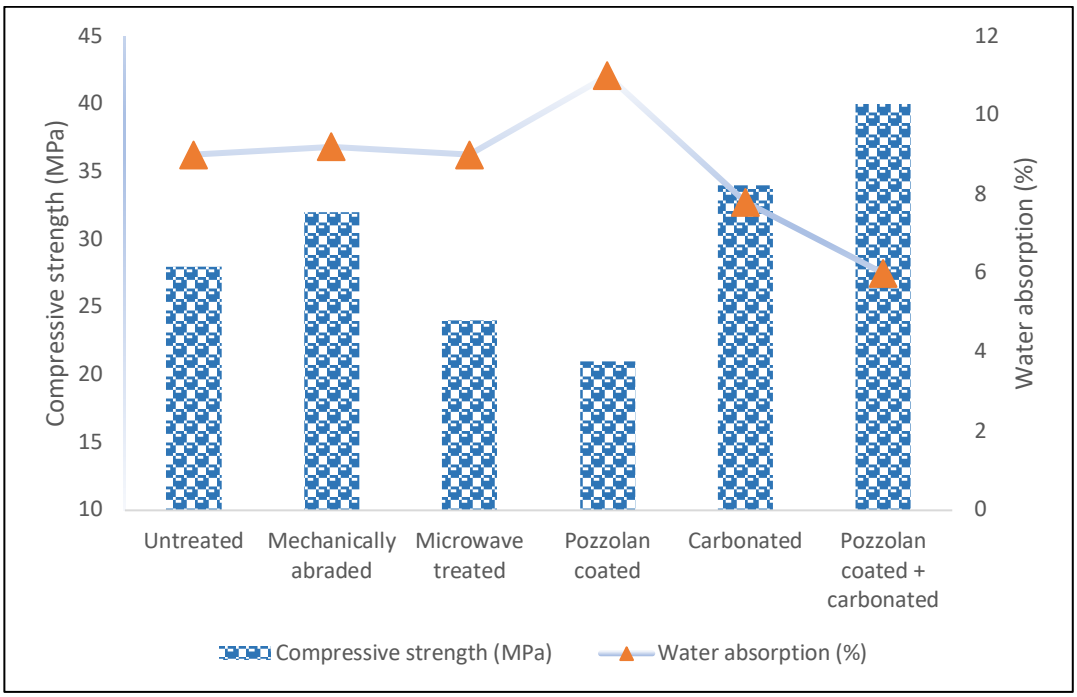

Figure 3: Properties of concrete with RCA

The representative microstructure of the untreated RCA sample showed a clear interfacial transition zone (ITZ) between the old and new mortar regions (Figure 4). Although ITZ disappeared in the treated RCA, pozzolan-coated RCA showed an extra layer between the new and old mortar regions (Figure 4d). This layer should be the coating which should densify the old mortar in RCA whereas, it resulted in an extra layer affecting the strength and water absorption values negatively. The microwave-treated RCA showed mending of the old mortar in the RCA region, however with a highly porous microstructure which explains the issue of increased absorption in this mix (Figure 4c). RCA carbonation improved the uniformity in the microstructure (Figure 4e, 4f) by strengthening the old mortar with calcium products formed by CO_2. Thus, pozzolanic coating enhanced the reaction and improved the binding of old and new mortar regions, resulting in a more uniform microstructure (Figure 4f). This explains the high strength achieved with carbonation alone and its combination with different coating methods.

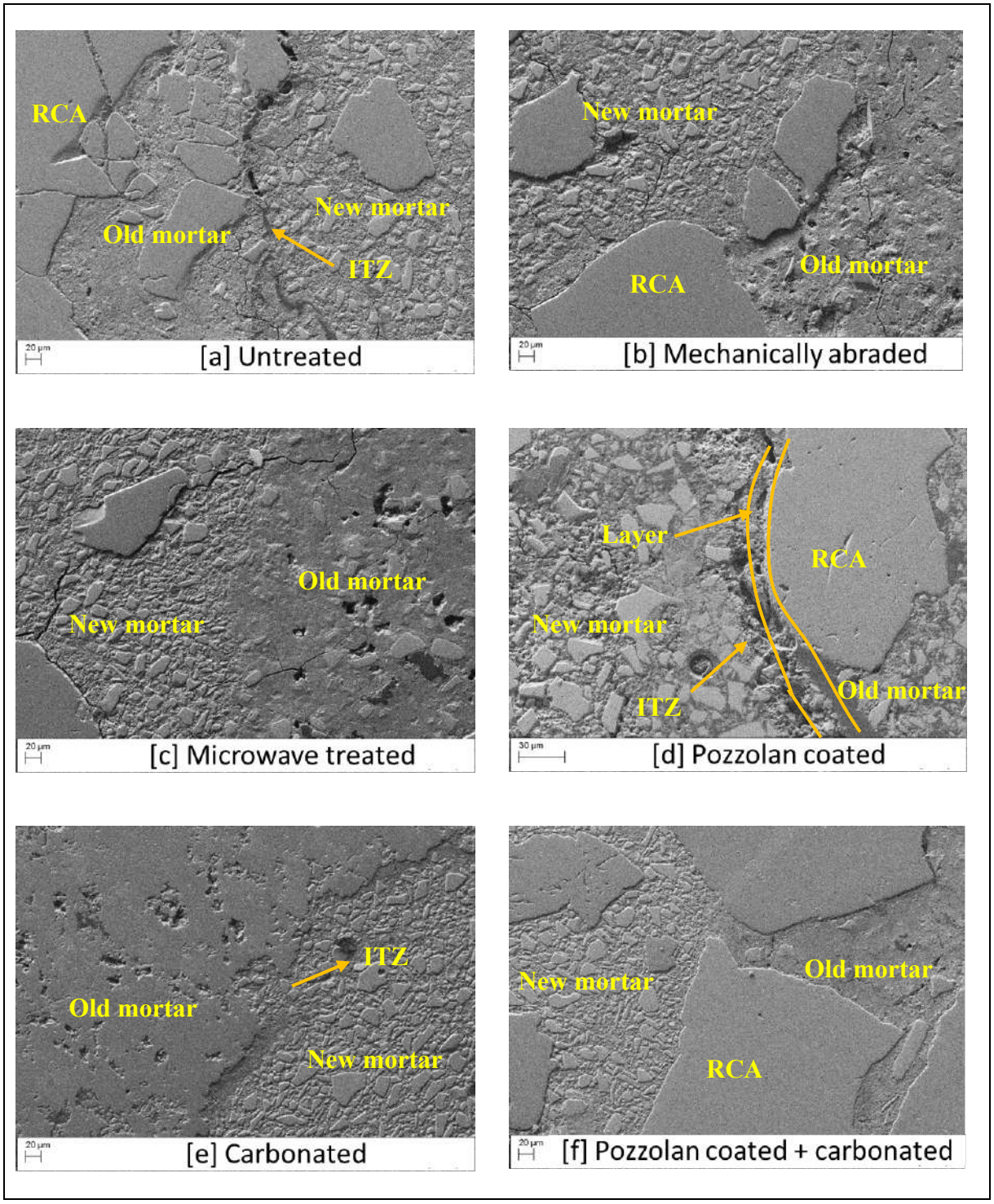

Figure 4: Representative microstructure of concrete produced with RCA

4. CONCLUSIONS

In this study, different RCA samples obtained from a single source were treated using the following four treatment methods: mechanical abrasion, microwave treatment, pozzolan coating, and carbonation. To understand the effects of different combinations of treatment methods, carbonation was attempted on pozzolan-coated RCA samples. Among the different treatments, carbonation appeared promising for improving the RCA performance. Carbonation products filled the pores in the old mortar region of the RCA, which helped in improving the ITZ between the old and new mortar regions. This was reflected in the strength improvement of the concrete formed of carbonated recycled concrete. Pozzolanic coating did not perform well when applied alone; however, its combination with carbonation outperformed other methods. Hence, it is worthy to attempt different combinations of treatment methods to utilize their benefits.

ACKNOWLEDGEMENTS

The authors acknowledge the financial support received for the project, Deconcrete [grant # KO 4068: eco-efficient arctic technologies cooperation] funded by Kolarctic CBC initiative of European Union.

REFERENCES

[1] EEA, Construction and Demolition Waste : challenges and opportunities in a circular economy, 2020.https://www.eea.europa.eu/publications/construction-and-demolition-waste-challenges/at_download/file.

[2] Betoniteollisuus ry, säästää ympäristöä ja luonnonvaroja, 2010.

[3] M. Behera, S.K. Bhattacharyya, A.K. Minocha, R. Deoliya, S. Maiti, Recycled aggregate from C&D waste & its use in concrete - A breakthrough towards sustainability in construction sector: A review, Constr. Build. Mater. 68 (2014) 501–516.

[4] C. Hoffmann, S. Schubert, A. Leemann, M. Motavalli, Recycled concrete and mixed rubble as aggregates: Influence of variations in composition on the concrete properties and their use as structural material, Constr. Build. Mater. 35 (2012) 701–709.

[5] J.M.V. Gómez-Soberón, Porosity of recycled concrete with substitution of recycled concrete aggregate: An experimental study, Cem. Concr. Res. 32 (2002) 1301–1311.

[6] A. Katz, Properties of concrete made with recycled aggregate from partially hydrated old concrete, Cem. Concr. Res. 33 (2003) 703–711.

[7] V. Spaeth, A. Djerbi Tegguer, Improvement of recycled concrete aggregate properties by polymer treatments, Int. J. Sustain. Built Environ. 2 (2013) 143–152.

[8] C. Shi, Z. Wu, Z. Cao, T.C. Ling, J. Zheng, Performance of mortar prepared with recycled concrete aggregate enhanced by CO2 and pozzolan slurry, Cem. Concr. Compos. 86 (2018) 130–138.

[9] B. Zhan, C.S. Poon, Q. Liu, S. Kou, C. Shi, Experimental study on CO2 curing for enhancement of recycled aggregate properties, Constr. Build. Mater. 67 (2014) 3–7.

[10] T. Luukkonen, Z. Abdollahnejad, J. Yliniemi, P. Kinnunen, M. Illikainen, Comparison of alkali and silica sources in one-part alkali-activated blast furnace slag mortar, J. Clean. Prod. 187 (2018) 171–179.

[11] P. Perumal, T. Luukkonen, P. Kinnunen, M. Illikainen, Design of ultra-high performance one-part geopolymer concrete with particle packing technology Ultra-High Performance Concrete with One-part Alkali- Activated Slag, in: 39th Cem. Concr. Sci. Conf., 2019.

[12] A. Akbarnezhad, K.C.G. Ong, M.H. Zhang, C.T. Tam, T.W.J. Foo, Microwave-assisted beneficiation of recycled concrete aggregates, Constr. Build. Mater. 25 (2011) 3469–3479.
[13] D. Kong, T. Lei, J. Zheng, C. Ma, J. Jiang, J. Jiang, Effect and mechanism of surface-coating pozzalanics materials around aggregate on properties and ITZ microstructure of recycled aggregate concrete, Constr. Build. Mater. 24 (2010) 701–708.
[14] J. Li, H. Xiao, Y. Zhou, Influence of coating recycled aggregate surface with pozzolanic powder on properties of recycled aggregate concrete, Constr. Build. Mater. 23 (2009) 1287–1291.
[15] C. Liang, B. Pan, Z. Ma, Z. He, Z. Duan, Utilization of CO2 curing to enhance the properties of recycled aggregate and prepared concrete: A review, Cem. Concr. Compos. 105 (2020) 103446.

STRENGTH, DURABILITY AND MICROSTRUCTURE OF CONCRETE MADE USING WASTE ELECTRICAL AND ELECTRONIC PLASTIC AS PARTIAL REPLACEMENT FOR THE NATURAL AGGREGATE IN CONCRETE

Lewis A. Parsons [(1)] and Sunday Nwaubani [(1)]

(1) School of Civil and Environmental Engineering, University of the Witwatersrand

ABSTRACT

Electronic waste (e-Waste) is the waste product derived from electrical and electronic equipment (EEE) which has reached its end of life. Although South Africa is one of the largest generators of e-Waste in Africa at 5.7kg/inhabitant, only 11% is recycled while a mere 25% of the plastic fraction termed waste electrical and electronic plastic (WEEP) is recycled per annum. This is due to the fact that WEEP contains a wide range of polymers and heavy elements at different stages of degradation. Thus, recycling of WEEP as replacement material for the natural aggregate in concrete can be advantageous. The aim of this research was to produce structural concrete with a minimum compressive strength of 25MPa at 28 days of curing while replacing both the coarse and fine natural aggregates simultaneously with different types of granulated WEEP in increments of 0%, 5%, 10%, 20% and 30% by volume while maintaining a constant w:c ratio of 0.52. The paper reviews the material and mineralogical properties, microscopy analysis of hardened concrete, compressive and tensile splitting strength and durability. Results showed that replacements of 30% WEEP attained the minimum compressive strength requirements while achieving acceptable water sorptivity and oxygen permeability indices.

Keywords: aggregate, concrete, durability, strength, waste electrical and electronic plastic.

1. INTRODUCTION

South Africa is one of the largest generators of e-Waste in Africa at 5.7kg/inhabitant/annum which is much compared to Africa's average e-Waste generation of 1.9kg/inhabitant/annum [1]. More troubling is the fact that only 11% of South Africa's annual e-Waste is recycled and that e-Waste volumes are expected to grow by 10% per annum [2]. This growth rate is influenced by: social and economic development, increased consumer demand, perceived obsolescence and shorter replacement cycles among others (ibid). Electrical and electronic plastic (EEP) is the plastic fraction used for insulation, noise reduction, sealing, housing, structural parts and functional parts in electrical and electronic equipment (EEE) and contributes to on average 30% by weight. The most common plastic types found in EEP include: acrylonitrile butadiene styrene (ABS), polypropylene (PP), polystyrene (PS), polycarbonate (PC) and polyurethane (PU) which represents more than 70% of plastics found in EEE.

On the other hand, waste electrical and electronic plastic (WEEP) is the plastic fraction derived from EEP once it has reached its end of life. Sadly, the recycling of WEEP is very low at recycling percentages of less than 25% per annum globally [3]. This may be due to the difficulties faced when recycling WEEP such as: numerous amounts of additives incorporated into EEP (cadmium, chlorine, antimony and brominated flame-retardant compounds), insufficient labelling of EEP according to its plastic type and the wide range of different types of resins used [4]. Furthermore, in both the use and recycling phase the polymers in EEP degrade resulting in plastics with unpredictable and insufficient properties [5]. As such, alternative methods must be investigated to utilise this problematic plastic waste.

One industry in which the use of WEEP is currently being considered, is in the construction sector. Previous studies have shown that the use of WEEP as a partial replacement for aggregates in concrete is possible. However, inconsistent or incomplete results were found among some literature. Lakshmi and Nagan conducted *Studies on Concrete Containing e-Plastic Waste* and found a significant decrease in the compressive strength of the control mix at 25% replacement of the coarse natural aggregate with WEEP dropping from 19.8MPa to 6.2MPa [6]. Liu *et al.*, investigated the *Performance of Recycled Plastic-Based Concrete* by replacing 20% of the fine natural aggregate with PC/ABS WEEP and found a decrease in the compressive strength from 44.7MPa to 28.6MPa [7]. It is clear that although some research has been conducted in the use of WEEP as replacement material for the natural aggregate, very little has been researched pertaining to the microscopy, strength and durability of concrete made using different types of WEEP as aggregate replacement material.

2. EXPERIMENTAL

2.1 Materials used

2.1.1 Binder material

A high strength, rapid hardening ordinary Portland cement (CEM I 52.5 R) was used as binder material in this study. Table 1 and 2 present the chemical oxide composition and characteristics of the cement.

The chemical oxide composition was determined by the author using a CAMECA SX5-FE electron probe micro analyser. The mean particle size was determined using an Anton Paar PSA 1190 particle size analyser while the specific density and surface was determined using a Pentrapyc 5200e gas pycnometer and NOVAtouch LX gas sorption analyser.

Table 1: Chemical oxide composition of Portland cement.

Chemical oxide composition (%)	Al_2O_3	CaO	Fe_2O_3	MgO	SiO_2
	1.01	67.05	0.68	1.23	23.52

Table 2: Characteristics of Portland cement.

Characteristics of Portland cement	Mean particle size (μ)	Specific density (g/cc)	Specific surface (m^2/g)
	16.199	3.632	1.934

2.1.2 Admixture

The superplasticiser Sika®ViscoCrete®-3088 was used in this study which is chemically based on an aqueous solution of modified polycarboxylate ethers.

2.1.3 Aggregates

This study used both the fine and coarse (13.2mm) crushed natural aggregate as well as granulated WEEP. Granulated ABS, chemically blended PC and ABS (PC/ABS) and high impact polystyrene (HIPS) WEEP was bought from e-Waste recycling companies in Gauteng, South Africa. The granulated WEEP used had a maximum size of 6.7mm. Fig. 1 provides a sample representation of the granulated ABS, PC/ABS and HIPS WEEP used while Fig. 2 presents the images of the aggregates surface topography at 5 000 times magnification using a Carl Zeiss Sigma Field Emission Scanning Electron Microscope (FESEM).

Figure 1: Granulated WEEP.

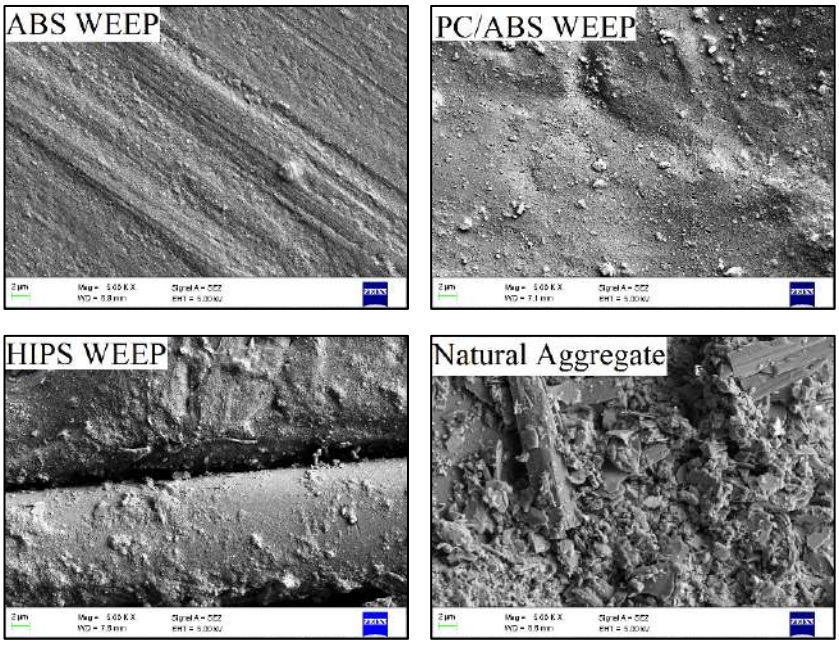

Figure 2: SEM imaging of the aggregates surface topography at 5 000 times magnification.

Table 3 presents the chemical compositions of all the different WEEP types used. The data was determined by the author using a CAMECA SX5-FE electron probe micro analyser. It is clear that ABS WEEP contained heavy elements in its polymetric matrix, namely: bromine (Br) and antimony (Sb), both of which are used as a flame retardant in EEP. Table 4 presents the particle density (SANS 5844), bulk density (SANS 5845), fineness modulus and dust content (SANS 1083) [8] [9] [10].

Table 3: Granulated WEEP elemental composition.

WEEP type	Normal weight (%) of elements						
	C	O	Cl	Br	Sb	N	Total
ABS	77.19	3.26	1.76	14.49	3.30	0.00	100
PC/ABS	91.65	1.03	0.00	0.00	0.00	7.33	100
HIPS	81.47	17.55	0.97	0.00	0.00	0.00	100

Table 4: Aggregate physical properties.

Physical properties	Stone	Sand	ABS	PC/ABS	HIPS
Particle density (kg/m³)	2 890	2 580	940	1 190	1 390
Bulk density (kg/m³)	1 660	2 060	520	580	580
Fineness modulus	-	3.4	-	-	-
Dust content (%)	2.1	8.3	-	-	-

2.2 Concrete mix design

The mix design replaced both the coarse and fine natural aggregate simultaneously by volume in percentages of 5%, 10%, 20% and 30% with either ABS, PC/ABS, HIPS or an equal blend of WEEP in a ratio of 1:1:1 using a water:cement (w:c) ratio of 0.52 and a superplasticiser to maintain a slump of 80mm $\pm$ 25mm. Figure 3 provides a description for the acronyms used to describe the mix designs presented in Table 5.

The natural aggregate and cement were added to a 50L pan mixer. In the use of WEEP as replacement for the natural aggregate, WEEP was added before the stone. This was done to prevent the granulated WEEP from bouncing out of the pan during the initial mixing. The dry materials were mixed for approximately 2 - 3 minutes, after which the potable water was added.

The fresh concrete was mixed for approximately 2 - 3 minutes. A slump test was performed according to SANS 5862-1 [11]. If the mix did not have a slump of 80mm ± 25mm, a superplasticiser was added directly into the fresh concrete and mixed for 1 - 2 minutes. Once the desired slump was achieved, compaction was carried out using a vibrating table. Concrete cube moulds were filled with approximately one third fresh concrete. They were then vibrated for approximately 5 - 8 seconds, after which they were filled with another third of the cubes volume and vibrated again.

It should be noted that replacing 30% of the natural aggregate with different types of WEEP by volume will vary the overall density of the mix design. This is because WEEP have different particle size densities as shown in Table 4.

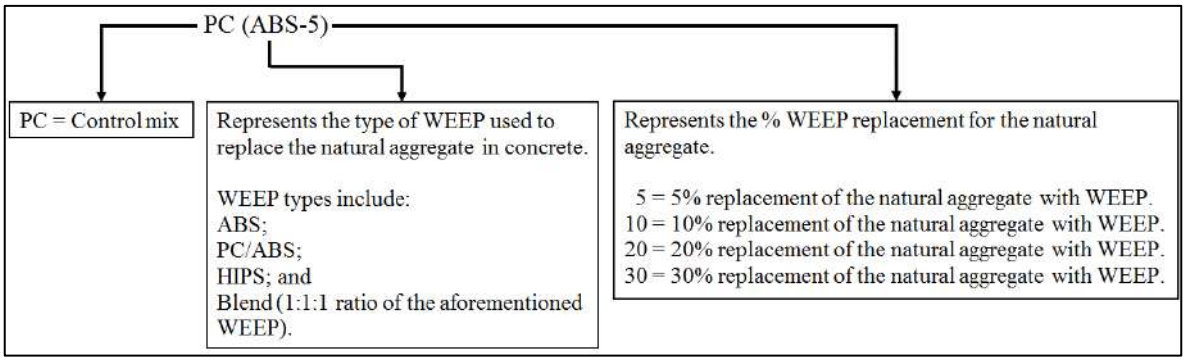

Figure 3: Mix design acronyms and meanings.

Table 5: Mix design.

Mix design	Sand	Stone	WEEP	Water	Cement	Total mass	Super-plasticiser	Slump
	kg/m³						% cement	mm
PC (Control)	931	706	0	231	444	2 312	0.00	80
PC(ABS-5)	908	688	14			2 285	0.00	75
PC(ABS-10)	884	671	28			2 259	0.00	70
PC(ABS-20)	838	635	57			2 205	0.09	65
PC(ABS-30)	791	600	85			2 152	0.16	68
PC(PC/ABS-5)	908	688	18			2 292	0.00	80
PC(PC/ABS-10)	884	671	36			2 272	0.00	80
PC(PC/ABS-20)	838	635	72			2 232	0.00	55
PC(PC/ABS-30)	791	600	108			2 193	0.12	55
PC(HIPS-5)	908	688	21			2 289	0.00	75
PC(HIPS-10)	884	671	42			2 266	0.00	75
PC(HIPS-20)	838	635	84			2 220	0.04	60
PC(HIPS-30)	791	600	126			2 174	0.12	60
PC(Blend-5)	908	688	18			2 289	0.00	65
PC(Blend-10)	884	671	36			2 266	0.00	65
PC(Blend-20)	838	635	71			2 219	0.06	60
PC(Blend-30)	791	600	107			2 173	0.18	65

2.3 Interfacial transition zone

The interfacial transition zone (ITZ) is often the weak link in concrete and is formed during compaction of fresh concrete whereby a film of water forms around the aggregate, leading to higher w:c ratios close around the aggregate [12]. Fig. 4 provides imaging of the ITZ between the natural aggregate in PC (Control) and WEEP in PC(Blend-30) at 5 000 times magnification. The ITZ is noticeable by the clear dark-sheath band between the natural aggregate and hardened cementitious paste (HCP) for PC (Control). Between the ABS WEEP and HCP there were numerous crystal formations as indicated by "1". These crystals were formed during the hydration process, whereby calcium hydroxide (CH) formed between the aggregate and bulk paste when critical saturation was reached due to the dissolution of calcium silicate, forming calcium and hydroxyl ions. CH grew into very large plate like crystals due to the excess water

around the aggregate producing a more porous system. As the hydration process continued these pores were filled with poorly crystallised calcium silicate hydrates, small crystals of ettringite and CH formed between the framework [12].

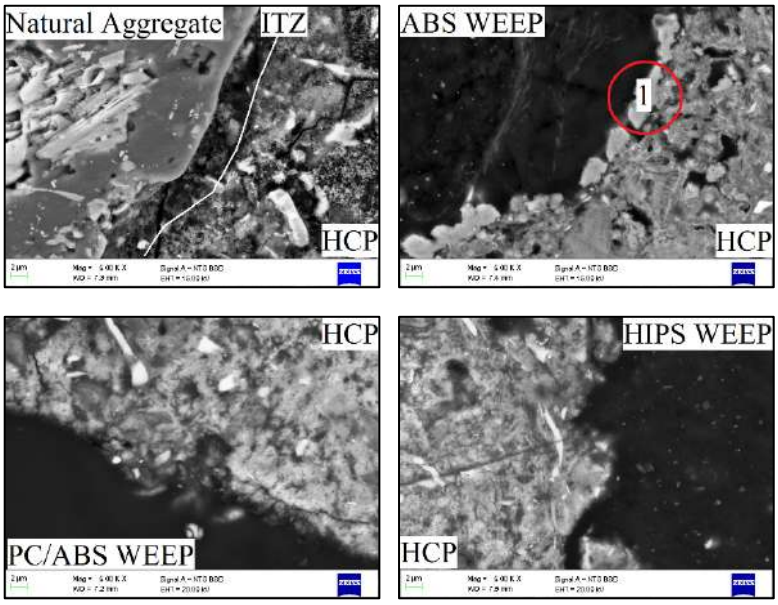

Figure 4: ITZ between aggregates used and the HCP.

3. RESULTS AND DISCUSSION

3.1 Hardened concrete properties

Concrete cubes of size 100 x 100 x 100 mm were cast for both the compressive and durability tests. Concrete cylinders of size of 150 x 300 mm were cast for the tensile splitting strength tests. The specimens were water cured at a temperature of 23°C $\pm$ 2. The compressive strength tests were performed at 3, 7, 28 and 90 days at 0%, 5%, 10%, 20% and 30% WEEP replacements while the tensile splitting strength and durability tests were performed at 28 days at 30% WEEP replacement.

3.1.1 Compressive strength results

The concrete cubes were tested in accordance to SANS 5863 [13]. The cubes were loaded using a cube press-foote machine which had a maximum loading capacity of 1 000kN. Fig. 5-8 compares the average compressive strengths of PC (Control mix) at different ages of curing, types of WEEP and percentage replacement levels.

The compressive strength of the mixtures containing WEEP were observed to decrease as the percentage of substitution increased. Furthermore, it is interesting to note that there was little difference in the compressive strength of concrete made with WEEP at 20% replacement. However, there was a large drop in strength for concrete made using ABS WEEP at 30% replacement.

Furthermore, it was found that replacements of 30% ABS WEEP continued to significantly reduce the compressive strength of PC (Control mix) by 55.1%, Blend WEEP by 37.7%, HIPS WEEP by 32.4% and PC/ABS WEEP by 32.0%. This could be as a result of the crystal

formation between the ABS WEEP and HCP reducing the bond between the HCP and ABS WEEP which in turn reduced the compressive strength more compared to other mixes.

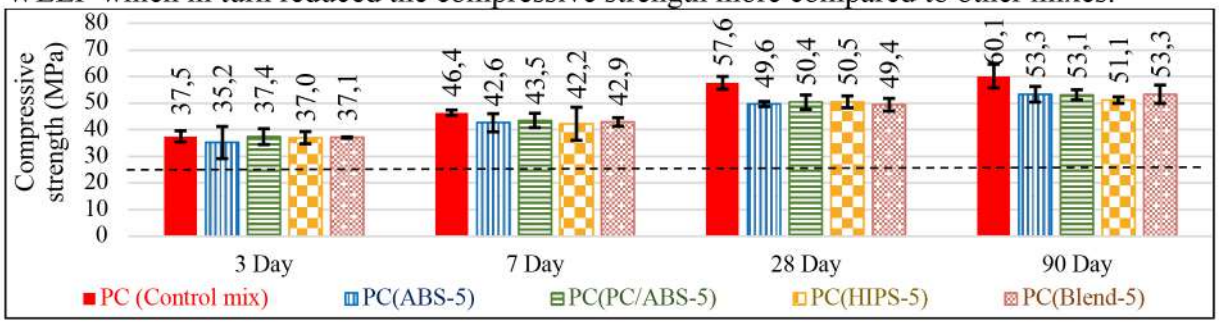

Figure 5: Compressive strength results at 3, 7, 28 and 90 days curing at 5% replacement.

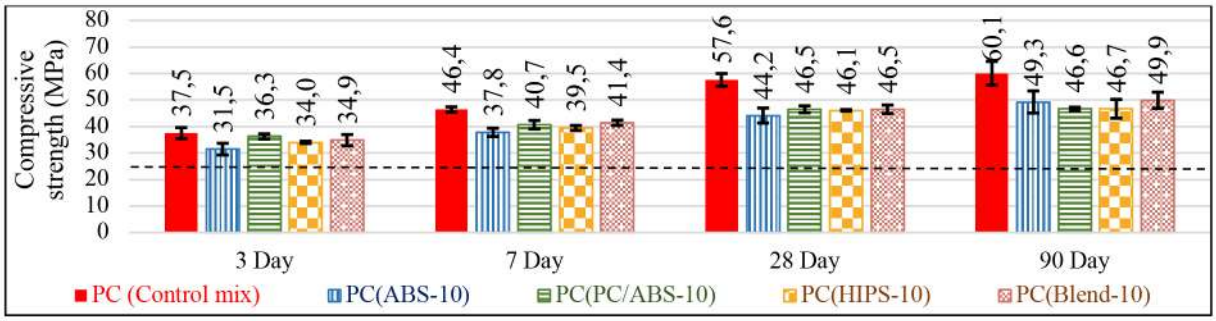

Figure 6: Compressive strength results at 3, 7, 28 and 90 days curing at 10% replacement.

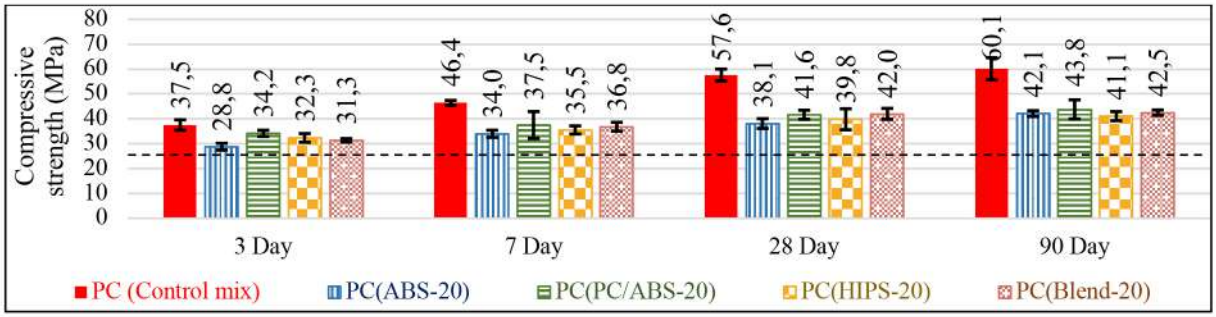

Figure 7: Compressive strength results at 3, 7, 28 and 90 days curing at 20% replacement.

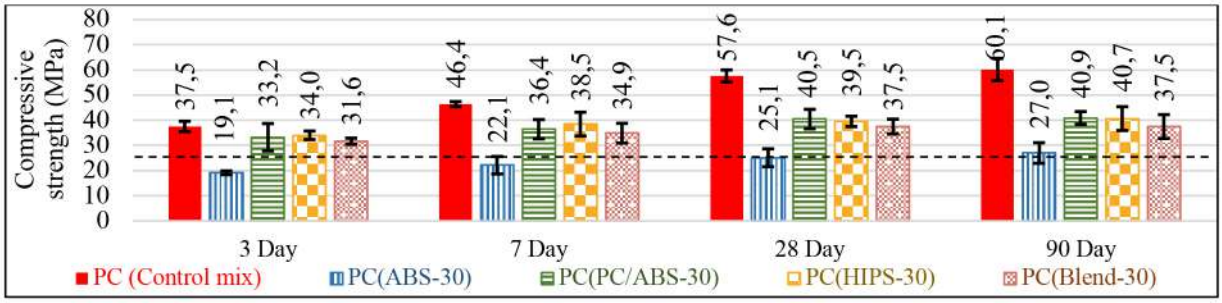

Figure 8: Compressive strength results at 3, 7, 28 and 90 days curing at 30% replacement.

3.1.2 Tensile splitting strength results

The tensile splitting strength test was conducted according to SANS 6256 [14]. The cylinders were loaded using an Amsler machine which has a maximum loading capacity of 2 000kN. The tensile splitting strength test results are presented in Fig. 9. It was observed that the tensile splitting strength of concrete made without WEEP replacement had a higher tensile splitting strength compared to concrete made with WEEP replacement.

There was little difference in the average tensile splitting strength between substitutions of HIPS or Blend WEEP. As with the average compressive strength of concrete, replacements with ABS WEEP yielded the lowest average tensile splitting strength results.

Here it is clear that ABS WEEP substitution decreased the average tensile splitting strength of concrete mixed with ABS WEEP the most at 14.4%, followed by Blend WEEP at 10.7%, HIPS WEEP at 10.2% and PC/ABS WEEP at 7.9%.

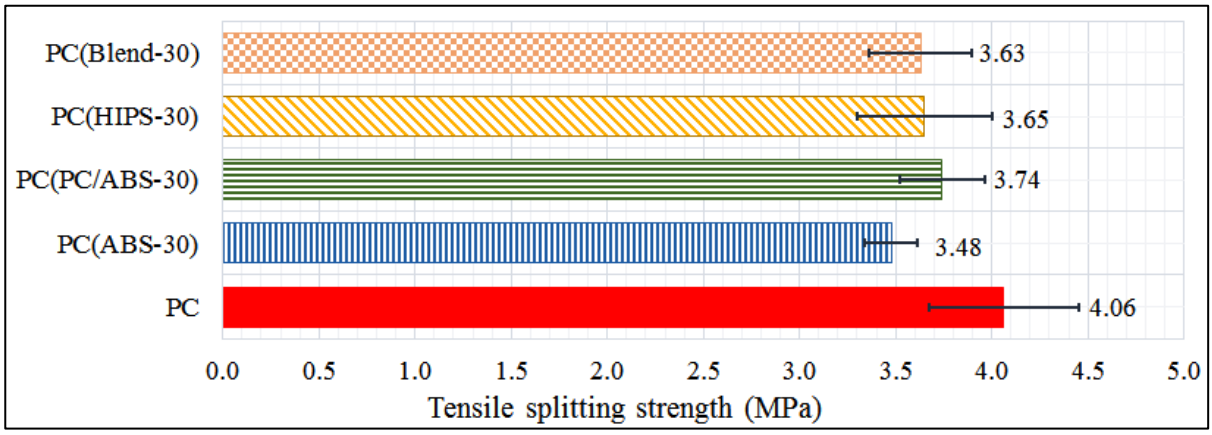

Figure 9: Tensile splitting strength results at 28 days.

3.2 Durability of concrete

3.2.1 Concrete durability indices

The durability of concrete in South Africa can be measured by the oxygen permeability index, water sorptivity and porosity, and chloride conductivity tests and should meet the acceptable limits for durability indexes [15], as presented in Table 6.

Table 6: Suggested ranges for durability of concrete [15].

Durability class	OPI (log scale)	Sorptivity (mm/√h)	Chloride conductivity (mS/cm)
Excellent	> 10	< 6	< 0.75
Good	9.5 - 10	6 - 10	0.75 - 1.50
Poor	9.0 - 9.5	10 - 15	1.50 - 2.50
Very poor	< 9	> 15	> 2.50

3.2.2 Oxygen permeability index

The oxygen permeability index (OPI) test was conducted according to SANS 3001-CO3-2 [16]. The average OPI results are graphically illustrated in Fig.10. All mixes had average OPI-values > 9.5, indicating a good durability class.

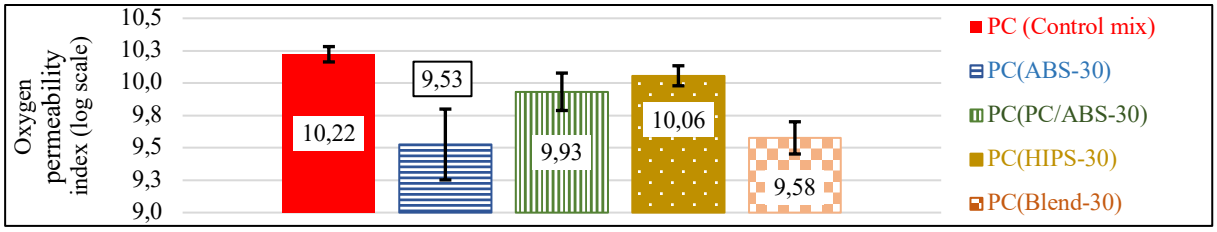

Figure 10: OPI for concrete containing no WEEP and containing 30% WEEP.

3.3.3 Water sorptivity

The water sorptivity test was conducted in accordance to the Durability Index Manual [17]. The average water sorptivity results are shown in Fig 11. It was observed that the water sorptivity decreased with an increase in WEEP replacements. This indicated that the overall durability class increased for the majority of concretes made using WEEP.

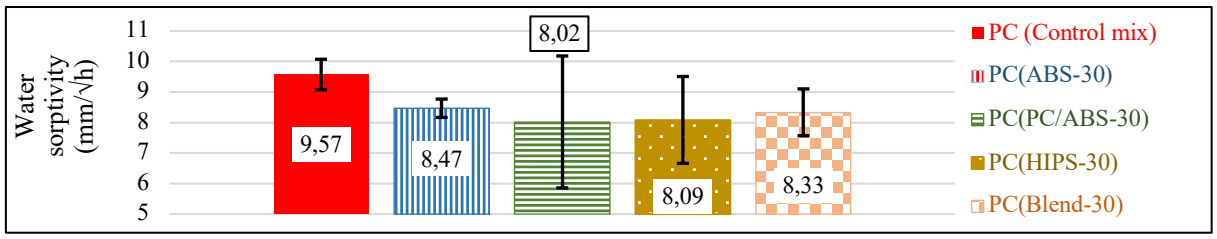

Figure 11: Water sorptivity for concrete containing no WEEP and containing 30% WEEP.

3.3.4 Chloride conductivity

The chloride conductivity test was conducted according to SANS 3001-CO3-3 [18]. The average water sorptivity results are graphically presented in Fig 12. Results clearly show that ABS WEEP had the overall highest chloride and is classified as having poor durability.

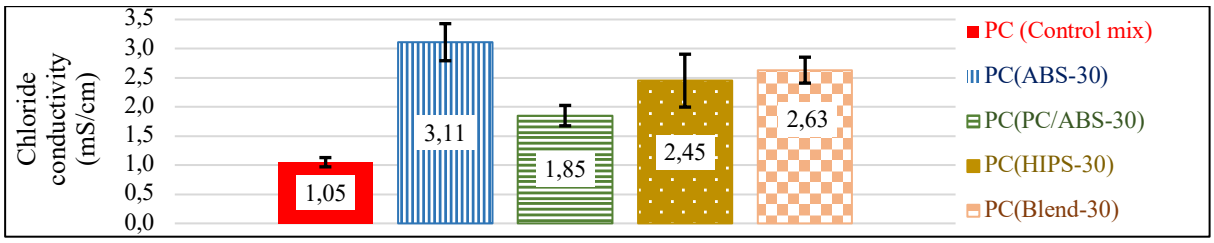

Figure 12: Chloride conductivity for concrete containing no WEEP and containing 30% WEEP.

4. CONCLUSION

The increase in EEE has resulted in vast quantities of WEEP discarded with no intention of re-use. This study has confirmed that ABS, PC/ABS, HIPS and an equal combination of the aforementioned WEEP can be used to partially replace both fine and coarse aggregates up to 30% and attain the minimum compressive strength requirements for structural concrete (> 25MPa) at 28 days. Replacement of WEEP for the natural aggregate reduced the compressive strength of concrete at 28 and 90 days while replacements of 30% ABS WEEP significantly decreased the compressive and tensile splitting strength of concrete the most. Concrete made using WEEP at 30% replacement for the natural aggregate had a good or higher durability result in the OPI and water sorptivity tests but poor or lower durability result in the chloride conductivity test.

ACKNOWLEDGEMENTS

The authors are grateful for the donations of cement and natural aggregate from AfriSam, superplasticiser and condensed silica fume from Sika and metakaolin from Kaolin-Group and Serina Trading Company. The authors acknowledge Anton Paar for testing the cement particle size, surface area and relative density. Lastly, the authors are grateful for the financial support from the Post Graduate Merit Award of the University of the Witwatersrand.

REFERENCES

[1] C. Baldé, V. Forti, V. Gray, R. Kuehr and P. Stegmann, "The Global e-Waste Monitor," *United Nations University, International Telecommunication and International Solid Waste Association,* 2017.

[2] M. Lydall, W. Nyanjowa and Y. James, "Mapping South Africa's Waste Electrical and Electronic Equipment (WEEE) Dismantling, Pre-Processing and Processing Technology Landscape," vol. 7574, Johannesburg, Gauteng: Mintek, 2017.

[3] S. Lundstedt, "Recycling and Disposal of Electronic Waste," Swedish Environmental Protection Agency, Bromma, 2011.

[4] P. Mahesh, P. Rajankar and V. Kumar, Improving Plastic Management in Delhi. A Report on WEEE Plastic Recycling, New Delhi: Toxics Link, 2012.

[5] E. Stenvall, Electronic Waste Plastics Characterisation and Recycling by Melt-processing, Gothenburg, Sweden: Department of Materials and Manufacturing Technology: Chalmers University of Technology, 2013.

[6] R. Lakshmi and S. Nagan, "Studies on Concrete Containing e-Plastic Waste," *International Journal of Environmental Sciences,* vol. 1, no. 3, pp. 270-281, 2010.

[7] F. Liu, Y. Yan, L. Li, C. Lan and G. Chen, "Performance of Recycled Plastic-Based Concrete," *Journal of Materials in Civil Engineering,* pp. A4014004-1-A4014004-9, 2015.

[8] SANS:5844, Particle and relative densities of aggregates, 2.2 ed., Pretoria, Gauteng: South African Bureau of Standards, 2014.

[9] SANS:5845, "Bulk densities and voids content of aggregates," 2.1 ed., Pretoria, Gauteng: South African Bureau of Standards, 2006.

[10] SANS:1083, "Concrete Tests-Aggregates From Natural Sources-Aggregates for Concrete," 2.4 ed., Pretoria, 2014.

[11] SANS:5862-1, "Concrete Tests. Consistence of Freshly Mixed Concrete: Slump Test," 2.1 ed., Pretoria, Gauteng: South African Bureau of Standards, 2006.

[12] Z. Li, Advanced Concrete Technology, Hoboken, New Jersey: JOHN WILEY & SONS, INC., 2011.

[13] SANS:5863, "Concrete Tests — Compressive Strength of Hardened Concrete," 2.1 ed., Pretoria, Gauteng: South African Bureau of Standards, 2006.

[14] SANS:6253, "Concrete Tests — Tensile Splitting Strength of Concrete," 1.1 ed., Pretoria, Gauteng: South African Bureau of Standards, 2006.

[15] M. Alexander, J. Mackechnie and Y. Ballim, "Use of Durability Indexes to Achieve Durable Cover Concrete in Reinforced Concrete Structures," *Materials Science of Concrete,* 2011.

[16] SANS:3001-CO3-2, "Part CO3-2: Concrete durability index testing — Oxygen permeability test," Pretoria, Gauteng: South African Bureau of Standards, 2015.

[17] Durability Index Manual, University of Cape Town, 2017.

[18] SANS:3001-CO3-3, "Part CO3-3: Concrete durability index testing — Chloride conductivity test," Pretoria, Gauteng: South African Bureau of Standards, 2015.

CAPILLARY PRESSURE MEASUREMENT OF CRUMB-RUBBER MASONRY CONCRETE BLOCK

Sanni M. Yinka [(1)], Leonard N Dugguh [(1)] and Laraiyetan E. Taiye [(2)]

(1) Department of Civil Engineering, Ahmadu Bello University, Zaria, Kaduna State, Nigeria

(2) Department of Civil Engineering, Kogi State Polytechnic, Lokoja, Kogi State, Nigeria

ABSTRACT

This paper experimentally investigates the capillary pressure and porosity of masonry concrete block containing waste tyre (crumb-rubber) with varying ratios ranging from 0 - 25%, which was used to partially replace coarse aggregate (granite) by volume. The bulk density of masonry concrete decreased by 5.4% with crumb-rubber content up to 25%. Porosity (*f*) of masonry concrete (24 hours water absorption, vacuum saturation, satiation, and vacuum satiation porosity) increased with an increase in crumb-rubber content. The capillary pressure test result for both the initial and refined (modified) method shows a rapid increase from 0% to 5% before gradually increasing with a further increase in crumb-rubber content up to 25%. The average capillary pressure value for the reference masonry concrete using the initial and refined method is 0.166MPa and 0.128MPa while the modified concrete with 25% crumb-rubber particles recorded 0.289MPa and 0.233MPa respectively indicating 74% and 82% increase respectively. Generally, the increase in capillary pressure can be directly linked to the increase in voids in the composite matrix which also increased the porosity. These results signify an increase in the capacity of modified masonry concrete to absorb water through the capillary rise.

Keywords: crumb-rubber; masonry concrete; capillary pressure and porosity

1. INTRODUCTION

Increasing amounts of solid waste materials are being investigated across the world to supplement natural components of typical building mixes, like concretes and mortars, due to environmental reasons. According to [8] each year about 9 million tonnes of waste rubber-tyres are disposed of all over the world, which was also estimated to be around 1 billion tyres withdrawn from use in the world annually. Based on 2018 statistics with a 15% annual generation rate, it is estimated that around 37 million waste tyres exist in Nigeria [6]. In Nigeria one of the most common ways of disposing of waste tyres is through open field disposal, open-air combustion most especially in our abattoir and the local commercial quarry where they serve as a source of fire for processing slaughtered animals and mining activities [5]. Many researchers have studied and developed various recycling methods for the re-use of waste tyres in construction materials [9].

Al-Sakini [1] has characterized crumb-rubber aggregate from end-of-life waste automobile tyres to have a low specific gravity (0.95 kg/m3), small water absorption (2-4%), low thermal

conductivity (0.14W/mk) high dynamic modulus and damping properties and high resistance to weather (i.e non-biodegradable).

Masonry concrete in form of concrete blocks is becoming widely accepted as a construction material in our buildings, hence the partial replacement of mineral aggregates with rubber-tyre particles having low water absorption in concrete blocks would be a very good and promising way to utilize the large quantities of waste rubber-tyres. The use of waste rubber-tyres particles in masonry hollow concrete blocks would not only make good use of such waste materials by converting waste into a resource but could help to enhance some masonry hollow concrete blocks inherent properties such as water absorption. Masonry concrete blocks are porous material that interacts with the surrounding environment; their durability depends largely on the movement of water and gas as it flows through it.

Capillary pressure is the energy required to transfer a unit mass of liquid from a partially saturated porous material to a reservoir of the same liquid at the same temperature and elevation [2]. Porosity and saturated permeability do not tell the whole story of water transport in porous materials. Water movement in porous building materials is almost completely driven by the action of capillary forces. [3] described a new experimental method of measuring directly the capillary pressure Ψ of a wetting front. They showed that the capillary pressure is a material property and it defines the effective strength of the capillary forces that drive the absorption in a porous material. The method measures the equilibrium pressure of the air displaced and compressed ahead of the advancing wetting front. The pressure of air trapped in the wetted region is taken as the capillary pressure of absorption, using the assumptions of the ideal gas law.

The objective of this study is to investigate the bulk density, porosity, and capillary pressure of the reference masonry concrete compared to the modified crumb-rubber masonry concrete.

2. MATERIALS AND METHODOLOGY

2.1 Material

Crumb-rubber masonry concrete consists of cement, natural aggregate (fine and coarse), crumb-rubber from waste tyre, and water as shown in Figure 1. A general-purpose blended limestone portland cement CEM II (42.5R MPa) that conforms to BS EN 197-1:2011 with a specific gravity (*G)* of approximately 3.15 was sourced from a retail outlet and used for this study. Ordinary tap water (potable drinking water) sourced from Civil Engineering Laboratory was used for all concrete mixes and curing. Natural sharp river quartzite sand smaller than 4.76mm but larger than 75μm that is free of clay, loam, dirt, and any organic or chemical matter with average specific gravity (saturated surface dry) of 2.65 and bulk density of 1,454 kg/m^3 was used as fine aggregate.

Figure 1: Crumb-Rubber Aggregate Used for Concrete Mix

Natural crushed (granite) with nominal maximum sizes of 9.52-10mm and sourced from a local commercial quarry with a specific gravity of 2.66 and bulk density of 1635kg/m3 was used as coarse aggregate. Coarse rubber aggregate (crumb-rubber) from scrap tyres with nominal maximum sizes of 4 - 9mm, the specific gravity of 1.14 and bulk density of 528 kg/m3 was used for this research. Crumb-rubber surface treatment method by soaking in sodium hydroxide (NaOH) solution was adopted for this research due to its effectiveness in enhancing the hydrophilic properties of the rubber and increasing the intermolecular interaction forces between rubber and calcium silicate hydrate (C-S-H) gel which enhances the strength of the composite matrix as reported by [4]. Two-kilogram (2kg) of Solid Caustic Soda (NaOH, Caustic Soda Pearls/Crystals ≥ 99.0%) was dissolved in 10 liters of water to form liquid caustic soda also called saturated sodium hydroxide solution (NaOH) with a concentration of 10% and pH of 14. Crumb-rubber particles were soaked in the saturated sodium hydroxide solution and stirred regularly to guaranty a uniform treatment of rubber particles for 24 hours under ambient conditions. The crumb-rubber particles were removed and washed with tap water and kept in laboratory condition for 24 h before use.

2.2 Mix Proportions

The mix design for the masonry concrete and crumb-rubber modified masonry concrete adopted was based on the absolute volume method according to BS EN 206:2013+A1:2016. Based on a preliminary estimate of the concrete mix design, a mix ratio of 1:1.5:3 with water/cement ratio of 0.42 and aggregate/cement ratio of 4.5:1 was used to produce a trial mix which was tested for compacting factor, strength, density and eventually subjected to adjustment before adopted and applied to all the concrete mixes. A total number of six (6) mixes were prepared: One control mix and five concrete mixes in which the 9.52-10 mm granite was replaced by crumb-rubber aggregate (4 - 9mm) at 5%, 10%, 15%, 20% and 25% by volume. The mix proportions were constant in terms of mix design ratio, water/cement ratio, sizes, type of natural and crumb rubber-tyre aggregate used for the study.

2.3 Sample Preparation

The sets of hardened masonry concrete blocks prism samples used in this work with dimensions 160 x 40 x 40mm, were derived from masonry hollow concrete blocks using a masonry cutting machine as shown in Figure 2.

Figure 2 : Masonry Concrete Samples for Water Absorption Coefficient Test

2.4 Experimental Procedures

(a) Bulk Density:

The bulk density of masonry concrete was determined from the eighteen (18) sample cured, oven-dried and heated until a constant weight was achieved. It was then cooled in a desiccator and weighed to the accuracy of 0.0018 after which they were transferred to a beaker and heated for 30 min to release the trapped air. They were cooled and the soaked weight (w) was measured. They were suspended in a beaker containing water placed on a balance. The suspended weight was taken and the bulk density was calculated from Equation 1:

$$\text{Bulk Density} = \frac{\rho w}{w - s}, Kg / m^3 \qquad \textit{Equation} \textbf{ (1)}$$

Where: w = Soaked weight, s = Suspended weight, and ρ = Density of water.

(b) Vacuum Saturation Porosity (*f*) Test:

Total accessible open porosity (*f*) was measured using this method as detailed in RILEM, CPC 11.3, and [7], although it is not a standard test method. In this method, the block was dried to constant mass at 70 °C ± 5 °C before being allowed to cool and weighed. The volume was determined. The eighteen (18) sample (average of three per test) was then placed in a vacuum chamber shown in Figure 3 which was connected by a hose to a rotary vacuum pump capable of producing a vacuum of ≈100 kPa. The chamber was evacuated and pumping was continued for 30 minutes. After which water was drawn into the vacuum chamber. When the sample had become fully immersed in the water drawn, the hose was removed from the water and air allowed to enter the vacuum tank so that atmospheric pressure forces water into the evacuated pores of the blocks. After 24 h of soaking the sample was removed from the water and weighed.

Figure 3: Vacuum Saturation Porosity (*f*) Test

The vacuum saturation porosity *(f)* was then calculated using Equation 2.

$$f' = \frac{\text{volume of water absorbed}}{\text{volume of sample}} \times 100\% \qquad \textit{Equation} \textbf{ (2)}$$

(c) Water Absorption (24 Hours Soak) Porosity (W_m) Test:

The water absorption porosity test was determined according to BS EN 772-21:2011. The eighteen (18) masonry concrete samples were dried to constant mass and allowed to cool to ambient temperature before being weighed and the dry mass (m_d) was recorded. Then they were placed on small pads in a tank of water at room temperature to allow water to be in contact with all faces. The masonry concrete blocks were left submerged for the desired time (24h in this study) then taken from the tank and surplus water is removed from their surfaces using a damp

cloth. They were weighed and the wet mass (m_w) was recorded. W_m was determined using Equation 3:

$$W_m = \frac{m_w - m_d}{m_d} \times 100 \qquad \textit{Equation (3)}$$

Where: m_w = mass of the wet sample, m_d = mass of the dry sample
The percentage was calculated at soaking times of 1min, 9 min, 25 min, 1 h, and 24 h.

(d) Satiation Porosity (f') Test:

The satiation porosity also known as effective porosity was determined from one-dimensional capillary absorption using a simple procedure of measurement with only one weighing needed at the point when the water has reached the top face of the sample. Eighteen (18) blocks were dried at 70 °C to constant mass, allowed to cool to ambient temperature, their volume determined before they were weighed and the dry mass recorded. They were placed on their bed faces on small pads in a tank to an immersion depth of approximately 5 mm of water at room temperature to allow water to be absorbed from the bed face only until the water reached the top of the block. They were then taken from the tank, surplus water removed using a damp cloth, weighed and the wet mass was recorded and converted to volume. f' is equally calculated from Equation 4.

$$f' = \frac{\text{volume of water absorbed}}{\text{volume of sample}} \times 100\ \% \qquad \textit{Equation (4)}$$

(e) Satiation Porosity (f'') Under Vacuum Test:

In this method, the satiation porosity was determined in the same way as the vacuum saturation porosity. The difference is that water was fed into the bottom of a vacuum tank and stopped when the block bed-face had an immersion depth of approximately 5mm. The eighteen (18) block samples remained under vacuum until the water reached the top of the block sample. Then the air was allowed to enter the vacuum tank and the block was removed from the water and weighed. The vacuum satiation porosity f'' was then calculated from Equation 4.

(f) Capillary Pressure (ψ) Measurement of Crumb-Rubber Masonry Concrete:

Capillary pressure was measured using three rectangular prisms of dimensions 160*40*40 mm for every sample which was cut from each type of block with the long axis of the prism parallel to the bed and stretcher faces of the block. After drying the samples to constant mass in an air oven at 70˚C, five faces (the four long faces and one small face) were sealed with several layers of impermeable membrane. The initial masses of the bars were recorded and they were then fully immersed in water as shown in Figures 4.

Figure 4: Samples Sealed with Impermeable Membrane, Weighed and placed in Water

The complete immersion of the samples enabled the detection of any air leaking through the sealed surfaces immediately by the appearance of bubbles. If bubbles appeared, the sample was recovered and recoated. The sealed sides ensured that absorption occurred only perpendicular to the inflow face.
The samples were weighed at regular intervals until there was no further change in mass. The volume of absorbed water was determined from the mass increase, giving the volume of pores filled with water. The capillary pressure was determined using Equation 6:

$$p_1 v_1 = p_2 v_2 \text{ \{ideal gas equation assuming constant temperature\}} \qquad \textbf{\textit{Equation}} \textbf{ (5)}$$

Where: P_1 = the pressure of the initial volume of air in the block before capillary absorption and it is equal to the atmospheric pressure (0.1 MPa), V_1 = Initial volume of air (mm^3) = vacuum saturation porosity * sample volume, P_2 = Final pressure after absorption = trapped air pressure (MPa) and V_2 = Final volume of air left after the capillary rise of water (mm^3).

$$p_2 = \frac{p_1 v_1}{v_2} \qquad \textbf{\textit{Equation}} \textbf{ (6)}$$

The capillary pressure (ψ) taken as P_2 was calculated from equation 6

3. RESULTS AND DISCUSSION

3.1 Bulk Density (ρ)

Bulk density for masonry concrete blocks determined is presented in Figure 5 which shows that the bulk density of masonry concrete decreased gradually with the increase in rubber content. The average bulk density of the reference masonry concrete is 2,577Kg/m^3 while the crumb-rubber masonry concrete with 25% crumb-rubber content recorded a bulk density of 2,439Kg/m^3 respectively which indicates a 5.4% decrease in density with 25% replacement of crumb-rubber.

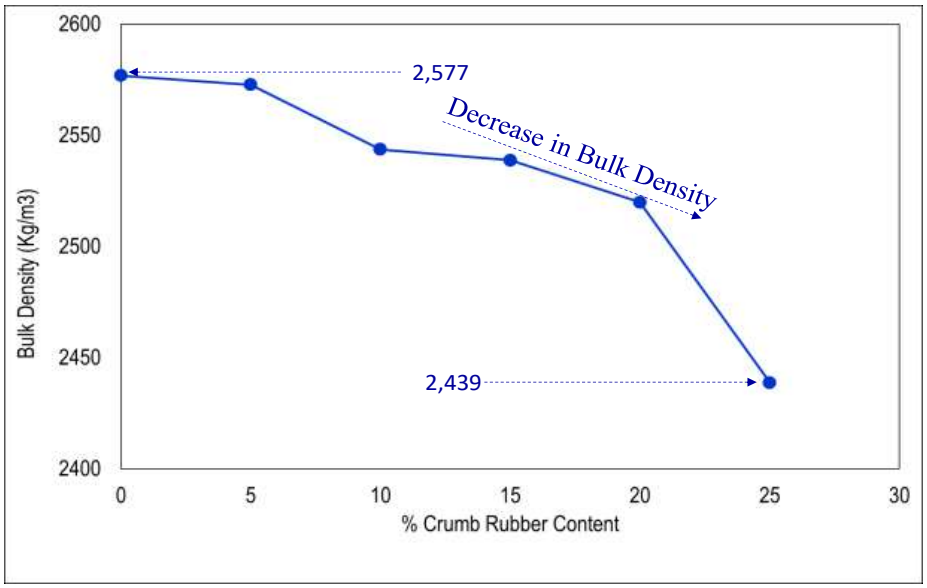

Figure 5: Bulk Density (Kg/m^3) of CR-MCB against % CR Content

3.2 Water Absorption (24Hours Soak) Porosity (*f*)

The 24 hours water absorption porosity test of masonry concrete is presented in Figure 6. The results indicate that increase in crumb-rubber content increased the porosity of masonry concrete samples by 21% with 25% crumb-rubber replaced in coarse granite aggregate.

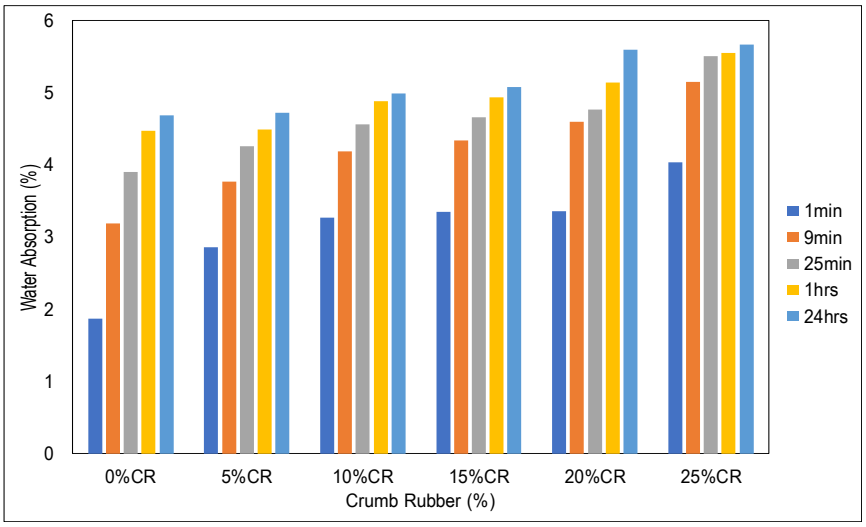

Figure 6: Water Absorption Porosity Test of CR-MCB against % CR Content

3.3 Vacuum Saturation Porosity (*f*)

The porosity of masonry concrete using vacuum saturation test is presented in Figure 7. The result of the vacuum saturation porosity measurements provides a true porosity, i.e., per cent by volume, unlike the 24 hours soaking porosity test which many others do refer to as a substitute for porosity but not a porosity. The results show that the reference masonry concrete samples ($0\%_{CR}$) have a porosity of 23.69% while the 5, 10, 15, 20 and 25% have a porosity of 23.75, 23.94, 24.03, 24.12 and 24.38% respectively.

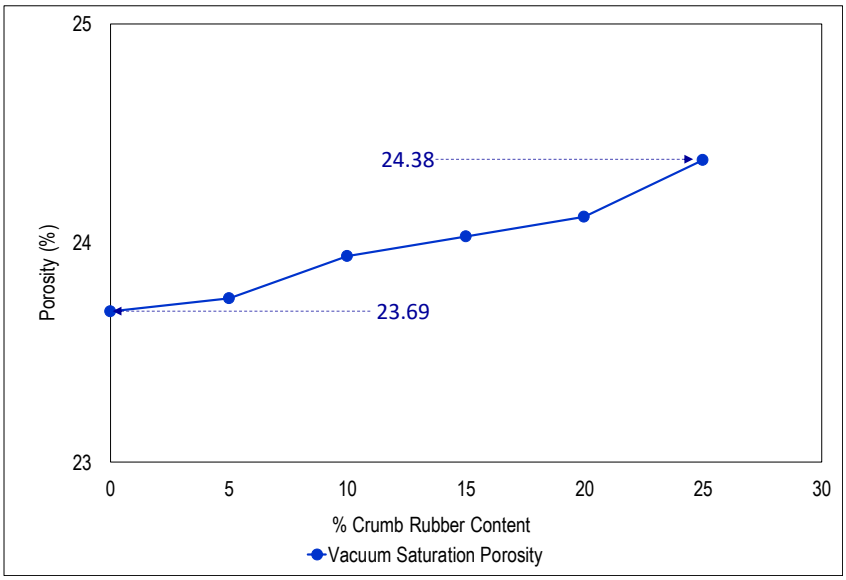

Figure 7: Vacuum Saturation Porosity (*f*) of CR-MCB against % CR Content

3.4 Satiation Porosity *(f')*

The results of satiation porosity also known as effective porosity of crumb-rubber masonry concrete blocks are presented in Figure 8. The results show that the reference masonry concrete blocks (0%$_{CR}$) have a porosity of 13.62% while the 5, 10, 15, 20 and 25% have a porosity of 13.78, 13.99, 14.10, 14.52 and 14.71% respectively.

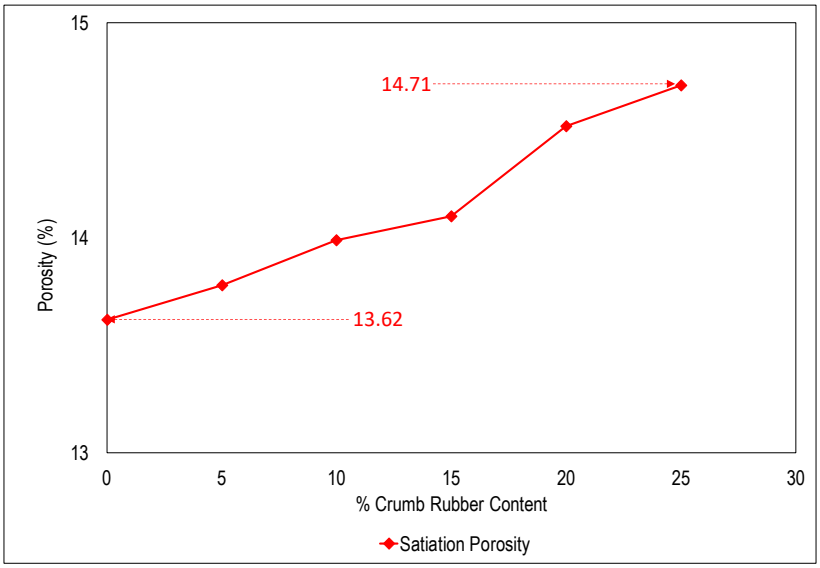

Figure 8: Satiation Porosity *(f')* of CR-MCB against % CR Content

3.5 Vacuum Satiation Porosity *(f'')*

The result of the vacuum satiation porosity measurements provides values very close to the vacuum saturation porosity (*f*) as shown in Figure 9. The results show that the reference masonry concrete (0%$_{CR}$) has a porosity of 23.63% while the 25%$_{CR}$ have a porosity of 24.36% which indicate an increase with about 3.1%.'

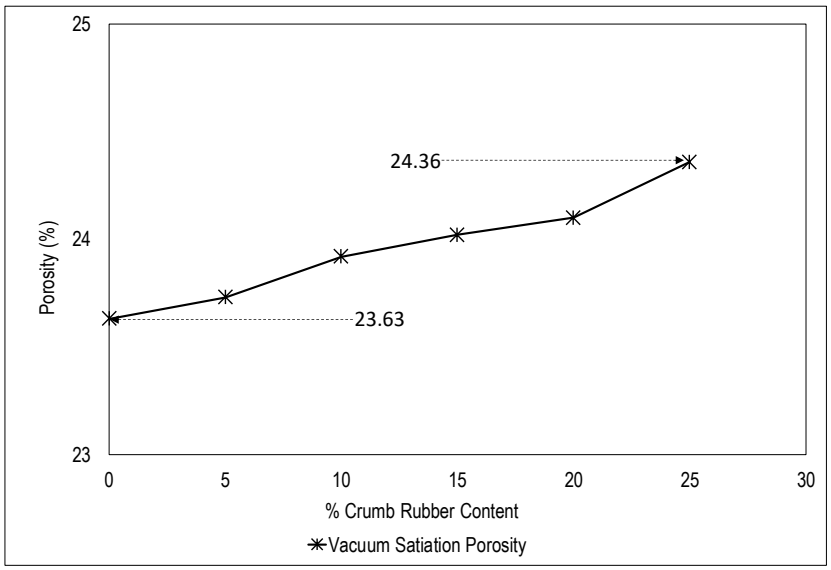

Figure 9: Vacuum Satiation Porosity (*f''*) of CR-MCB against % CR Content

3.6 Capillary Pressure (ψ)

The capillary pressure test result for both initial and refined (modified) methods is presented in Figure 10 which shows that the capillary pressure of crumb-rubber masonry concrete increased rapidly from 0% to 5% crumb-rubber content before gradually increasing with further increase in crumb-rubber content up to 25%.

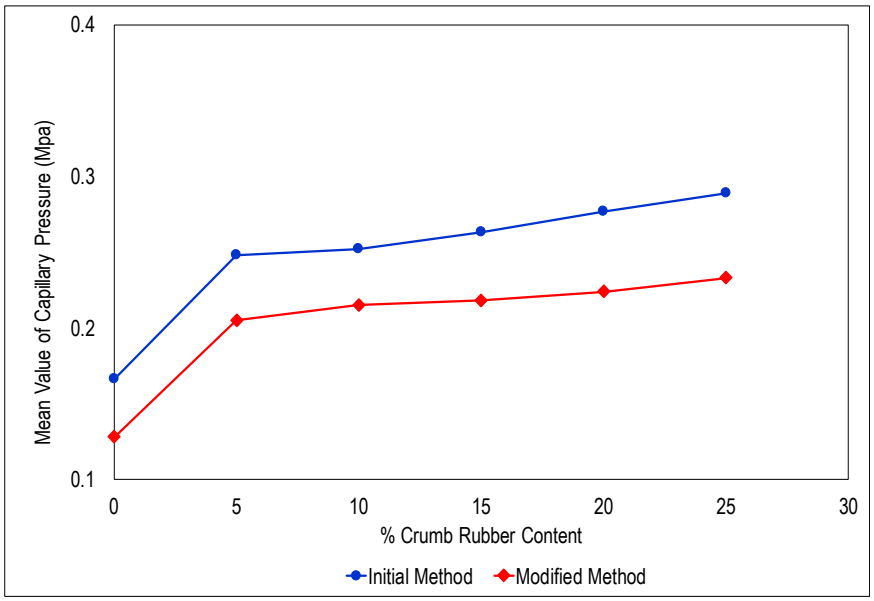

Figure 10: Capillary Pressure (ψ) of CR-MCB against % CR Content

The average capillary pressure value for the reference masonry concrete using the initial method is 0.166MPa while the masonry concrete with 25% crumb-rubber content recorded capillary pressure of 0.289MPa which indicates a 74% increase in capillary pressure with 25% replacement of crumb-rubber. For the refined (modified) method, average capillary pressure of 0.128MPa was recorded for the reference masonry concrete while the masonry concrete with 25% crumb-rubber content recorded capillary pressure of 0.233MPa which indicates 82%.

4. CONCLUSIONS

i. The bulk density of masonry concrete decreased with a percentage increase in crumb-rubber content up to 25%. The reference masonry concrete recorded 2,578Kg/m^3 while 25% crumb-rubber modified masonry concrete has a bulk density of 2,439Kg/m^3 which indicates a decrease of 5.37%.

ii. Porosity *(f)* of masonry concrete samples (24 hours water absorption, vacuum saturation, satiation, and vacuum satiation porosity) increased with an increase in crumb-rubber content varying from 5, 10, 15, 20 and 25%. The increase in the porosity is related to the higher content of entrained air along with poor interfacial contact between the crumb-rubber particles and the cement paste, the masonry concrete mixes caused by the hydrophilic (non-polar) nature of crumb-rubber particles attracting air around the surface of the aggregate during the mixing process causes a weaker bond between the non-polar and the polar particles, pores in crumb-rubber particles and the complex morphology of crumb-rubber.

iii. Capillary pressure (ψ) of masonry concrete increased rapidly from 0.166MPa to 0.248MPa for 0% and 5% crumb-rubber content before gradually increasing up to 0.289MPa for crumb-rubber content up to 25%. Generally, the increase in capillary pressure for both the initial and refined method with an increase in crumb-rubber content can be directly linked to the increase in the volume of pore spaces (voids) as a result of weak bonding between the crumb-rubber and the concrete composite which increased the porosity and results to increase in the volume of capillary rise.
iv. The result signifies an increase in the capacity of the modified masonry concrete to absorb water through the capillary rise.

REFERENCES

[1] Al-Sakini (1998), ''Behaviour and Characteristics of chopped worn-out tyres lightweight concrete'', Msc Thesis university of Technology, Baghdad, Iraq.
[2] Hall, C. (1994). ''Barrier performance of concrete- a review of fluid transport theory,'' Materials, and Structures, 27(169): p. 291-306.
[3] Ioannou, I., Hall C., Wilson M. A., Hoff W. D., and Carter M. A. (2003). ''*Direct measurement of the wetting front capillary pressure in a clay brick ceramic,''* Journal of Physics D-Applied Physics, 2003. 36(24): p. 3176-3182.
[4] Mohammadi, I. (2014). ''Investigation on the Use of Crumb Rubber Concrete (CRC) for Rigid Pavements,'' University of Technology Sydney.
[5] Ocholi, A, Ejeh S.P and Sanni M.Y., (2014). ''An Investigation into the Thermal Performance of Rubber-Concrete'', Academic Journal of Interdisciplinary Studies MCSER Publishing, Rome-Italy Vol 3 No 5 July 2014 Doi:10.5901/ajis. 2014.v3n5p29.
[6] Ocholi, A, Sanni M.Y and Ejeh S.P., (2018). *''The impact resistance effect of partially replacing coarse aggregate with ground-rubber aggregate in concrete''*. Nigeria Journal of Technology (NIJOTECH) pp.330-337 http://dx.doi.org/10.4314/njt.v37i2.7
[7] Wilson, M., Carter, M. & Hoff, W. (1999). *''British Standard and Rilem Water Absorption Tests,''*: A Critical Evaluation. Materials and Structures, 32(8), pp. 571-578.
[8] Yang, Y. Chen, J., and Zhao, G. (2000). "*Technical Advance on the Pyrolysis of Used Tires in China,"* Dept. of Chem. Eng., Zhejiang University, Hangzhou, 310027, P.R. CHINA.
[9] Yunping, Xi, Paria Meshin, Okpin na, and Yue Li. (2010), *"Premixed Rubberized Insulation Mortar (PRIM)",* University of Colorado at boulder.

FRAMEWORK FOR ASSESSING THE VIABILITY OF LATERITE AS A SOURCE OF ALUMINOSILICATES IN GEOPOLYMERISATION

Victor S. Gilayeneh [(1)] and Sunday Nwaubani [(1)]

(1) School of Civil and Environmental Engineering, University of the Witwatersrand

ABSTRACT

As the search for eco-friendly and affordable cement intensifies, geopolymer technology has become a viable option. Geopolymer technology offers a greener and cheaper means of producing cement-based materials which exhibit performance comparable to Portland cement. This technology could be instrumental in addressing the needs for adequate housing and other civil infrastructures in middle- and low-income countries. However, the utilisation of geopolymer technology depends on the accessibility of a steady source of aluminosilicates. One material that meets such a criterion is laterite. Laterite is abundantly found in most countries, situated in the tropical and subtropical regions of the world. Despite this, the potential of laterite as a source of aluminosilicates is yet to be exploited, and one of the limitations impeding the acceptance and development of geopolymer cement derived from laterite is the lack of information regarding its durability performance. Consequently, this paper presents the framework of an ongoing study on the viability of laterite as a source of aluminosilicates in geopolymerisation, with emphasis on the transport properties and corrosion of steel in laterite-based geopolymer concrete. For this investigation, imaging analysis and nano-analytics will be employed to probe the microstructure. It is envisioned that the findings of this study will fill the current gap in knowledge regarding the afore-mentioned properties and further the use of laterite as a source of aluminosilicates in producing green and affordable cement.

Keywords: geopolymer, laterite, microstructure, steel corrosion, transport properties

1. INTRODUCTION

The need for eco-friendly and affordable cement is the current driving force behind the research and development of alternative cements, such as those based on alkali or acid activation technology. One novel class of materials that falls in this category is geopolymer. Geopolymers are inorganic polymeric materials synthesised from the reaction of aluminosilicate materials (usually called the precursors) with an alkaline or acidic reagent. These materials consist of chains or networks of molecules linked by covalent bonds and have a broad range of applications [1].

Geopolymer technology presents a promising opportunity of producing low cost and green cement-based materials, which is much needed in the least developed and developing countries, where the needs for low-cost housing, road infrastructure, water reticulation system, to name a few, are ostensible. However, the utilisation of this technology strongly depends on the accessibility of a steady source of aluminosilicates, as the availability of locally sourced

precursors is an essential factor in determining the acceptance and utilisation of alkali-activated binders [2].

Considering that access to industrial wastes in underdeveloped and less-industrialised countries is a major problem, the need for other sources of aluminosilicate materials is self-evident if geopolymer technology is to be utilised. Thus, the only available source of aluminosilicates that should be exploited in these regions is geological materials [3]. One potential geological material that could be used as a source of aluminosilicates and exists in vast quantities exceeding the likely global production of cement-based materials [2], but has not received the deserved attention, is laterite or lateritic soil.

Laterite is a reddish or rust-coloured soil found mostly in the tropics and subtropics, developed as the result of long and intensive weathering of the underlying parent rock. This material is poorly crystallised, rich in iron and aluminium; and mainly consists of goethite, hematite, kaolinite, and gibbsite minerals. Laterite has long had a history of being used as a construction material. Dating back as far as 1000 years ago in Southeast Asia, laterite soil was cut in the form of large blocks and used in the construction of temples [4]. Apart from being used as a compressed stabilised earth block (CSEB) in modern time [5], laterite has also found usage in road construction, as road base material and road surface pavement [6], in the development of earth dams and the concrete industry as Portland cement replacement material. It has been proven that calcined laterite has pozzolanic properties and can be used as cement replacement in the production of Portland cement-based materials [7, 8]. Laterite or lateritic soil, as a construction material, suits the context of sustainability and is promising for middle- and low-income countries, most notably regarding chemical activation.

Despite being a potential source of aluminosilicates, laterite has received less attention from researchers. There are scant publications on the use of laterite as an aluminosilicate precursor compared to the vast publications and reviews available on the properties, characterisations and performance of alkali-activated binders based on metakaolin, fly ash, and blast-furnace slag [9], which are considered the most-used aluminosilicate precursors [10]. Although there is a substantial amount of information on the mostly used aluminosilicate precursors, knowledge of these materials is not easily transferable, given that the properties and performance of alkali-activated binders strongly depend on the chemical and mineralogical compositions of the aluminosilicate precursors as well as the mix design, activators, and the curing process. Thus, other potential sources of aluminosilicates, such as laterite, must be subjected to full scrutiny.

2. LATERITE AS A SOURCE OF ALUMINOSILICATES

Laterite, as a source of aluminosilicates, has just attracted attention in recent time, and most of the publications on the use of laterite as a source of aluminosilicates are under the name geopolymer. It is worth mentioning that this review only captures work on lateritic material sourced from the tropics or subtropics. Results from previous investigations indicate that laterite-based geopolymer is suitable for construction purposes. However, these investigations lack comprehensive information about the durability performance of laterite-based geopolymer. Obonyo et al. [11] investigated the suitability of using laterite as a solid precursor in geopolymerisation. In their study, portions of the laterite ranging from 15 – 35% by weight were calcined at 700 °C to serve as nucleation sites for the geopolymerisation. The authors examined the final product for stability in water, biaxial flexural strength, pore size distribution and the microstructure. They found that the final product exhibited excellent stability in water,

low porosity and water absorption, and flexural strength comparable to that of conventional concrete. Lamougna et al. [12] examined the influence of curing temperature and the amount of sodium hydroxide (NaOH), the sole activator, on the compressive strength of laterite-based geopolymer. The authors reported that both the curing temperature and alkali concentration influenced strength development.

Similarly, studying the potential of utilising laterite as a raw material in geopolymerisation, Gualtieri et al. [13] studied the mechanical and microstructural properties of phosphoric acid activation and sodium silicates activation of laterite and found that the laterite-based geopolymer synthesised with phosphoric acid exhibited better mechanical properties and low porosity than the sodium silicates activation. Lamougna et al. [14] investigated the effects of replacing laterite with slag and calcite on the development of laterite-based inorganic polymer. The replacement level ranged from 5 – 50% and 2 – 20%, for the slag and calcite, respectively. The authors reported the calcite to have little influence while the replacement of the laterite with slag from 20% and above, had significant improvement on the compressive strength and the microstructure.

Studying the influence of calcination temperature on fully indurated laterite, Kaze et al. [15] examined water absorption, flexural strength, and the microstructure of laterite-based geopolymer. The authors reported 500 °C to be the optimum calcination temperature in terms of flexural strength and dense microstructure. Still concerned with the performance of laterite-based geopolymer, Kaze et al. [16] investigated the flexural strength, water absorption, porosity and microstructure of laterite-based geopolymer containing rice husk ask (RHA) at 10 – 40% replacement level, cured at room temperature and 90 °C. The authors reported significant improvement in the mechanical properties and microstructure of the laterite-based geopolymer containing RHA at higher replacement level and curing temperature. Kaze et al. [17] also investigated the effect of silicate modulus with varying NaOH concentration on the initial and final setting times, compressive strength and microstructure of laterite-based geopolymer cured at room temperature and found the setting times to decrease with increasing NaOH concentration while the compressive strength and microstructure improved with increasing concentration of NaOH and decreasing silicate modulus.

As stated above, the current research on the activation of laterite as a cement-based material has focused chiefly on strength development, the influence of curing temperature, soundness in water, and the microstructure. None has detailed neither the flow behaviour of the fresh mix nor the durability performance regarding corrosion of steel, the most common deterioration mechanism associated with reinforced concrete [18] or the transport properties, which often serve as indicators of durability [19]. These are essential aspects that should be understood if alkali- or acid-activated laterite is to be utilised as cement-based material.

3. SCOPE OF THE ONGOING INVESTIGATION

The focus of this investigation is on the durability aspects of steel corrosion in laterite-based geopolymer concrete and its transport properties. However, the scope of this investigation also covers the rheology, setting times (initial and final) and reaction kinetics of the fresh mix, as well as strength development and microstructural analyses of the hardened laterite-based geopolymer concrete.

4. EXPERIMENTAL FRAMEWORK

4.1 Laterite Characterisation

Various techniques will be employed in characterising the physical and chemical properties of the laterite. The physical properties of interest are the particle size distribution, specific gravity, surface area and SEM micrography, while those of the chemical are the oxide composition, mineralogical phases, and elemental composition.

As illustrated in Figure1, the characterisation of the laterite will begin with preliminary chemical analyses (XRF & XRD) to establish whether the material is suitable for this investigation. Subsequently, the laterite will be milled to pass a sieve size of 45 μm, and thermal analyses (DSC-TGA) will be conducted to determine the dehydroxylation temperature, followed by the calcination of a portion of the milled laterite. Next, the final chemical analyses (XRF, XRD and SEM/EDS) will be conducted for both calcined and uncalcined parts of the laterite. Then, the particle size distribution (PSD), specific gravity (SG), surface area (SA) and SEM micrography will be obtained.

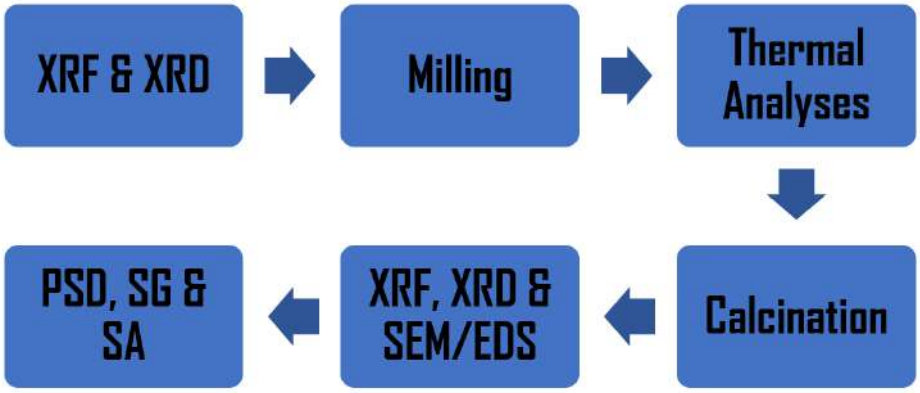

Figure 1: Flowchart of the Laterite Characterisation Process.

4.2 Concrete Mix Designs

Two (2) categories of mixes will be considered in this investigation, Geopolymer Mixes and Hybrid Mixes. Each category will comprise two mixes: consisting of calcined and uncalcined laterite. The geopolymer mixtures will consist solely of laterite as the precursor (100% laterite), while the hybrid will consist of 70 – 80% laterite & 20 – 30% Portland cement.

All mixes will be activated with the same activator(s). The optimum mix design of the geopolymer mixtures will be achieved after several trial mixes, and the critical factors to be considered during the mix design process are the workability, setting at ambient temperature and strength development. The liquid-to-solid ratio, type of activator(s) and concentration will be determined during the trial mixes. Once the optimum mix design is established, the hybrids will be tailored to suit the sole laterite mixes in terms of consistency and workability.

4.3 Rheology, Setting time and Reaction Kinetics

The rheology of the fresh mix will be examined by a free flow test (slump) which will evaluate workability and consistency. Vicat apparatus will be used for the determination of the initial and final setting times, and the reaction kinetics (heat evolution) will be studied by measuring the heat released during the geopolymerisation process with an isothermal calorimeter.

4.4 Strength Development

The strength development of the mixes will be explored using the compressive strength and splitting tensile strength tests. The compressive and splitting tensile strengths tests will be conducted in accordance with the South African National Standards, and the trend of strengths development will be tracked up to 52 weeks after casting.

4.5 Microstructural Analyses

The microstructural analyses cover phase identification of the products of geopolymerisation and analyses of the pore structures (porosity, pore size and pore size distribution). The pore structures will be analysed by SEM imaging and mercury intrusion porosimetry (MIP), whereas the phase identification involves XRD and EBSD in combination with EDS. EDS and EBSD will consist of both micro- and nanoscale analyses. The TGA technique will also be employed in the microstructural characterisation to complement results of the XRD and EBSD/EDS analyses.

4.6 Durability Performance

4.6.1 Transport Properties

The transport properties of the laterite-based geopolymer concrete will be studied from the perspective of resistance to penetration. The resistance to penetration will be evaluated against gas permeation, moisture absorption, and chloride diffusion, and these will be assessed by the South African Durability Indexes.

4.6.2 Steel Corrosion Resistance

The steel corrosion resistance of laterite-based geopolymer concrete will be evaluated based on chloride-induced corrosion since chloride is the most aggressive corrosion-inducing species in the environment. This corrosion resistance study involves the depth of chloride penetration, the electrical resistivity, the half-cell potential, the corrosion rate, and the mass loss of the rebars. A Coulostat meter will be employed to measure the corrosion rate, electrical resistivity of the specimens and the half-cell potential of the rebars. The mass loss of the rebars will be evaluated by gravimetric analysis. A resistivity meter and half-cell meter will also be used to verify or complement the electrical resistivity and half-cell potential measurements, respectively, obtained from the Coulostat meter.

5. CONCLUDING REMARKS

This study seeks to examine the viability of laterite as a source of aluminosilicates with emphasis on the durability performance of laterite-based geopolymer concrete, which covers steel corrosion and the transport processes of gas permeation, moisture absorption, and chloride diffusion. These are essential durability aspects that should be understood if alkali- or acid-activated laterite is to be utilised as cement-based materials. It is anticipated that the findings of this study will fill the current gap in knowledge regarding the corrosion of steel in laterite-based geopolymer concrete and its durability-related transport properties and promote the use of laterite as a source of aluminosilicates in producing green and affordable cement.

REFERENCES

[1] Davidovits, J., 'Introduction', in *Geopolymer Chemistry and Applications*, 5th edition., 2020.
[2] Provis, J. L., 'Alkali-activated materials', *Cem. Concr. Res.*, vol. 114, pp. 40–48, 2018.
[3] Mcintosh, A., Lawther, S. E. M., Kwasny, J., Soutsos, M. N., Cleland, D., and Nanukuttan, S., 'Selection and characterisation of geological materials for use as geopolymer precursors', *Adv. Appl. Ceram.*, vol. 114, no. 7, pp. 378–385, 2015.
[4] Schellmann, W., 'Home - An Introduction in Laterite'. [Online]. Available: http://www.laterite.de.
[5] Lemougna, P. N., Melo, U. F. C., Kamseu, E., and Tchamba, A. B., 'Laterite based stabilized products for sustainable building applications in tropical countries: review and prospects for the case of Cameroon', *Sustainability*, vol. 3, no. 1, pp. 293–305, 2011.
[6] Cabrera, J. G. and Nwaubani, S. O., 'Strength and chloride permeability of concrete containing red tropical soils', *Mag. Concr. Res.*, vol. 45, no. 164, pp. 169–178, Sep. 1993.
[7] Nwaubani, S. O., 'Properties, Hydration and Durability of Pozzolanic Mortars and Concrete', PhD Thesis, Department of Civil Engineering, University of Leeds, 1990.
[8] Pera, T. M. J. and Ambroise, J., 'Action of some aggressive solutions on Portland and calcined laterite blended cement concretes', *Spec. Publ.*, vol. 132, pp. 763–780, 1992.
[9] Heah, C. Y., Kamarudin, H., Mustafa Al Bakri, A. M., Bnhussain, M., Luqman, M., Khairul Nizar, I., Ruzaidi, C. M., and Liew, Y. M., 'Study on solids-to-liquid and alkaline activator ratios on kaolin-based geopolymers', *Constr. Build. Mater.*, vol. 35, pp. 912–922, Oct. 2012.
[10] Yang, K.-H., Song, J.-K., and Song, K.-I., 'Assessment of CO2 reduction of alkali-activated concrete', *J. Clean. Prod.*, vol. 39, pp. 265–272, Jan. 2013.
[11] Obonyo, E. A., Kamseu, E., Lemougna, P. N., Tchamba, A. B., Melo, U. C., and Leonelli, C., 'A sustainable approach for the geopolymerization of natural iron-rich aluminosilicate materials', *Sustainability*, vol. 6, no. 9, pp. 5535–5553, 2014.
[12] Lemougna, P. N., Madi, A. B., Kamseu, E., Melo, U. C., Delplancke, M.-P., and Rahier, H., 'Influence of the processing temperature on the compressive strength of Na activated lateritic soil for building applications', *Constr. Build. Mater.*, vol. 65, pp. 60–66, Aug. 2014.
[13] Gualtieri, M. L., Romagnoli, M., Pollastri, S., and Gualtieri, A. F., 'Inorganic polymers from laterite using activation with phosphoric acid and alkaline sodium silicate solution: mechanical and microstructural properties', *Cem. Concr. Res.*, vol. 67, pp. 259–270, 2015.
[14] Lemougna, P. N., Wang, K., Tang, Q., Kamseu, E., Billong, N., Melo, U. C., and Cui, X., 'Effect of slag and calcium carbonate addition on the development of geopolymer from indurated laterite', *Appl. Clay Sci.*, vol. 148, pp. 109–117, 2017.
[15] Kaze, R. C., à Moungam, L. B., Djouka, M. F., Nana, A., Kamseu, E., Melo, U. C., and Leonelli, C., 'The corrosion of kaolinite by iron minerals and the effects on geopolymerization', *Appl. Clay Sci.*, vol. 138, pp. 48–62, 2017.
[16] Kaze, R. C., à Moungam, L. M. B., Cannio, M., Rosa, R., Kamseu, E., Melo, U. C., and Leonelli, C., 'Microstructure and engineering properties of Fe2O3 (FeO)-Al2O3-SiO2 based geopolymer composites', *J. Clean. Prod.*, vol. 199, pp. 849–859, 2018.
[17] Kaze, C. R., Djobo, J. N. Y., Nana, A., Tchakoute, H. K., Kamseu, E., Melo, U. C., Leonelli, C., and Rahier, H., 'Effect of silicate modulus on the setting, mechanical strength and microstructure of iron-rich aluminosilicate (laterite) based-geopolymer cured at room temperature', *Ceram. Int.*, vol. 44, no. 17, pp. 21442–21450, 2018.
[18] Angst, U. M., 'Challenges and opportunities in corrosion of steel in concrete', *Mater. Struct.*, vol. 51, no. 1, p. 4, Jan. 2018.
[19] Otieno, M., Alexander, M. G., and Beushausen, H., 'Transport Mechanisms', in *Transport Mechanisms, Corrosion of Steel and Corrosion Assessment in Concrete*, Concrete Materials and Structural Integrity Research Group, 2010.

PERFORMANCE OF GEOPOLYMER CONCRETE SUBJECTED TO HCl IN STATIC AND DYNAMIC TEST CONDITIONS

Mandla Dlamini [(1)] and Mark Alexander [(2)]

(1) University of Cape Town, Engineering and the Built Environment, South Africa; Council for Scientific and Industrial Research (CSIR), Smart places, Pretoria South Africa.

(2) University of Cape Town, Engineering and the Built Environment, South Africa;

ABSTRACT

Geopolymer cements are alumino-silicate based binders, currently touted to be potential alternatives to traditional cement binders. Geopolymers are suggested to possess numerous beneficial properties, such as high chemical stability (durability), high-temperature stability and, low carbon footprint. This study sought to assess the performance of fly as set of fly ash-based geopolymer concretes under acid testing (HCl). The mineral acid testing program attempted to determine the performance of geopolymer concrete specimens under static corrosion and erosion-corrosion. Static corrosion was simulated using HCl immersion tests while erosion-corrosion was simulated using the dynamic HCl test rig developed at the University of Cape Town. Portland cement and calcium aluminate cement concrete mixed with calcareous aggregates (dolomite) were used as control specimens, while geopolymer concretes made use of both siliceous and calcareous aggregates. The corrosion testing showed that the resistance of geopolymer concretes exposed to hydrochloric acid in dynamic and static conditions was significantly greater than Portland cement concrete and calcium aluminate concrete. The study also showed that the acid resistance of geopolymers can further be improved by pairing them with siliceous aggregates instead of calcareous aggregates.

Keywords: geopolymers, hydrochloric acid, resistance, concrete.

1. BACKGROUND

Geopolymers have been touted as promising binders possessing superior acid resistance compared to traditional cement types [1] [2]. Acid resistance is a desirable property for infrastructure such as concrete sewer pipe, which is subjected to a complex biogenic corrosion process known as microbially-induced corrosion (MIC). Therefore a significant amount of attention has been placed on the resistance of concrete to microbially-induced acid corrosion. It is important to note that MIC is a complex phenomenon, wherein complexity arises from, complex sewer exposure conditions (sewer biome, temperature/client, effluent flow regimes etc.), the complexity of concrete as a composite material, and the complex interactions of acids, bacteria and corrosion products.

Previously, researchers focusing on MIC resistance of concrete have cautioned against the use of mineral acid testing to assess the performance of cementitious materials subjected to microbially-induced corrosion (MIC) [3] [4]. This view is partly based on results emanating

from mineral acid tests that did not correspond to field measurements [3]. Furthermore, researchers [5] [4] suggest, in addition to the chemical stability of concrete, certain protective mechanisms between the concrete substrate and acid-producing bacteria (sulfur-oxidizing bacteria) have a strong bearing on corrosion performance [6]. One such mechanism by which the concrete substrate is thought to influence corrosion is by means of the bacterio-static effect, which manifests either through the presence of toxic materials within sound concrete [7], or the liberation of toxic corrosion products during corrosion [6].

A second resistance mechanism is the release of protective precipitates such as alumina gel (AHx) in corroding calcium aluminate cement concretes, which are thought to act as a physical barrier, blocking acids from sound concrete [5].It should be noted that the two corrosion protection mechanisms identified above are not exhaustive and that they occur in addition to the chemical resistance of concrete. Thus, chemical stability plays a significant role in concrete's resistance to both mineral acid corrosion and microbially-induced corrosion. To select durable materials for these corrosive environments, this study proposed that mineral acid tests could be a useful tool to measure the performance of competing concrete mixtures if the limitations of these tests are understood.

2. MATERIALS AND METHODS

2.1 Materials

The types of cement used to produce concrete test specimens are shown in Table 1 together with data on their relative densities. Portland cement and calcium aluminate cement were intended to be used in control specimens.

Table 1: Cement types used in the study

Cement type and origin	Relative density (of Hardened cement paste)	Loose bulk density (kg/m^3)
CEM I, 52.5 R, Portland cement from PPC	3.1	1260
Cement Fondu-calcium aluminate cement (Brand: Imerys)	3.3	1370
Fly ash-based geopolymer cement developed by CSIR Smart Places.	2.5	1020

Two classes of aggregate were used in the experiment, namely siliceous and calcareous aggregates. The five aggregate types are listed below in Table 2.

Table 2: Aggregates used in the study

Aggregate type	Fineness modulus	Chemical class
Granite	4.65	Siliceous
Ferro-quartz	4.79	Siliceous
Dolerite	4.95	Siliceous
Andesite	4.99	Siliceous
Dolomite	5.28	Calcareous

2.1.1 Concrete mix designs

A total of 7 concrete mixes were prepared for corrosion testing. All concrete mixes prepared in the study were "dry" mixes, which were subsequently compacted to achieve a dense concrete matrix. The control specimens were produced from Portland cement and calcium aluminate cements paired with dolomite aggregate according to the recipe provided in Table 3.

Table 3: Mix design of control specimens

Concrete mix component	**Mix proportion as a percentage of the total mass**	**Mix Ratio (by mass)**
CAC/PC	23%	1
Dolomite aggregate (fine: coarse ratio = 33:44)	77 %	3.35
Water-cement ratio	0.37	

Geopolymer cement was paired with all 5 types of aggregate according to the mix recipe provided in Table 4.

Table 4: Mix design of geopolymer concrete specimens.

Concrete mix component	**Mix proportion as a percentage of the total mass**	**Mass Mix Ratio**
Fly ash-based geopolymer	17%	1
Aggregate (fine: coarse ratio = 33:44)	83 %	4.89
Geopolymer solids to geopolymer liquids ratio (similar to water-cement ratio)	0.37	

*Concrete specimens prepared for the static test did not include coarse aggregate, however, the ratio of aggregate to binder was kept constant.

* Because the density of fly ash-based geopolymer binder is significantly lower than Portland and calcium aluminate cement (see Table 1), the proportion of binder in the geopolymer concretes was reduced to have the volumetric ratio of binder to aggregate in the control specimens approximately equivalent to the Portland cement and calcium aluminate cement concrete mixes.

2.2 Materials characterisation (XRD)

To identify the crystalline phases of hardened cement paste and aggregate, X-Ray diffraction analysis was employed. The materials were analysed with a Malvern Panalytical Aeris diffractometer with PIXcel detector and fixed slits with Fe filtered Co-Kά radiation. The phases were identified using X'Pert Highscore plus software.

2.2.1 Static corrosion testing

Mineral acid attack under static conditions involved placing 50 mm concrete cubes in a hydrochloric acid bath (Figure 1). The pH was maintained between 1 and 1.1 by adding

concentrated acid into the PVC bucket while measuring the pH using a calibrated pH meter. Furthermore, the acid was fully replaced every 24 hours. The concrete cube specimens were first placed in water for 4 hours and their saturated surface dry mass was recorded together with their dimensions. Four cubes of the same type are placed into 5 Litres of acid (HCl) solution of pH 1. Four concrete specimens of each mix design were placed in a container and submerged in 5 litres of pH 1 acid solution. Therefore, the total initial surface area subjected to acid attack for each specimen was 150 cm^2, and the total initial surface area of concrete specimens within a bucket containing 5 litres of pH 1 acid was 600 cm^2. The ratio of initial surface area to the volume of pH 1 acidic solution is 0.12 m^2/m^3 ($600cm^2/5000cm^3$).

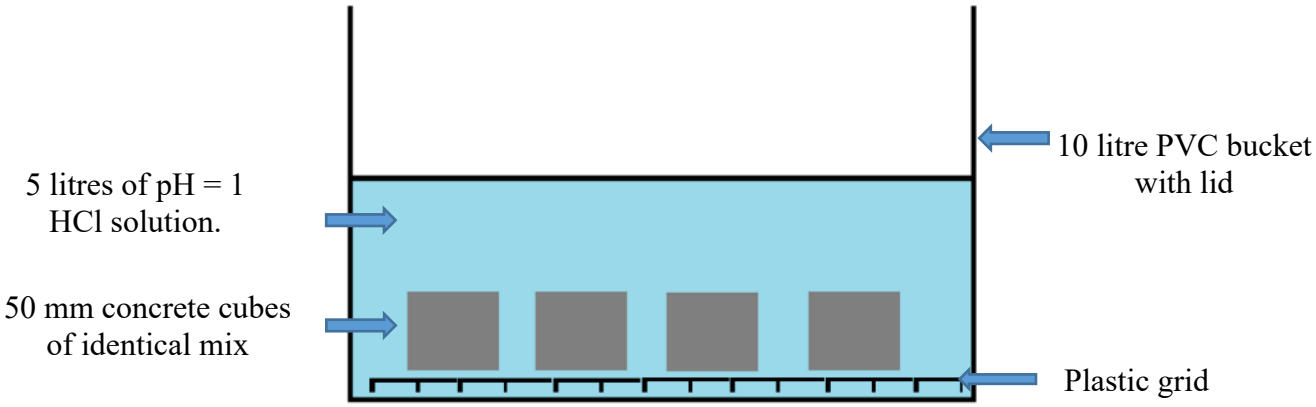

Figure 1: Static test configuration

The effect of corrosion on the concrete specimens was measured by taking the mass of the corroding specimens over a period of 800 hours. Mass measurements were taken twice every 24 hours.

2.2.2 Dynamic hydrochloric acid testing

The dynamic acid test involves subjecting concrete specimens to both acid attack and abrasion simultaneously, making it a highly aggressive test. This test is typically conducted over 48 hours, however clear have been observed within 24 hours of testing ([8], [9]). A compartment was filled with approximately 50 ℓ of a hydrochloric solution (pH=1). Cored cylindrical concrete specimens (78 mm diameter × 125 mm) were firstly pre-saturated with tap water for four hours. Thereafter they were immersed in the acid tank and rotated at approximately 16 revolutions per minute over rubberised rollers driven by rubber pulleys connected to an electric motor (Figure 2). A PVC brush is lowered onto the surface of the specimen to dislodge any loose erodible material forming at the surface of the specimen.

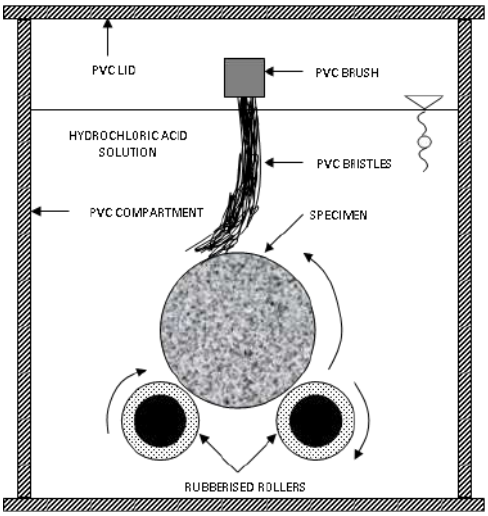

Figure 2: Dynamic acid test configuration

The effect of corrosion on the concrete specimens was measured by taking the mass of the corroding specimens over a period of 48 hours. Mass measurements were taken every two hours.

3. RESULTS

3.1 XRD analysis of hardened cement pastes

Table 5, Table 6 and Table 7 show the minerals identified from XRD analysis and their proportions within the hardened cement binders. Furthermore, data on the solubility of the minerals identified via XRD analysis was collected from a mineral solubility database [10]. The hardened geopolymer paste was found to be primarily made up of amorphous content, while the crystalline phases were largely made up of mullite and quartz. In Portland cement hydrated paste, calcium bearing minerals such as calcite, Portlandite and hatrurite are soluble in acids. The amorphous phases are likely to be calcium silicate hydrates (C-S-H). X-ray diffraction graphs of Portland cement paste typically exhibit very broad bands due to their low crystallinity. The hydrated CAC paste has a high proportion of amorphous content. Krotite (12.8%), srebrodolskite (7.1%) and katoite (6.7%) make up the bulk (29.9%) of crystalline content.

Table 5: Mineralogy of hardened geopolymer cement paste obtained by quantitative XRD analysis and the solubility of the identified mineral.

Mineral	**Percentage**	**Chemical formula**	**HCl solubility**	**H_2SO_4 solubility**
Quartz	8.7%	SiO_2	Insoluble	Insoluble
Mullite	13.9%	$3Al_2O_3{\cdot}2SiO_2$	Insoluble	Insoluble
Hematite*	0.9%	Fe_2O_3	Soluble	Insoluble
Sillimanite	3.5%	Al_2SiO_5	Insoluble	Insoluble
Calcite*	1.0%	$CaCO_3$	Soluble	Soluble
Amorphous content	72.0%			

Table 6: Mineralogy of hydrated PC paste obtained by quantitative XRD analysis

Mineral	Percentage	Chemical formula	HCl Solubility	H_2SO_4 solubility
Quartz	0.5%	SiO_2	Insoluble	Insoluble
Mullite	0.7%	$3Al_2O_3 \cdot 2SiO_2$	Insoluble	Insoluble
Calcite*	2.0%	$CaCO_3$	Soluble	Soluble
Portlandite*	6.3%	$Ca(OH)_2$	Soluble	Soluble
Hatrurite *	11%	$Ca_3(SiO_4)O$	(No data)	(No data)
Gypsum	0.5%	$CaSO_4$	Soluble	Insoluble
Amorphous	79%			

Table 7: Mineralogy of hydrated CAC paste obtained by quantitative XRD analysis

Mineral	Percentage	Chemical formula	HCl solubility	H_2SO_4 solubility
Cristobalite	0.5%	SiO_2	Insoluble	Insoluble
Quartz	0.3%	SiO_2	Insoluble	Insoluble
Magnetite	0.2%	$FeO \cdot Fe_2O_3$	Soluble	Insoluble
Katoite	6.7%	$Ca_3Al_2(SiO_4)(OH)_8$	(no data)	(no data)
Dolomite	1.4%	$CaMg(CO_3)_2$	Soluble (if heated)	Insoluble
Srebrodolskite	7.1%	$Ca_2Fe^{3+}{}_2O_5$	(no data)	(no data)
Hedenbergite	0.1%	$CaFe^{2+}Si_2O_6$	Insoluble	(no data)
Krotite	12.8%	$CaAl_2O_4$	(no data)	(no data)
Chromite	1.2%	$FeCr_2O_4$	Insoluble	Insoluble
Amorphous	70.1%			

3.2 XRD of Aggregates

Ferro-quartz XRD results show a high proportion of quartz mineral with minute quantities of hematite and biotite. Quartz has high chemical stability and thus can be considered fully resistant to acid attack. Biotite and hematite are both soluble in concentrated acids however, their contribution to total acid resistance is negligible as they constitute only 1% of the mineralogy of the ferro-quartz aggregate.

Table 8: Mineralogy of ferro-quartz aggregate obtained by quantitative XRD analysis

Mineral	Percentage	Chemical formula	HCl solubility	H_2SO_4 solubility
Quartz	99%	SiO_2	Insoluble	Insoluble
Hematite	0.1%	Fe_2O_3	Soluble	Insoluble
Biotite	0.9%	$K(Mg,Fe)_3AlSi_3O_{10}(OH)2$	Insoluble	Soluble

The mineralogy of dolomite is mainly constituted by dolomite crystals (75%) and quartz (24.1%). This aggregate, therefore, has high acid solubility as quartz constitutes only a quarter of its mineral composition.

Table 9: Mineralogy of dolomite aggregate obtained by quantitative XRD analysis

Mineral	Percentage	Chemical formula	HCl solubility	H_2SO_4 solubility
Quartz	24.1%	SiO_2	Insoluble	Insoluble
Dolomite	75.7%	$CaMg(CO_3)_2$	Soluble	Soluble
Biotite	0.3%	$K(Mg,Fe)_3AlSi_3O_{10}(OH)2$	Soluble	Soluble

Labradorite is the main mineral found in dolerite aggregate at 58.5%. This feldspar mineral is soluble in HCl and H2SO4. The reaction of labradorite feldspar with aqueous solutions at pH = 1 and 2.0 produce a surface that is depleted in calcium and aluminium and is enriched in silicon [11].

Table 10: Mineralogy of dolerite aggregate obtained by quantitative XRD analysis

Mineral	Percentage	Chemical formula	HCl solubility	H_2SO_4 solubility
Quartz	3.7%	SiO_2	Insoluble	Insoluble
Augite	16.8%	$(Ca,Na)(Mg,Fe,Al,Ti)(Si,Al)_2O_6$	Insoluble	Insoluble
Smectite 14	6.9%	$A_{0.3}D_{2-3}[T_4O_{10}]Z_2 \cdot nH_2O$	Insoluble	(no data)
Labradorite	58.5%	$((Ca, Na)(Al, Si)_4O_8)$	Soluble	Soluble
Muscovite	1.4%	$KAl_2(AlSi_3O_{10})(F,OH)_2$	Insoluble	Insoluble
Enstatite, ferroan	12.7%	$Mg_2Si_2O_6$	Insoluble	Insoluble

Andesite aggregate has two minerals regarded as being acid-soluble, clinochlore and clinozoisite. They constitute 13% and 5.8% of andesite's mineralogy respectively. Clinochlore, a mineral belonging to the chlorite group of minerals is soluble in acids is reported to be soluble in HCl [10].

Table 11: Mineralogy of andesite aggregate obtained by quantitative XRD analysis

Mineral	Percentage	Chemical formula	HCl solubility	H_2SO_4 solubility
Microcline	3.1%	$KAlSi_3O_8$	Insoluble	Insoluble
Quartz	11.9%	SiO_2	Insoluble	Insoluble
Clinochlore	13%	$Mg_5Al(AlSi_3O_{10})(OH)_8$	Soluble	Soluble
Actinolite	18.1%	$Ca_2(Mg,Fe)_5Si_8O_{22}(OH)_2$	Soluble	(no data)
Diopside, ferroan	6.1%	$CaMgSi_2O_6$	Insoluble	Insoluble
Albite	42.1%	$Na(AlSi_3O_8)$	Insoluble	Insoluble
Clinozoisite	5.8%	$\{Ca_2\}\{Al_3\}(Si_2O_7)(SiO_4)O(OH)$	Soluble	Insoluble

The mineralogy of granite aggregate is largely made up of acid-insoluble minerals. The major minerals detected by XRF are albite (48.3%), microcline (15.9%) and quartz (32.7%). Small amounts of soluble minerals are also present in the form of clinochlore and actinolite.

Table 12: Mineralogy of granite aggregate obtained by quantitative XRD analysis

Mineral	**Percentage**	**Chemical formula**	**HCl Solubility**	**H_2SO_4 solubility**
Albite	48.3%	$Na(AlSi_3O_8)$	Insoluble	Insoluble
Biotite	2.4%	$K(Mg,Fe)_3AlSi_3O_{10}(OH)2$	Insoluble	Soluble
Microcline	15.9%	$KAlSi_3O_8$	Insoluble	Insoluble
Quartz	32.7%	SiO_2	Insoluble	Insoluble
Clinochlore llb-2	0.6%	$Mg_5Al(AlSi_3O_{10})(OH)_8$	Soluble	Soluble
Actinolite	0.1%	$Ca_2(Mg,Fe)5Si_8O_{22}(OH)_2$	Insoluble	(no data)

3.3 HCl corrosion testing

The corrosion rates observed in both the static HCl test and the dynamic HCl test were generally linear when measured in terms of mass loss over time for the specimens tested. The averaged corrosion rates for each concrete mix type are ported in Table 13 for the static HCl test and Table 14 for the dynamic HCl test.

Table 13: Ranked performance of GP/PC/CAC concrete mixes tested in the static HCl test

Rank in resistance	Concrete mix	Corrosion rate ($mg/cm^2/hr$)
1	GP-ferro-quartz	0.056
2	GP-granite	0.0587
3	GP-andesite	0.086
4	GP-dolerite	0.14
5	CAC-dolomite	0.27
6	GP-dolomite	0.54
7	PC-dolomite	3.85

Table 14: Ranked performance of GP/PC/CAC concrete mixes tested in the dynamic HCl test

Rank in resistance	Concrete mix	Corrosion rate ($mg/cm^2/hr$)
1	GP-ferro-quartz	0.19
2	GP-granite	0.44
3	GP-andesite	0.46
4	GP-dolerite	4.43
5	GP-dolomite	21.1
6	PC-dolomite	34.12
7	CAC-dolomite	52.1

4. DISCUSSION

XRD analysis showed that the three binders consisted of mostly amorphous phases. The amorphous content of Portland cement was 79%, calcium aluminate cement 70.1% and the amorphous content of geopolymer cement was 72%. Thus, only the mineralogy of the crystalline phases was characterised. Of significance was that the fly ash-based geopolymer's mineralogy consisted of acid-insoluble minerals (under ambient temperature and pressure). Mullite (13.9%) and quartz (8.7%) were the main insoluble minerals in geopolymer hardened cement paste. Much of the insoluble mullite was attributed to fly ash used in the geopolymer binder. The crystalline phase Portland hardened cement pastes consisted mainly of portlandite (6.3%) and haurite (11%), which are acid-soluble minerals. The crystalline phase of calcium aluminate cement hardened paste was found to consist mainly of krotite (12.8%) and katoite (6.7%), the solubility of these minerals was not established. On the other hand, the mineralogy of aggregates was analysed to consist of crystalline phases (99% or more).

Even though this study was focused on geopolymers, the control specimens also exhibited noteworthy behaviour. The performance of the CAC-dolomite concrete mix in the dynamic HCl test was significantly poorer than its performance in the static HCl test. The reduced performance of the CAC-dolomite concrete mix in the dynamic HCl test is attributed to the protection provided by alumina gel (AHx) being rendered ineffective by the abrasive action of the bristles in the dynamic HCl test. Under the static HCl test, the most resistant fly ash-based GP concretes (GP-ferro-quartz) provided a 69-fold improvement in acid corrosion resistance when compared to PC-dolomite concretes and a 4.82 fold improvement in acid corrosion resistance when compared to CAC-dolomite concretes. CAC-dolomite concrete was found to have the highest difference in performance between the dynamic HCl test and the static HCl test.

The results from the dynamic acid test showed that the resistance fly ash-based GP concretes under erosion-corrosion is significantly higher than both CAC and PC concretes. Under the dynamic HCl test, the best performing fly ash-based GP concrete (GP-ferro-quartz) provided up to a 180-fold improvement in resistance when compared to PC-dolomite concretes, and up to a 275-fold improvement in resistance when compared to CAC-dolomite concretes. Furthermore, the highest acid resistance was achieved using geopolymer concretes with siliceous aggregates. In the geopolymer concrete mixes, aggregates with a low proportion of soluble minerals such as ferro-quartz and granite produced concrete mixes with the highest acid resistance.

5. CONCLUSION

The study showed that geopolymer concretes offer a significant improvement to traditional binders under static and dynamic HCl testing. Static testing is used to approximate the conditions under static corrosion whereas dynamic testing is used to approximate the condition of erosion-corrosion. The resistance of geopolymer concrete to HCl corrosion can generally be improved by paring geopolymer cement with siliceous aggregates in the concrete mix. The study found that geopolymer cement paired with ferro-quartz aggregate yielded the lowest corrosion rates in both the static and dynamic HCl test. Calcium aluminate cement concrete paired with dolomite aggregate provided with lowest resistance in the dynamic HCl test. This result is attributed to effectiveness of a protective gel in calcium aluminate cement, referred to as alumina gel (AHx) by researchers [6] [5] is rendered ineffective under dynamic HCl test conditions.

REFERENCES

[1] T. Bakharev, "Resistance of geopolymer materials to acid attack," *Cement and concrete research,* pp. 658-670, 2005.

[2] Grengg, "Microbially induced acid corrosion in sewer environments," Graz University of Technology, 2017.

[3] M. Kiliswa, "Composition and microstructure of concrete mixes subjected to biogenic acid corrosion and their role in corrosion prediction of concrete outfal sewers.," University of Cape Town, 2016.

[4] N. De Belie, J. Monteny and L. Taerwe, "Apparatus for accelerated degradation testing of concrete specimens," *Materials and Structures,* vol. 45, 2002.

[5] R. Letourneux and K. Scrivener, "High performance concretes from calcium aluminate cements," *Cement and concrete research,* vol. 29, pp. 1215-1223, 1999.

[6] J. Herrison and F. Saucier, "Use of calcium aluminate cements in H2S biogenic environment," Institute of of Concrete Technology, 2015.

[7] M. G. Alexander and C. Fourie, "Performance of sewer pipe concrete mixtures with Portland and calcium aluminate cements subjected to mineral and biogenic acid attack," *Materials and Structures,* vol. 44.

[8] C. Fourie, "MSc Thesis: Acid resistance of sewer pipe concrete," University of Cape Town, 2007.

[9] N. Motsieloa, "MSc Thesis: Acid resistance of sewer pipe," University of Cape Town, 2012.

[10] J. Crawford, "Solubility data on 646 common and not so common minerals," [Online]. Available: https://www.mindat.org/article.php/553/Solubility+Data+on+646+Common+and+Not+So+Common+Minerals. [Accessed 01 February 2020].

[11] W. Casey, H. Westrich, W. Aronld and J. Banfield, "The surface chemistry of disolving labodorite feldspar," *Geochimica et Cosomichimica,* vol. 53, 1989.

INFLUENCE OF BLENDED CEMENTS ON CORROSION RATE OF STEEL IN REINFORCED CONCRETE STRUCTURES IN A MARINE TIDAL ZONE – A REVIEW

Luthando Ngcotwana [(1)], Rakesh Gopinath [(1)] and Mike Otieno [(2)]

(1) Department of Civil Engineering, Central University of Technology

(2) School of Civil and Environmental Engineering, University of the Witwatersrand, Johannesburg

ABSTRACT

Reinforced concrete structures in the marine environment experience early deterioration problems due to chloride-induced steel corrosion. High chloride concentrations available and the waving action in exposure conditions such as the marine tidal zone makes the steel reinforcement vulnerable to corrosion. For this reason, modern procedures for reinforced concrete design are aimed at designing concrete that can resist weathering as well as corrosion to maintain quality and serviceability when exposed to the harsh marine environment. The use of blended cements in modern concrete production is notably increasing. This is because the introduction of supplementary cementitious materials (SCMs), such as ground granulated blast furnace slag (GGBS), fly ash (FA), silica fume (SF), etc., to produce blended cements in concrete technology produces dense and impermeable concretes. However, SCMs show different characteristics and performance under different exposure conditions. The main aim of this paper is to critically review the influence of blended cements on the rate of corrosion in concrete exposed in a marine tidal zone. This paper also explores the suitability of the classification of exposure zone in the marine environment used in European standards (EN 206), adopted in South Africa.

Keywords: blended cement, reinforced concrete, chloride-induced corrosion, corrosion rate, marine tidal zone.

1 INTRODUCTION

Reinforced concrete (RC) structures in the marine environment experience premature deterioration problems due to chloride-induced steel corrosion. High chloride concentrations available and the waving action in exposure conditions such as the marine tidal zone make the steel reinforcement vulnerable to corrosion. Depending on the exposure conditions, chloride ions in seawater can penetrate the concrete by diffusion, convection, permeation, and wick action [1]. However, a combination of convection and diffusion is the dominant mode of chloride transport in a marine tidal exposure conditions.

For steel corrosion to be initiated, a certain amount of chlorides (referred to as chloride threshold) at the level of steel is required [2, 3, 4]. Consequently, the passive protective oxide

layer around the steel reinforcement, which is formed as a result of high pH conditions (ranging from 12 – 13) in the concrete pore structure is disturbed and subsequently leading to corrosion initiation [5]. The corrosion initiation is followed by the formation of cracks, spalling of cover concrete, etc. in the propagation phase [6]. The propagation phase is mostly influenced by the availability of moisture and oxygen [1, 5].

Modern design procedures are aimed at designing RC structures that can resist weathering and corrosion to maintain quality and serviceability when exposed to the harsh marine environment. The use of blended cements incorporating supplementary cementitious materials (SCMs), such as ground granulated blast furnace slag (GGBS), fly ash (FA) and silica fume (SF) in modern concrete production has therefore increased. This is because blended cements produce dense and impermeable concretes [7] that improve the durability of RC structures [9,10].

This paper critically reviews the influence of blended cements on steel corrosion in RC structures in a marine tidal zone. This will enable engineers with the knowledge to enhance the service life of reinforced concrete structures with blended cements. It also explores the suitability of the classification of exposure zone in the marine environment used in European standards [11], adopted in South Africa [12].

2 SUPPLEMENTARY CEMENTITIOUS MATERIALS

Supplementary cementitious materials (SCMs) are used to partially replace a portion of plain Portland cement (PC). FA, GGBS, and SF are the most commonly used SCMs in South Africa. These materials are categorised as pozzolans and hydraulic materials [13]. The incorporation of SCMs in concrete improves its durability properties through pozzolanic or hydraulic activity, or a combination [13].

For example, low calcium FA, SF and other natural pozzolans such as metakaolin (calcined clay) and volcanic ash exhibit pozzolanic behaviour when used in concrete, whereas high calcium FA exhibits both pozzolanic and hydraulic reactions. In contrast, GGBS exhibits limited hydraulic behaviour due to its ability to form hydration products when in contact with only water [13]. For this reason, hydraulic SCMs can, independently of plain PC, harden or gain strength, however when jointly used with PC, chemical reactions are accelerated [13].

Guneyisi et al. [14] studied the properties of different SCMs and their durability performance when used in concrete. A performance variation in reinforcement corrosion and concrete resistivity was observed, where other SCMs yielded better resistance to reinforcement corrosion than others, based on their replacement levels. Further, they highlighted that the performance variation was attributed to SCM physical, chemical, and mineralogical composition as a result of their production and the properties of the raw material used. Other studies found that SCMs reduce the amount of calcium hydroxide in concrete due to the dilution effect and pozzolanic reaction [15, 16]. As a result, the reduction of calcium hydroxide weakens the passivity of the reinforcing steel [17]. Therefore, careful consideration of the type and the content of the SCM to be used in a particular concrete mixture is paramount because of the varying impact of SCM on concrete properties, which in turn influences their durability performance. The reader is referred to Thomas [13] for in-depth details on the origin of SCMs.

3 THE INCLUSION OF BLENDED CEMENTS IN CONCRETE

3.1 Influence of blended cements on corrosion rate

Lopez-Calvo et al. [18] studied the influence of cover depth on the corrosion of steel in high-performance concrete (HPC) against the concrete quality and specimen crack width in laboratory simulated tidal conditions. The concrete contained corrosion inhibitors and 20% fly ash. A reduction in corrosion rate was observed in concrete specimens containing fly ash, regardless of the concrete cover and crack width. Similarly, Otieno et al. [19] conducted an experimental study on chloride-induced corrosion of steel in an accelerated (cyclic wetting and drying) and natural marine environment. A variation in cover depth of 20 mm and 40 mm was employed. The concrete specimens were made of 100% PC and a partial replacement of the Portland cement with SCMs (30% FA or 50% GGBS). They observed that the inclusion of SCMs results in a significant decrease in corrosion rate at a given cover depth.

In a recent study, Baten et al. [20], checked the corrosion vulnerability of RC structures using different blended cements and a variation in cover depth. In concrete mixes containing 30 - 40% of GGBS, the results yielded moderate resistance to corrosion. The study further pointed out that the performance of GGBS concretes improved with the increase in cover thickness and higher compressive strength values. Whereas concrete mixed with 30 - 40% FA yielded higher corrosion resistance even at lower cover depths but with slow strength development. The high corrosion resistance may be attributed as a result of higher silica content and a larger amount of calcium-silicate-hydrate (C-S-H) in FA concretes, with the latter leading to a more refined pore structure, hence stifled corrosion [21].

Further, Otieno [10] showed that the diffusion coefficient values of GGBS concrete, at different water to cement (w/c) ratios, were lower than those of FA concretes. This indicated that, based on the replacement levels used in that study, GGBS concrete had better durability performance than FA concrete concerning the ingress of chlorides, moisture and oxygen, hence lower corrosion risk. The better performance of GGBS than the other SCMs was also observed in a review by Yi et al. [22]. These studies reveal that SCMs show different characteristics and performance. Hence, it is important to provide engineers with enhanced knowledge to specifically select binder types suitable for a particular exposure zone, consequently assisting in improving the service life predictions of structures in the tidal zone of the marine environment.

Scott and Alexander [23] studied the influence of binder type, cracking and concrete cover on the rate of corrosion and resistivity in chloride-contaminated concrete. The specimens were exposed to cyclic wetting and drying. The results showed that SCM concretes (incorporating FA, GGB and SF) had higher resistivity compared to PC concrete, thus reducing the rate of corrosion of reinforcement. Therefore, they concluded that in blended concretes, concrete resistivity governs the occurrence of corrosion and results in low oxygen diffusion. Also, the results of Chang et al. [24] concur with these findings. Where the incorporation of GGBS resulted in low oxygen diffusion due to a denser microstructure exhibited by blended concrete. Therefore, an understanding of the influence of oxygen and moisture content on the corrosion rate is significant, especially for structures in a marine tidal zone, taking into account the influence of drying and wetting durations and SCMs under varied cover depths.

3.2 Influence of blended cements on chloride ingress

Chloride ingress is the primary cause of corrosion of reinforcement in chloride contaminated reinforced concrete structures. The concrete pore solution, concrete quality, exposure conditions, curing regime, cement composition, etc. influence chloride penetration into concrete [25].

Simcic et al. [26] investigated the chloride penetration profiles for mixtures exposed to cyclic wetting and drying conditions for 21, 42, 84, 105, and 126 days. The concrete mixtures incorporated unmodified and modified (with fly ash) cement. From their results, modified concrete showed lower chloride concentrations compared to the unmodified concrete in each observation. This was as a result of the dense microstructure in modified concrete. Also, Thomas and Moffatt [27] reached similar conclusions, where concretes incorporating SCMs (such as GGBS, FA and SF) yielded lower chloride penetrations than the PC concrete for structures exposed to different marine conditions (including tidal zone) for 25 years.

The use of supplementary cementitious materials as a partial replacement for Portland cement in concrete applications shows a high chloride binding capacity and great resistance to chloride penetration to the level of reinforcing steel [25, 26, 27, 28, 29], thereby limiting the rate of corrosion in blended concretes. Furthermore, Chalhoub et al. [30] investigated the critical chloride threshold values as a function of cement type and steel surface. It was found that a low w/c ratio increased the chloride threshold value. Furthermore, blended concretes also exhibited higher chloride threshold values for the same low w/c ratio. These findings support the conclusion by Angst et al. [31] that concrete quality (which is affected by w/c ratio and cement type) influences the transport mechanism of aggressive fluids and gasses in concrete in aggressive environments such as the marine tidal zone, hence the significance of concrete quality in concrete durability assessments as well as service life predictions.

Moradllo et al. [32] quantified the convection zone depth and its influence on chloride profiles and service life prediction of concrete structures in a marine tidal zone for five years. The convection zone is generally known to consist of high chloride concentrations. Two w/c ratios (0.35 and 0.5) and silica fume were used in the mix. The concrete with low w/c ratio of 0.35 yielded a 50% decrease in the convection zone depth compared to a w/c ratio of 0.5 due to the high permeability of the latter.

Guneyisi [33] examined the effect of initial curing on chloride ingress and corrosion resistance using different binders. The results showed that initial curing had an influence on chloride penetration for all concretes. Nevertheless, the rate of chloride ingress and corrosion was found to be dependent on the w/c ratio as well as the cement type. Similarly, the influence of w/c ratio as well as cement type on chloride diffusion and corrosion rate was also noted by van der Wegen et al. [34].

4 REVIEW OF EXPOSURE CLASSIFICATION IN SANS 10100-2: 2013

This section explores the suitability of the classification of exposure zones in the marine environment used in European standards (EN 206-1), adopted in South Africa (SANS 10100-2) [35]. The standard classifies the marine tidal zone and splash and spray zone as the most severe exposure conditions. However, the results from the field observations presented in Moore [1] challenge this classification because of a notable difference in corrosion severity, with the tidal zone exhibiting little or no signs of corrosion. Furthermore, findings from

laboratory investigations of the same study, suggest an adjustment of the tidal zone to the submerged category based on the thickness of concrete cover (greater than 30 mm). However, it should be noted that the study only focussed on the use of PC in concrete, and due to the difference in concrete resistivity, concrete pore solution, oxygen diffusion rate, etc., when using blended cements, the results may differ. Hence, there is a need for further research when using SCMs.

Therefore, the classification of exposure classes indicating the severity of corrosion damage need to be refined taking into account the type of cement used and cover depth adopted. This will enable more precise durability design specifications depending on the exposure classes, leading towards sustainable design practice.

5 CONCLUSIONS

In this study, a review of the influence of blended cements on the corrosion rate of reinforced structures is presented. The study also explores the suitability of the exposure zone classification in the marine environment as per the adopted standard in South Africa. The following conclusions can be drawn:

- The inclusion of SCMs such as fly ash, ground granulated blast-furnace slag and silica fume, as partial replacement for PC, results in a more refined concrete microstructure and high concrete resistivity. Consequently, it leads to a reduction in the corrosion rate. Notably, GGBS concretes are reported to exhibit better durability performance than other SCMs from the reviewed studies.
- SCMs as a partial replacement for Portland cement in concrete applications show a high chloride binding capacity and great resistance to chloride penetration. Furthermore, the reviewed literature also reveals that the w/c ratio is influenced by the performance of SCMs to inhibit chloride penetration, where chloride ingress was inhibited even at relatively high w/c ratios. In addition, the concrete cover was shown to influence the reduction of diffusion of oxygen to the level of the reinforcement.
- Studies from the literature suggest that the current exposure zone classification of the marine tidal zone must be adjusted to the submerge category taking into account the influence of cover depth. However, more research, based on more field investigations and the incorporation of SCMs, is needed to support this notion.

ACKNOWLEDGEMENT

The authors would like to acknowledge the financial support from the merSETA grant as well as the National Research Foundation.

REFERENCES

1. Moore, A. ‘Effect of oxygen availability on the corrosion rate of reinforced concrete in marine exposure zones: inference from site and lab studies’, MSc Eng. Thesis, 2019 (Department of Civil Engineering, University of Cape Town, Cape Town, South Africa).
2. Alonso, C., Castellote, M. & Andrade, C. ‘Chloride threshold dependence of pitting potential of reinforcements’, *Journal of Electrochimica Acta* 47 (2002):3469-3481.
3. Otieno, M. ‘Corrosion propagation in cracked and un-cracked concrete’, MSc Eng. thesis, 2008 (Department of Civil Engineering, University of Cape Town, Cape Town, South Africa).

4. Babaee, M. & Castel, A. 'Chloride diffusivity, chloride threshold, and corrosion initiation in reinforced alkali-activated mortars: Role of calcium, alkali, and silicate content', *Cement and Concrete Research* 111 (2018):56-71.
5. Broomfield, J.P. 'Corrosion of Steel in Concrete: Understanding, Investigation and Repair', 2nd ed. Tailor & Francis Group (London, England, 2006).
6. Tuutti, K. 'Corrosion of Steel in Concrete', Report No. 4, Swedish Cement and Concrete Research Institute (Stockholm, Sweden, 1982).
7. Zhang, J., Shi, C., Zhang, Z. & Ou, Z. 'Durability of alkali-activated materials in aggressive environments: a review of recent studies', *Construction and Building Material* 152(2017) 598-613.
8. Wu, K., Long, J., Xu, L. & De Schutter, G. 'A study on the chloride diffusion behaviour of blended cement concrete in relation to aggregate and ITZ', *Construction and Building Material* 223 (2019) 1063-1073.
9. Xu, H., Chen, Z., Xu, B. & Ma, D. 'Impact of low calcium fly ash on steel corrosion rate and concrete-steel interface', *The Open Civil Engineering Journal* 6 (2012) 1-7.
10. Otieno, M. The development of Empirical Chloride-induced corrosion rate prediction model for cracked and un-cracked steel reinforced concrete structures in the marine tidal zone. PhD thesis, 2014 (Department of Civil Engineering, University of Cape Town, Cape Town, South Africa).
11. *EN 206-1*. 'Concrete - specification, performance, production and conformity', European Standard, 2013.
12. *SANS 10100-2*. 'The Structural Use of Concrete Part 2: Materials and Execution of work', SABS, 2013 (Pretoria, South Africa, 2013).
13. Thomas, M. 'Durability of Concrete'. *Supplementary Cementing Materials in Concrete*, Chapter 9, CRC Press, Taylor & Francis Group, 2013 (Boca Raton, FL, USA, 2013) 103-160.
14. Guneyisi, E. Ozturan, T. & Gesoglu, M. 'A study on reinforcement corrosion and related properties of plain and blended cement concretes under different curing conditions', *Cement and Concrete Composites* 27 (4) (2005) 449-461.
15. Zhang, Y.M. Sun, W. Yan, H.D. 'Hydration of high-volume fly ash cement pastes', *Cement and Concrete Composite* 22 (6) (2000) 445-452.
16. Detwiler, R. 'The role of Fly Ash Composition in Reducing Alkali-Silica Reaction', PCA R&D Serial No. 2092. Portland Cement Association, (Skokie (Illinois), United States of America, 2002).
17. Poursaee, A. 'Corrosion of steel bars in saturated $Ca(OH)_2$ and concrete pore solution', *Concr Res Lett,* 1(3) (2010) 90-97.
18. Lopez-Calvo, H.Z., Montes-García, P., Jiménez-Quero, V.G., Gómez-Barranco, H., Bremner, T.W. & Thomas, M.D.A. 'Influence of crack width, cover depth and concrete quality on corrosion of steel in HPC containing corrosion inhibiting admixtures and fly ash', *Cement and Concrete Composites* 88 (2018) 200-210.
19. Otieno, M., Beushausen, H. & Alexander, M. 'Chloride-induced corrosion of steel in cracked concrete - Part I: Experimental studies under accelerated and natural marine environments', *Cement and Concrete Research* 79 (2016) 373-385.
20. Baten, B., Torsha, T. & Manzur, T. 'Corrosion vulnerability of reinforced concrete structures with different blended cement due to chloride ingress', *Materials Today: Proceedings* (2020).
21. Baten, B., Manzur, T. & Ahmed, I. 'Combined effect of binder type and target mix-design parameters in delaying corrosion initiation time of concrete', *Construction and Building Materials* 242 (2020) 118003.
22. Yi, Y., Zhu, D., Guo, S., Zhang, Z. & Shi, C. 'A review on the deterioration and approaches to enhance the durability of concrete in the marine environment', *Cement and Concrete Composites* 113 (2020) 103695.
23. Scott, A. & Alexander, M.G. 'The influence of binder type, cracking and cover on corrosion rates of steel in chloride contaminated concrete', *Magazine of Concrete research* 59 (7) (2007) 495-505.

24. Cheng, A., Huang, R., Wu, J. & Chen, C. 'Influence of GGBS on durability and corrosion behavior of reinforced concrete', *Materials Chemistry and Physics* 93 (2005) 404-411.
25. Shi, X., Xie, N., Fortune, K. & Gong, J. 'Durability of steel reinforced concrete in chloride environments: An overview', *Construction and Building Materials* 30 (2012) 125-138.
26. Simcic, T., Pejovnik, S., De Schutter, G. & Bosiljkov, V.B. 'Chloride ion penetration into fly ash modified concrete during wetting–drying cycles', *Construction and Building Materials* 93 (2015) 1216-1223.
27. Thomas, M.D.A. & Moffatt, E.G. 'The Performance of Concrete in a Marine Environment', *6th International Conference on Durability of Concrete Structures*, Leeds, 18-20 July 2018, (Leeds, United Kingdom, 2018).
28. Thomas, M.D.A. & Bamforth, P.B. 'Modelling chloride diffusion in concrete: Effect of fly ash and slag', *Cement and Concrete* Research 29 (4) (1999) 487-495.
29. Tadayon, M.H., Shekarchi, M. & Tadayon, M. 'Long-term field study of chloride ingress in concretes containing pozzolans exposed to severe marine tidal zone', *Construction and Building Materials* 123 (2016) 611-616.
30. Chalhoub, C., François, R. & Carcasses, M. 'Critical chloride threshold values as a function of cement type and steel surface condition', *Cement and Concrete Research* 134(2020) 106086.
31. Angst, U., Geiker, M.R., Alonso, M.C., Polder, R., Isgor, O.B., Elsener, B., Wong, H., Michel, A., Hornbostel, K. & Gehlen, C. 'The effect of the steel–concrete interface on chloride-induced corrosion initiation in concrete: a critical review', RILEM TC 262-SCI, *Materials and Structures* 52 (4) (2019) 88.
32. Moradllo, M.K., Sadati, S., & Shekarchi, M. 'Quantifying maximum phenomenon in chloride ion profiles and its influence on service-life prediction of concrete structures exposed to seawater tidal zone - A field oriented study', *Construction and Building* Materials 180 (2018) 109-116.
33. Guneyisi, E., Ozturan, T. & Gesoglu, M. 'Effect of initial curing on chloride ingress and corrosion resistance characteristics of concretes made with plain and blended cements', *Building and Environment* 42 (7) (2007) 2676-2685.
34. van der Wegen, G., Polder, R.B. & van Breugel, K. 'Guideline for service life design of structural concrete - A performance based approach with regard to chloride induced corrosion', *Heron* 57 (3) (2012) 153-168.
35. Ballim, Y., Alexander, M. & Beushausen, H. 'Durability of Concrete', In ed. Owens, G, *Fulton's Concrete Technology*, Chapter 9 (Cement & Concrete Institute, Midrand, South Africa, 2009) 155-188.

THE INFLUENCE OF STEEL FIBRE REINFORCEMENT ON THE BALLISTIC RESISTANCE OF CONCRETE

Jurie F. Adendorff [(1)], Elsabe Kearsley [(1)]

(1) Department of Civil Engineering , University of Pretoria

ABSTRACT

This study involves research on the influence of steel fibre reinforcement on the ballistic resistance of concrete. Concrete panels were cast with varying thicknesses and fibre volumes and subjected to a kinetic energy related ballistic attack. A .30-'06 hunting rifle using specially loaded ammunition was used to simulate the kinetic energy of ballistic attacks performed by an AK-47. The failure mechanism has been identified to consist of the Crater and Crushed Aggregate regions which are dependent on the Compressive Strength of the concrete and the Scab region, which is dependent on the Tensile Strength of the concrete. The ballistic resistance of the concrete panels was determined by taking volumetric measurements of the failure regions. Ultrasonic Pulse Velocity tests were conducted to determine the crack formation and propagation caused by the ballistic attacks. By incorporating the use of steel fibres, the Compressive and Tensile Strength of the concrete panels were improved which led to an increase in ballistic resistance of the concrete panels as well as an increase in damage mitigation. It has also been found that an increase in the thickness of the concrete panels led to an increase in overall ballistic resistance of the concrete panels.

Keywords: concrete ballistics, fibre reinforcement, impact testing

1. INTRODUCTION

"*Sweat saves blood*" – Erwin Rommel.

Radicalized terrorist groups have become a problem as of late. These groups target the civilian population with mass shootings and explosives. It is therefore important to design and construct infrastructure to protect those who may be a target. Some countries experience a high crime rate consisting of criminal activities that includes gun related violence with drive-by shootings as an example. These activities influence the lives of innocent civilians and lives may be lost. It is thus important to find building materials that can withstand impact loading by absorbing energy without shattering under impact. Unreinforced concrete is normally deemed to be brittle, and it is known that steel fibres can be added to concrete mixtures to improve ductility and increase absorption before fracture [1].

There are existing standards for the development and standardization of ballistic protection, for both vehicles and body armour. NIJ [2], Alpineco [3] and NATO's STANAG [4] are but a few of the standards specifying the standardization of ballistic armouring, but none of them include the standardization, development and applications for the ballistic resistance of concrete. Although extensive research has been conducted on the impact resistance of concrete

[1, 5-10, 12, 13], only limited design guidelines have been developed that can be used to design concrete exposed to high impact loading.

In this study, the effect of steel fibre reinforcement on the ballistic resistance of concrete was investigated. The study is of experimental nature. Research was conducted on the failure mechanism of concrete under high velocity impacts and the material properties that were sought after to increase the ballistic resistance of concrete, such as an increase of both compressive and tensile strengths. Experiments were set up and performed in order to determine any significant performance improvements of the concrete panels. The experiments were divided into two groups, the first comprised of a range of tests to determine the material properties of the concrete used to construct the panels and the second, to determine the ballistic performance and resistance of the concrete panels. The results were analysed, and various conclusions have been reached regarding the relationships between the material properties of the concrete and the ballistic resistance that the panels provided.

2. FAILURE MECHANISM OF CONCRETE UNDER HIGH VELOCITY IMPACTS

When a projectile traveling at a high velocity impacts a concrete target, it induces a longitudinal compressive wave. Depending on the thickness of the concrete, the compressive wave reflects back as a tensile wave once it hits the unconfined face at the back of the target. If the amplitude of this tensile wave exceeds the tensile strength of the concrete, it forms cracks in the concrete and propagate existing cracks [9].

The failure mechanism of concrete under high velocity impacts can be divided into three regions [9], as illustrated in Figure 1. The first region is the crater and crushed aggregate region. This region is dependent on the compressive strength of the concrete. Literature has shown that the crater is of conical shape and the volume of the crater is inversely proportional to the square root of the compressive strength [10]. The second region is the cracking region, which is dependent on the tensile strength of the concrete. The third region is the scab region. Scabbing is the loss of material at the back of the concrete target. This region is dependent on the tensile strength as well as the thickness of the concrete target. Due to the dependency of the scab region on the thickness of the concrete target, it may or may not occur. If the concrete target is of sufficient thickness, the longitudinal wave induced by the impact may dissipate and scabbing will not occur.

It is important to now clarify the definition of perforation. If the velocity of the projectile is such that it penetrates the target and the tip of the projectile protrudes from the back of the target, or the projectile leaves a hole such that light can shine through, the velocity of the projectile meets the U.S. Army's criterion for perforation [11]. If the velocity of the projectile enables it to pass through the target but has no energy, the velocity of the projectile meets the U.S. Navy's criterion of perforation [11]. The use of the above-mentioned definitions for perforation depends solely on the practical application of the target. For the purpose of the study, the U.S. Army's criterion for perforation will be used.

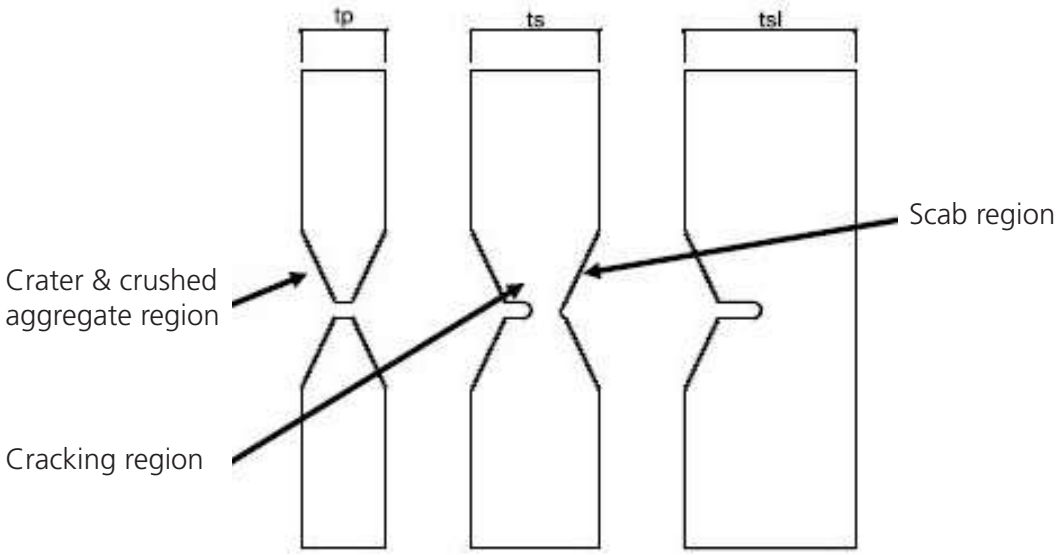

Figure 1: Failure Mechanism of Concrete Under High Velocity Impacts [10]

Various thickness definitions may be given to the concrete target, which consists of combinations of the three regions of the failure mechanisms as well as referring to perforation [12]. The Perforation Thickness (t_p) may be defined as the maximum thickness at which a projectile will perforate the target. All three failure regions are found in the Perforation Thickness, where the crater and scab regions may be directly linked together (given that the target is thin enough) or they may be connected via a "tunnel" caused by the penetration of the projectile. An increase in thickness leads to the Scabbing Thickness (t_s), which is the minimum thickness at which scabbing occurs without perforation taking place. An increase in thickness surpassing the Scabbing Thickness leads to the Scabbing Limit Thickness (t_{SL}). This is the minimum thickness of the target to prevent scabbing from occurring.

3. MIX DESIGN AND MATERIAL PROPERTIES

The mix design consisted of a CEM II 52.5N Portland Cement, Undensified Silica Fume, Fly Ash, Ground Granulated Blast Furnace Slag, Dolomite sand (< 4.5mm), Dolomite stone (< 9.5mm), Spring Steel Micro Fibres, Polypropylene Fibres and CHRYSO OPTIMA 100 Superplastisizer. A water-cement ratio of 0.4 was used. Spring Steel Micro Fibres with 2500MPa tensile strength, 13mm in length, 0.2mm in diameter and aspect ratio of 65 were used. The amount of steel fibres varied for four different mixes. Mix 1, the control, had 0.0% fibres, whereas mixes 2, 3 and 4, contained 1.5%, 3.0% and 4.5% fibres respectively, with relation to volume. Polypropylene fibres were added to the mix to reduce the amount of initial shrinkage cracks that could propagate further during the ballistic testing. The mixing, casting and curing took place in the Civil Engineering Laboratory of the University of Pretoria. Table 1 contains the material properties of the various mix designs and Table 2 contain the respective standard deviations. The compressive strength as indicated in Table 1 is the average 28-day water cured strength obtained from three 100mm cubes while the indirect tensile strength was obtained from four split cylinder tests conducted on 100mm diameter cylinders. The direct tensile strength was taken from the average of 3 prisms in the shape of a "dog-bone" with a square cross-section

of 50mm sides. The "dog-bones" were pulled along the longitudinal axis until failure occurred. The direct tensile test also indicated that the failure mechanism of the fibres within the concrete matrix was of shear failure where the fibres pulled out of the matrix instead of fracturing. This was due to a weak bond-strength and indicated that the full tensile potential of the fibres was not utilised. The modulus of elasticity was determined by taking the average of measurements from two cylinders, 200mm in length and 100mm in diameter, cured for 28-days.

Table 1: Summary of Material Properties

Fibre Percentage [%]	Compressive Strength [MPa]	Tensile Strength [MPa]		Modulus of Elasticity [GPa]
		Direct	Indirect	
0.0	78.3	3.5	4.9	33
1.5	103.8	4.7	9.7	37
3.0	114.6	5.9	13	44
4.5	115.3	7.2	14	41

Table 2: Standard deviations of Material Properties

Fibre Percentage [%]	Compressive Strength [MPa]	Tensile Strength [MPa]		Modulus of Elasticity [GPa]
		Direct	Indirect	
0.0	4.22	0.40	0.34	0.71
1.5	6.56	0.56	0.17	0.62
3.0	5.55	0.32	0.88	1.05
4.5	2.79	0.39	0.49	1.60

4. BALLISTIC TESTING AND RESULTS

The ballistic testing was performed at the Bluegum Valley Shooting Range located near Bronkhorstspruit. It is an outdoor shooting range located within a plantation. The trees of the plantation as well as the embankments situated on the sides provide for excellent wind protection.

The targets were placed 20m from the firing station and velocity measurements were taken at 10m from the target. The method of exponential decay, shown in equation 1, was used to calculate the impact velocity of the projectile, assuming a constant drag coefficient, C_d, of 0.33 with v_I as the impact velocity [m/s], v_X the velocity at point of measurement [m/s], X as the distance from the target [m], ρ_{air} the density of air at standard conditions (1.225kg/m^3), m as the mass of the projectile [kg] and d as the projectile diameter [m]. The mean projectile mass was 9.23g reaching an impact velocity of 780m/s, producing 2 808J of kinetic energy.

$$v_I = v_X * e^{\frac{-X*\rho_{air}*\pi*C_d*d^2}{8m}} \qquad \textbf{Equation (1)}$$

The firing station consisted of an elevated table and the rifle, a .30-'06 SAKO, was propped up with a special sandbag used for precision shooting. The rifle has a 1:12 twist rate. A Prochrone Chronometer was used for velocity measurements as shown in Figure 2 (a). A steel frame was constructed to hold the concrete panels in a fixed position. Pieces of threaded rod were used to screw the panels tightly in place. The threaded rods, however, did not screw directly to the concrete panels. Pieces of flat bar were used to distribute the forces evenly. The influence of the addition of steel fibre reinforcement with respect to the ballistic resistance of concrete panels is clearly illustrated in Figure 2 (b), (c). The unreinforced concrete panel was completely destroyed due to its brittle nature.

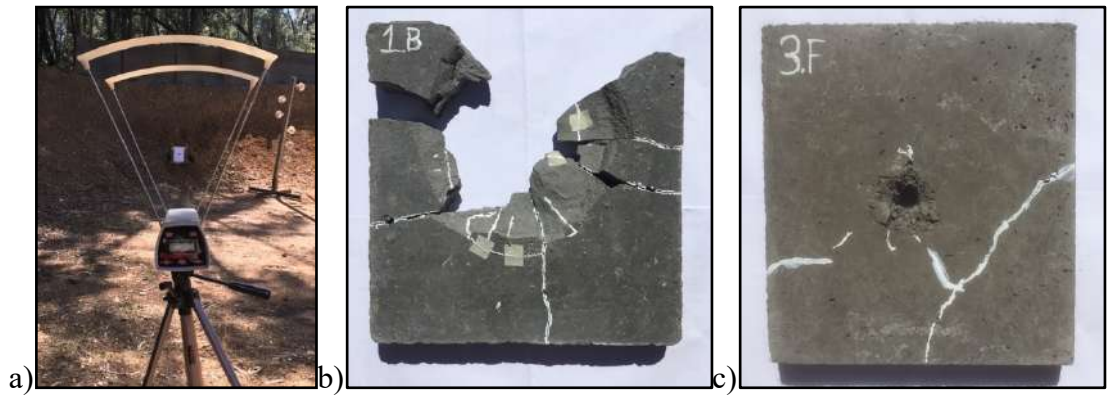

Figure 2: a) Prochrono chronometer, b) unreinforced concrete panel, c) fibre reinforced concrete panel

The following measurements were taken in order to gauge the ballistic performance of the fibre reinforced concrete panels: crater diameter and volume, perforation percentage and the Ultrasonic Pulse Velocity over the thickness of the panel both before and after being subjected to ballistic attack.

When examining the crater inflicted by the projectile, a general trend can be found. It can be seen in Figure 3 that for both the diameter and the volume of the crater, a decrease in size occurs with an increase in the percentage volume of steel fibres. It can also be seen from the same graphs in Figure 3, that with an increase in compressive strength, a decrease in crater diameter and volume occurs. This confirms that the crater and crushed aggregate region is indeed dependent on the compressive strength of the mix, as stated in the literature. When examining the crater diameter alone, it can be seen that the 50mm panel experienced the least amount of damage. This is due to the 100% perforation that occurred for mixes 1 and 2 containing 0.0% and 1.5% volume steel fibres respectively, as can be seen in Figure 3. With 100% perforation, the projectile leaves the panel with residual velocity and therefore the panel has less kinetic energy to absorb. With mixes 3 and 4 containing 3.0% and 4.5% volume of fibres, an increase in compressive strength occurred. In conjunction with the increase of compressive strength, the increase of volume of fibres lead to the formation of a mesh that enabled the panel to capture the projectile, thus resulting in perforation percentages less than 100%.

When examining the 75mm and 100mm panels, both a decrease in crater diameter and volume occurred. This is due not only to the increase in both compressive strength and volume of fibres, but also due to the increase in thickness of the panels. An increase in the thickness

leads to an increase in the energy absorption capability of the panels, due to the increased longitudinal wave dissipation that occurs.

Lastly, regarding the perforation percentage, panel thickness and compressive strength, it can be seen that for the thicker panels (75mm and 100mm) that neither the fibre percentage nor the compressive strength of the mixes have a significant effect on the perforation percentage. When concrete is subjected to high strain-rates, it experiences an increase of compressive strength [13]. This is caused by the combination of the lateral inertial confinement effect as well as material behaviour. This increase of compressive strength can be quantified by the Dynamic Increase Factor (DIF) and is dependent on aggregate properties and specimen size [13]. Therefore, an increase in specimen size will cause an increase in the DIF which results in a decrease in perforation percentage.

When examining the thinner panel (50mm) in this regard it can be seen that a significant increase in compressive strength occurs with the addition of 1.5% volume fibres, but no decrease in perforation percentage occurs. When the volume of fibres was increased from 1.5% to 3.0%, a slight increase in compression strength occurred, but a significant reduction in the perforation percentage occurred. This suggests that the quasi-static compressive strength does not play a role in the perforation percentage of the concrete panels, but rather the volume of fibres present in the mix and the thickness of the panels. The explanation for this is the combination of the longitudinal wave dispersion that occurs as well as the mesh-formation that is provided from the fibres.

When considering the ultrasonic pulse velocity of the panels it can be seen from Figure 3 that after the ballistic attack, a general decrease in the difference in ultrasonic pulse velocity, ΔUPV, (from before being subjected to ballistic attacks) occurs with an increase in volume of fibres in the mixes. When examining the 75mm and 100mm panels, it can be noted that there is a slight increase in ΔUPV from 3.0% to 4.5% volume fibres. This is due to dispersion problems of the fibres within the matrix. Voids are formed within the matrix which increase the readings obtained from the ultrasonic pulse velocity tests. Furthermore, an increase in the modulus of elasticity occurs with the addition of fibres but tapers down from 3.0% to 4.5% volume fibres. This is due to dispersion problems of the fibres.

When observing the significant increase in modulus of elasticity that occurs with the fibre volume increase from 1.5% to 3.0%, it can be seen that the ΔUPV reading remains almost constant for the 100mm panel and only decreases slightly for the 75mm panel. This indicates that the modulus of elasticity is a weak indicator of the energy absorption capabilities of the concrete panels under high velocity ballistic attacks and that the volume of fibres yet again has the greatest effect. The ultrasonic pulse velocity readings of the 50mm panels were neglected due to unreliable readings which was caused by the increase in damage experienced by the panels during the ballistic attacks.

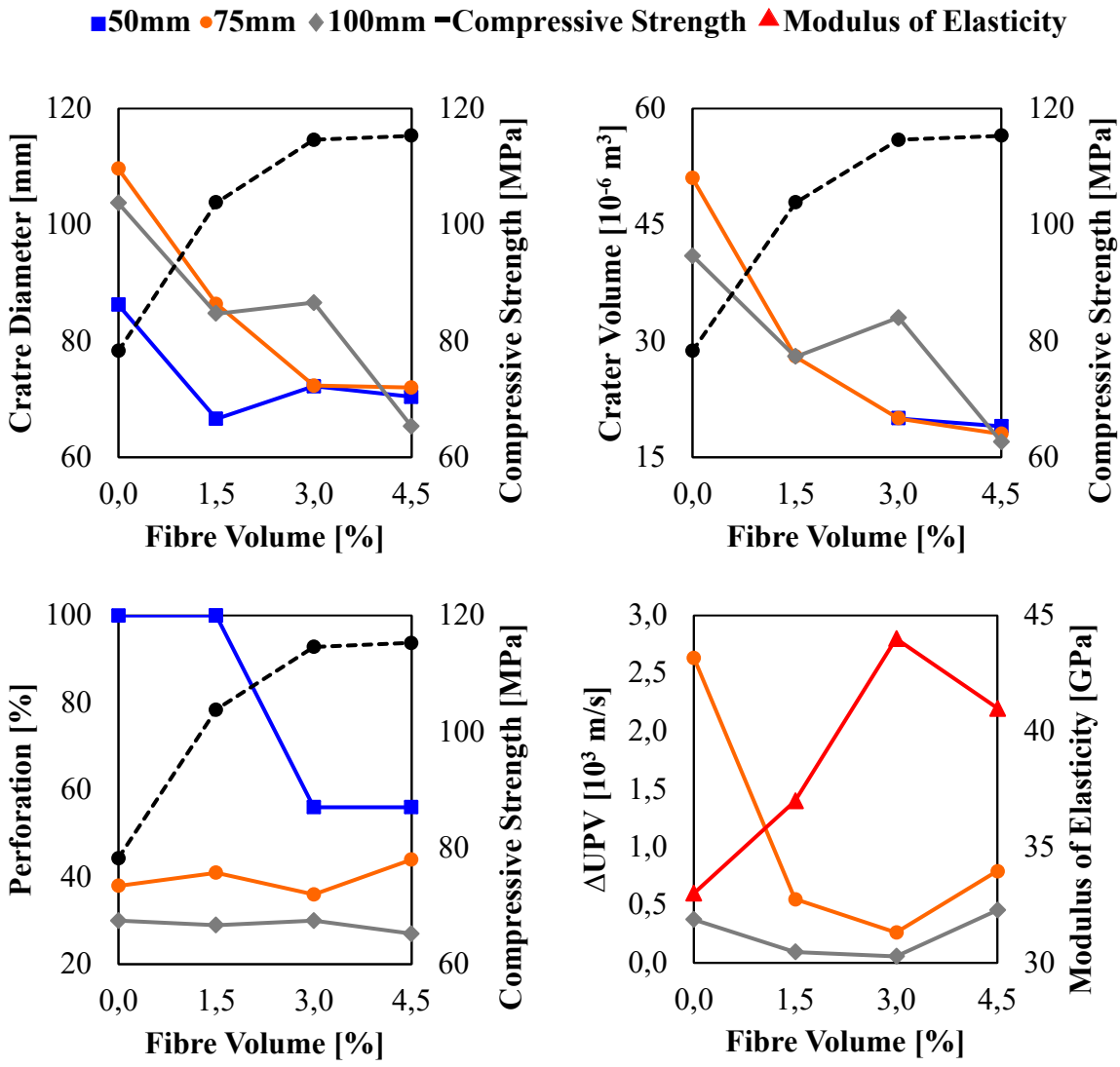

Figure 3: Crater diameters and -volumes, perforation percentage and difference in ultrasonic pulse velocity for all panels whilst considering the compression strengths and modulus of elasticity of the mixes

5. CONCLUSIONS

It can be concluded that an increase in the volume of fibres in this specific concrete mix contributes to a positive influence on the material properties beneficial to the ballistic resistance of the concrete panels. An increase in the volume of fibres resulted in an increase in the compressive and tensile (both direct and indirect) strengths of the concrete mix. This led to a decrease in crater diameter and volume as well as penetration depth. It should be noted that a fibre volume saturation point was reached in the vicinity of 4.5% volume fibres. An increase in fibre volume past this saturation point will lead to a decrease in strength and ballistic resistance. An increase in the volume of fibres also contributed to an increase in damage mitigation of the

concrete panels (i.e., crack formation and propagation), as can be seen from the results of the ultrasonic pulse velocity tests.

It was also found that the ballistic resistance of the concrete panels is dependent on the thickness of the panels. An increase in the thickness of the panels lead to better dissipation of the shockwave induced by the impact of the projectile. This increase of shockwave dissipation resulted in less damage occurring in terms of volume loss as well as in the formation and propagation of cracks in the concrete surrounding the point of impact.

It can be concluded that the crater diameter and volume are indeed dependent on the compressive strength of the concrete panels as suggested by the literature. The perforation percentage of thicker panels (75mm and 100mm) is solely dependent on the thickness of the panels and is not affected by the volume of fibre and compressive strength. The perforation percentage of thinner (50mm) panels is dependent on the volume of fibres and not the compressive strength. Finally, the volume of fibres in the concrete panels have a greater contribution to energy absorption and damage mitigation than the modulus of elasticity.

REFERENCES

[1] Yoo, D. and Banthia, N. 2019. Impact Resistance of Fiber-reinforced Concrete – A Review. *Cement and Concrete Composites,* 104, p. 103389.

[2] NIJ programs & services. 1993. [Washington, D.C.?]: U.S. Dept. of Justice, Office of Justice Programs, National Institute of Justice.

[3] Alpineco.com. 2019. *Alpine Armoring USA | Armored Vehicles - SUVs - Sedans - SWATs*. [online] Available at: https://www.alpineco.com/ [Accessed 23 Feb. 2019].

[4] Test methodology for protection of vehicle occupants against anti-vehicular landmine effects. 2007. [Neuilly-sur-Seine Cedex, France]: North Atlantic Treaty Organisation, Research & Technology Organisation.

[5] Yu, R., van Beers, L., Spiesz, P., & Brouwers, H. 2016. Impact resistance of a sustainable Ulta-High Performance Fibre Reinforced Concrete (UHPFRC) under pendulum impact loadings. *Construction and Building Materials*, 107, pp. 203-215.

[6] Banthia, N., Chokri, K., Ohama, Y., & Mindess, S. 1993. Fiber-Reinforced Cement Based Composites Under Tensile Impact. *Advanced Cement Based Materials*, 1, pp. 131-141.

[7] Banthia, N., Mindess, S., & Trottier, J.-.F. 1996. Impact Resistance of Steel Fiber Reinforced Concrete. *ACI Materials Journal*, 93(5), pp. 472-479.

[8] Suaris, W., & Shah, P. 1982. Inertial Effects in the Instrumented Impact Testing of Cementitious Composites. *Cement, Concrete, and Aggregates*, 3(2), pp. 77-83.

[9] Prakash, A., Rao, A. and Srinivasan, S. 2017. Investigations on Steel Fibre Reinforced Cementitious Composite Panels under High Velocity Impact of Short Projectiles. *Procedia Engineering*, 173, pp. 331-338.

[10] Clifton, J. 1982. *Penetration resistance of concrete*. Washington: U.S. Government printing Office, pp. 3-7.

[11] Backman, M. 1976. *Terminal ballistics*. China Lake, Calif.: Naval Weapons Center, pp. 53-76.

[12] Fang, Q. and Wu, H. (n.d.). *Concrete structures under projectile impact*. pp. 9-10.

[13] Hao, Y., Hao, H. and Li, Z. 2010. Numerical Analysis of Lateral Inertial Confinement Effects on Impact Test of Concrete Compressive Material Properties. *International Journal of Protective Structures,* 1(1), pp. 145-167.

EXPERIMENTAL STUDY ON THE EFFECT OF FLEXURAL REINFORCEMENT RATIO ON PUNCHING SHEAR STRENGTH OF FLAT SLAB WITHOUT SHEAR REINFORCEMENT

Abdelrhman M. A. Ahmed [(1)], Abdallah A. A. Alballa [(1)] and Dr. Mohemmed T. M. Abdelsalam [(1)]

(1) Department of Civil Engineering, University of Khartoum

ABSTRACT

Experimental investigations of six flat slab specimens were carried out in structural laboratory at University of Khartoum to investigate the influence of the flexural reinforcement ratio in punching strength. All slab specimens were 1.5m x 1.5m x 0.15m with 0.2m x 0.2m column constructed at the centre of slab. The main variable was the flexural reinforcement ratio which varied between 0.15% and 1.2%. The results of punching shear strengths of tested slabs were compared with those evaluated from different codes of practice, namely; BS8110, EC2, ACI318-11 and fib MC2010. Investigations showed that increasing the reinforcement ratio increases the punching capacity, but strongly decreases the deformation capacity of the tested slabs, hence their ductility. However, the increase in punching capacity appeared to be less significant in specimens with reinforcement ratios larger than 1%. Punching strength predictions using BS8110 & EC2 agreed fairly well with those from the tests. In regard to ACI 318-11 it was demonstrated that the code could lead to unsafe design for slabs with low reinforcement ratios. Conversely, fib MC 2010 predictions gave the best agreement with the test results.

Keywords: flexural reinforcement ratio; punching shear; flat slabs; critical shear crack theory; design codes.

1. INTRODUCTION

Flat slab system is the one of the best 20th century discoveries. It has an advantage of overcoming other systems cons which make it the ideal structural form for architects and contractors .The superiority of flat slab floor supported directly on columns, over other forms of construction when looked at from the standpoint of lower cost, better lighting, greater neatness of appearance, and increased safety and rapidity of construction, is so generally, or rather universally conceded as to render any reliable information relative to the scientific computation of stresses in this type of construction of great interest [1].

However flat slab system has a prominent drawback. With its small slab-column connection, the high stress in the column support may cause (the so-called punching shear failure). At the moment when the punching occurs [2] the column and slab physically separate from one another, which significantly disturbs the balance of the system formed by those elements. Often, such disturbance may cause collapse of great proportions due to redistribution of load to other elements that are not design to transfer such forces. This phenomenon occurs suddenly (brittle fracture), which is why it has to considered with great care during design of slabs supported on columns only.

2. CODE OF PRACTICE

The critical sections of the slab for moment and shear are either at or close to the perimeter of the loaded area, and hence it would be expected that moment-shear interaction would occur. This complicates the classification of the modes of failure at the connection. However, there is a change in the characteristic of the failure mode and load-deflection curves measured for slabs with different reinforcement ratios [3]. Most design codes base their verifications on a critical section, with the punching shear strength of slabs without shear reinforcement defined as a function of the concrete compressive strength and often of the reinforcement ratio. Four codes of practice are considered in comparisons with test data (BS8110, EC-2, ACI-318 2011 and MC-2010). It follows different formats ACI318-11 has a format which proportional to compressive strength and it doesn't count on reinforcement ratio.

$$V_c = \left(\frac{1}{3}\right).\lambda.\sqrt{f'_c}.b_o.d \qquad \textbf{Equation (1)}$$

Where λ is the modification factor for lightweight concrete, taken as unity for normal weight concrete in the present paper.

BS8110 has a format which proportional to compressive strength, reinforcement ratio and size effect.

$$0.79\left\{\frac{100.A_s}{b_v.d}\right\}^{\frac{1}{3}}.\left\{\frac{400}{d}\right\}^{\frac{1}{4}}.\left\{\frac{f_{cu}}{25}\right\}^{\frac{1}{3}}.\frac{1}{\gamma_m} \qquad \textbf{Equation (2)}$$

With a limitation of 0.03 for the reinforcement ratio and a minimum value of 0.67 for the size effect.

EC-2 equation depends on parameters same as BS8110 parameters

$$V_{Rd,c} = C_{Rdc}.K.(100\rho.f_{ck})^{\frac{1}{3}} + K.\sigma_{CD} \qquad \textbf{Equation (3)}$$

Where b_o is the control perimeter located 2d from the face of the column, ρ accounts for the bending reinforcement ratio (with a maximum value of 0.02) and K is a factor accounting for size effect defined by the following expression:

$$K = 1 + \sqrt{\frac{200\ \text{mm}}{d}} = 1 + \sqrt{\frac{7.87\ \text{in}}{d}} \leq 2 \qquad \textbf{Equation (4)}$$

Model Code 2010 proposes simplified formulas derived on the basis of Critical Shear Crack Theory CSCT for Calculation of load-rotation behavior. With respect to Eq (5) various methods can be used to estimate the load–rotation behavior necessary to calculate the punching shear strength. The values of the various mechanical parameters in the formula can be assessed with different degrees of accuracy, leading to the levels-of-approximation (LoA) approach.

$$V_{Rc} = K_{\psi} \frac{\sqrt{f_{ck}}}{\gamma_m} b_0 d_v$$ **Equation (5)**

with f_{ck} in [MPa].

The parameter k_{ψ} depends on the deformations (rotations) of the slab around the support region and is calculated as:

$$K_{\psi} = \frac{1}{1.5 + 0.6.\psi.d.k_{dg}} \leq 0.6$$ **Equation (6)**

3. RESEARCH SIGNIFICANT

Current methods for the design of punching shear reinforcement are based on empirical formulations to estimate the contributions of concrete and shear reinforcement at failure. This approach in some cases, leads to very conservative estimates of punching shear strength of flat slabs, however it may also overestimate the contribution of concrete or the shear reinforcement. This paper presents the results of an experimental test campaign on the punching shear strength of slabs in which the reinforcement ratio and bars diameter were varied. The tests focus mainly on slabs with low reinforcement ratios.

4. EXPERIMENTAL PROGRAM

The research presented herein basically focuses on the investigation of effect of flexural reinforcement ratio on punching shear resistance of flat slabs. All the investigated specimens refer to simply supported slabs with central square columns. Thus, the research focuses primarily on symmetrically loaded slabs.

The experimental study consists of six slab specimens with same geometry dimensions. However, different reinforcement bar diameters were used as follows:

Four basic slabs with the same reinforcement distribution on both directions but different bars diameter (8mm, 10mm, 2mm and 16 mm bar). One slab specimen with nominal reinforcement as a reference. One-way slab specimen to investigate the behavior of slab with different reinforcement distribution on the longitudinal and transverse directions and its crack pattern at failure and to compare it with the other slab specimens.

5. TEST SETUP

The tests were carried out in the reinforced concrete laboratory of the Faculty of Engineering, University of Khartoum. A very rigid steel frame consisting of horizontal and vertical I-sections was used as a base to support a slab specimen. The load was applied vertically using a hydraulic jack (Figure1) with maximum capacity 50 ton in centric of the column of slab. During every test, the load was applied in steps of 2 tons to avoid local failure in the column gypsum board were inserted between the steel cradles and the top surface of the slabs. Between load steps the hydraulic jack was kept constant for 5-10 minutes for inspection and measurements. The specimens were positioned on 1-m frame so that the research team was able to observe the bottom face of the slabs during testing. After the peak load was reached, the hydraulic jack was

further increased to record the post-punching behavior of the slabs.

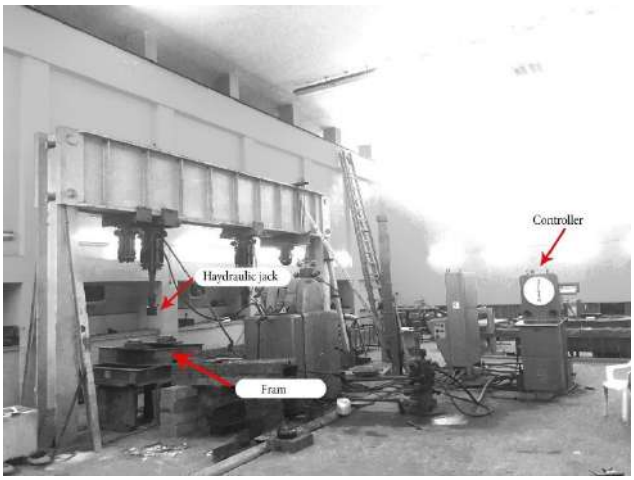

Figure 1 : Hydraulic jack And Loading Frame

Figure 2 : Slab during test

5. MEASUREMENT

Vertical deflection was monitored at the middle of the bottom surface of the slab (tension). one dial gauge was used. In addition, total station system was used to measure the deflection at the edges of the slab specimens. Steel strains were measured and recorded by using a digital data logger device connected to the strain gauges by wires and the readings were taken at each increment of loading. Finally, crack pattern was inspected at failure.

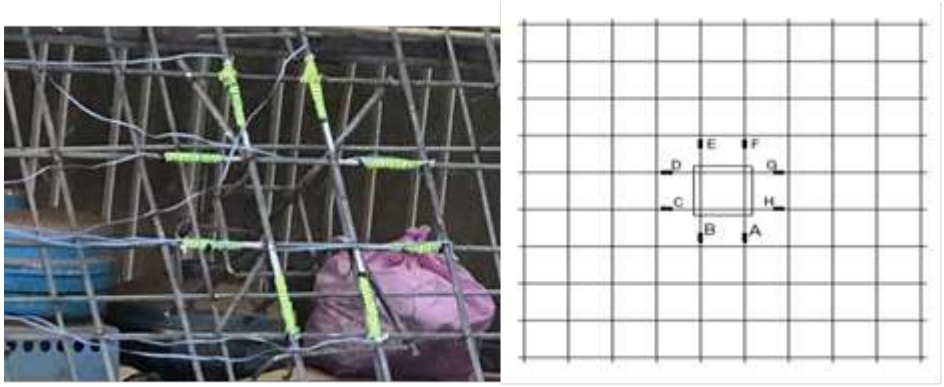

Figure 3 : Position of Strain Gauges

7. RESULT AND ANALYSIS

The test results for slab specimens are presented in terms of the (load/deflection) response, the strain in flexural reinforcement and the crack patterns for slabs at failure. It also compares the results of punching shear strengths of tested slabs with those evaluated using current code predictions (BS8110, EC2, ACI318-11 and MC2010).

7.1 Load deflection response/ Load-rotation response

As shown in Figure (4), slab specimens test with the less reinforcement ratio had the more ductility. And there was a significant improvement in the maximum deflection recorded by the dial gauge for slabs with a smaller reinforcement ratio.

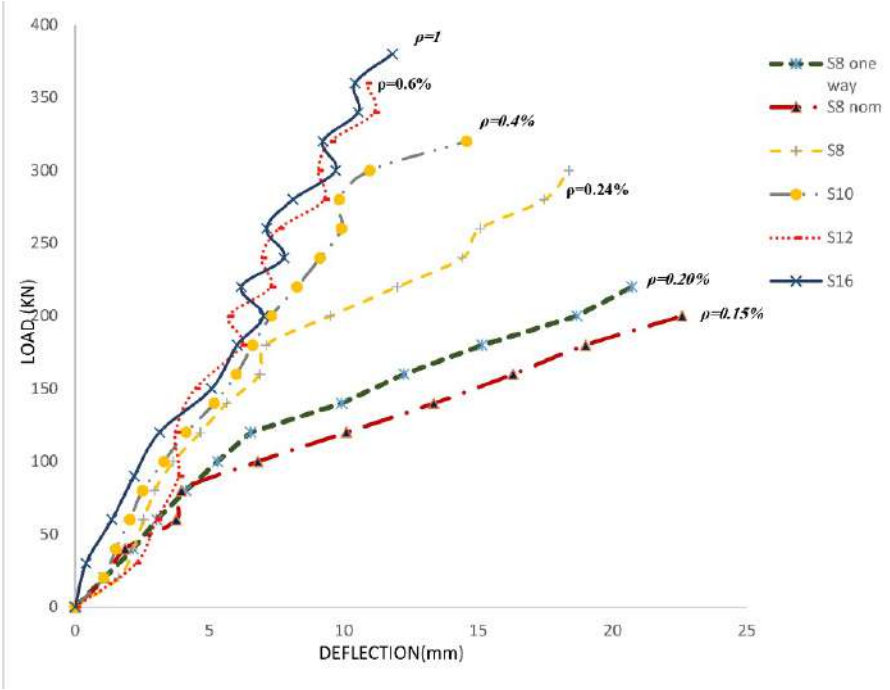

Figure 4 : Load vs Deflection at Center of Slab

7.2 Strain in flexural reinforcement

In all slab specimens there was no significant yielding of reinforcement, except S8 nominal which it had yielding of reinforcement when failure occur. However, this result ensures that all slab specimens were occur due to punching. Figure (5) shows load strain response for slab specimens

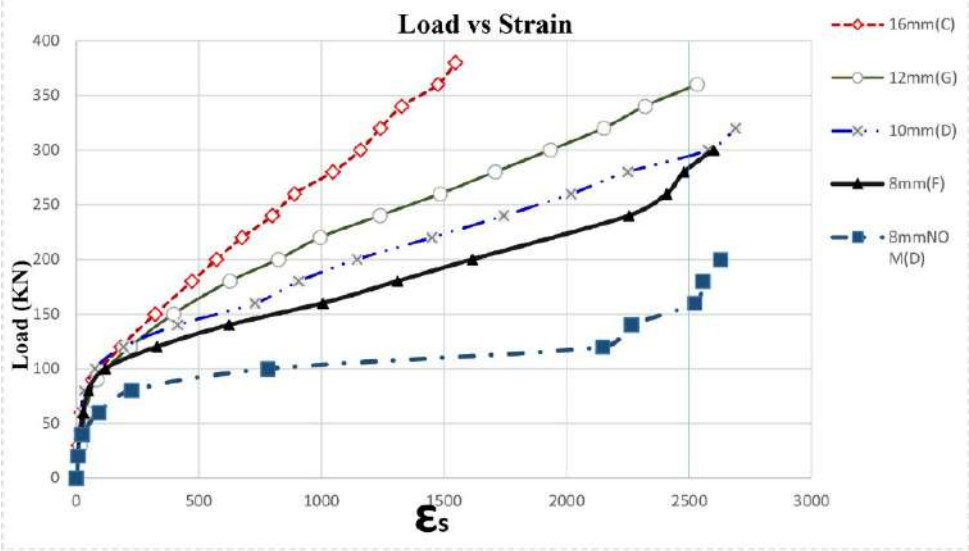

Figure 5 : Load vs Strain for All Specimens

7.3 Crack pattern and failure mechanism

Figures (6) illustrates the crack pattern at the top surface of the slap after punching failure, also shows the column penetration into the slab specimens. The inclination of the failure surface was rather steep for members with "relatively" large amounts of shear reinforcement. For lower amounts of shear reinforcement, the angle of the failure surface was somewhat flatter. It can be noted that the parameter of punching was getting smaller with the increase of reinforcement.

For slab specimens with the symmetrical reinforcement in its both directions, when the load is applied, the first crack was appeared as a roughly circular crack around the perimeter of the loaded area "beneath the column", then extended from the critical perimeter when the load is increased. At about half of the failure load, the diagonal crack was developed in the slab. These cracks were appearing with different amounts, slabs with "relatively" high reinforcement ratio had a few several cracks with small width. For slabs with low reinforcement ratio, cracks were too many than the slab with high reinforcement ratio because of the inter actions of shear and moment and too much bigger in width. For slab (S8 one-way), cracks were firstly appeared in the weak axis within the loaded area and then extended from the loaded area in one direction. For all slab specimens punching shear failure occurred without the yielding of reinforcement

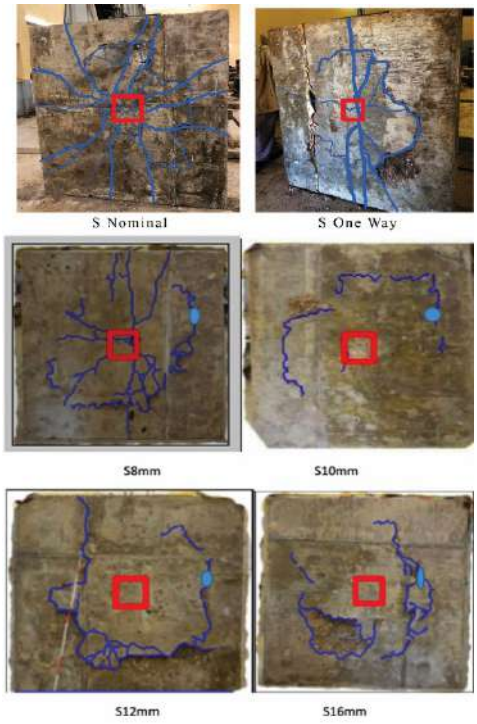

Figure 6 : Crack Patterns for tested slabs

8. COMPRESSION OF VARIOUS CURRENT CODE PREDICTION

The code provisions were investigated with respect to the predicted punching strength and the influence of the reinforcement ratio. For this, the punching strength was calculated accordingly to the provisions of the previously mentioned codes as a function of the investigated parameter. Table 1 lists the measured punching strength, maximum rotation at failure and it compares the experimentally obtained punching strength to the calculated punching strength.

Table (1) : Predictions punching strength using BS8110,EC2,ACI318 and MC2010 and from the tests

Specimens	Ψ	V_{BS}	V_{EC2}	V_{ACI}	$V_{R,test\ (KN)}$	$V_{R,test}/V_{R,BS}$	$V_{R,test}/V_{R,EC2}$	$V_{R,test}/V_{R,ACI}$
$S_{8\ nominal}$	0.0287	184.93	178.05	361.77	212.90	1.15	1.20	0.59
$S_{8\ one\text{-}way}$	0.0276	184.93	193.87	361.77	235.40	1.27	1.21	0.65
S8	0.0233	219.21	211.10	361.77	312.00	1.42	1.48	0.86
S10	0.0194	249.96	239.69	353.95	333.50	1.33	1.39	0.94
S12	0.0148	272.73	260.60	337.82	367.90	1.35	1.41	1.09
S16	0.0157	318.64	301.93	322.86	372.80	1.17	1.24	1.16
Average						1.28	1.32	0.88
Coefficient of variation (COV)						0.083	0.091	0.259

Figure 7 shows the ratio of the experimentally obtained punching strength of the tests to the predicted strength as a function of the flexural reinforcement ratio. It can be noted that all the codes predict a punching failure even for low flexural reinforcement ratios, which correspond to the experimental observations and generally none of the models leads to an obvious trend with respect to the flexural reinforcement ratio. Nevertheless, ACI 318-11 seems to lead to lower ratios of experimentally obtained and predicted strength for lower flexural reinforcement ratios than in the case of higher flexural reinforcement ratios. For slab with low reinforcement ratios, ACI predicts strengths that are clearly larger than those given by the other codes. BS 8110 and EC2 showed conservative predictions when compared to tests result within this research and a better COV was obtained (8% and 9% respectively). Moreover, the punching strengths evaluated from BS8110 and EC2 agree reasonably well with those from the test. It can be noted that the effect of reinforcement ratio in the punching strength had been delimited in specimens with a large reinforcement ratio which observed in slab (S12 and S16). This is consistent with the maximum limit for reinforcement ratio set by EC2 (2%) and BS 8110(3%).

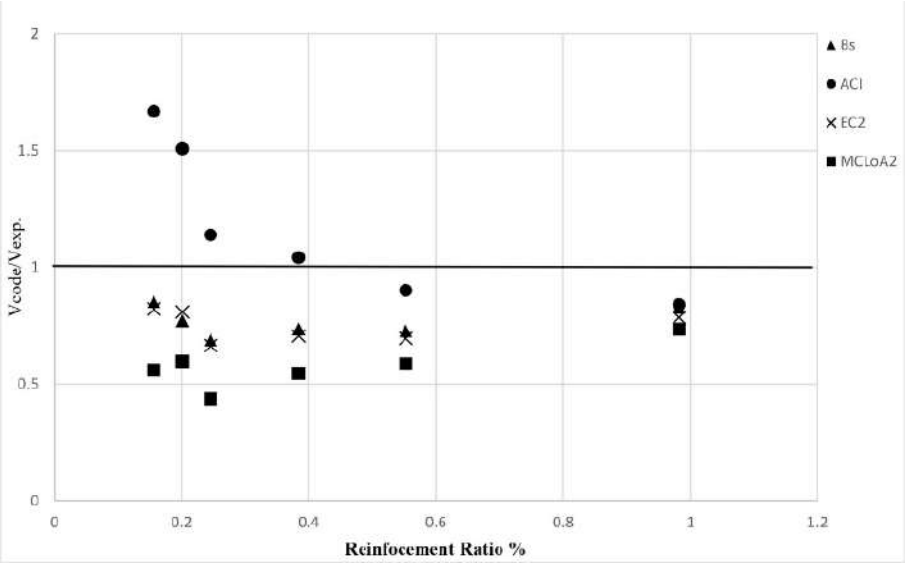

Figure 7 : Comparaison of (V_{code}/V_{exp}) vs ρ%

MC 2010 (LoA4) predictions (shown in Figure 8 and Table 2) of punching strength show an excellent agreement, with an average value of the ratio between the measured- to predicted average failure load of 1.12 and with small value of the coefficient of variation (COV) (7.5%). Figure 28 shows that the accuracy can be increased thereafter by performing additional analyses and it is allowing a better estimation of the physical parameters required by the design equations. (LoA4) shows an increase in the strength as the flexural reinforcement ratio increases. While (LoA2) predictions were conservative when compared to tests result with average failure load 1.338, except for S16 which had a larger LoA2 prediction than LoA4 prediction.

Table (2): Compression between test results for MC 2010

Specimens	Ψ	VR, LoA2	VR, LoA4	VR,test/VR,LoA2	VR,test/VR,LoA4
S8 nominal	0.0287	121.41	215.00	1.45	0.99
S8 one-way	0.0276	143.09	224.00	1.27	1.05
S8	0.0233	138.32	263.00	1.43	1.19
S10	0.0194	185.43	296.00	1.36	1.13
S12	0.0148	219.56	315.00	1.31	1.17
S16	0.0157	282.65	309.00	1.15	1.21
Average				1.34	1.12
Coefficient of Variation (COV)				0.091	0.075

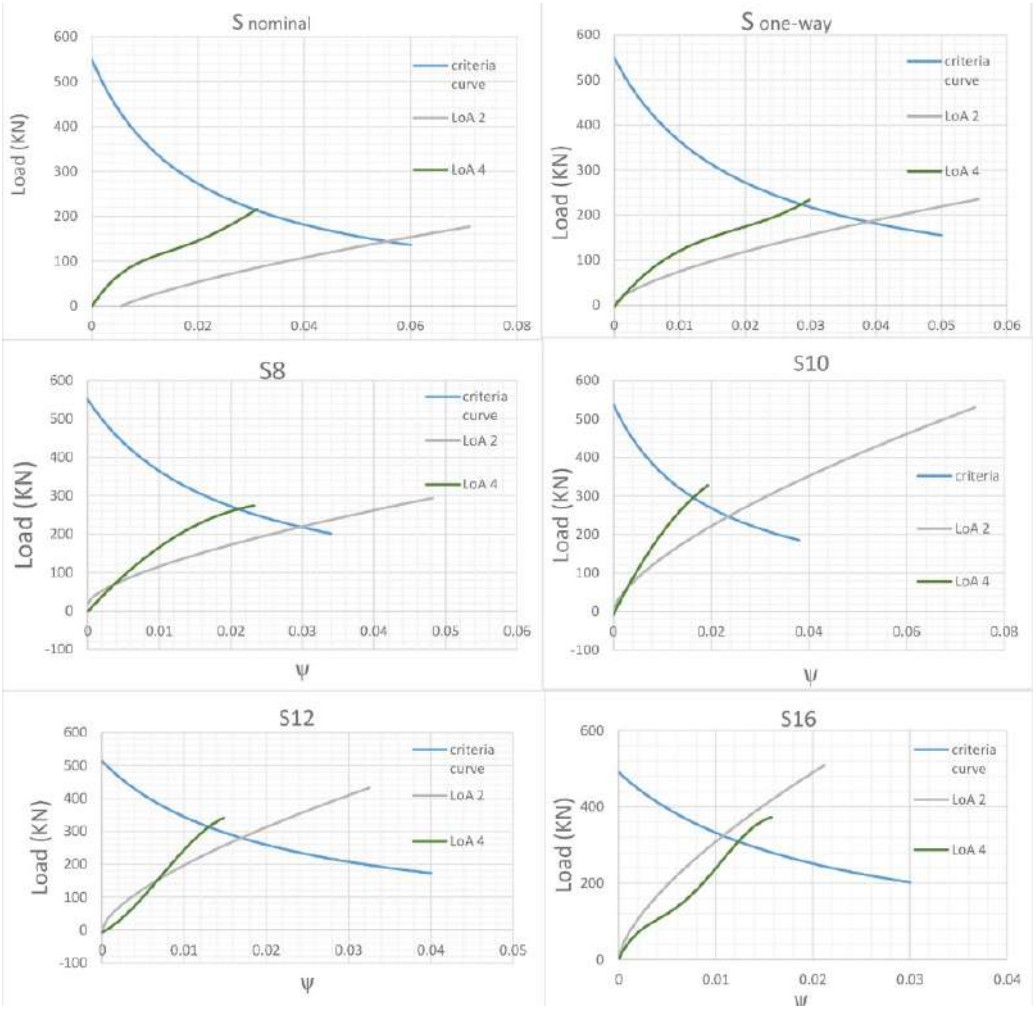

Figure 8: Predictions of punching strength for all specimens by LoA2 and LoA4

9. CONCLUSION

Increasing the reinforcement ratio increases the punching capacity, but strongly decreases the deformation capacity of the slab and the ductility of flat slab. However, the effect has a less significant in slabs with large reinforcement ratios which is suitable with EC2 and BS 8110 limitations for reinforcement ratio:

1. Increasing the reinforcement ratio decreases the interactions of shear and moment on the loaded area, because of that the increasing of the reinforcement ratio decreases the cracks and its developing.
2. ACI 318-11 does not only exhibit a large COV when compared with test results (26%), but it does not include the reinforcement ratio effect, which leads to unsafe designs in low reinforcement ratio slabs, also, even though flat slab tends to have relatively high flexural reinforcement ratios at column supports; ACI strength has a reverse relationship with the increasing of the bars diameter.
3. BS 8110 and EC2 showed conservations of the punching strength when compared to test results within this research. While the ratios of the predicted to the experimentally obtained punching strength are in an acceptable range.
4. MC 2010 predictions showed that adding additional analyses gives more accuracy to the predictions. However, MC 2010 showed the best agreement between the test results and codes predictions.

REFERENCES

[1] Eddy, T., 1914. The Theory of the Flexure and Strength of Rectangular Flat Plates Applied to the Reinforcement Concrete Floor. s.l.:s.n..

[2] Bartulac, M. D. D. D. I. .., 2015. ACI STRUCTURAL JOURNAL,,. “Punching Strength of flat slab with and without shear reinforcement “ , pp. 771-786 pp.

[3] Boon diagon, l, 1997. “Punching Shear Capacity of Flat Slab Column-Junction”. s.l.:s.n.

A REVIEW OF MATERIAL SPECIFICATIONS FOR 3D PRINTING TECHNOLOGIES AND ALKALI-ACTIVATED MATERIALS CONTRIBUTION

Ndapandula P. Kawalu [(1)], Abdolhossein Naghizadeh [(2)] and Jeffrey Mahachi [(1)]

(1) Department of Civil Engineering, University of Johannesburg

(2) Department of Civil Engineering Sciences, University of the Free State

ABSTRACT

Geopolymer concrete is an environmentally friendly substitute for conventional concrete which uses Portland cement. Geopolymer binders are prepared by activating aluminosilicate materials with alkaline agents. The present study aims to report on recent developments of the 3D printing of geopolymer mixes by looking at the fresh hardened properties and how each of these properties are affected and can be optimised. The review was carried out by analysing literature and the authors' approaches in selecting 3D printable geopolymer mixes with improved fresh and hardened properties. Properties of 3D printed geopolymer are significantly affected by material composition, showing the importance of material optimisation. Properties are also positively affected by fibre inclusion; however, it reduces the geopolymer mix's workability. Therefore, the use of fibres should be studied thoroughly. Overall, geopolymer binders yield adequate printable properties. Finally, recommendations are provided in order to improve the 3D printing process and materials.

Keywords: 3D printing, waste, by-product, geopolymer, concrete.

1. INTRODUCTION

1.1. 3D Printing Technology

Generally, 3DP is an emerging technology in which a final product is produced through depositing printed material layer by layer [1]. Employing 3DP technology in the construction industry can eliminate formwork, which would account for a maximum of approximately 54% and 75% of the project time and cost, respectively [2]. Construction waste produced is further reduced as 3DP technology produces little to no waste [3]. One of the significant challenges in 3DP of concrete is developing a printable mixture as it is required to have low flowability with self-compacting behaviour, although these are contradicting goals [1].

1.2.Geopolymer Concrete

Different types of materials, including industrial wastes and by-products, can be used to prepare 3D printing of geopolymer mortars. In 3DP of concrete, OPC is mainly used as the

main binder and may partially be replaced by supplementary cementitious materials, including Pozzolanic materials [4]. Production of OPC negatively affects the environment; it requires high amounts of energy and is considered one of the top contributors to carbon emissions [5], [6]. Geopolymer cement (GPC) has been introduced as an alternative binder as one of the solutions to this problem because it has a low carbon footprint [7]. Geopolymers are synthesised inorganic materials produced through dissolution and polycondensation of aluminosilicate materials by highly alkaline agents through a geopolymerization reaction. [8, 9]. GPC mainly uses by-products such as fly ash (FA) and ground granulated blast furnace slag (GGBS) as binders, and their abundance and availability paved the way for the use of these materials in the construction industry [10].

Several kinds of research on the 3DP of geopolymer concrete have been reviewed in the current study to provide an overview of the critical parameters and materials that have been suggested as to be used as 3DP mixtures, especially industrial wastes and by-products.

2. 3D PRINTABLE GEOPOLYMER MATERIALS

Binder phases to be used in the 3DP of geopolymers include FA, GGBS, MK etc., while silica sand and river sand are mainly used as a fine aggregate in 3DP processes, ranging in 0-3mm particle size fractions. FA is mainly preferred over GGBS as a sole binder due to its higher fire resistance and lower shrinkage [11]. The size of the 3D printer in use mainly determines the size of aggregate be adopted as the mix needs to pass through the printer's nozzle [12]. Sodium or potassium hydroxide and sodium or potassium Silicate are some of the used alkali activators in the formation of geopolymers [5,13]. Sodium-based activators have been reported to have better properties such as open time, workability, and compressive strength than potassium-based activators. Borax and sucrose powder are some of the retarders used in the preparation of GPC mixes, while Sodium carboxymethyl cellulose (CMC) powder and sodium carboxymethyl starch are used as a viscosity modifying agents [14–17]. Table 1 (all values are mass ratios of binder, except for the fibres) gives optimum geopolymer mixes suitable for 3DP processes. Optimising materials used in the 3DP of GPC is vital as they affect different properties of geopolymers suggested by different studies [2, 15, 19, 20].

Table 1: Optimum geopolymer mixes suitable for 3DP processes.

Reference	Binder Phase			SS/SH*	a/b*	Aggregate	Agg/B*	Admixture	Fibres
	FA	GGBS	SF						
[18]	0.6	0.25	0.15	2	-	Silica Sand 0-1mm	1	-	-
[16]	1	-	-		0.38	Silica Sand 465&271µm	1.5	0.012 CMC	
[14]	1	-	-	2.5	-	Silica Sand 172&898µm	1.5	0.020 CMC and 0.002 Borax	-
[1]	0.78	0.14	0.08	-	0.4	River sand < 2mm	1.4	-	-
[19]	1	-	-	-	-		1.5	0.028 CMC	0.25% PP*
[20]	1	-	-	1	0.52	River sand < 0.3mm	1	-	0.5% PP*, 1% Steel

*SS/SH – sodium silicate solution to sodium hydroxide solution ratio
*a/b – activator to binder ratio
*Agg/Binder – aggregate to binder ratio
*PP - Polypropelene

3. PROPERTIES OF 3DP CONCRETE MIXTURES

3.1. Fresh Properties of 3DP mixtures

3.1.1. Workability/Flowability

Workability (slump/flow) refers to how easily concrete can be placed and compacted without segregation and is measured by carrying out a mini-slump or slump flow test [21, 22, 16]. Workability of 3D printable GPC paste is significantly affected by fibres inclusion, fine aggregate size, sodium hydroxide molarity, type of activator, and solids and liquid ratios [18–[20]. Flowability suitable for 3DP processes has been reported in the ranges of 126 and ±158mm. Workability is affected by setting time, as a short setting time may lead to a loss of workability required for 3DP [23]. It is also reduced by increased GGBS contents as Chougan et al. [18] reported a significant increase in workability with a reduced GGBS content (lower than 15%) and a reduced aggregate size for a FA/GGBS/SF-based GPC. Workability was affected by the activator type as mixes prepared with potassium-based activator yielded lower workability compared to those prepared with sodium-based activators. The optimum mix (mix details in Table 1) exhibited a slump-flow of 126mm [24]. Vlachakis et al. [25] suggested an optimum solid to liquid ratio of 0.85 for a suitable 3D printable mix with sufficient workability for metakaolin-based geopolymer mix as ratios of 0.8 and 0.9 were either too wet or too dry for 3D printing. Polypropylene (PP) reduces workability of geopolymer paste, regardless of the content used, as these fibres absorb a lot of geopolymer paste [26]. Nematollahi et al. [19] suggested a maximum inclusion of 0.25% (vol) of PP fibres in FA-based geopolymer for adequate workability of 3DP processes. Most research that studied fibre inclusion effects on 3DP of geopolymers did not include effect on fresh properties such as workability.

3.1.2. Extrudability

Extrudability refers to how easily a mix is transferred from the pump to the nozzle of the 3D printer for extrusion [22]. This parameter is evaluated by the visual inspection method, ensuring no pipe block during printing [27]. Extrudability is mainly affected by mixture proportion. Aggregate to binder ratios of 1.5 and less lead to more extrudable mixtures, while ratios beyond 1.7 were not extrudable as mixes were too stiff [1]. Kashani and Ngo [23] found an optimum mix with a 0.33 water-to-solids (w/s) ratio and 8% activator content for the 3DP of FA/GGS/SF geopolymer mix to have better extrudability than mixes prepared with 0.31 and 0.35 w/s ratios and 10% activator content. Factors such as activator type and silicate modulus have an insignificant effect on FA/GGBS-based GPC mixtures' extrudability [24].

3.1.3. Buildability

Buildability/Shape retention ability refers to how the extruded layer/s can hold the preceding layers and keep its extruded shape under self-weight without falling apart [22], [28]. 3DP requires high buildability as a low buildability of 3DP material may lead to deformation during printing layers, causing the entire printed structure to collapse [6]. High buildability may be attained by a low liquid-to-binder ratio (0.21-0.33), low CMC contents, utilising sodium-based activators and shorter open time. Kashani and Ngo [23] reported that mixes prepared with a w/s ratio of 0.35 had poor buildability as the layers printed collapsed after extrusion. Those

prepared with a w/s ratio of 0.33 exhibited acceptable buildability. Specimens prepared with potassium-based activator failed in retaining their shape when printed than those prepared by sodium-based activators [24]. Buildability can be enhanced by adding rheology modifiers such as nano-clays, as Panda et al. [1] suggested the addition of 1.2% nano-clay to optimise buildability for large scale 3DP.

3.1.4. Open time

Open time can be described as the time needed to print the subsequent layer.[1, 23]. Open time is crucial as a printed layer needs to acquire adequate strength to support and at the same time be wet enough and fuse with the subsequent layers. Open time is directly affected by setting time; therefore, a shorter setting time may indicate a shorter open time. Short open time is a sign of quick strength gain; however, it can cause the pipe's clogging and hardening of the material in the reservoir (as the material loses workability) [23]. Furthermore, a shorter setting time can lead to faster curing and should the subsequent layer be printed on a fully cured substrate layer, it will cause a weak interfacial bond strength, thus causing a cold joint in the printed layers [26]. Though short open time is a sign of quick strength gain, meaning the printed layer will have adequate strength to support the subsequent layers, Kashani and Ngo [23] suggested a longer setting time as yield stress is sometimes enough to support a limited number of subsequent layers. Open time for successful printing has been reported between 15-20 minutes and has been affected by, GGBS content, activator type and SiO_2/Na_2O ratio (molar ratio) [14, 18, 29]. Increasing GGBS content from 5-15% reduces the setting time of FA-based geopolymer mortar; thus, the mortar cannot be used for a long time [1].

Bong et al. [24] reported a shorter open time of 15 minutes with potassium-based activator compared to 29 minutes recorded for sodium-based activator. Additionally, a shorter open was reported due to a reduced molar ratio, which affected the interlayer bond strength [29].

The above discussed fresh properties are fundamental as there is no use of formwork in 3DP processes, and they lead to a successful printing and affect mechanical properties after setting [21, 23]. It is thus important to optimise material composition in order to enhance these fresh properties for 3DP.

3.2.Hardened Properties of 3DP mixtures

3.2.1. Compressive Strength

Effect of material composition

Materials used in the preparation of geopolymers are crucial as they determine the mechanical properties of the 3D printed mix as material composition affects strength differently. Utilising GGBS in GPC mixes can provide denser microstructures, which further results in early age compressive strength [21]. Panda et al. [21] showed that adding GGBS to FA-based GPCs increased 7d compressive strength of the 3D printed mixes to 18.4 MPa. Xia et al. [30] suggested a minimum amount of 50% GGBS required to set FA/GGBS GPC binder at ambient temperatures, yielding 7d compressive strength of 24.9 MPa. Less than 50% GGBS reduced the strength, and 100% GGBS increased compressive strength. Strength is greatly affected by liquid content used; Kashani and Ngo [23] recorded a 21d compressive strength of approximately 58 MPa for a GGBS:FA:SF, activated by 8% sodium metasilicate powder at an optimum w/s ratio of 0.33%. Results showed that the strength was negatively affected by increasing the w/s ratio over 0.33 and activator content over 10%. Admixtures used also have an effect on the strength gain of 3D printed geopolymer mixes as Sun et al. [17] reported that

increased sodium carboxymethyl starch (CMS) content, a viscosity modifying agent, results in a reduction in compressive strength of the printed specimen. The 28d compressive strength reduced from 87 MPa (mixes without CMS) to ±56 MPa (mixes with 8% CMS). Bong et al. [24] reported increased 3d compressive strength from 8.5 to 16.6 MPa, with an increase in sodium-based alkali content and silicate modulus for FA/GGBS based GPC

Effect of Fibre inclusion

Fibres have been introduced to 3DP mixes to reduce the use of steel [31]. The strength of 3DP GPC concrete mixtures is influenced by the inclusion of different types of fibres used. Nematollahi et al. [19] reported an increased compressive in 3D printed GPC mixes containing PP fibre inclusion compared to those without fibres, the optimum inclusion of 0.25% (vol.) PP fibres led to increased compressive strength of 35.8MPa from 22.3MPa. Anything beyond 0.25% reduced and compressive strength. Korniejenko et al. [32] suggested incorporating an optimum of 0.5% short (30-50 mm) green tow flax and carbon fibres reinforcement in FA-based 3D printed GPCs, as anything beyond that decreases the rate of compressive strength gain at each age. Overall, the outcome of fibre inclusion on the compressive strength was insignificant as the fibre led to a 6% increase. Bong et al. [15] reported a 7d maximum compressive strength of 49.1 MPa for 3D printed FA/GGBS GPC mixes with wollastonite microfiber addition, while those without fibre recorded a compressive strength of 48.3MPa, showing an insignificant effect of fibres. Chougan et al. [18] recommended 1% nano graphite platelets inclusion to FA, GGBS and SF binder GPC for 3DP and exhibited better compressive strength compared to 3D printed and cast specimen without nano graphite platelets.

Effect of curing conditions

Findings reported in the literature show that comparable results have been obtained with different curing conditions, as summarised in Table 2 below. According to the study done by Nematollahi et al. [34], the compressive strength cured at room temperature was comparable to that of the study carried out by Korniejenko et al. [32], whose specimens were cured at 75 ˚C for 24 hours. In other studies, similar results were obtained for different curing temperatures as Panda et al. [33], and Bong et al. [14] reported similar compressive results for specimens cured at room temperature and those cured at elevated temperatures of 60 ˚C by Nematollahi et al. [34]. It should be noted that all the studies used different materials, and where similar materials were used, different compositions of the used materials were adopted and thus each affecting the end results in different ways.

Table 2. 28d Flexural and Compressive Strength of 3DP FA-Based GPC cured at different temperatures

Reference	Curing temperature	28d Compressive Strength (MPa)
[35]	70˚C - 48 hrs	25
[14]	Ambient temp	34
[34]	60˚C - 24 hrs	35
[33]	Ambient temp	36
[32]	75˚C - 24 hrs	48
[34]	Ambient temp	43.2

Compressive strength is a crucial property of concrete as it can represent its quality in terms of mechanical behaviour. The compressive strength of geopolymer binder is affected by curing conditions, the properties of GPC binders, mixture composition and other factors, including water content, activator to binder ratio, type and concentration of alkaline activators and admixtures used [36, 37]. Results also show that ambient cured specimens can attain comparable results compared to heat-cured specimens.

3.2.2. Interlayer/Tensile Bond Strength

Sufficient bond strength between printed layers is required for adequate mechanical properties as it distributes the applied loads through the printed structure and affects the structural integrity of the printed structure. It is influenced by the time gap (open time), as an increase in the time gap reduces the tensile bond strength. This is due to the induction of voids at the interface and adhesion reduction due to the increased time gap [11, 38]. Panda et al. [33] recorded a maximum bond strength of 16.3 MPa for FA/GGBS/SF 3DP GPC paste. Bond strength was reduced by a longer open time (over 20 minutes), longer printing time gap and higher printing speed. Bong et al. [14] recorded a 7d 0.9 MPa bond strength by optimising the mix described in Table 1, showing the importance of mixture optimisation on the bond strength of 3D printed specimens. The recorded strength is suggested to be enough to prevent interfacial shear failure as failure mode in flexural strength testing was tensile and not shear. Furthermore, bond strength is affected by curing type and printing time gap, as a reduction in bond strength was observed with oven-cured specimens and longer layer time intervals (printing time gap/interval) [34, 39]. Additionally, bond strength is affected by buildability as it can be enhanced by an improvement in buildability [26].

4. CONCLUSIONS AND RECOMMENDATIONS

This study reviewed applications of industrial wastes or by-products, including fly ash and ground granulated blast-furnace slag, as binder phases in the 3DP of geopolymer concrete mixtures. In the reviewed literature, geopolymer cement has been suggested as a suitable binder phase to prepare 3D printable mixes. Literature showed that that 3DP technology is sustainable and leads to a greener environment. Fresh and hardened properties were affected by the mixtures' material composition (GGBS, fibre inclusion, w/s, etc), showing the importance of material optimisation to obtain printable results and curing conditions. Fibre increases compressive strength but has adverse effects on workability; thus, a small percentage of fibre inclusion is recommended. There is a lack of literature on one-part binder-based geopolymer, which may pave the way for future research. The authors recommend extensive experimental works on evaluating a wider range of geopolymer binders as 3D printing materials instead of FA and GGBS.

There are limited studies in the literature that have been carried out on applying waste materials and industrial by-products in the binder phase of 3D printing concretes. Therefore, further studies are required to explore the potential re-use of different waste materials.

REFERENCES

[1] Panda, B. and Tan, M. J., 'Experimental study on mix proportion and fresh properties of fly ash based geopolymer for 3D concrete printing', *Ceramics International*. 44 (9) (2018) 10258-10265.

[2] Paul, S. C., van Zijl, G. P., Tan, M. J. and Gibson, I., 'A review of 3D concrete printing systems and materials properties: Current status and future research prospects', *Rapid Prototyping Journal*. 24 (4) (2018) 784-798.
[3] Sanjayan, J. G. and Nematollahi, B., '3D concrete printing for construction applications', *3D concrete printing technology* (2019) 1-11.
[4] Panda, B., Ruan, S., Unluer, C. and Tan, M. J., 'Improving the 3D printability of high volume fly ash mixtures via the use of nano attapulgite clay', *Composites Part B: Engineering*. (165) (2019) 75-83.
[5] Naghizadeh, A. and Ekolu, S. O., 'Investigation of mixture factors influencing alkali-silica reaction in fly Ash-based geopolymer mortars' *Proceedings*, 71st RILEM Annual Week & ICACMS 2017, Chennai, (2017) 95–400.
[6] Tay, Y. W., Panda, B., Paul, S. C., Tan, M. J., Qian, S. Z., Leong, K. F. and Chua, C. K., 'Processing and properties of construction materials for 3D printing', *Materials Science Forum.* 861 (2016) 177-181.
[7] Hossain, M. M., Karim, M. R., Hossain, M. K., Islam, M. N. and Zain, M. F. M., 'Durability of mortar and concrete containing alkali-activated binder with pozzolans: A review', *Construction and Building Materials*. 93 (2015) 95-109.
[8] Wongpa, J., Kiattikomol, K., Jaturapitakkul, C. and Chindaprasirt, P., 'Compressive strength, modulus of elasticity, and water permeability of inorganic polymer concrete', *Materials & Design*. 31(10) (2010) 4748-4754.
[9] Davidovits, J., 'Geopolymer Chemistry and Applications', 5th Edn (Saint-Quentin: Institut Géopolymère, 2020).
[10] Jawahar, J G, Lavanya, D & Sashidhar, C 2016. Performance of fly ash and GGBS based geopolymer concrete in acid environment. *International Journal of Research and Scientific Innovation*, 3(8):101-104.
[11] Le, T. T., Austin, S. A., Lim, S., Buswell, R. A., Law, R., Gibb, A. G. and Thorpe, T., 'Hardened properties of high-performance printing concrete', *Cement and Concrete Research*. 42(3) (2012) 558-566.
[12] Paul, S.C., Tay, Y.W.D., Panda, B. and Tan, M.J. 'Fresh and hardened properties of 3D printable cementitious materials for building and construction', *Archives of civil and mechanical engineering*, (18) (2018) 311-319.
[13] Aleem, M.A. and Arumairaj, P.D. "Geopolymer concrete–a review", *International journal of engineering sciences & emerging technologies*, 1(2) (2012) 118-122.
[14] Bong, S. H., Nematollahi, B., Nazari, A., Xia, M. and Sanjayan, J., 'Method of optimisation for ambient temperature cured sustainable geopolymers for 3D printing construction applications', *Materials*. 12(6) (2019) 902.
[15] Bong, S.H., Nematollahi, B., Arunothayan, A.R., Xia, M. and Sanjayan, J., 'Effect of Wollastonite Micro-Fiber Addition on Properties of 3D-Printable 'Just-Add-Water' Geopolymers', in Concrete and Digital Fabrication- Digital Concrete, Proceedings of the Second RILEM International Conference, Eindhoven University of Technology, July, 2020 (Digital Conference, 2020) 3-11.
[16] Nematollahi, B., Vijay, P., Sanjayan, J., Nazari, A., Xia, M., Naidu Nerella, V. and Mechtcherine, V., 'Effect of polypropylene fibre addition on properties of geopolymers made by 3D printing for digital construction', *Materials*. 11 (12) (2018) 2352.
[17] Sun, C., Xiang, J., Xu, M., He, Y., Tong, Z. and Cui, X., '3D extrusion free forming of geopolymer composites: Materials modification and processing optimisation', *Journal of Cleaner Production.* 258 (2020) Available from https://doi.org/10.1016/j.jclepro.2020.120986
[18] Chougan, M., Ghaffar, S. H., Jahanzat, M., Albar, A., Mujaddedi, N. and Swash, R., 'The influence of nano-additives in strengthening mechanical performance of 3D printed multi-binder geopolymer composites', *Construction and Building Materials*. 250 (2020) Available from https://doi.org/10.1016/j.conbuildmat.2020.118928
[19] Nematollahi, B., Xia, M., Sanjayan, J. and Vijay, P., 'Effect of type of fiber on inter-layer bond and flexural strengths of extrusion-based 3D printed geopolymer', *Materials science forum.* 939 (2018) 155-162.

[20] Al-Qutaifi, S., Nazari, A. and Bagheri, A. ‘Mechanical properties of layered geopolymer structures applicable in concrete 3D-printing’, *Construction and Building Materials,* (176) (2018) 690-699.
[21] Panda, B., Unluer, C. and Tan, M. J., 'Investigation of the rheology and strength of geopolymer mixtures for extrusion-based 3D printing', *Cement and Concrete Composites*. 94 (2018) 307-314.
[22] Kim, K. K., Yeon, J., Lee, H. J. and Yeon, K. S., 'Feasibility Study of SBR-Modified Cementitious Mixtures for Use as 3D Additive Construction Materials', *Polymers*. 11(8) (2019) 1321.
[23] Kashani, A. and Ngo, T. D., 'Optimisation of mixture properties for 3D printing of geopolymer concrete', in International Symposium on Automation and Robotics in Construction, Berlin, July, 2018 1-8.
[24] Bong, S. H., Nematollahi, B., Nazari, A., Xia, M. and Sanjayan, J. G., 2018. 'Fresh and hardened properties of 3D printable geopolymer cured in ambient temperature', in Concrete and Digital Fabrication- Digital Concrete, Proceedings of the First RILEM International Conference, Zurich, September, 2018 (Digital Conference, 2018) 3-11.
[25] Vlachakis, C., Biondi, L. and Perry, M. ‘3D printed smart repairs for civil infrastructure’, In *9th European Workshop on Structural Health Monitoring Series (EWSHM)*, *Manchester, United Kingdom,* (2018) 1-12.
[26] Khan, M. A., 'Mix suitable for concrete 3D printing: A review', *Materials Today.* 32 (2020*)* 831-837
[27] Le, T. T., Austin, S. A., Lim, S., Buswell, R. A., Law, R., Gibb, A. G. and Thorpe, T., 2012a. 'Mix design and fresh properties for high-performance printing concrete', *Materials and Structures*. 45(8) (2012) 1221-1232.
[28] Kruger, J., Zeranka, S. and van Zijl, G., '3D concrete printing: A lower bound analytical model for buildability performance quantification', *Automation in Construction*. 106, (2019) 9.
[29] Panda, B., Mohamed, N. A. N., Tay, Y. W. D. and Tan, M. J., 'Bond strength in 3D printed geopolymer mortar', in Concrete and Digital Fabrication- Digital Concrete, Proceedings of the First RILEM International Conference, Zurich, September, 2018 (Digital Conference, 2018) 200–206.
[30] Xia, M., Nematollahi, B. and Sanjayan, J., 2019. 'Printability, accuracy and strength of geopolymer made using powder-based 3D printing for construction applications', *Automation in Construction*. 101 (2019) 179-189.
[31] Hambach, M., Rutzen, M. and Volkmer, D. ‘Properties of 3D-printed fiber-reinforced Portland cement paste’, *In 3D Concrete Printing Technology* (2019) 73-113.
[32] Korniejenko, K., Łach, M., Chou, S. Y., Lin, W.T., Cheng, A., Hebdowska-Krupa, M., Gądek, S. and Mikuła, J., 'Mechanical Properties of Short Fiber-Reinforced Geopolymers Made by Casted and 3D Printing Methods: A Comparative Study', *Materials*. 13(3) (2020) 579.
[33] Panda, B., Paul, S. C., Mohamed, N. A. N., Tay, Y. W. D., & Tan, M. J., 2018d. ‘Measurement of tensile bond strength of 3D printed geopolymer mortar’, *Measurement*, (113) (2018) 108–116.
[34] Nematollahi, B., Bong, S. H., Xia, M. and Sanjayan, J., 'Digital Fabrication of 'Just-Add-Water'Geopolymers: Effects of Curing Condition and Print-Time Interval', in Second RILEM International Conference on Concrete and Digital Fabrication, Netherlands, July, 2020 (Eindhoven University of Technology, Netherlands, 2020) 93–102.
[35] Alghamdi, H., Nair, S.A. and Neithalath, N. ‘Insights into material design, extrusion rheology, and properties of 3D-printable alkali-activated fly ash-based binders’, *Materials & Design*, 167 (2019) Available from: https://doi.org/10.1016/j.matdes.2019.107634
[36] Bagheri, A. and Cremona, C., 'Formulation of mix design for 3D printing of geopolymers: A machine learning approach', *Materials Advances*. 1(4) (2020) 720-727.
[37] Naghizadeh, A. and Ekolu, S. O., 'A comprehensive mix design method of fly ash geopolymer mortars', *Construction and Building Materials*. 202 (2019) 704-717.
[38] Tay, Y. W. D., Ting, G. H. A., Qian, Y., Panda, B., He, L. and Tan, M. J.' Time gap effect on bond strength of 3D-printed concrete', *Virtual and Physical Prototyping*. 14(1) (2019) 104-113.
[39] Wolfs, R. J. M., Bos, F. P. and Salet, T. A. M., 'Hardened properties of 3D printed concrete: The influence of process parameters on interlayer adhesion', *Cement and Concrete Research*. 119 (2019) 132-140.

THE SUSCEPTIBILITY OF SELECTED NAMIBIAN AGGREGATES TO ASR

Philemon A. Arito [(1)], Petrina T. Johannes [(1)] and Martin T. Mulundu [(1)]

(1) Department of Civil and Environmental Engineering, University of Namibia

ABSTRACT

This paper investigates the potential alkali silica reactivity of selected Namibian aggregates from certified quarries in the following towns: Opuwo, Omakange, Tsumeb, Otjiwarongo, Walvis Bay and Windhoek. The susceptibility of the selected aggregates to alkali silica reaction (ASR) was investigated using laboratory-made cement-based mortar bar specimens cast according to ASTM C1260 specifications. Six mortar mixes were used to cast the test specimens. Three replicate specimens were cast for each mortar mix. The concentration of reactive silica in the aggregates was determined using X-Ray Fluorescence (XRF). From the test results, it can be concluded that the susceptibility of the aggregates under investigation to ASR was minimal. All aggregates, except for those sourced from Windhoek, were non-reactive. Aggregates from Windhoek exhibited slow/mild potential to alkali silica reactivity. An increase in SiO_2 content in aggregates resulted in a corresponding increase in the susceptibility to ASR and the percentage expansion.

Keywords: alkali silica reaction, XRF, aggregates, mortar bar

1. INTRODUCTION

Alkali aggregate reaction (AAR) is a global problem that has been observed in many concrete structures. It was first reported by Stanton in the USA in 1938 and has been researched extensively since then [1–3]. AAR is an adverse chemical reaction between the alkali in concrete pore solution and the reactive compounds in aggregates. It can be classified into three broad categories depending on the nature of the aggregate involved in the process: alkali-silica reaction, alkali-silicate reaction and alkali-carbonate-rock reaction.

Alkali silica reaction (ASR) is the chemical reaction that occurs between the alkaline concrete pore solution and the metastable forms of silica found in aggregates such as volcanic glasses, cristobalite, tridymite and opal. It can also refer to the reaction between the concrete pore solution and aggregates containing or comprising cherts, chalcedony, microcrystalline quartz, cryptocrystalline quartz or strained quartz. It entails the formation of two types of gel products, namely a non-swelling calcium-alkali-silicate hydrate (C-N(K)-S-H) and a swelling gel alkali-silicate-hydrate (N(K)-S-H) [2–4]. ASR is deemed safe if only the non-swelling gel is formed and unsafe if both products are formed. For the swelling gel to form, four conditions ought to be met simultaneously: (i) a sufficient amount of alkali (generally believed to be higher than 0.6% in terms of sodium oxide equivalent) should be present in the concrete; (ii) a reactive form of silica in sufficient quantity (generally in the aggregates) is required; (iii) a source of soluble calcium (such as portlandite) to react with dissolved silica and form the deleterious gel; and (iv) a sufficient source of moisture is required. ASR will not occur if any of the four

mentioned conditions fails to exist. ASR results from a series of reaction processes which occur sequentially, namely: the dissolution of metastable silica, the formation of non-colloidal silica sol, the gelation of the latter and the swelling of the gel [2, 3, 5, 6].

ASR is influenced by: aggregate type, content of reactive aggregate, porosity of aggregate, mineralogy of the reactive silica, diffusivity of the relevant ions, source and concentration of ions, the presence of a pozzolan, the quantity of free $Ca(OH)_2$ in the hydration process, aggregate size, the property of the reaction product and exposure conditions [2, 3, 5–9]. A detailed explanation on how each of these parameters influence ASR can be obtained from the cited literature. The expansive gel formed due to ASR induces tensile stresses in the concrete. These stresses result in cracks which would compromise the aesthetics, durability and structural integrity of the affected concrete structures. The negative effects of ASR have been countered in practice through the use of low-alkali cements (sodium oxide equivalent lower than 0.6%), chemical admixtures containing lithium and calcium nitrate, concrete moisture control, use of non-reactive aggregates and the partial replacement of cement with supplementary cementitious materials (SCMs) [1–4, 7, 8, 10–12].

Whereas extensive studies on the susceptibility of aggregates from various localities to ASR have been reported in literature [1–3]; research on the susceptibility of Namibian aggregates to ASR has not been reported. Consequently, many engineers and contractors in Namibia have continued to specify and use concrete without an in-depth knowledge on their susceptibility to ASR. Chatterji [7], Rashidi et al [13] and Mahomed [2] report that a proper understanding of the composition and behaviour of aggregates ought to inform the assessment of the susceptibility of an aggregate to ASR. Considering the lack of local research on the susceptibility of Namibian aggregates to ASR, this study sought to: (i) investigate the elemental composition of selected Namibian aggregates from six towns; and (ii) assess the potential reactivity of the selected aggregates to ASR using the accelerated mortar bar test as described in ASTM C 1260 [14]. The chemical composition of the aggregates was examined using X-Ray Fluorescence (XRF). The results from this study would inform the selection of suitable aggregate sources for use in the construction of concrete buildings and infrastructure in Namibia.

2. EXPERIMENTAL METHODOLOGY

The following materials were used to cast the mortar mixes for this study:

i. Cement: CEM I, 42.5 N (meeting ASTM C 150 requirements); percentage alkalis = 0.9521% Na_2Oeq (Sourced from a local cement plant).
ii. Fine aggregates: passing through the 4.75 mm sieve and retained on the 150 μm sieve (sourced from different quarries across Namibia).
iii. Sodium hydroxide (NaOH): concentration = 1.0 ± 0.01 N (Source: Biodynamics, Windhoek, Namibia).

Coarse aggregates samples were collected randomly from certified quarries that supply aggregates for use in construction in the following towns in Namibia: Opuwo, Omakange, Tsumeb, Otjiwarongo, Walvis Bay and Windhoek. The sampling was done according to Method MB1 of TMH5 [15]. The samples were labelled as S1 (Walvis Bay), S2 (Opuwo), S3 (Tsumeb), S4 (Otjiwarongo), S5 (Omakange) and S6 (Windhoek). The labelled samples were oven-dried, cooled, crushed and sieved according to ASTM C33 [16], ASTM C136 [17] and

ASTM C 1260 [14] specifications. The portion of the graded fine aggregate that passed through the 4.75 mm sieve and was retained on the 150 µm sieve was separated for use in this study.

A 1kg aggregate from each quarry was pulverised, packed in a plastic bag and sent to the Ministry of Mines and Energy in Windhoek for X-Ray Fluorescence (XRF) analysis. XRF was used to determine the elemental composition of each aggregate sample. The relative density of the graded aggregates from each source was determined using a pycnometer according to TMH1 Method B15 [18] specifications. The proportioning of the materials for casting the mortar mixes was determined. A mortar mix was cast from each aggregate source. The mass of each mix constituent was determined on the basis of the relative density (r.d) of each aggregate as presented in Table 1 The equations that were used to determine the aggregate proportions are presented in ASTM C 1260 [14] and Strack et al [6].

Table 1: Mix design proportions per batch (aggregates with relative densities ≥ 2.45)

Material	Quantity	
	Relative density ≥ 2.45	Relative density < 2.45
Cement (g)	440.0	440.0
Water (ml)	206.8	206.8
Graded aggregate (g)	990.0	440.0
Water:cement (w/c) ratio	0.47	0.47

The constituents of each mortar mix were mass batched and mixed using a mixer, paddle and a mixing bowl. Mixing was done according to ASTM C 305 [19]. Three specimens were cast from each of the six mixes. 18 No. 25 x 25 x 285 mm mortar bar specimens were cast within 2 minutes and 15 seconds after mixing and placed in steel moulds in two approximately equal layers. Each layer was hand compacted with a tamper. The top surface of each specimen was levelled and smoothened with a trowel. The freshly cast specimens were marked then kept in a moist cabinet (temperature = 23 ± 2 ^{o}C; relative humidity = 100%) for 24 ± 2 hours before demoulding. Figure 1 shows a freshly-cast mortar bar in a moist cabinet.

Figure 1: A freshly-cast mortar bar in a moist cabinet.

Specimens were removed from the cabinet and dried using a towel to a saturated surface dry (SSD) condition. A digital Vernier calliper was used to measure the initial length of each

specimen immediately after its removal from the cabinet (Figure 2). Measurements were made to the nearest 0.002 mm. Utmost care was taken to prevent the loss of moisture in the specimens.

Figure 2: Length measurements using a digital Vernier calliper

The accelerated mortar bar test – despite its limitations as presented in Chatterji [7], Kandasamy and Shehata [11], Rashidi et al [13], Mahomed [2] and Strack et al [6] - was used to test for the potential alkali silica reactivity of the aggregates in accordance with ASTM C 1260 [14]. The constraints of limited time for this research and the unavailability of equipment informed the adoption of this test method. The SSD mortar bar specimens were immersed fully in a storage container with potable tap water at a temperature of 23 ± 2 ºC. The container was then sealed and placed in an oven maintained at 80 ± 2 ºC for 24 hours. The hot mortar bar specimens were removed from the oven, one at a time, and their surfaces dried using a towel. A zero length reading was taken and recorded. Thereafter, the mortar bar specimens were immersed in a container with 1.0 N sodium hydroxide solution (NaOH) at 80 ± 2 ºC for 14 days. The change in length in each specimen was monitored throughout the 14 days of immersion in NaOH. Length measurements were taken at 1, 5, 7, 12 and 14 days after immersion in NaOH. The percentage expansion in each specimen was calculated as per the ASTM C 1260 [14] recommendations. The mean percentage expansion of each mortar mix was calculated from three test results.

3. RESULTS AND ANALYSIS

3.1 Elemental composition

The elemental composition of the aggregates under investigation were determined using XRF analysis. The XRF results are presented in Figure 3. From the XRF results it can be observed that silica content in the aggregates decreased in the following order: S6, S2, S1, S5, S3 and S4. Based on the geological map of Namibia [20], it can be inferred that the variations in silica content can be attributed to the mineralogy of the rocks from which the aggregates were sourced. The silica content is generally high in aggregate sources that contain quartzite and granite (e.g., S1 and S6).

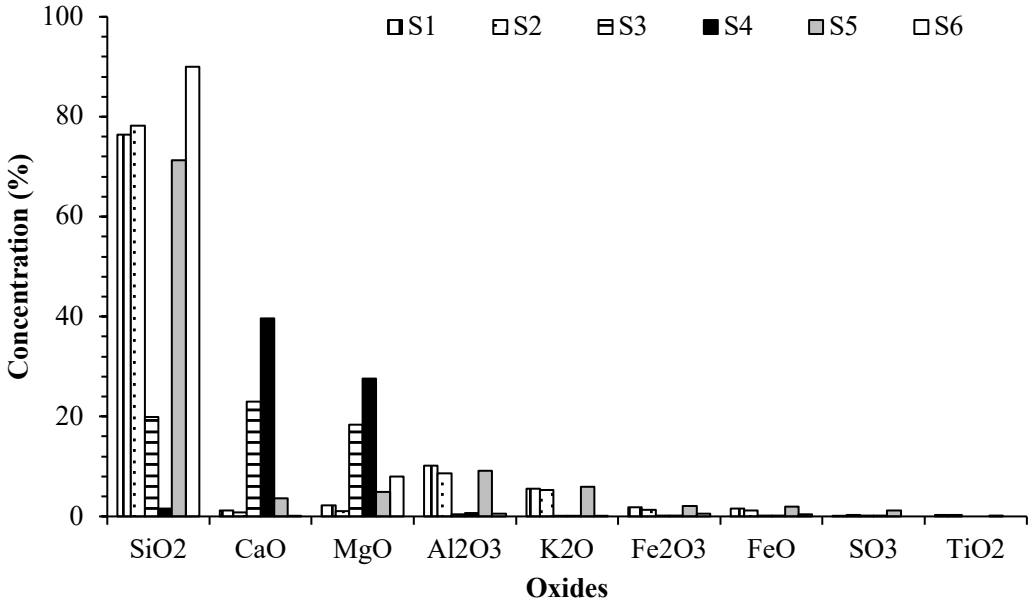

Figure 3: Elemental composition of aggregates

3.2 Mortar bar test results

The test results from the mortar bar test are presented in Figure 4. From Figure 4, it can be observed that aggregates from Windhoek (S6) exhibited the largest percentage expansion while aggregates from Otjiwarongo (S4) exhibited the least percentage expansion after 14 days of immersion in 1.0 N sodium hydroxide (NaOH) solution. The percentage expansion in the other aggregates varied between these two values.

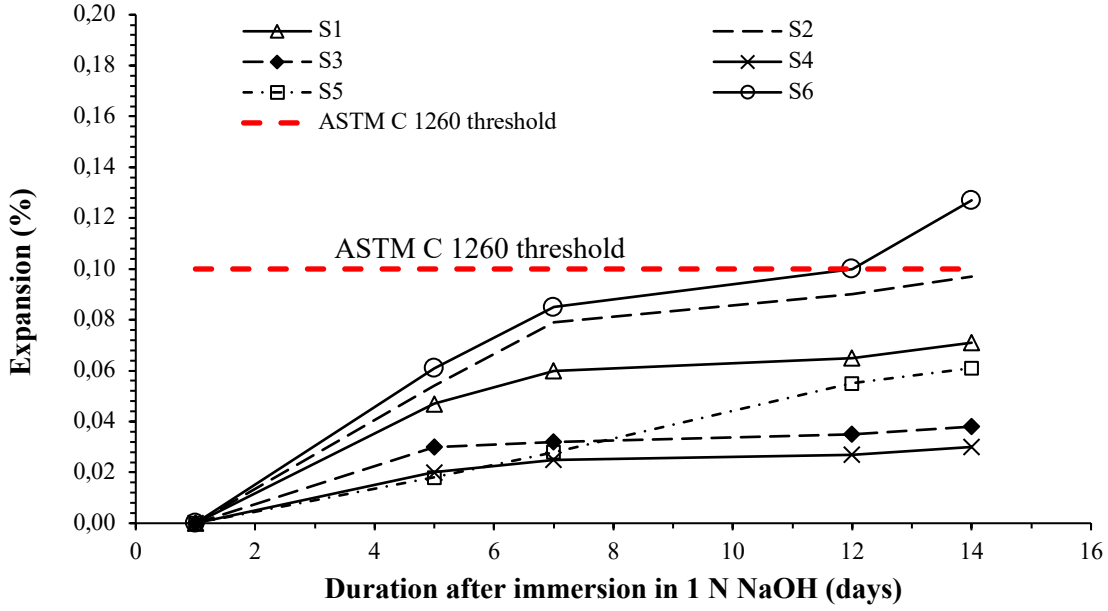

Figure 4: Mortar bar results

The relationship between silica content and the percentage expansion after 14 days of immersion in NaOH solution in each aggregate is presented in Figure 5.

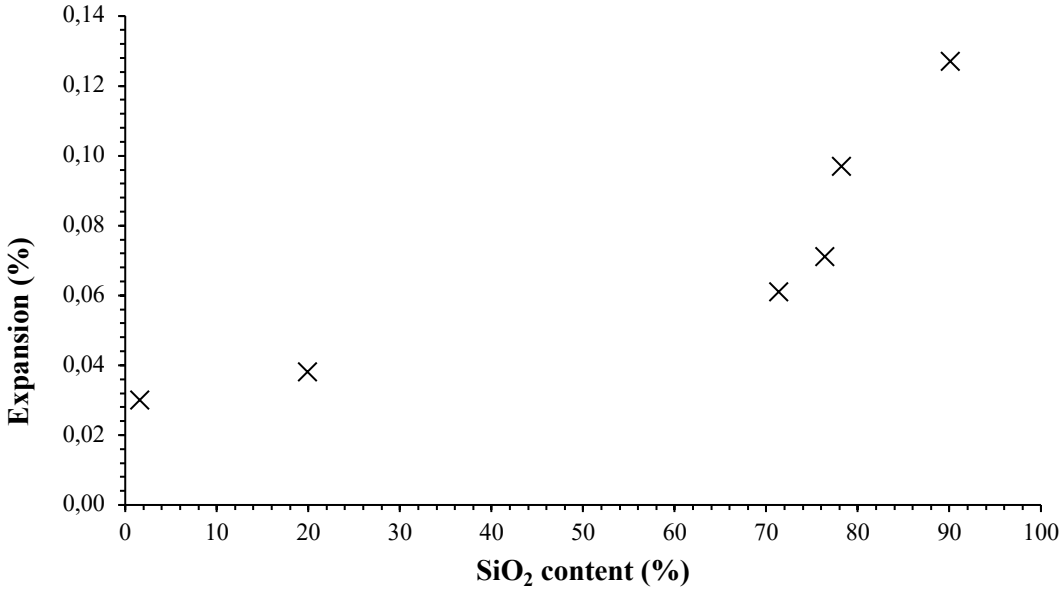

Figure 5: Silica content versus percentage expansion after 14 days of immersion in NaOH

The percentage expansion in the aggregates after 14 days of immersion in 1 N NaOH is closely related to their silica content as shown in Figure 5. A juxtaposition of Figure 3 and Figure 5 reveals that very strong positive correlation - with a correlation coefficient of 0.9 - exists between silica content and the percentage expansion in the aggregates after 14 days of immersion in NaOH. Thus, it can be concluded that an increase in silica content will result in an increase in percentage expansion. The expansion in the aggregates was also observed to be closely related to the Ca/Si ratio. The reported observations are consistent with literature [2,3,5–7]. The percentage expansion was larger in aggregates with low Ca/Si ratio than in those with high Ca/Si ratio. Aggregates with a low Ca/Si produces a net negative charge in the C-S-H gel. This negative charge would absorb the cations in the pore solution which would consequently increase the percentage expansion and the susceptibility to ASR. Aggregates from Windhoek (S6) had the most silica content (90.1%) while those from Otjiwarongo (S4) had the least silica content (1.6%). All the aggregates under investigation, except for those from Windhoek, can be classified as 'innocuous' as per the ASTM C 1260 [14] specifications. The aggregates from Windhoek, however, are potentially reactive. Thus, their use in concrete ought to be carefully informed, especially in critical infrastructure such as dams where the susceptibility to ASR would result in disastrous consequences.

A strong positive correlation – with a correlation coefficient of 0.5 - exists between the silica content and the percentage expansion in the aggregates from 5 to 14 days. Thus, it can be inferred that an increase in silica content will result in an increase in the percentage expansion due to ASR. A negative correlation with a correlation coefficient of 0.6 exists between Ca/Si ratio and the expansion at 14 days. Similarly, a weak negative correlation coefficient exists between the Ca/Si ratio and the percentage expansion in the aggregates from 5 to 14 days. It

can thus be inferred that a reduction in the Ca/Si ratio will increase the percentage expansion in the aggregates at 14 days and the percentage change in length from 5 to 14 days. Further studies, however, ought to be done to investigate this relationship in detail. Also, it can be observed that the high alkali content of the cement used in this study (i.e., 0.9521 Na_2O eq) could contribute to the susceptibility to ASR; especially in instances where reactive or mildly reactive aggregates are used. Utmost caution ought to be observed while using this cement – especially in the construction of critical infrastructure such as dams which would be adversely affected by ASR.

4. CONCLUSIONS

The susceptibility of selected Namibian aggregates to ASR attack has been discussed. From the test results, the following conclusions can be made:

i. The silica content of Namibian aggregates varies widely depending on their geology.
ii. The susceptibility to ASR increases with an increase in silica content.
iii. The percentage expansion due to ASR increases with an increase in silica content.
iv. The susceptibility of the selected Namibian aggregates to ASR is generally low. All the aggregates under investigation, except for those from Windhoek, are non-reactive. Aggregates from Windhoek exhibited slow/mild potential of alkali silica reactivity.

ACKNOWLEDGEMENTS

The authors wish to acknowledge with gratitude the following for financial support and materials for this research: Ohorongo Cement Company, Ministry of Mines and Energy (Republic of Namibia), the University of Namibia, and The Carnegie Corporation of New York.

REFERENCES

[1] S. Diamond, Alkali silica reactions – some paradoxes, Cem. Concr. Compos. 19 (1997) 391–401.
[2] Z.L. Mahomed, Alkali-aggregate reaction in Western Cape concrete, University of Cape Town, 2018.
[3] R.B. Figueira, R. Sousa, L. Coelho, M. Azenha, J.M. de Almeida, P.A.S. Jorge, C.J.R. Silva, Alkali-silica reaction in concrete: Mechanisms, mitigation and test methods, Constr. Build. Mater. 222 (2019) 903–931. https://doi.org/10.1016/j.conbuildmat.2019.07.230.
[4] G.J.. Xu, D.F. Watt, P.P. Hudec, Effectiveness of mineral admixtures in reducing ASR expansion, Cem. Concr. Res. 25 (1995) 1225–1236.
[5] S. Chatterji, Concrete durability and CaO/SiO2 mole ratio of CSH, Cem. Concr. Res. 25 (1995) 929–932.
[6] C.M. Strack, E. Barnes, M.A. Ramsey, R.K. Williams, K.L. Klaus, R.D. Moser, Impact of aggregate mineralogy and exposure solution on alkali-silica reaction product composition and structure within accelerated test conditions, Constr. Build. Mater. 240 (2020) 117929. https://doi.org/10.1016/j.conbuildmat.2019.117929.
[7] S. Chatterji, Chemistry of alkali–silica reaction and testing of aggregates, Cem. Concr. Compos. 27 (2005) 788–795. https://doi.org/10.1016/j.cemconcomp.2005.03.005.
[8] W. Aiqin, Z. Chengzhi, T. Mingshu, Z. Ningsheng, ASR in mortar bars containing silica glass in combinations with high alkali and high fly ash contents, Cem. Concr. Compos. 21 (1999) 375–381.
[9] H. Bouzabata, S. Multon, A. Sellier, H. Houari, Swellings due to alkali-silica reaction and delayed ettringite formation: Characterisation of expansion isotropy and effect of moisture conditions, Cem. Concr. Compos. 34 (2012) 349–356. https://doi.org/10.1016/j.cemconcomp.2011.10.006.

[10] B. Qinghan, S. Nishibayashi, W. Xuequan, A. Yoshino, Preliminary study of effect of LiNO2 on expansion of mortars subjected to alkali-silica reaction, Cem. Concr. Res. 25 (1995) 1647–1654.
[11] S. Kandasamy, M.H. Shehata, The capacity of ternary blends containing slag and high-calcium fly ash to mitigate alkali silica reaction, Cem. Concr. Compos. 49 (2014) 92–99. https://doi.org/10.1016/j.cemconcomp.2013.12.008.
[12] T. Oey, E.C. La Plante, G. Falzone, Y.-H. Hsiao, A. Wada, L. Monfardini, M. Bauchy, J.W. Bullard, G. Sant, Calcium nitrate: A chemical admixture to inhibit aggregate dissolution and mitigate expansion caused by alkali-silica reaction, Cem. Concr. Compos. 110 (2020) 103592. https://doi.org/10.1016/j.cemconcomp.2020.103592.
[13] M. Rashidi, M.C.L. Knapp, A. Hashemi, J.-Y. Kim, K.M. Donnell, R. Zoughi, L.J. Jacobs, K.E. Kurtis, Detecting alkali-silica reaction: A multi-physics approach, Cem. Concr. Compos. 73 (2016) 123–135. https://doi.org/10.1016/j.cemconcomp.2016.07.001.
[14] ASTM, C 1260: Standard test method for potential alkali reactivity of aggregates (Mortar-bar method), 2014.
[15] CSRA, TMH5 - Sampling methods for roads construction materials: Method MB1 – sampling of stockpiles, 1981.
[16] ASTM, C 33: Standard specification for aggregates, 2018.
[17] ASTM, C 136: Standard test method for sieve analysis of fine and coarse aggregates, 2019.
[18] CSIR, TMH1 – Standard methods of testing road construction materials: Method B15 – the determination of the dry bulk density, apparent relative density and water absorption of aggregate passing the 4,75 mm sieve, 1986.
[19] ASTM, C 305:Standard practice for mechanical mixing of hydraulic cement pastes and mortars of plastic consistency, 2014.
[20] T. Becker, K.. Hoffmann, U.. Schreiber, Geological survey of Namibia, Windhoek, 1998.

COMBINED ACTION OF CHLORIDE-INDUCED STEEL CORROSION AND ASR IN RC STRUCTURES – A REVIEW AND ONGOING STUDY

Williams Dunu [(1)] and Mike Otieno [(1)]

(1) School of Civil and Environmental Engineering, University of the Witwatersrand, Johannesburg.

ABSTRACT

Chloride-induced corrosion of steel reinforcement and alkali-silica reaction (ASR) are major forms of deterioration in reinforced concrete (RC) structures. While the damage in RC structures due to either chloride-induced or ASR have been extensively researched, the combined effect of both has not been given much attention. RC structures can exhibit alkali-silica reaction and be exposed to corrosive condition (chloride-induced corrosion) in a marine environment, and information is needed on how the combined actions of the deterioration mechanisms affect RC structures. This paper presents a review of the literature on the combined effect of both deterioration mechanisms. The paper also presents an ongoing study on the combined actions of alkali-silica reaction and chloride-induced corrosion on the durability performance of a reinforced concrete structure.

Keywords: chloride-induced corrosion, alkali-silica reaction, corrosion rate, service life

1. INTRODUCTION

Corrosion of steel reinforcement is one of the major causes of deterioration of reinforced concrete structures. While chloride-induced corrosion has been extensively researched, the combined effect of alkali-silica reaction and chloride-induced steel corrosion has not been given much attention, because of insufficient information on the combined action of ASR and chloride-induced steel corrosion in RC structures [1].

ASR is a reaction between alkali hydroxide in the pore solution of a hydrated cement paste (HCP) in the concrete and reactive silica in aggregates. Three things that need to be present for ASR to take place [2] include reactive aggregates, high alkali content in the pore solution, and high moisture content (> 80% relative humidity). The product of this reaction is referred to as ASR gel (A-S-H), which can also be converted to calcium silicate hydrates (C-S-H) gel because of the calcium ions present in the pore solution. ASR gel is porous and has a high surface area which has the affinity to absorb moisture from the surrounding pore solution and environment, this results in the expansion of the concrete and its structural degradation due to crack formation. The ASR gel forms in and around the aggregates, interfacial transition zone (ITZ), and in the concrete pores, the gel may fill the ITZ, pores, and concrete cracks thereby creating a barrier against the easy transportation of chlorides from the concrete surface to the steel reinforcement [21].

Right from Stanton's discovery of ASR in 1940, this defect has been known to occur in various concrete structures such as dams, bridge piers and decks, pavements and other

concrete structures [21]. In investigations on concrete structures and laboratory concretes, Sibbick and Page, [19]assessed the effect of NaCl exposure on ASR in concrete concerning the alkali content of the concrete and the C_3A content of the cement. They proposed a reaction scheme in which, firstly, the ingress of NaCl increases the NaOH concentration of the pore solution owing to the reaction of chloride with the C_3A hydration products and portlandite. Secondly, the increase in OH^- concentration promotes the neutralization of the acidic silanol groups (SiOH) at the SiO_2 surface and thus the formation of negatively charged SiO^- surfaces. This paper presents a review of the combined effect of ASR and chloride-induced corrosion of steel in reinforced concrete structures.

2. CAUSES OF CONCRETE DETERIORATION

Alkali-aggregate reaction (alkali-silica reaction and alkali-carbonate reaction) and chloride-induced corrosion of steel are among the several causes of concrete deterioration. Some other causes are swelling due to expansion of the cement (from free lime or ettringite), external factors such as cycles of freezing and thawing or the attack on concrete by water in forms such as acidic water and sulphate-rich water In many cases, there may be a combination of causes, so that when there is an alkali-aggregate reaction in the concrete, for instance, the effects of other factors may be aggravated [11].

2.1 Alkali-silica reaction

Alkali-silica reaction is a harmful reaction (expansion and cracks) that occurs between the alkaline pore solution of concrete and several forms of reactive silica found in many natural and artificial aggregates [4] Dissolution of the silica structure occurs by the constant attack of hydroxyl ions, after which the dissolved silica structure behaves as a hygroscopic compound and absorbs water from the surrounding environment. Alternatively, the dissolved silica can cross-link (e.g. in the presence of Ca^{2+} ions), coagulate, and form ASR gel. Right from Stanton's discovery of ASR in 1940, this defect has been known to occur in various concrete structures such as dams, bridge piers and decks, pavements and other concrete structures [21]. Three things need to be present for ASR to take place [2]:

i. The presence of reactive aggregate
ii. High-alkali content in the pore solution (pH 12.5 and above); and
iii. A high moisture content, usually a relative humidity from 80% and above.

At the initial stage of ASR, the hydroxyl ions in the pore solution of a hydrated cement paste (HCP) react with Si-O-Si bonds (siloxane group) of reactive silica in aggregates to produce silicic acid (Si-OH) and alkali silicate ($Si-O^-$). Then the silicic acid reacts with the hydroxyl ions (OH^-) and metal alkali that forms alkali-silica gel by liberating water. Finally, the expansion occurs due to the hydration of the alkali-silica gel [16]. Later, the hydrated alkali-silica gel gets defused from aggregate to cement paste and reacts with the calcium ions Ca^{2+}. This generates an alkali-calcium-silicate hydrate gel. These products absorb moisture from the surroundings and expand in volume. Excessive expansion can cause cracking of aggregate and cement paste to initiate the degradation of concrete [16].

2.2 Corrosion of steel in concrete

Corrosion of steel reinforcement embedded in concrete has been viewed as the main hazard which reduces the durability of reinforced concrete structures [15, 18, 14]. The

lifespan (service life) of the RC structure mainly comprises two phases: the corrosion initiation and propagation phases. Over the years, steel corrosion due to chloride ingress or carbonation has been identified as the main cause of durability failure and hence reduced the service life of RC structures [4]. For RC structures in marine environments and where de-icing salts are used, chloride-induced corrosion has been identified as the dominant cause of durability failure [20].

Steel corrosion in concrete is a process in which iron is dissolved at the anode and oxygen is reduced at the cathode [3].

3. COMBINED ACTION OF CHLORIDE-INDUCED STEEL CORROSION AND ASR IN RC STRUCTURES

Significant research [9, 14, 8, 7] has been conducted on the damage in RC structures due to either ASR or chloride-induced corrosion, but combined actions of both mechanisms have not been fully researched and understood [21] RC structures can exhibit alkali-silica reaction and be exposed to corrosive condition (chloride-induced corrosion) in a marine environment. Information is needed on how the combined actions of the deterioration mechanisms affect RC structures.

Since ASR leads to cracking in concrete and cracks enhance chloride transportation, it is anticipated that ASR will increase the rate of chloride penetration in concrete thereby reducing the time to active corrosion. Though ASR in concrete results in cracks, the reaction product can fill the ITZ between the aggregates, cracks and voids particles thereby creating a barrier to chloride penetration [12]. The ASR product may retard the ingress of chloride into concrete and consequently delay the corrosion initiation of steel in concrete. Studies have shown that ASR can reduce the transport rate of chlorides and time to corrosion initiation of steel reinforcement in concrete [10, 21] However, there is a need to investigate how the combined actions of ASR and chloride-induced corrosion influence the durability performance of RC structures. Interestingly, the few studies that have been carried out to investigate the influence of ASR and chloride-induced corrosion of steel on RC structures had been performed primarily on corrosion initiation [10, 21] but there is no information on durability performance of RC structures under the combined actions of ASR and chloride-induced corrosion. To ensure that structures maintain adequate durability during their service life, engineers need to understand the combined action of ASR and chloride-induced corrosion of steel which can impair the durability performance of RC structures.

3.1 Existing work on the combined effect of chloride-induced steel corrosion and ASR in RC structures

Studies have confirmed that cracks in the RC provide pathways to the surface of steel reinforcement for aggressive agents[14, 16]. Trejo *et al* [21], investigates the influence of ASR on chloride transport characteristics and time to corrosion initiation. The following conclusions were drawn:

i. The formation of ASR gel in specimens containing a reactive fine aggregate resulted in expansion and cracking of the specimens containing reactive aggregate, but this was not observed in the specimens containing nonreactive aggregate.
ii. The specimens containing reactive and nonreactive aggregate showed similar times to corrosion initiation.

iii. Specimens containing nonreactive aggregate exhibited a higher corrosion rate than the specimens containing reactive aggregate. This indicates that ASR resists the transport of chlorides and the presence of ASR gel can act as a barrier against chloride transport in concrete, resulting in the lower overall penetration rate of the chlorides.
iv. Energy dispersive X-ray (EDX) results show a statistically significantly lower chloride value in the ASR gel than the HCP.

4. SCOPE OF THE ONGOING STUDY

The study according to [21], that had been carried out to assess the influence of these combined deterioration mechanisms on reinforced concrete structures was performed primarily on corrosion initiation and therefore, a comprehensive research study is needed to investigate the interacting effect of these two deterioration mechanisms. The experimental work of the ongoing study will comprise the following laboratory test assessment; aggregate reactivity test will be carried out using a standardized test method [17] to determine the most reactive among the selected aggregates and adopt it for the research work. Corrosion assessment and alkali-silica reaction test will be conducted on concrete beam specimens using the coulostatic method to monitor corrosion initiation and corrosion propagation of steel in concrete beam specimen and a standardized test method (ASTM C129) will be used to determine dimensional length change due to ASR. Durability index tests will be conducted on the discs extracted from the concrete cube specimens, one set of specimens with reactive and non-reactive aggregates and the second set of specimens with non-reactive for fine and coarse aggregates to determine the influence of alkali-silica reaction on the durability properties in concrete structures.

This ongoing research will take into account relevant quantifiable parameters such as time to corrosion initiation, rate of corrosion propagation, durability index tests (chloride conductivity index, oxygen permeability index, water sorptivity index) which will provide useful data that can be utilized in the prediction of the service life of reinforced concrete structures exposed to the combined actions of alkali-silica reaction and chloride-induced corrosion in a marine environment. This ongoing research will provide the information that will enhance the knowledge of engineers on the combined effect of both mechanisms on reinforced concrete structures in a marine environment. The ongoing experimental work is described in the flow chart, as shown in Figure 1 :

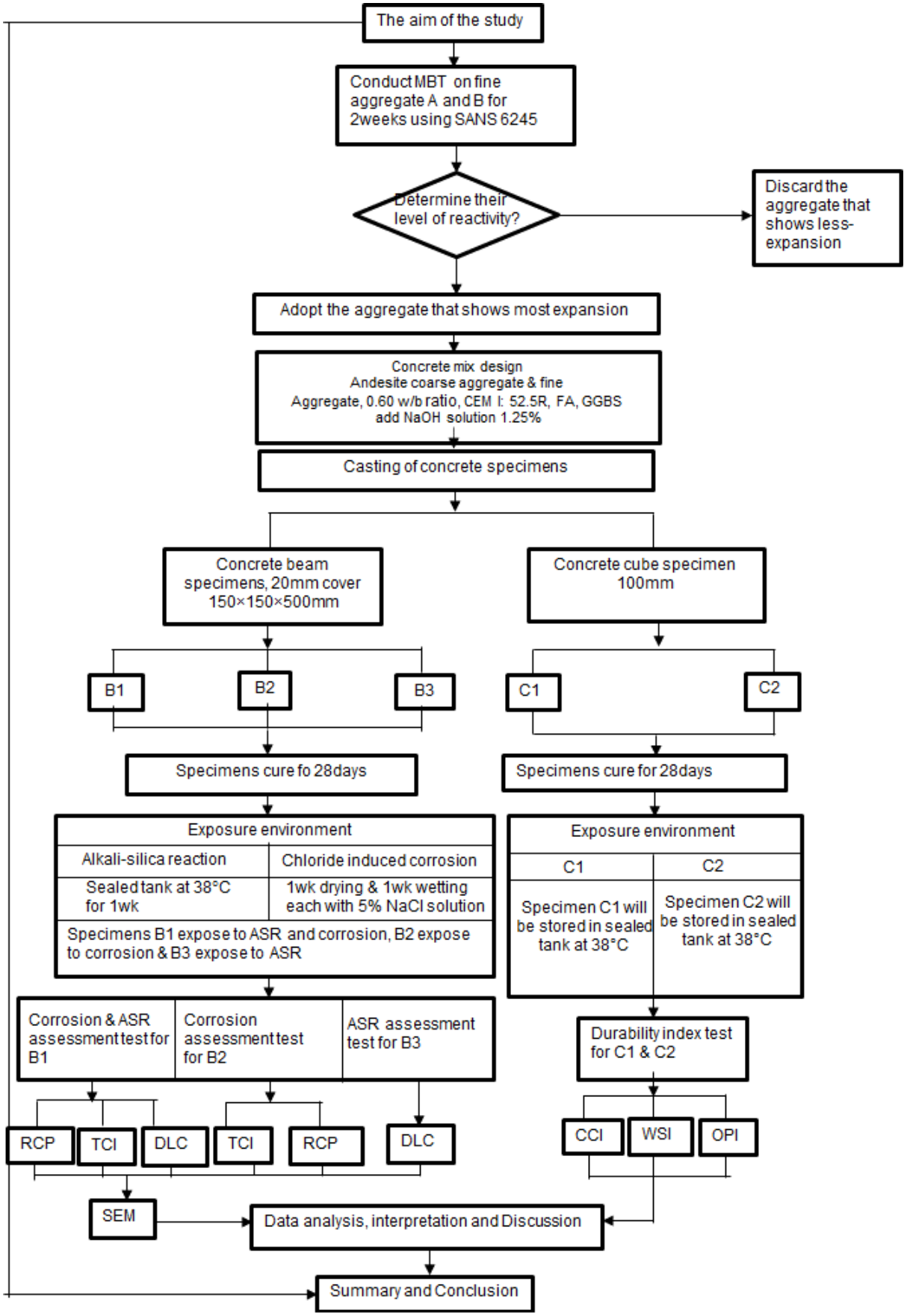

Figure 1: Flow chart showing detail research scope

The specimens used in the ongoing experimental work were designed to have a basis of comparison of results are as follows:

i. Beam specimens (B1) containing reactive fine and non-reactive coarse aggregates were produced. A 12mm steel reinforcement bar was placed at a cover depth of 20mm from the concrete face that was exposed to chlorides. The objective of these specimens to create a scenario of alkali-silica reaction and steel corrosion simultaneously.
ii. Beam specimens (B2) containing non-reactive coarse aggregate and non-reactive fine aggregate were produced. A 12mm steel reinforcement bar was placed at a cover depth of 20mm. This was done to create a scenario of steel corrosion only.
iii. Beam specimens (B3) containing reactive fine aggregate and non-reactive coarse aggregate were used. No steel reinforcement bar was embedded (plain concrete). This was designed to create a scenario of alkali-silica reaction only.
iv. Cube specimens (C1 and C2) specimen C1 containing non-reactive coarse and reactive fine aggregate. This specimen is designed to have an alkali-silica reaction. Specimen C2 containing non-reactive coarse and fine aggregate. This was done to have cube specimens without alkali-silica reaction. Other abbreviations used in the flow chart are presented in Table 1:

Table 1: Abbreviation meaning

Abbreviation	Meaning
MBT	Mortar bar test
FA	Fly ash
GGBS	Ground granulated blast-furnace slag
RCP	Rate of corrosion propagation
TCI	Time of corrosion initiation
DLC	Dimensional length change
CCI	Chloride conductivity index
WSI	Water sorptivity index
OPI	Oxygen permeability index
SEM	Scanning electron microscopic

5. CLOSING REMARKS

This paper has presented a review of the combined action of chloride-induced steel corrosion and ASR in RC structures. The following salient points can be drawn from this review:

i. Investigating the combined action of these deterioration mechanisms will give a good understanding of RC structures that exhibit alkali-silica reaction and be exposed to chloride-induced corrosion in the marine environment.
ii. The formation of ASR gel can fill the cracks and interfacial zone of the aggregates thereby influencing the chloride transport in concrete, resulting in the lower overall penetration rate of the chlorides and higher time of corrosion initiation to take place.

iii. Comprehensive work should be done on the combined action of chloride-induced steel corrosion and ASR by taking cognisance of relevant quantifiable parameters such as time to corrosion initiation, rate of corrosion propagation, durability index tests (chloride conductivity index, oxygen permeability index, water sorptivity index). This will give sufficient information on the durability performance of RC structures under the combined action of ASR and chloride-induced steel corrosion.

iv. To ensure that structures maintain durability during their service life, there is a need for engineers to have a robust knowledge of the combined effect of both mechanisms on reinforced concrete structures in a marine environment.

REFERENCES

[1] Angst, U. M., Elsener, B., Larsen, C. K and Vennesland, O. (2011) 'Chloride induced reinforcement corrosion: Electrochemical monitoring of initiation stage and chloride threshold values', *Corrosion Science*, 53(4), pp. 1451–1464. doi: 10.1016/j.corsci.2011.01.025.

[2] Angulo-Ramírez, D. E., Mejía de Gutiérrez, R. and Medeiros, M. (2018) 'Alkali-activated Portland blast furnace slag cement mortars: Performance to alkali-aggregate reaction', *Construction and Building Materials*, 179, pp. 49–56. doi: 10.1016/j.conbuildmat.2018.05.183.

[3] Beushausen, H., Otieno, M. B. and Alexander, M. G. (2012) *Corrosion of steel in reinforced concrete : Influence of binder type, water/binder ratio, cover and cracking*. Ninth edit. Cape Town: Concrete Materials and Structural Integrity Research Unit Department of Civil Engineering, University of Cape Town.

[4] Fang, C., Gylltoft, K., Lundgren, K. and Plos M. (2006) 'Effect of corrosion on bond in reinforced concrete under cyclic loading', *Cement and Concrete Research*, 36(3), pp. 548–555. doi: 10.1016/j.cemconres.2005.11.019.

[5] Fournier, B. and Bérubé, M.-A. (2000) 'Alkali-aggregate reaction in concrete: a review of basic concepts and engineering implications', *Canadian Journal of Civil Engineering*, 27(2), pp. 167–191. doi: 10.1139/cjce-27-2-167.

[6] François, R. and Arliguie, G. (1998) 'Influence of Service Cracking on Reinforcement Steel Corrosion, *Journal of Materials in Civil Engineering*, 10(1), pp. 14–20. doi: 10.1061/(ASCE)0899-1561(1998)10:1(14).

[7] Giaccio, G., Torrijos, M.C., Milanesi, C and Zerbino, R. (2019) 'Alkali–silica reaction in plain and fibre concretes in field conditions', *Materials and Structures/Materiaux et Constructions*, 52(2), pp. 1–15. doi: 10.1617/s11527-019-1332-2.

[8] Karthik, M. M., Mander, J. B. and Hurlebaus, S. (2018) 'Experimental Behavior of Large Reinforced Concrete Specimen with Heavy ASR and DEF Deterioration', *Journal of Structural Engineering*, 144(8), p. 04018110. doi: 10.1061/(ASCE)ST.1943-541X.0002102.

[9] Michel, A., Otieno, M., Stang, H and Geiker, M. R. (2016) 'Propagation of steel corrosion in concrete: Experimental and numerical investigations', *Cement and Concrete Composites*. Elsevier Ltd, 70, pp. 171–182. doi: 10.1016/j.cemconcomp.2016.04.007.

[10] Mitsunori KAWAMURA, Kunio TAKEMOTO, M. I. (2015) 'Alkali-silica reaction and corrosion of steel reinforcement in mortars containing a reactive aggregate and chloride', pp. 2–4. Available at: https://www.jstage.jst.go.jp/article/jscej1984/1992/451/1992_451_99/_article/-char/en.

[11] Nvmahure (2008) 'Monograph on Alkali Aggregate Reaction'. Available at: http://csmrs.gov.in/WriteReadData/Publication/MonographonAlkaliAggregateReactionConcrete.pdf.

[12] Otieno, M. B., Alexander, M. G. and Beushausen, H.-D. (2010) 'Corrosion in cracked and uncracked concrete – influence of crack width, concrete quality and crack reopening', *Magazine of Concrete Research*, 62(6), pp. 393–404. doi: 10.1680/macr.2010.62.6.393.

[13] Otieno, M., Beushausen, H. and Alexander, M. (2016a) 'Chloride-induced corrosion of steel in cracked concrete - Part I: Experimental studies under accelerated and natural marine environments, *Cement and Concrete Research*. Elsevier Ltd, 79, pp. 373–385. doi: 10.1016/j.cemconres.2015.08.009.
[14] Otieno, M., Beushausen, H. and Alexander, M. (2016b) 'Chloride-induced corrosion of steel in cracked concrete - Part II: Corrosion rate prediction models', *Cement and Concrete Research*. Elsevier Ltd, 79, pp. 386–394. doi: 10.1016/j.cemconres.2015.08.008.
[15] Pang, L. and Li, Q. (2016) 'Service life prediction of RC structures in the marine environment using long term chloride ingress data: Comparison between exposure trials and real structure surveys', *Construction and Building Materials*. Elsevier Ltd, 113, pp. 979–987. doi: 10.1016/j.conbuildmat.2016.03.156.
[16] Parmar, H. S., Gupta, T. and Sharma, R. K. (2019) 'A Critical Review on Mitigation of Alkali-Silica Reaction in Concrete, 8(0), pp. 34–40.
[17] SANS 6245 : 2006 SOUTH AFRICAN NATIONAL STANDARD Potential reactivity of aggregates with alkalis (accelerated mortar prism method)', 2006, pp. 0–8.
[18] Shi, X., Xie, N., Fortune, K and Gong, Jing. (2012) 'Durability of steel-reinforced concrete in chloride environments: An overview', *Construction and Building Materials*. Elsevier Ltd, 30, pp. 125–138. doi: 10.1016/j.conbuildmat.2011.12.038.
[19] Sibbick, R. G. and Page, C. L. (2009) 'Mechanisms affecting the development of alkali-silica reaction in hardened concretes exposed to saline environments, *Magazine of Concrete Research*, 50(2), pp. 147–159. doi: 10.1680/macr.1998.50.2.147.
[20] Torres-Luque, M., Bastidas-Arteaga, E., Schoefs, F., Sanchez-Silva, M and Osma, J. F. (2014) 'Non-destructive methods for measuring chloride ingress into concrete: State-of-the-art and future challenges', *Construction and Building Materials*. Elsevier Ltd, 68, pp. 68–81. doi: 10.1016/j.conbuildmat.2014.06.009.
[21] Trejo, D., Mazarei, V., Ideker, J. H and Isgor, O. B. (2017) 'Influence of alkali-silica reaction reactivity on corrosion in reinforced concrete, *ACI Materials Journal*, 114(5), pp. 723–731. doi: 10.14359/51689895.
[22] Yu, L., Francois, R., Dang, V. H., L'hostis, V and Gagne, R. (2015) 'Development of chloride-induced corrosion in pre-cracked RC beams under sustained loading: Effect of load-induced cracks, concrete cover, and exposure conditions', *Cement and Concrete Research*. Elsevier Ltd, 67, pp. 246–258. doi: 10.1016/j.cemconres.2014.10.007.

CORROSION PREDICTION MODELS FOR BIOGENIC ACID ATTACK CONCRETE IN SEWERS

Alice T. Bakera [(1)], Mark G. Alexander [(1)], and Hans Beushausen [(1)]

(1) Department of Civil Engineering, University of Cape Town

ABSTRACT

Among assets of urban infrastructure of modern societies, sewer systems are very crucial. They protect humans against water-borne diseases and other threats attributed to water, air and land pollution. Sewer systems consist of pipelines, manholes, pumping stations, storm overflows, and screening chambers, which are commonly made of concrete. Despite concrete being robust, versatile, and economical, its long-term performance in sewer environments can be problematic due to biogenic acid attack. Designing a durable concrete to resist this attack has been a challenge for many decades. This is because the attack is complex and depends on numerous influencing factors. Further, existing corrosion prediction models are limited mainly to Portland Cement (PC) based concretes, which do not perform well. Other binders exists that have been proved to perform better, however limited tools for modelling their performance are available. The purpose of this paper is, therefore, to review the existing prediction models for concrete in sewers, point out their applications and limitations, and indicate means of applying their principles to improve a widely used prediction model, the 'Life Factor Method'.

Keywords: durability, sewer concrete, biogenic acid attack

Symbols

A = Alkalinity of the concrete material (g $CaCO_3$ per g concrete material)
A_c = Concrete surface area,
A_S = Scaling constant
C_{avg} = Average (annual) corrosion rate (mm/year)
C_{max} = Maximum concrete corrosion rate (mm/year)
ϕ_{sw} = Average H_2S flux to the pipe wall (g/m^2/h)
P = Perimeter of the pipe wall above the sewage surface (m)
a and c = Aggregate and cement content in concrete (kg aggregate or cement/m^3 concrete)
$S_{(-II)}$ = Sum of H_2S, HS^-, and S^{2-} concentrations in the water phase (g S/m^3)
S_{SO_4} = Sulphate concentration (g S/m^3)
P_{H_2S} = H_2S partial pressure in the gas phase (ppm)
$S_{H_2SO_4}$ = Sulphuric acid concentration in the water film of moist sewer surface (g S/m^3)
S_O = dissolved oxygen concentration (g O_2/m^3)
d_{corr} = Surface corrosion depth (m)
d = Density of concrete (kg/m^3)
k = Efficiency factor
H = Concrete moisture content
Ea = Activation energy (kJ/mol)
V_w = Gas volume (m^3)
V_g = Water volume (m^3)
σ_{conc} = Specific mass of the concrete material (g/m^3)
r# = process rate (/day)
eqv = Equivalent
agg. = Aggregate
AH_3 = Aluminium hydroxide gel
CaO = Calcium oxide phase in cement and aggregate
CH = Calcium hydroxide
$CaCO_3$ = Calcium carbonate
FeO(OH) = Iron oxyhydroxide
Al, Ca, and Fe = Aluminium, Calcium, and Iron
100/56 = Molar mass ratio of $CaCO_3$ and CaO
$[H_2S]_{aq}$ = Hydrogen sulphide concentration in the sewage (mg/l)
q = Sewer headspace aggressiveness factor

R_{Cwc} = Stoichiometric constant of chemical oxidation of sulphide in bulk water (g S/g O_2)
R_{Cwb} = Stoichiometric constant of biological oxidation of sulphide in bulk water (g S/g O_2)
R_{Cfb} = Stoichiometric constant of biological oxidation of sulphide in biofilm (g S/g O_2)
R = Universal gas constant (8.314 J/mol/K)
RC_{eff} = Effective resistance capacity
s = Hydraulic gradient (m/m)
V = Hydraulic velocity (m/s)
W = Sewage surface width (m)

1. INTRODUCTION

Biogenic acid attack results from the biological activity of bacteria on sewer concrete surfaces. The bacteria produce sulphuric acid that corrodes the concrete matrix and underlying steel reinforcement [1]. In this context, sewer concrete must be designed with a high potential for resisting the attacking acid. The resisting potential can be achieved by providing concrete with high acid neutralization capacity and/or components that retard or stop the growth of the acid-producing bacteria (bacteriostatic capacity) [2]. However, designing such concrete requires the designer to understand the overall deterioration mechanisms and interaction between the attacking acid and resisting concrete, determine the deterioration rate, and predict the service life of sewer concrete. These can be aided by the use of adequate and reliable service life prediction models [3].

The desired service life of a sewer is about 100 years which is sufficient time for a sewer to serve with routine maintenance but without major repairs being necessary. However, achieving this lifetime is challenging due to changes in sewer environmental conditions, on-going changes in construction materials and techniques, and inadequate knowledge about the mechanisms of the attack. Because of these factors, most existing corrosion prediction models are inadequate, and some of them become obsolescent.

Most existing and preferred models such as the 'Life Factor Method' have been developed based on sewer conditions of earlier periods. Authorities set regulations controlling the quantity and quality of wastewater released from industries, but domestic wastewater also consists of components that facilitate the growth of bacteria [4]. Environmental changes also pose challenges for sewers, for example, countries affected by drought. With limited usage of water, the wastewater flow declines with increasing retention time and concentration of biodegradable matter and nutrients for bacteria growth which, eventually, lead to high production of hydrogen sulphide gas [5].

Ongoing changes in construction materials due to technological developments also affect the development of service life prediction tools. Several modern materials (e.g. newer cement, modern chemical admixtures, antimicrobial additives, etc.) are being introduced into the industry with, in many cases, unknown levels of performance. With sewer deterioration rates being relatively slow in general, the industry is often not willing to invest time and money in studying and understanding newer materials or establishing prediction models that can accommodate these materials. Despite the advancement and availability of computer-based platforms for modelling and simulation, there are fewer incentives for researchers to readily utilize them. Even when these platforms are applied, there is limited information or field data to assist in calibration.

Therefore, the aim of this paper is to review various corrosion prediction models and understand their applications and limitations. With this understanding, a commonly used

prediction model in the design of concrete sewers, the 'Life Factor Method', can be modified in such a way it can be easily applied by engineers in the field.

2. LIFE FACTOR METHOD (LFM) - 1977

The Life Factor Method (LFM) (Equations 1.1 to 1.3) is, in many cases, the preferred approach for predicting corrosion rate of concrete subjected to the biogenic acid attack in sewers [6]. The corrosion rate (C_{avg}) is determined by combining four stages of biogenic corrosion, which are (i) hydrogen sulphide generated in the bulk wastewater ($[H_2S]_{aq}$), (ii) hydrogen sulphide emission into the sewer headspace (hydrogen sulphide flux: ϕ_{sw}), (iii) hydrogen sulphide absorbed and oxidised to sulphuric acid (efficiency factor: k), and (iv) concrete neutralization potential (alkalinity: A).

$$C_{avg} = 11.4\mathrm{k}\frac{\phi_{sw}}{A} \qquad \textbf{Equation (1.1)}$$

$$\phi_{sw} = 0.69(\mathrm{sV})^{0.375}[H_2S]_{aq}\frac{W}{P} \qquad \textbf{Equation (1.2)}$$

$$\mathrm{A} = \frac{c(CaO_{cement}) + a(CaO_{agg})}{d}\mathrm{x}\frac{100}{56} \qquad \textbf{Equation (1.3)}$$

The LFM model was first used in 1976 to design Portland Cement (PC)-based concrete pipes for the central trunk sewer by the city of Sacramento, California, U.S.A., and later, expanded to other countries such as South Africa. During its application, it was observed that the predicted corrosion depths were often smaller than the actual depths measured in most sections of sewers, and that the worst corroded areas coincided with the 'tidal' zone at the average daily sewage flow level, and also at the crown and at regions with high flow turbulence [7–10]

This variability in corrosion depths was attributed to either assumption made during the introduction of certain parameters such as the efficiency factor (k) and H_2S flux (ϕ_{sw}), or the exclusion of other parameters related to turbulence and the critical corroded area, during model development. Based on these observations, in 1992, two factors; the crown corrosion factor (CCF), ranging from 1.5 to 2.0, and turbulence corrosion factor (TCF), ranging from 1.0 to 2.5 for areas with 'typical' turbulent flow conditions, and 5.0 to 10.0 for very turbulent junctions, were introduced in equation 1.1, to produce equation 1.4 [7].

$$C_{max} = \left(11.4\mathrm{k}\frac{\phi_{sw}}{A}\right).CCF.TCF \qquad \textbf{Equation (1.4)}$$

However, equation 1.4 fails to take into account further recent findings concerning the corrosion process and associated influencing factors [11]. It is observed that the corrosion rate depends on various sewer environmental factors that include the H_2S gas concentration, Relative Humidity (RH) and temperature, and not merely on the bulk wastewater sulphide concentration [12,13]. It was also discovered that pipe corrosion was critically related to properties of concrete other than those allowed for in the original model, (i.e. material factor), which includes the concrete transport properties and the chemical and biological interactions with the oxidised sulphide and bacteria proliferating on the concrete exposed surface[14–16].

3 IMPROVED LIFE FACTOR METHOD - 2016

Before the mix designs were finalised, 3 trial mixes were done in accordance with the South African Concrete & Cement Institute (C&CI) design method, to determine the optimum moisture content to theoretically achieve a 75mm slump for the control mix design. Three different mix designs with water contents ranging between 225 kg/m^3; 215 kg/m^3 and 205 kg/m^3, were done using a principle of ratios. This method was used to ensure that no material was wasted, and excess water used whilst conducting three different slump tests each having different water contents. The method of ratios consisted of designing the initial mix in accordance with the C&CI method, and then performing numerous ratio calculations to determine the new quantities. The recorded slumps can be seen in Figure 1.

With reference to the C&CI method as well as the new optimum water content, the mix designs were scaled to the required volumes for each batch consisting of cubes for compressive strength tests and beams for dynamic loading tests. A constant w/c ratio of 0,45 was used throughout the seven different batches, with the batch quantities for the treated and untreated rubber staying constant. Table 1 shows the final mix designs for the four different batches.

In a study conducted at the University of Cape Town in 2016 [17], regarding the application of the LFM model at the Virginia Experimental Sewer (VES) in South Africa, it was observed that the model adequately predicted the total sulphides in the sewer and the biogenic corrosion rate of plain PC concrete mixtures, but could not predict corrosion rates of concretes consisting of blends of PC and other supplementary cementitious materials, or of Calcium Aluminate Cement (CAC) based systems. According to [17], this was related to the inability of the LFM to incorporate the different chemistries of various binders.

Therefore, the LFM model was empirically refined by replacing the alkalinity factor (A) with an 'effective resistance capacity' (RC_{eff}), and introducing a 'sewer headspace aggressiveness factor' (q), giving rise to the 'Improved LFM' – equations 1.5 and 1.6. RC_{eff} was introduced on the basis that using the alkalinity factor as the rate-controlling parameter of the concrete corrosion rate was inadequate and inaccurate. Other binder chemical compositions which include larger amounts of, e.g., Al_2O_3, and Fe_2O_3, were found to contribute significantly to neutralizing the attacking acid and providing the possible bacteriostatic effect. Also, the sewer headspace aggressiveness factor was introduced due to the influence of sewer headspace temperature and RH of a particular sewer.

$$C_{avg} = 11.4\mathrm{k}\frac{\phi_{sw}}{\left(RC_{eff}\right)^{1.49}}q \qquad \textbf{Equation (1.5)}$$

$$RC_{eff} = \left(\mathrm{CaCO_3}_{eqv.agg}\right) + \left(CH_{eqv.CAC}\right) + \left(\frac{CH^{-1}_{eqv.PC}}{100}\right) + \left(AH_{3_{eqv}}\right) + \left(FeO(OH)_{eqv}\right) + \left(\frac{Al}{Ca}\right) + \left(\frac{Fe}{Ca}\right) \qquad \textbf{Equation (1.6)}$$

4 CURRENT CHALLENGES WITH THE IMPROVED LFM MODEL

Despite the 2016 improvement, the LFM model is still limited. Binder constituents such as CaO, Al_2O_3, and Fe_2O_3 used to evaluate the effective resistance capacity are observed to influence the corrosion rate in ways counter to how they are quantified in the Improved LFM model. According to [11, 18], the presence of iron phases in concrete under attack leads to the formation of iron oxide precipitates which cause internal cracking in the intact zone of the concrete. The cracking then contributes to the transport of aggressive components into the intact zone, thereby accelerating the attack. On the other hand, the aluminium phase has been considered to contribute to the bacteriostatic effect. However, [19] found that, in the presence of aluminium ions in concrete, the microorganisms readily adapt and consequently continue to proliferate. Because of the lack of clarity in these crucial aspects, a clear understanding of their roles must be established, which will result in further modifications and improvements to the LFM.

Further, the 'sewer aggressiveness factor' which was introduced in the improved LFM conflicts with the 'efficiency factor'. Both factors are empirically evaluated and are functions of sewer headspace conditions, especially temperature and RH. According to [17], the sewer aggressiveness factor accounts for the influence of sewer headspace temperature and RH. However, a range of values has not been evaluated, but can conceivably differ from one sewer to another. According to [10], the efficiency factor also has never been measured; the value chosen depends on engineering judgement. Its value approaches unity when the rate of acid formation is slow, and maybe as low as 0.3 to 0.4 when the rate of acid formation is rapid and if much condensate is formed (e.g. warm wastewater and cold pipe wall). Thus, these factors need re-consideration and reconciling.

Using field data from the VES [17], the improved LFM model could be made to adequately predict the performance of PC and CAC based mixtures. However, its performance was unclear when predicting the corrosion rates of concretes made with other modern binder systems such as Alkali-Activated Cements (AAC) and Calcium Sulpho-Aluminate cement (CSA). Therefore, there is a further need to study or refine the model to increase its broader usage.

Regardless of the challenges, the LFM is a practical and useful model which can be easily applied by engineers. Therefore, modifying this model can significantly contribute to sewer design and applications. Figure 1 shows the LFM timeline and developments made to date. Applying the principles used in developing other corrosion prediction models likely could assist in improving the LFM model. Therefore, the following section reviews other corrosion rate prediction models; through understanding their principles, vital information can be extracted and applied in the LFM modification.

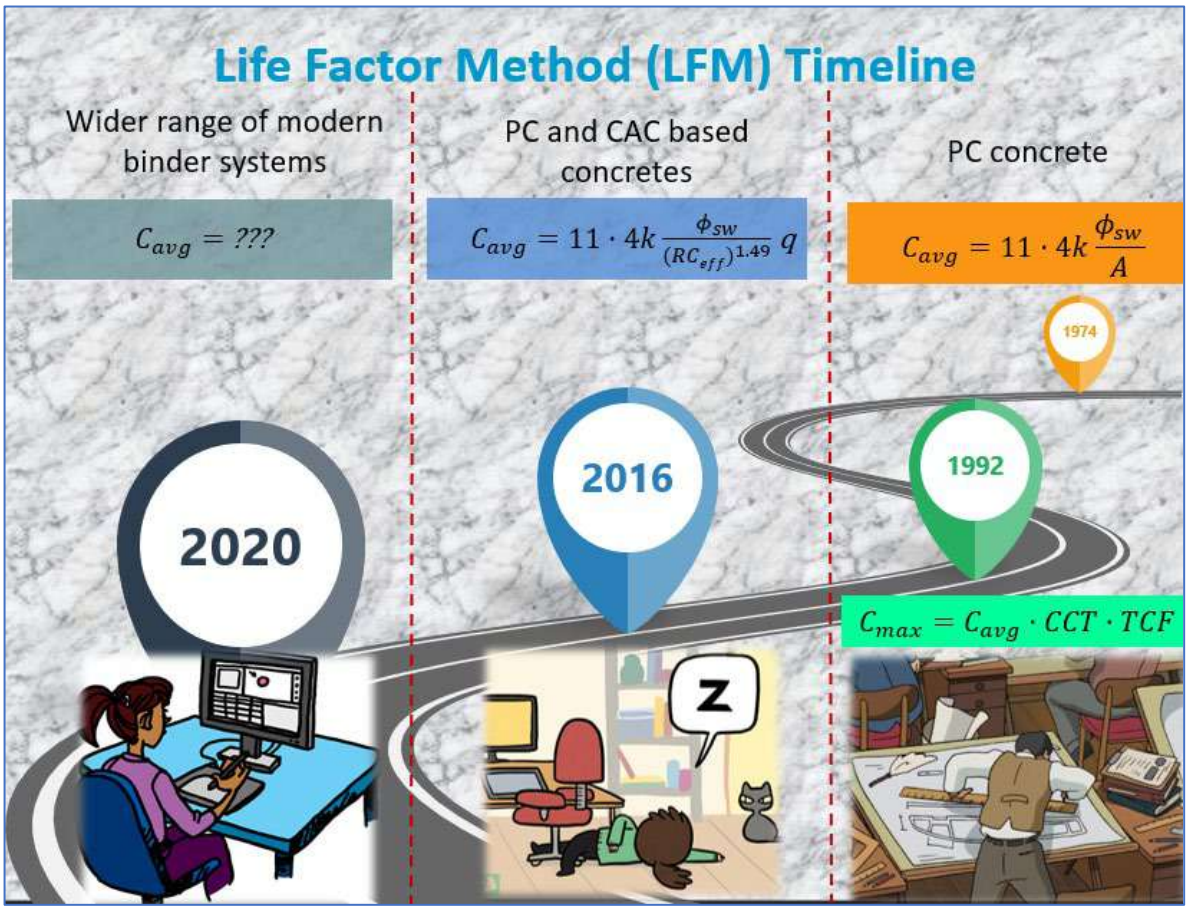

Figure 1: Life Factor Method (LFM) timeline from 1974 to 2016. The challenge is to 'improve' this model to be applicable to modern binder systems.

5. OTHER CORROSION RATE PREDICTION MODELS

5.1 WATS Model - 2013

Wastewater Aerobic-Anaerobic Transformations in Sewers (WATS) model is a conceptual and numerical model which is mainly applicable for simulating sewer processes and predicting hydrogen sulphide gas associated problems in both gravity sewers and force (pumped) mains. The main objective of the WATs model is to manage and control sewer processes that lead to concrete corrosion, human health impacts, and odour nuisance caused by hydrogen sulphide and volatile organic compounds [20, 21].

The model consists of various components and their corresponding transformation processes expressed by rate equations and stoichiometric constants. A combination of the rate equations and stoichiometric constants results in several coupled differential equations which can only be solved numerically [20]. The transformation processes, i.e. aerobic, anoxic, or anaerobic transformations can be divided into five conceptual process elements, i.e. sulphur cycle, aerobic, heterotrophic transformations of organic matter, aerobic transformations of organic carbon and sulphur, anoxic, heterotrophic transformations of organic matter, and aerobic and anaerobic transformations or organic carbon and sulphur. Therefore, the central elements and the backbone of the WATS process concept are the sulphur cycle and the carbon cycle.

Regarding concrete corrosion, only sewer process elements for the sulphur cycle formulation are included. The sulphur cycle concerns both anaerobic and aerobic processes and includes all phases leading to concrete corrosion; the biofilm, the water phase, the sewer headspace, and the surfaces exposed to the sewer headspace. The matrices presented in Table 1 are considered as the differential of the first row being equal to the sum of the processes listed in the respective column. For instance, the rate of surface concrete corrosion is given in Equation 1.7. A complete WATS model contains fifteen coupled differential equations that are solved by Euler approach. For more details regarding the model, see [21].

Table 1: WATS Sewer Process Model for Formulation of Sulphur Cycle as a Process Matrix [21]

Process rate	$\frac{d}{dt}(S_{SO_4})$	$\frac{d}{dt}(S_O)$	$\frac{d}{dt}(S_{(-II)})$	$\frac{d}{dt}(P_{H_2S})$	$\frac{d}{dt}(S_{H_2SO_4})$	$\frac{d}{dt}(d_{corr})$
H_2S formation in biofilm, r1	-1		1			
Chemical oxidation of sulphide in bulk water, r2	1	$-\frac{1}{R_{Cwc}}$	-1			
Biological oxidation of sulphide in bulk water. r3	1	$-\frac{1}{R_{Cwb}}$	-1			
Oxidation of sulphide in biofilm, r4	1	$-\frac{1}{R_{Cfb}}$	-1			
H2S emission, r5			-1	$\frac{RT}{32}\frac{V_w}{V_g}$		
H_2S oxidation at the concrete surface, r6				-1	$\frac{RT}{32}$	$\frac{100k}{\sigma_{conc}ART}\frac{V_g}{A_c}$

$$\frac{d}{dt}(d_{corr}) = \frac{100k}{\sigma_{conc}ART} x \frac{V_g}{A_c} x\, r6 \qquad \textbf{Equation (1.7)}$$

The WATS model clearly shows the relationship between the physical, chemical, and biological processes of sewer deterioration, although it neglects sulphide production in the biofilms. Each process in the model is described by an equation and depends on the user's choice among a large panel of empirical equations [22]. Compared with the LFM, the WATS model incorporates more variables which also makes it more complex for engineering application, and beside the concrete alkalinity, other chemical compositions of concrete responsible for neutralising the attacking acid are not considered [17].

5.2 Bi-linear model - 2015

Wells and Melchers [23] developed a bi-linear model for predicting sewer pipe corrosion (equation 1.8). The model relates concrete corrosion rates to the sewer environmental conditions, i.e. sewer headspace temperature, H_2S concentration and RH. The influence of sewer headspace temperature is expressed as a function of the activation energy using the

Arrhenius relationship. The corrosion rate of concrete is directly related to the square root of H_2S concentration in the sewer headspace. The influence of RH was evaluated based on a relationship between the sewer RH and concrete moisture content, expressed as a function of the concrete pore size distribution, the geometry and tortuosity of the individual pores, and the temperature of the concrete wall relative to that of the sewer headspace. Finally, the rate of corrosion is considered to be directly proportional to the moisture content in the concrete pores. Hence, equation (1.8) is used to predict the corrosion rate of concrete corresponding to a certain sewer environment. While the bi-linear model considers factors that most prediction models fail to incorporate, it still ignores the material factor.

$$C_{avg} = A_S \, x \, {P_{H_2S}}^{0.5} x \left(\frac{0.1602H - 0.1355}{1 - 0.977H}\right) x \, e^{Ea/RT} \qquad \textbf{Equation (1.8)}$$

5.3 ATIR Model – 2005 and 2016

The "Säure, Angriff, Transport, Instationär, Reaktion" (SATIR) model [24, 25] is a numerical model for simulating the degradation of concrete exposed to static or flowing acidic media. The simulation describes the degradation process by diffusion of acid species through the initial porosity of the concrete at the exposed surface, and the subsequent corroded layer produced by the dissolution of the paste matrix, and if needed, the dissolution of the aggregates, as shown in Figure 2.

The dissolution of the paste matrix and aggregate particles produces hydroxyl and other dissolved ions associated with calcium, aluminium, iron and sulphur. The hydroxyl ions neutralize protons of the attacking acid, while other ions diffuse toward the concrete surface leaving a porous corroded layer. The growth of the corroded layer depends on the diffusion rate of acid through the corroded layer, and subsequent reaction with the intact front and the precipitation of calcium salt. The degree of corrosion is defined by the thickness and porosity of the corroded layer and, if abrasion effects occur, the thickness of removed material [24, 25].

For simplicity, the SATIR model considers only one transport process, i.e. diffusion. It entails mathematical equations that explain the aggressiveness of the attacking acid and its state, i.e. static or flowing, the dissolution of the paste matrix, the diffusion of species through concrete pore solution at a certain depth, the aggregate solubility and distribution in near-surface concrete, the loss of concrete surface and the precipitation of gypsum. These equations are found in [24, 25].

The model clearly shows the chemical and transport interaction between the attacking acid and the exposed concrete. It covers the simulation of all chemically attacking acids (strong to weak acids), on PC concrete. In the case of biogenic sulphuric acid attack, the model is applicable only after the onset of sulphuric acid production since it ignores the influence of sewer headspace conditions and the biological factors related to the production of the acid. It principally focuses on the material properties and their role in the final corrosion process. However, the model regards the neutralisation capacity of the concrete only as the total calcium, calculated from the calcium content of the binder and the binder content of the concrete, and not as an alkalinity factor as in the LFM and WATS models.

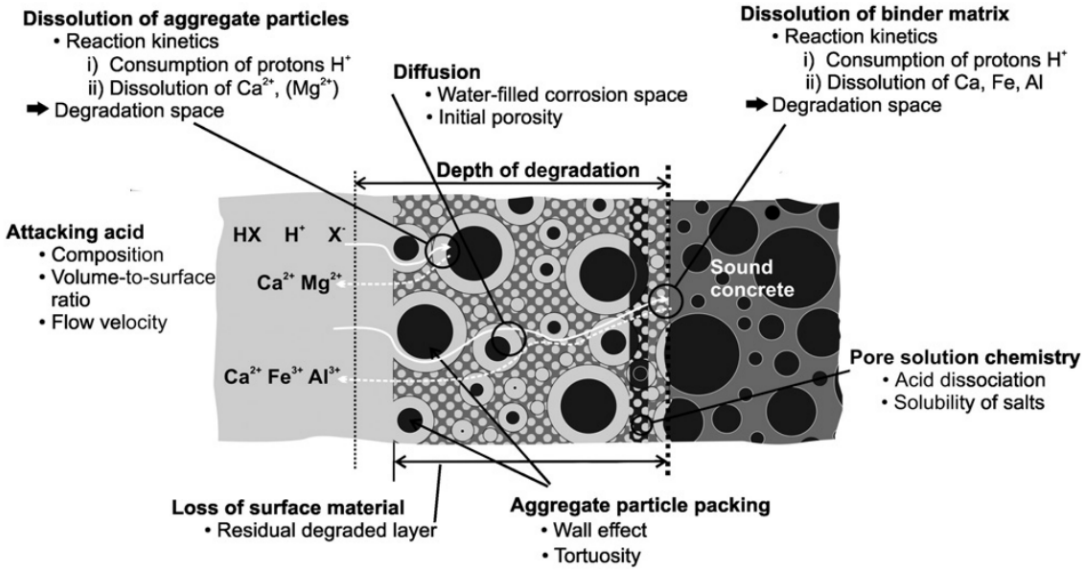

Figure 2: Process and conditions considered by the SATIR Model [24]

6 DISCUSSION AND CONCLUSION

Based on the reviewed models, it is observed that most fail to effectively and efficiently incorporate the material factor in the prediction of concrete corrosion. However, some useful principles for improving the LFM model were highlighted in the review. The WATS model provides the principles for incorporating microbial growth rate, the bi-linear model for incorporating the sewer headspace conditions, and the SATIR model for understanding the chemical and transport interactions between concrete components and the attacking acids.

Primarily, the corrosion rate is evaluated by balancing the factors involved in acid attack and acid resistance. Acid attack consists of factors involved in the production of sulphuric acid, including the sewer environmental conditions and the microbial growth rate. Acid resistance is mainly governed by the material factor which neutralizes the attacking acid and possibly limits the microbial activity. The material factor entails transport processes such as diffusion and capillary action of acid species into the concrete and dissolved ions into the corroded layer, and chemical reactions such as dissolution and precipitation of the concrete components and ionic exchange within the pore solution. The overall interaction between the chemical reactions and transport processes is complex and involves a wide range of parameters which might be complicated to assess individually.

However, it is important to define, understand, and quantify the influence of each parameter (chemical reaction and transport processes) in order to identify the key parameters which can be coupled in the LFM model as the material factor. In this regard, a reactive transport model is considered to be a useful tool which can assist in identifying these parameters. A reactive transport model is a numerical modelling approach whereby thermodynamic equilibria of the chemical reactions in the mineral phases and pore solution are coupled with transport by diffusion and capillary action in order to evaluate the influence of various mineral species involved in concrete corrosion. While there are various reactive transport models in the literature, in this study, HYTEC, will be applied [26, 27].

REFERENCES

[1] C. Grengg, F. Mittermayr, N. Ukrainczyk, G. Koraimann, S. Kienesberger, M. Dietzel, Advances in concrete materials for sewer systems affected by microbial induced concrete corrosion: A review, Water Res. 134 (2018) 341–352.

[2] C. Grengg, M.W. Kiliswa, F. Mittermayr, M.G. Alexander, Microbially-induced Concrete Corrosion- A worldwide problem, Microorg. Mater. Interact. (2016) 1–19.

[3] M.G. Alexander, H. Beushausen, Durability, service life prediction, and modelling for reinforced concrete structures – review and critique, Cem. Concr. Res. 122 (2019) 17–29.

[4] T. Hvitved-Jacobsen, B. Jütte, P.H. Nielsen, N.A. Jensen, Hydrogen Sulphide Control in Municipal Sewers, Pretreat. Chem. Water Wastewater Treat. (1988) 239–247.

[5] C. Chappelle, H. Mccann, D. Jassby, K. Schwabe, L. Szeptycki, Managing Wastewater in a Changing Climate, Public Policy Institure Calif. (2019) 31.

[6] J. Vollertsen, A.H. Nielsen, H.S. Jensen, T. Wium-Andersen, T. Hvitved-Jacobsen, Corrosion of concrete sewers-The kinetics of hydrogen sulfide oxidation, Sci. Total Environ. (2008).

[7] EPA, Detection, Control, and Corrction of hydrogen sulphide corrosion in existing wastewater system, United States Environ. Prot. Agency. (1992) 1.

[8] EPA, Hydrogen Sulfide Corrosion in Wastewater Collection and Treatment System Report nO. 430/09-19-009, United States Environ. Prot. Agency. (1991) 82.

[9] EPA, Design Manual: Odor and Corrosion Control in Sanitary Sewerage Systems and Treatment Plants, United States Environ. Prot. Agency. (1985).

[10] EPA, Process design manual for sulphide control in sanitary sewerage systems, United States Environ. Prot. Agency. (1974) 136.

[11] G. Jiang, J. Keller, P.L. Bond, Z. Yuan, Predicting concrete corrosion of sewers using artificial neural network, Water Res. (2016).

[12] G. Jiang, X. Sun, J. Keller, P.L. Bond, Identification of controlling factors for the initiation of corrosion of fresh concrete sewers, Water Res. 80 (2015) 30–40.

[13] G. Jiang, J. Keller, P.L. Bond, Determining the long-term effects of H2S concentration, relative humidity and air temperature on concrete sewer corrosion, Water Res. 65 (2014) 157–169.

[14] V. Chalupecký, T. Fatima, J. Kruschwitz, A. Muntean, Macroscopic corrosion front computations of sulfate attack in sewer pipes based on a micro-macro reaction-diffusion model, ArXiv Prepr. ArXiv …. (2012) 1–10.

[15] L. De Windt, P. Devillers, Modeling the degradation of Portland cement pastes by biogenic organic acids, Cem. Concr. Res. 40 (2010) 1165–1174.

[16] H.S. Jensen, A.H. Nielsen, T. Hvitved-Jacobsen, J. Vollertsen, Modeling of Hydrogen Sulfide Oxidation in Concrete Corrosion Products from Sewer Pipes, Water Environ. Res. 81 (2009) 365–373.

[17] M.W. Kiliswa, Composition and microstructure of concrete mixtures subjected to biogenic acid corrosion and their role in corrosion prediction of concrete outfall sewers, University of Cape Town, South Africa., 2016.

[18] G. Jiang, E. Wightman, B.C. Donose, Z. Yuan, P.L. Bond, J. Keller, The role of iron in sulfide induced corrosion ofsewer concrete, Water Res. 49 (2014) 166–174.

[19] A. Buvignier, Caractérisation du rôle de l'aluminium dans les interactions entre les microorganismes et les matériaux cimentaires dans le cadre des réseaux d'assainissement École doctorale et discipline ou spécialité, 2018.

[20] A.H. Nielsen, J. Vollertsen, H.S. Jensen, H.I. Madsen, T. Hvitved-Jacobsen, Aerobic and Anaerobic Transformations of Sulfide in a Sewer System – Field Study and Model Simulations, Proc. Water Environ. Fed. 2006 (2014) 3654–3670.

[21] T. Hvitved-Jacobsen, J. Vollertsen, A.H. Nielsen, Sewer Processes: Microbial and Chemical Process Engineering of Sewer Networks, Second Edition, Second, CRC Press; Taylor & Francis Group, London, New York, 2013.

[22] L. Carrera, F. Springer, G. Lipeme-Kouyi, P. Buffiere, A review of sulfide emissions in sewer networks: Overall approach and systemic modelling, Water Sci. Technol. 73 (2016) 1231–1242.
[23] T. Wells, R.E. Melchers, Modelling concrete deterioration in sewers using theory and field observations, Cem. Concr. Res. 77 (2015) 82–96.
[24] R.E. Beddoe, Modelling acid attack on concrete: Part II. A computer model, Cem. Concr. Res. 88 (2016) 20–35.
[25] R.E. Beddoe, H.W. Dorner, Modelling acid attack on concrete: Part I. The essential mechanisms, Cem. Concr. Res. 35 (2005) 2333 – 2339.
[26] F. Schmidt-Döhl, F.S. Rostásy, Model for the calculation of combined chemical reactions and transport processes and its application to the corrosion of mineral-building materials: Part I. Simulation model, Cem. Concr. Res. 29 (1999) 1039–1045 A.
[27] F. Schmidt-Döhl, F.S. Rostásy, Model for the calculation of combined chemical reactions and transport processes and its application to the corrosion of mineral-building materials: Part II. Experimental verification, Cem. Concr. Res. (1999).

EFFECT OF CORROSION OF LAP-SPLICED STEEL REINFORCEMENT ON THE FLEXURAL STRENGTH OF REINFORCED CONCRETE BEAMS

Anele Mahlawe [(1)] and Mike Otieno [(1)]

(1) School of Civil and Environmental Engineering, University of the Witwatersrand, Johannesburg

ABSTRACT

The study aimed to investigate the effect of corrosion on the flexural strength of reinforced concrete (RC) beams with steel lap-splicing in the central constant moment region. A total of 24 RC 100 × 165 × 1500 mm beams were cast. Accelerated chloride-induced corrosion was used to induce steel corrosion in the central constant moment region. Only 6 RC beams (i.e. six – 3 with spliced, and 3 without spliced flexural reinforcement) were corroded for each design code, the remaining 6 were used for reference purposes. The reference beam specimens were tested 28 days after casting to determine their respective ultimate flexural strength while the corroded beams were tested once the desired corrosion level was reached, using a 4-point bending configuration. The applied load, mid-span deflection and mode of failure were recorded until failure load was reached. The results showed an increase in deflection and a decrease in ultimate strength in the corrosion-damaged specimens. The failure mode of non-lapped beams remained ductile, while on lap-spliced beams the failure mode changed from ductile to brittle.

Keywords: flexural strength, Lap-spliced reinforcement, Accelerated corrosion

1. INTRODUCTION

The use of spliced steel reinforcement in concrete structures is inevitable in day-to-day construction due to reasons such as steel fabrication, transportation limitations, steel workshop fabrication (limited available length) and construction joints. The required length of steel bars may exceed a standard stock length of 13 m, or the steel bar may be too long to be transported conveniently. Splicing of reinforcement steel is provided by several means such as welding, mechanical couplers, bar overlapping with a minimum length specified by design codes [8]. Splicing is intended to ensure safe load transfer between the spliced bars and between the spliced bars and the surrounding concrete. A lap-splicing method which requires the overlapping of two parallel bars is considered the most economical and practical technique commonly used to transfer forces between lapped steel bars in a reinforced concrete member. One of the main challenges with reinforced concrete (RC) structures is their deterioration due to corrosion of the embedded reinforcement. This brings about a reduction in the load-carrying capacity of structural members [2].

This study examined the influence of corroded lap-spliced reinforcement on flexural strength of RC beams. A comparison of lap length requirements were carried out between the South

African standard code of practice SANS 10100-1 [7] and the European standard code of practice EN 1992-1-1 [3].

2. EXPERIMENTAL PROGRAMME

2.1 Description and casting of specimens

A total of 24 RC beam specimens were manufactured for the experimental work. For specimens with lap spliced reinforcement, the lap splicing was located within the maximum moment span as shown in Figures 1 and 2. The RC beam specimens were divided into two groups (Type A and Type B). The design for Type A and Type B beams was carried out according to relevant requirements of SANS 10100-1 and Eurocode 2, respectively. The required tension reinforcement area was 154 mm^2 for SANS standard and 129 mm^2 for Eurocode standard; therefore 2Y10 bars were adopted for Type A beams and 3Y8 bars for Type B beams. Table 1 summarises the number and type of test specimens used in the study.

After casting, RC beams and companion cubes were left in the moulds for 24 hours in the laboratory (at room temperature), covered with polyethene sheeting. After 24 hours, the formwork was removed and the RC beams and cubes were cured in a water tank at 23 ±2 °C. RC beams were cured for a period of 21 days while cubes for concrete compressive strength tests were cured for 7 and 28 days.

Table 1: Specimens details

Beam Type	Guidelines used for splicing of flexural steel	Splice length	Number of specimens	Specimen treatment	Specimen label
A	SANS 10100-1	40Ø = 400 mm	3	Steel corroded	SANS-S-C
		40Ø = 400 mm	3	Steel not corroded	SANS-S-NC
		Flexural steel not spliced	3	Steel corroded	SANS-NS-C
		Flexural steel not spliced	3	Steel not corroded	SANS-NS-NC
B	Eurocode 2	36Ø = 288 mm	3	Steel corroded	EC2-S-C
		36Ø = 288 mm	3	Steel not corroded	EC2 -S-NC
		Flexural steel not spliced	3	Steel corroded	EC2 -NS-C
		Flexural steel not spliced	3	Steel not corroded	EC2 -NS-NC

Note: S: Spliced; NS: Not spliced; C: Corroded; NC: Not corroded

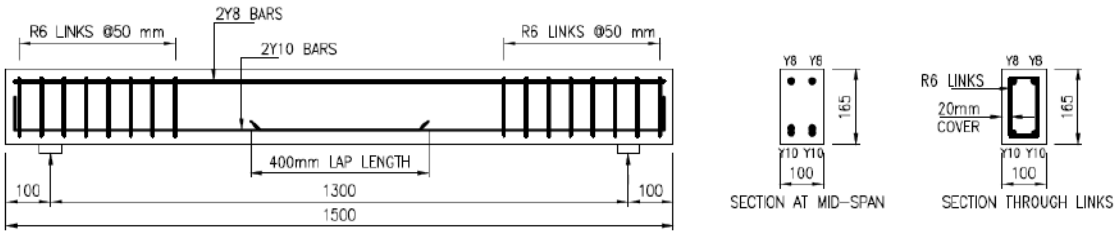

Figure 1: Type A RC beams geometry and reinforcement details

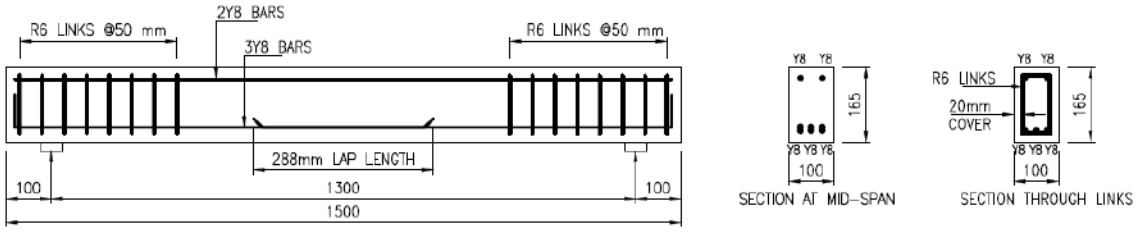

Figure 2: Type B RC beams geometry and reinforcement details

2.2 Concrete mix proportions

A summary of the concrete mix proportions (per cubic meter) used in this study is given in Table 2.

Table 2: Concrete mix proportions

Water content (kg/m^3)	**CEM I 52.5R (kg/m^3)**	**Fine aggregate (kg/m^3)**	**Coarse aggregate (kg/m^3)**	**w/c ratio**	**28 day strength (MPa)**
195	390	368	1005	0.50	52.50

2.3 Accelerated corrosion process

Impressed current technique was used to accelerate steel corrosion. In this study, the tensile steel reinforcement was corroded in the region corresponding to moment span or lapped splices in the case of lap-spliced steel. The beams were turned upside down to build the pond in the tension face. The region corresponding to lap-spliced steel reinforcement was saturated with a 5% solution of sodium chloride to supply chlorides required to accelerate steel de-passivation and function as an electrolyte solution in the corrosion cell. This was achieved by building a reservoir on the surface of RC specimens in accordance with the previous work carried out by Yoon, *et al*. [9] & Malumbela *et al*. [4]. The tension reinforcement (anode) was connected to the positive terminal of the applied external direct current, while the stainless steel bar (cathode), placed inside the sodium chloride solution reservoir pond was connected to the negative terminal of the external power supply. The arrangement of the accelerated corrosion set-up is given in Figure 3.

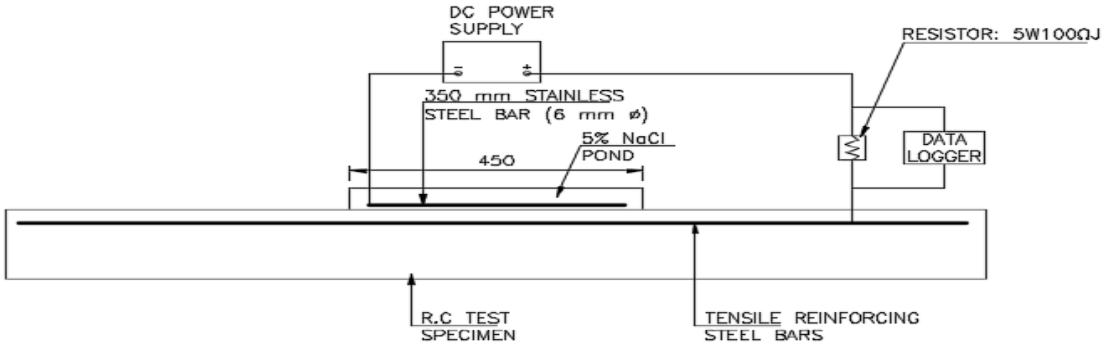

Figure 3: Accelerated corrosion set-up of beam specimens

A 20% loss of cross-sectional area was chosen as the desired corrosion to ensure that a significant effect of corrosion is attained. A lower corrosion degree, in the case of non-lap spliced beams would not have shown a significant effect of corrosion due to partial load factors used by South African standard code of practice SANS 10100-1 [7] and European standard code of practice EN 1992-1-1 [3]. The required current was calculated using Faraday's law.

Each RC beam was connected to a DC power supply unit. A constant voltage was supplied to steel reinforcement through a resistor of known resistance. A data logger (Agilent 34970A) was connected to the circuit to record the voltage across the resistor at a five second interval. The applied voltage was monitored regularly and the corrosion acceleration test was stopped once the required current was achieved. The current through the resistor was determined using Ohm's law.

2.4 Flexural tests

The reference (non-corroded) beams were tested immediately at 28 days after casting to determine their respective flexural load capacity while the corroded beams were tested once the desired corrosion level was reached. As shown in Figure 4, beams were simply supported, with a span of 1300 mm between the supports and loaded with two equal point loads placed symmetrically between the supports to produce a four-point bending.

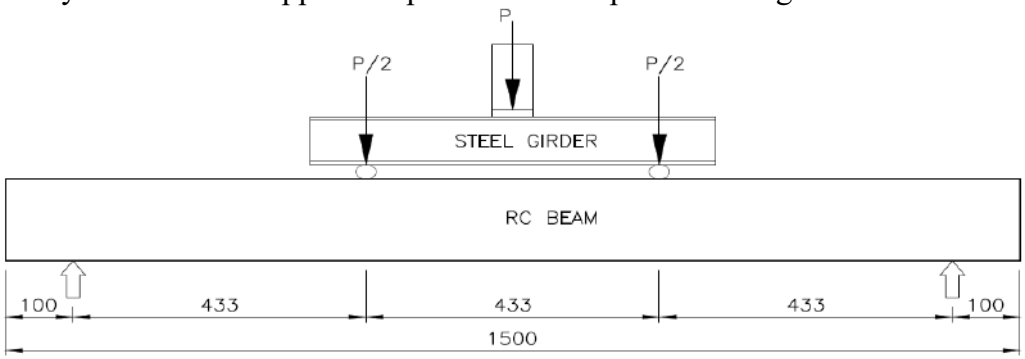

Figure 4: Loading test arrangement (dimensions in millimetres)

This loading arrangement produced zero shear force between the loading points, thus resulting in pure bending. SANS 5864 [6] recommends loading to be kept at a constant rate of 0.03 + 0.01 MPa/s until failure. For this study, the applied load was kept constant at 2 kN per minute and increased progressively until failure. The response behaviour of RC beams was examined through measurements of applied loads and mid-span deflection using a dial gauge. The results obtained from corroded beam specimens were compared with those obtained from reference (non-corroded) RC beams. The maximum load at failure was recorded for the calculation of flexural strength using Equation 1.

$$f_{cf} = \frac{Fl}{bd^2}$$ **Equation (1)**

where f_{cf} is the Flexural strength (MPa); F is the maximum load at failure (N); I is the distance between axes of supporting rollers (mm); b is the width of specimen (mm) and d is the depth of specimen (mm).

2.5 Assessment of corrosion in corroded RC beams

Upon completion of flexural tests, the tensile reinforcements were extracted from corroded beams and cleaned with a wire brush to remove the corrosion products and residues of concrete adhered to the surface of the bars for determination of corrosion level. After cleaning, the bars were physically measured using a Vernier Callipers and the bar diameter loss was determined using Equation 2.

$$D_{loss} = D_i - D_f$$ **Equation** (2)

where D_{loss} is the diameter loss (mm); D_i is the initial steel diameter before corrosion (mm) and D_f is the final steel diameter after the removal of corrosion products (mm). From equation 2, the initial and final areas of steel bars were calculated for the determination of the cross-sectional area loss.

3. RESULTS AND DISCUSSION

3.1 Visual observations

A longitudinal surface crack through the concrete cover on the ponding surface was first observed after 6 days of corrosion acceleration tests. The surface crack was followed by the formation of two side cracks at the interface between tensile steel reinforcement and concrete cover. Rust stains were then observed on the ponded surface, followed by corrosion products exuding through the surface crack. Concrete cracking provided an easy passage for NaCl solution to reach the embedded steel reinforcement. This cracking occurred along the line of the reinforcement in the NaCl pond and on both sides of the RC beams at the level of concrete cover. The typical visible damage due to corrosion is presented in Figure 5.

a) Cracking on the ponded surface

b) Cracking on the vertical side of beam

Figure 5: Typical corrosion-induced cracking

3.2 Mid-span deflections of reference beams

All reference (non-corroded) beams showed higher ductile behaviour. After the elastic limit, there was still a good amount of load increase before the maximum failure load was reached. The load-midspan deflection curves of SANS 10100-1 reference beams are given in Figure 6.

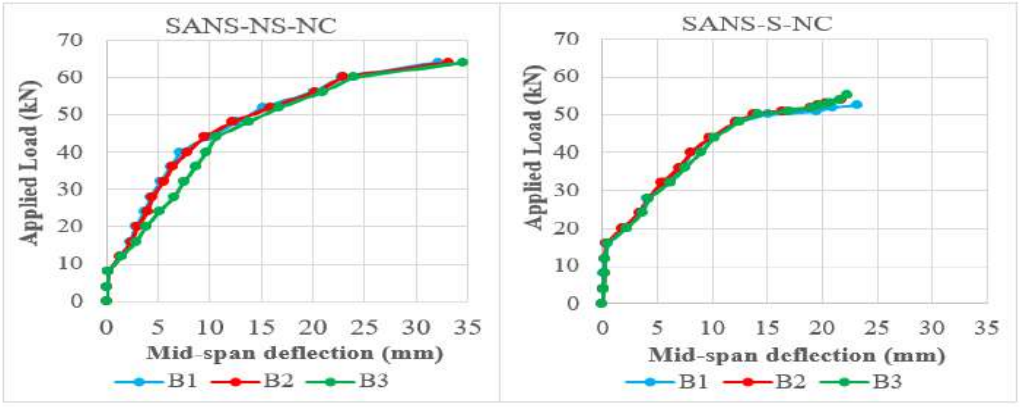

Figure 6: Typical load-midspan deflection curves of reference beams

Lap-spliced beams showed a decrease in flexural stiffness and load-carrying capacity compared to non-lap spliced beams, as a result, the average failure load of SANS 10100-1 lap-spliced beams was 16% less than that of non-spliced reference beams. The behaviour of Eurocode 2 lap-spliced beams was observed to resemble that of SANS 10100-1 lap-spliced beams. The average failure load of Eurocode 2 lap-spliced beams was 15% less than that of Eurocode 2 non-spliced beams.

3.3 Mid-span deflections behaviour of corroded beams

All non-spliced corroded beams behaved in a manner similar to non-spliced reference beams. These beams indicated a ductile behaviour as they showed a plastic behaviour after yield points, with load increase before the maximum failure loads were reached.

When comparing load-midspan deflection curves of SANS 10100-1 non-spliced corroded beams with SANS 10100-1 non-spliced reference beams, the failure load was observed to be 13% less than that of reference beams. In Eurocode 2 beams, the failure load was observed to be 11% less than that of Eurocode 2 reference beams.

In the case of lap-spliced corroded beams, both SANS 10100-1 and Eurocode 2 beams behaved in a similar manner. The failure of all lap-spliced corroded beams occurred suddenly after the widening of the side longitudinal crack, followed by the spalling of concrete cover in the lapped zone and slipping of longitudinal bars. SANS 10100-1 corroded lap-spliced beams showed a 65% reduction in failure load compared to lap-spliced reference beams. Eurocode 2 corroded lap-spliced beams showed a 50% reduction in failure load. The load-midspan deflection curves for SANS 10100-1 corroded beams are given in Figure 7.

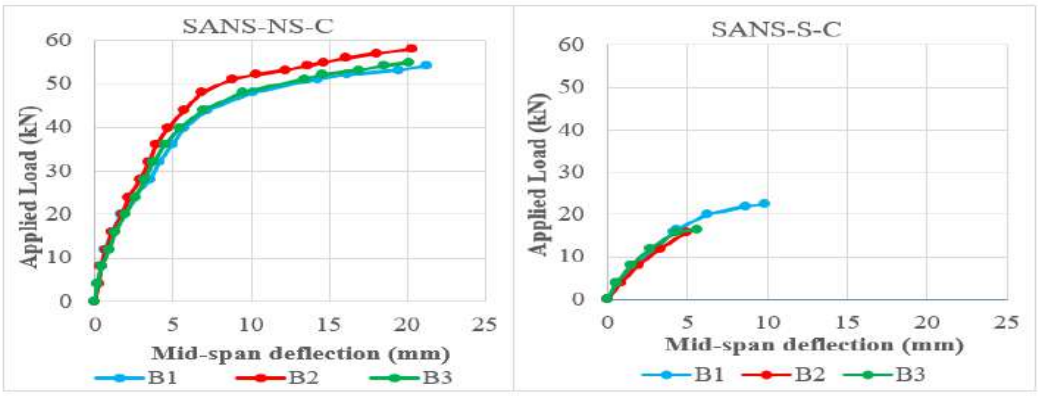

Figure 7: Typical load-midspan deflection curves of corroded beams

3.4 Flexural capacity of RC beams

The general observation was that an increase in degree of steel reinforcement corrosion results in a reduction of flexural capacity with deflections reaching the limit earlier than normal state. The flexural behaviour of SANS 10100-1 lap-spliced beams was observed to be similar to that of Eurocode 2. However, the general trend observed was a greater flexural capacity loss on lap spliced beams compared to non-lap spliced beams. The failure of all lap-spliced beams occurred suddenly and was reached immediately after the widening of the side longitudinal crack, followed by the spalling of concrete cover in the lapped zone and slipping of longitudinal bars. When the entire concrete cover was removed in the corroded region, the slippage of steel reinforcement was measured to range between 3 to 8 mm and between 2 and 7 mm on Type A and Type B beams, respectively. The morphology of corrosion on steel reinforcement resembled a combination of general and some pitting corrosion.The corrosion degree and loss of ultimate capacity of corroded beams are given in Table 3 and Figure 8 respectively.

Table 3: Loss in steel cross-section area (%)

SANS-NS-C	SANS-S-C	EC2-NS-C	EC2-S-C
47.8	14.5	37.7	27.9
14.6	21.9	25.5	27.0
31.2	17.4	34.5	29.0

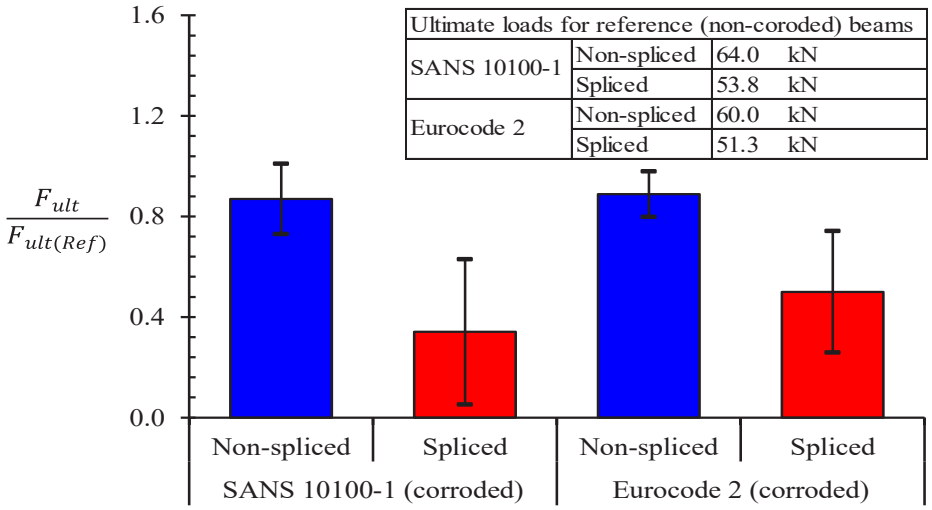

Figure 8: Ultimate load ratio of corroded beams to non-corroded beams

3.5 Flexural ductility of steel corrosion-damaged RC beams

When both non-lap spliced and lap-spliced corroded beams were compared with the reference beams, the results indicated a reduction in stiffness on all lap-spliced corroded beams with increasing mid-span deflections at a loading less than that applied on reference beams. A sudden and brittle bond failure was displayed in lap-spliced beams. This is despite the lower corrosion rate on lap-spliced beams compared to non-lap spliced beams. This behaviour may be attributed to the loss of bond between the concrete and steel reinforcement which led to a drop in anchorage capacity at the splice zone and thus, slipping of steel reinforcement.

The general trend was a reduction of flexural ductility of corroded beams with increasing steel cross-sectional loss. Figure 9 shows the influence of corrosion on the ductility of SANS 10100-1 beams. The Eurocode 2 beams showed a similar behaviour to SANS 10100-1 beams.

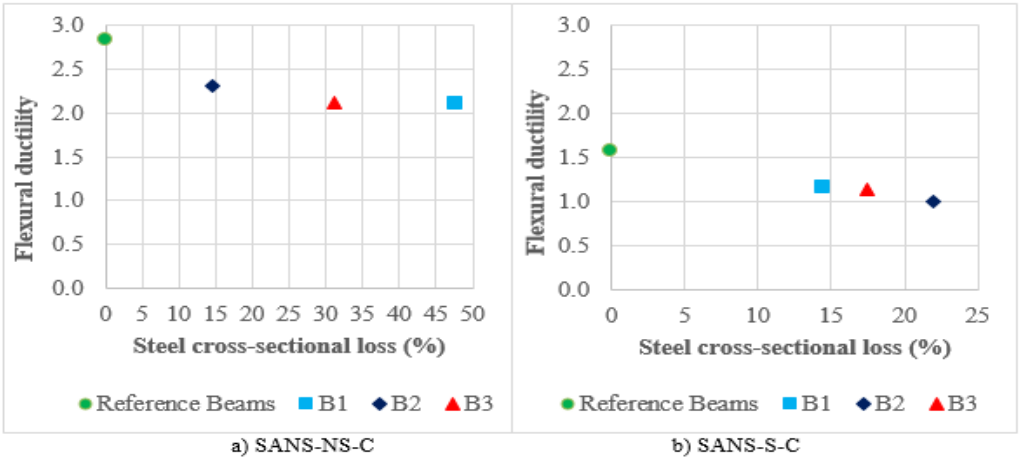

Figure 9: Flexural ductility vs steel cross-sectional loss

4. CONCLUSIONS

The main conclusions drawn from this study are reported as follows:

1. All RC beams experienced some variation between target and actual corrosion. This can be attributed to the variation in concrete resistivity and penetrability due to cracking.
2. When comparing results obtained in reference beams with results obtained in corroded beams, the consequences of steel reinforcement corrosion (i.e. reduction of steel cross-section, bond loss at the steel-concrete interface and longitudinal cracking at a steel-cover interface) resulted in a significant reduction of RC beam flexural capacity.
3. The general trend observed in lap-spliced beams was decreasing load carrying capacity and increasing deflections with increasing amounts of corrosion.
4. The ductility in corroded beams containing lap-spliced steel reinforcement was significantly reduced, as a result the failure of these beams changed from a ductile response (observed in reference beams) to a brittle response.
5. The corroded non-lap spliced beams carried more load after yielding of steel reinforcement before the failure load was reached, while the failure of lap-spliced beams occurred suddenly and was reached immediately after the widening of the side longitudinal crack.

ACKNOWLEDGEMENTS

The support of The Concrete Institute, The National Research Foundation, AfriSam and the Department of Environment, Forestry and Fisheries (DEFF) is greatly acknowledged.

REFERENCES

[1] Addis, B., & Goodman, J. (2009). *Concrete mix design. In G. Owens, ed. Fulton's Concrete Technology* (9th Ed.). Cement and Concrete Institute (CNCI).

[2] Castel, A., François, R., & Arliguie, G. (2000). Mechanical behaviour of corroded reinforced concrete beams—Part 1: Experimental study of corroded beams. *Materials and Structures*, *33*(9), 539–544.

[3] EN 1992-1-1. (2004). Eurocode 2—Design of concrete structures–Part 1-1. *Brussels: CEN European Committee for Standardization*.

[4] Malumbela, G., Alexander, M., & Moyo, P. (2010). Variation of steel loss and its effect on the ultimate flexural capacity of RC beams corroded and repaired under load. *Construction and Building Materials*, *24*(6), 1051–1059.

[5] SANS 5861-3. (2006). *Making and curing of test specimens*. South African Standard Code of practice.

[6] SANS 5864. (2006). *Concrete tests—Flexural strength of hardened concrete*. South African Standard Code of practice.

[7] SANS 10100 -1. (2000). *The Structural Use of Concrete. Part 1: Design*.

[8] Tarabia, A. M., Mahmoud, Z. I., Shoukry, M. S., & Abudina, A. A. (2016). Performance of RC slabs with lap splices using headed bars. *Alexandria Engineering Journal*, *55*(3), 2729–2740.

[9] Yoon, S., Wang, K., Weiss, W. J., & Shah, S. P. (2000). Interaction between loading, corrosion, and serviceability of reinforced concrete. *Materials Journal*, *97*(6), 637–644.

Corrosion of Reinforcing Steel induced by Combined Penetration of Chlorides and Carbon Dioxide in Concrete with Construction Cold Joints

James. W. Teggin [(1)] and Sunday. O. Nwaubani [(1)]

(1) School of Civil and Environmental Engineering, University of the Witwatersrand

ABSTRACT

Corrosion of reinforcement is regarded as the most destructive mechanism that influences the durability of reinforced concrete structures worldwide. Practically, the existence of chlorides and carbon dioxide is necessary to consider as it increases the corrosion risk due to population growth and urbanisation. Defects such as cracks and cold joints affect the transport of gasses, ions and moisture into concrete to cause rapid corrosion activity. The synergy of chloride built -up at defects and on-going progression of carbonation thus forms the focus of this study. The use of pozzolanic materials was the basis of comparison due to a shift to lower the production of Portland cement. Corrosion was monitored for a 294-day period to relate to the transport properties, penetration states and damages which manifested. The corrosion monitoring found a faster initiation time due to a joint and higher corrosion rate in propagation, when there was adequate carbonation. The influence of carbonation resided primarily in the long-term by increasing the penetration depth of chlorides and corrosion rate. The cement extenders were less resistant to carbonation, although the microstructure changes restricted the corrosion rate with a sufficient cover depth. The corrosion damages to the steel and cover concrete at completion of exposure revealed that the cold joint and carbonation increased the corrosion rate.

Keywords: corrosion, chlorides, carbonation, cold joint, cement extenders

1. INTRODUCTION

Chloride ingress and carbonation are the most severe mechanisms of corrosion, the former being the main reason for premature degradation. Atmospheric carbonation is the main reason for the alkalinity reduction of concrete, and has contributed largely since the industrialisation. The trends of population and urbanisation in marine environments require the consideration of the interaction of the two mechanisms, which has found to be synergistic by nature. Early studies suggest that only chlorides in the pore solution contribute to corrosion while chlorides bound to the microstructure, do not. The bound chloride was found to play a role to increasing the penetration depth once an adequate proportion is released [5]. This may take place when there is a partial reduction of the alkalinity (or pH) in the pore solution. All mineral cements bind chlorides in the paste to some degree, to hinder their diffusion in the pore solution [6].

The interaction of chlorides in carbonated concrete occurs in environments such as highly-urbanised coastal areas and to a lesser degree, any marine settlement. Most studies are based on the penetration of chlorides and carbonation in isolation howeve recent studies showed the

deterioration to be more severe due to combined action. There is however a disparity in the resistance to penetration where the conditions which favour the penetration of one agent may hinder the other. A continuous approach in the form of cyclic exposure has been effective to the synergy of combined exposure, which is generally the case within a marine settlement. Corrosion is also accelerated by the cyclic effect as there is oxygen at the cathodic and a sufficient electrolyte for ion transport.

The cyclic regimes of exposure are more effective the combined attack when compared to isolated regimes [18]. Chloride availability was reduced however the loss of binding capacity near the surface caused an increase in the penetration depth. Pre-carbonation is also effective in causing the enrichment of chlorides to the bulk although similarly the carbonation rates are lower due to moisture in the pores [7]. The alkalinity reduction by carbonation is influential even monthly in concrete which is pre-contaminated by chlorides [17]. The synergy of chloride penetration within carbonated concrete has thus been found regardless of the exposure in studies that are based in a laboratory setting. A loss of the binding capacity is concerning when there are defects as these tend to create a build-up of the chlorides over time which may diffuse to the steel.

The transport of corrosive agents in concrete is increased in the vicinity of defects as the penetrability is no longer based on concrete quality. The defect of interest is the cold joint due to a lack of knowledge on their durability compared to that of the mechanical resistance. Cold joints are present at the start of exposure and extensively used at successive placements of concrete to limit cracking by loading. A cold joint in specimens has caused an increase in the chloride diffusion in an accelerated test when compared to monolithic concrete [16]. Reinforced concrete specimens that contain cold joints are considered to be pre-damaged due to the rapid corrosion activity which is created [8]. A cold joint spans to the steel which may not be the case with other defects, such as shrinkage cracks, as there is still cover concrete to provide resistance.

The presence of a cold joint from the start of exposure and carbonation may increase the potential of cracks, to accelerate the corrosion rate. Monitoring in structures from the start of exposure thus encapsulates the concrete quality that controls the initiation time and formation of defects. Carbonation progress within chloride-contaminated concrete may be detected in corrosion monitoring schemes, once it has affected enough of the cover layer. The monitoring of electric potential increased the corrosion severity due to the carbonation up to 182 days of exposure [10]. The potential alone is limited in reflecting corrosion severity alone due to the many factors which are influential and thus the corrosion rate is used in conjunction. The corrosion rate supplemented the potential behaviour in concretes that had admixed chloride up to over 1000 days of accelerated carbonation [9]. The aim herein was to asses the corrosion risk of faster chloride ingress in concretes that have a cold joint and may become subjected to carbonation in highly-urbanised environments.

2. EXPERIMENTAL PROGRAMME

2.1 Materials used

The main cementing binder was rapid-hardening Portland cement under the 52.5R class in class in SANS 50197-1 [11]. Fine fly ash emanating from the Kriel station colliery was the least-reactive of the cementitious materials and conforms to SANS 50450-1 [12]. A highly reactive metakaolin, grade K40 from Kaolin Group was used for comparison of pozzolanity between the cement extenders. Metakaolin characteristics are not formalised in South Africa

with common cement extenders such as fly ash, slag or silica fume. The oxide compositions of 52.5 R cement (CEM 52.5 R), fly ash and metakaolin are listed in Table 1.

Table 1: Binder oxide compositions

Compound	CaO	S_iO_2	Al_2O_3	Al_2O_2	SO_3	Fe_2O_3	MgO	K_2O	TiO_2	Na_2O	Na	Mn_2O_2	P_2O_5
CEM 52.5 R	65.1	20.8	4.6		3.0	2.7	1.7	0.5	0.4	0.2		0.1	0.1
Fly ash	6-9.5	50-52.5	28.5-30.5			2-3	2-2.5	<1	1.5-2		<1.5		
Metakaolin		56.8		43.5		0.5		0.1	1.3				

2.2 Concrete mix design

The South African Cement and Concrete Institute procedure, described in Alexander, et al., (2009), was used and the final trial proportions are in Table 2. The ordinary concrete consists of 100% rapid-hardening cement (CEM 1) and the cement extenders concretes were replaced with 30% fly ash (FA) or metakaolin (MK). The stone and sand were both andesite which has a high density of 2.9 compared to natural stones, typically in a range of 2.6-2.95 [1]. The fineness modulus of 3.31 was due to adeficiency in the fine fractions so the sand contents were higher than in concretes with larger stone. The stone with a nominal size of 6.7 mm was suitable to the low cover depths that were used, to achieve a better state of homogeneity of the concrete. The sand contents of the cement extender concretes were lower to maintain the volumetric requirement of the mixtures.

Table 2: Concrete mixes

Material (kg/m^3)	100 % CEM 1	70/30 CEM 1/FA	70/30 CEM 1/MK
CEM I 52, 5 R	500	350	350
Fly ash	0	150	0
Metakaolin	0	0	150
Concrete stone	477	477	477
Crusher sand	1179	1114	1144
Mixing water	275	275	275
Slump (mm)	120	140	100

2.3 Test specimens

Reinforced beams contained a Y12 bar longitudinally-placed with electrical connectivity so the corrosion monitoring could be performed non-destructively. The dimensions were 100x 100x500 mm and the steel bars were placed at cover depths of 20 mm and 10 mm. The 500 mm long steel bars were chamfered either end then drilled into to attach a copper lead wire for a connection to the steel. Before moulding, the steel bars were wire-brushed and degreased, which is indispensable to a bond with epoxy at the bar ends. Cubes with 100x100x100 mm were used to measure the carbonation depth, to estimate that in the cover region of the beams. Carbonation in the plain cubes was thus an underestimate when considering the cold joint and cracks present in some of the beams. Separate cubes with the same dimensions were used for circular discs according to SANS 3001-CO3-1 [13], with a 70 mm diameter and 30 mm thickness. Cold joints were formed in half the beams and discs in 2 successive casts using a time delay of 24 hours, and orientated so that the penetration could occur along their plane.

2.4 Exposure conditions

The specimens were exposed after 28 days of curing, in a manner that was intended to be favourable to the chloride penetration and carbonation, by a cyclic manner of application. The sequence of periods in the combined exposure consisted of 3 days of chloride solution, 2 days drying in ambient conditions and 9 days of carbon dioxide. Specimens under isolated chloride exposure were dried in ambient conditions for the rest of 14-day cycles and the 2-day period before carbonation was intended on a partially-saturated surface. Chloride exposure was done by ponding a solution with 5% sodium-chloride in distilled water on the beams according to ASTM C1543 [2], while the cubes were submerged. The carbonation was accelerated by maintaining a concentration of carbon dioxide of 5% in a closed system to a toletance of 0.5%. A saturated solution of magnesium chloride was placed within the carbonation chamber to lower the relative humidity to close to the optimal range of 40-60% [1].

2.5 Testing

The resistance to the permeation of gasess, chloride and moisture was determined using the South African durability indices, with 4 circular discs at each age. The oxygen permeability (OPI) and conductivity (CCI) tests are in SANS 3001-CO3-2 [14] and SANS 3001-CO3-3 [15] respectively, and the sorptivity (WSI) test is not yet formalised. The early-age durability was tested after 28 days of curing where after further testing was done at 56 and 90 days to identify the long-term changes. These parameters were representative of the microstructure formation to provide resistance to chloride penetration and carbonation. The influence of the cold joint on concrete penetrability was determined after 28 days only, as this was the duration before the beams were first exposured. The cold joint was in the direction of exposure so that the penetration could take place in a localised manner along its plane.

The beams were sampled for chloride at the completion of the 21-cycle exposure period (of 294 days) whereas the carbonation was also measured at 10 cycles. Chloride profiles in the beams were established as the concentrations in 5 mm depth increments spanning the cover region. A drill with a 22 mm thick masonry drill bit attachment was used to sample the beams while firmly clamped. The samples were analysed with the Dionex X-120 apparatus which operates based on ion chromatography to obtain the total chloride concentration. Carbonation of the cubes was measured with a phenolphthalein indicator solution to represent the cover region of the beams. The carbonation depth at 10 cycles and at the completion at 21 cycles was calculated as the average over the 5 points measured in the carbonated regions.

The corrosion monitoring of the beams intended to detect the existence of active corrosion and quantify the corrosion rate that could be sustained. The behaviour of the electric potential, corrosion rate and concrete resistivity were established as time series' of the instantaneous states for 294 days. The monitoring frequency was based on the exposure periods; 1 day after the ponding to incorporate a drying period and on removal from the carbonation chamber. A baseline was taken 1 day after 28 days of curing, and 2 readings were taken to overcome the contact resistance in sets of 3 beams. Half the beams contained a cold joint at the mid-span for comparisons to that monolithically-cast over the entire volume. The potential behaviours were classified with ranges in ASTM C876 [3] to determine the initiation time.

The damages that accumulated in the propagation phase, characterised by active conditions were assessed as the cell formation on the steel bar and resulting cover cracking. The cracking was assessed as the coverage and width to identify the permeability changes that accelerated the corrosion formation on the underlying steel bar. The crack patterns were established by

mapping the exposed surface in 10 mm increments with the origin at midspan, and averaging the minimum and maximum measurements. The corrosion patterns were similarly established once the embedded steel had been removed, and the pits were found after wire-brushing.

3. EXPERIMENTAL RESULTS

3.1 Transport properties

The oxygen permeability indicies (OPI) found that the majority of the transport resistance to gasses, moisture and ions took place within 28 days. The 28-day OPI results fell within the excellent quality range (> 10) in Alexander, et al., [1] which grades the resistance from the durability indices. Both of the cement extenders reduced the gas permeability by within 5% due to their ability to refine the pores and capillaries. The fineness of the binders was similar due to a high cement grade so the refinement was limited to smaller pores compared to typical cements. The water sorptivity indices (WSI) found that more than 99% of the 90-day result in the ordinary and fly ash concrete had yielded at an age of 28 days. There were changes in the metakaolin concrete where the WSI reduced by 22% into the excellent concrete quality range (WSI < 6) at 90 days. The 28-day WSI values of the fly ash and metakaolin concretes were a respective 15% and 18% lower than the ordinary concrete due to their refinement effects.

The chloride conductivity indices (CCI) found a high resistance due to the metakaolin due to its reactivity and alumina content. The fly ash had about two-thirds of the alumina compared to the metakaolin and its reactivity and its low reactivity left the concrete susceptible to chloride penetration. The CCI of the fly ash concrete increased from a poor quality range at 28 days, to a good quality range (CCI < 1.5) at 90 days, similar to the ordinary concrete. The metakaolin reduced the CCI value by 44% at 28 days and then yielded a further reduction by 22% at 90 days, into the excellent quality range (CCI < 0.75). The higher resistance with metakaolin has been found in the durability indices of concretes with replacement levels up to 20% [4]. The resistance of the fly ash concrete is similar to studies where there is a delayed reactivity, to increase the chloride penetration.

The cold joint (CJ) in half of the circular discs was formed so that the direction of transport (of gasses, moisture and ions) was along the joint plane. The defect increased the penetrability of the 30 mm thick discs at 28 days in terms of all the durability indices by up to 21.5%. The joint preparation reflects in the amount of voids present along its plane and their connectivity, most influential nearer the surface. The disc preparation removes larger imperfections which presented a larger degree of influence in the surface region of beams. The chloride resistance is similar to studies that include a joint in diffusion tests, where the diffusion coefficients can be increased by up to 20% [16].

3.2 Penetration state

Chloride profiles were established in 5 mm depth increments spanning the cover region of beams in terms of the total chloride content. The cold joint was at mid-span in half the beams in the direction of exposure so that the penetration could occur to the steel at this plane. The chloride concentrations in the 20 mm cover ordinary concrete beams were up to 78 % larger than that monolithically-cast in depth increments up to 10 mm. The carbonation depth in the plain cubes of 7.4 mm equated to 37% of the 20 mm cover depth and increased the chloride concentrations at the steel by 46% in the cold joint beams. The carbonation in the plain cubes was an estimate of the cover region of beams that did not account for the influence of a cold

joint or cracks. The increase in chloride availability in the 15-20 mm increment in monolithic beams was minor thus the influence of carbonation was dependent on chlorides at the joint. Chloride concentrations in all the 10 mm cover beams were up to 75% larger up to a depth of 10 mm compared to the corresponding beams of a 20 mm cover depth. There were cracks in the 10 mm cover beams which were widest near the joint due to the rapid corrosion activity.

The fly ash concrete was least-resistant to chlorides due to the high chloride concentrations and chloride enrichment towards the steel due to carbonation. The chloride concentrations at the steel in the 20 mm cover cold joint beams were 143% larger than that monolithically-cast due to the loss of binding in carbonated concrete. The increase in chloride concentration at the steel in the monolithic beams was minor even though the carbonation was 20% deeper than the ordinary concrete. The chloride concentrations in the 10 mm cover beams were 18% larger than that in the corresponding 10 mm cover ordinary concrete beams. The cracking in the 10 mm cover fly ash concrete beams was most severe in the coverage and width over the bar length. The metakaolin yielded the highest resistance where the chloride concentrations at the steel in the 20 mm cover monolithic beams were 100% lower than the ordinary concrete. The low-carbonation resistance resulted in 66% of the cover region in the 20 mm beams being influenced from the measurement in the cubes. The majority of the steel within the 10 mm cover beams was thus affected although the chloride concentrations were insignificant.

The chloride profiles are consistent with studies on combined attack such as Yoon [18] and Malheiro, et al, [7], which are based on accelerated carbonation. The defects played a role herein by increasing the chloride availability that could diffuse to the steel once there was an adequate carbonation depth. The carbonation depths of the plain cubes under the combined attack at 21 cycles were such that most of the chlorides in the cover region of the beams were freed up within the timeframe of exposure.

3.3 Corrosion state

The concrete resistance was more informed with the corrosion rate due to limitations of the potential alone to representing the progress in the long-term. The durations in active or severe conditions of the copper-copper sulphate half-cell, and highest corrosion rates are shown in Table 3 to summarise the corrosion resistance. The main factors to the resistance were a cover reduction and chloride availability at defects, while the carbonation was apparent in the long-term. The 20 mm cover monolithic beams (M-20-I) remained in passive conditions throughout while the cold joint (CJ) caused rapid corrosion activity changes that reached active corrosion in all concretes. The cover reduction from 20 to 10 mm resulted in a faster drop into active conditions thus higher corrosion rates could be sustained over the course of exposure. The fly ash and metakaolin restricted the corrosion rates at a cover depth of 20 mm due to the oxygen availability (lower OPI) and higher resistivity. The resistivity ranges of both cement extender concretes were increased throughout, by up to around 5 times in the metakaolin concrete.

Table 3: Corrosion resistance of beam sets

Corrosion resistance									
CEM		M-20-I	M-20-C	CJ-20-I	CJ-20-C	M-10-I	M-10-C	CJ-10-I	CJ-10-C
	Active state	0	0	4	4	15	15	18	19
	Severe state	0	0	0	0	0	0	0	0
	Min (mV)	-149	-140	-396	-388	-463	-425	-468	-468
	Max ($\mu A/cm^2$)	1.0	1.1	7.5	7.6	21.2	25.1	21.5	36.3
Fly ash		M-20-I	M-20-C	CJ-20-I	CJ-20-C	M-10-I	M-10-C	CJ-10-I	CJ-10-C
	Active state	0	0	0	1	10	12	19	7
	Severe state	0	0	0	0	0	0	0	12
	Min (mV)	-135	-157	-342	-357	-375	-483	-485	-520
	Max ($\mu A/cm^2$)	0.4	0.6	2.5	3.2	9.0	40.4	40.3	62.1
Metakaolin		M-20-I	M-20-C	CJ-20-I	CJ-20-C	M-10-I	M-10-C	CJ-10-I	CJ-10-C
	Active state	0	0	0	0	6	9	9	18
	Severe state	0	0	0	0	0	0	0	5
	Min (mV)	-193	-206	-348	-341	-360	-436	-383	-507
	Max ($\mu A/cm^2$)	1.5	1.4	4.1	4.2	6.9	16.7	8.1	34.6

The proximity of the steel to the surface contamination is evident with the cover reduction from 20 to 10 mm due to the high corrosion rates that could be sustained. The carbonation fronts were at or near the steel in the 10 mm cover beams which was reflected by an increased corrosion severity under the combined exposure (C). The corrosion rates of the carbonated cold joint beams were highest due to the earlier cracking time that could sustain the corrosion at the latter. The resistivity ranges of the 10 mm cover beams were not influenced by a cover reduction as the potential and rate as this was dependent mainly on the proximity of the steel.

3.4 Corrosion damage

The crack width related to the time that the corrosion appeared to be accelerated and their origin was invariably nearer the mid-span in cold joint beams. No corrosion was found on the steel in the monolithic 20 mm cover beams which were passive throughout whereas the cold joint beams were corroded in a close proximity to the joint. The thicker cover in the 20 mm cover beams reduced the penetrability over the entire bar length, thus areas of the bars were not corroded. The corrosion damages to the steel in the 10 mm cove beams were much larger and deeper such that there was more mass loss visible to the naked eye. Most of these pitting forms were near the joint, and over larger areas within the carbonated beams as more of the chlorides could diffuse to the steel. These crack widths were not as influential to the chloride penetration as on the corrosion rate due to the effects of washout at the surface.

4. CONCLUSIONS

- The cold joint reduced the initiation time and increased the corrosion rate in propagation.
- The carbonation increased the corrosion rate after sufficient exposure in the long-term.
- The chloride penetration was based on availability at the surface and carbonation depth.

REFERENCE

[1] Alexander, M. et al., 2009. *Fultons concrete technology.* 9 ed. Midrand, South Africa: Cement & Concrete Institute (C & CI).

[2] ASTM, 1999. *ASTM C 1543 – 02 Standard Test Method for Determining the Penetration of Chloride Ion into Concrete by Ponding,* s.l.: ASTM International.

[3] ASTM, 1999. *ASTM C876 − 09 Standard Test Method for Corrosion Potentials of Uncoated Reinforcing Steel in Concrete,* s.l.: ASTM International.

[4] Bakera, A. & Alexander, M. G., n.d. *Properties of Western Cape Concretes with Metakaolin.* Cape Town, South Africa, University of Cape Town.

[5] Glass, G. K., Hassanein, N. M. & Buenfeld, N. R., 1997. Neural network modelling of chloride. *Magazine of Concrete Research,* Volume 49, p. 323–335.

[6] Glass, G. K. & Buenfeld, N. R., 1997. Presentation of the chloride threshold for corrosion of steel. *Corrosion Science,* 39(5), pp. 1001-1013.

[7] Malheiro, R. et al., 2016. *Proceedings of the 7th International Conference on Safety and Durability of Structures: Chloride penetration into carbonated concrete.* Portugal, s.n.

[8] Miyazato, S.-i. & Otsuki, N., 2010. Steel Corrosion Induced by Chloride or Carbonation in Mortar with Bending Cracks or Joints. Journal of Advanced Concrete Technology, 8(2), pp. 135-144.

[9] Moreno, E. I. & Sagues, A. A., 1998. Carbonation-induced corrosion of blended-cement concrete mix designs for highway structures. *NACE International.*

[10] Pakawat, S. & Uomoto, T., 2005. Effect of Cyclic Exposure of Carbonation and Chloride on Corrosion of Reinforcing Steel in Concrete. *Seisan-Kenkyu,* 57(2), pp. 29-32.

[11] SANS, 2011. SANS 50197-1 Cement Part 1: Composition, specifications and conformity criteria for common cements, Pretoria: South African National Standard.

[12] SANS, 2014. *Fly ash for concrete: Part 1: Definition, specifications and conformity criteria,* s.l.: SANS.

[13] SANS, 2015. *SANS 3001-CO3-1:2015 Civil engineering test methods Part CO3-1: Concrete durability index testing — Preparation of test specimens,* s.l.: SANS.

[14] SANS, 2015. *SANS 3001-CO3-2:2015 Civil engineering test methods Part CO3-2: Concrete durability index testing — Oxygen permeability tes,.*s.1: SANS.

[15] SANS, 2017. *SANS 3001-CO3-3:2015 Civil engineering test methods Part CO3-3: Concrete durability index testing — Chloride conductivity test,* s.l.: SANS.

[16] Sung-Won, Y. & Seung-Jun, K., 2016. Effects of cold joint and loading conditions on chloride diffusion in concrete containing GGBFS. Construction and Building Materials, Volume 115, p. 247–255.

[17] Wang, Y., Basheer, P. A. M., Nanukuttan, S. & Bai, Y., 2016. Influence of Chloride Ions on the Process of Carbonation in Concretes. London, University College London, U.K..

[18] Yoon, I., 2007. Deterioration of Concrete Due to Combined Reaction of Carbonation and Chloride Penetration: Experimental Study. *Key Engineering Materials,* Volume 348-349, pp. 729-732.

ULTIMATE TENSILE STRENGTH OF CORRODED STEEL REINFORCEMENT BARS IN CRACKED CONCRETE EXPOSED TO 1D AND 2D CHLORIDE INGRESS

Ze Gyang Zakka [(1)] and Mike Otieno [(1)]

(1) School of Civil and Environmental Engineering, University of the Witwatersrand, Johannesburg, South Africa.

ABSTRACT

This paper presents the ultimate load of corroded high yield steel reinforcement bars. The steel bars were embedded in cracked concrete beam specimens made with PC(70)/FA(30) and PC(50)/SL(50) binders with a water/binder ratio of 0.40. Based on the position of the steel bar in the beam specimens (in middle or at an orthogonal edge), the beams were exposed to 1D or 2D chloride ingress and subjected to 2-week wetting (with 5% NaCl) and 2-week air-drying cycles in the laboratory for 110 weeks after which the corroded steel bars were extracted and tested. The steel bars in concretes exposed to 1D chloride ingress had isolated corrosion pits while both uniform and isolated corrosion pits were observed in specimens exposed to 2D chloride ingress. In comparison to non-corroded steel bars, the ultimate tensile strength of specimens exposed to 1D chloride ingress reduced by 0.6 % and 2.2 %, while that of specimens exposed to 2D chloride ingress reduced by 3.3 % and 6.1 % in the PC/FA and PC/SL concrete, respectively. There was a significant reduction in the ultimate load and ductility of the corroded steel bars exposed to 2D chloride ingress when compared to those exposed to 1D chloride ingress.

Keywords: ultimate tensile strength, steel corrosion, 1D chloride ingress, 2D chloride ingress.

1 INTRODUCTION

Corrosion of steel reinforcement is a common form of deterioration in steel reinforced concrete (RC) structures. In addition to serviceability failures such as cracking of the concrete cover, delamination, spalling and increased deflections, it also results in ultimate limit state failures such as the reduction in the effective steel cross-sectional-area (CSA) and a loss in steel-concrete interface (SCI) bond which leads to a reduction in the load carrying capacity of these structures due to loss of composite action [1, 2, 4, 6, 7]. In severe cases, the loss in the steel CSA due to corrosion can lead to a change in the mode of structural failure from plastic to brittle failure due to loss in the steel ductility. This is not desirable.

In the past 3 to 4 decades, research on steel corrosion in RC has focused on deterioration due to 1-directional (1D) chloride ingress, which is typical in slabs and walls. While valuable results and predictive models have been developed using this approach, it does not depict the ingress of corrosion agents at the intersection of the non-planar surfaces of concrete columns, beams and corbels which can be modelled using either 2-directional (2D) or 3-directional (3D) approaches [3, 8, 9]. In particular, the 2D approach is recommended for the orthogonal edges

of beams and columns while a 3D approach is recommended for the exposed terminal ends of columns and in corbels – see Figure 1. In this paper, the reported results were obtained from an investigation of the effect of 1D and 2D chloride ingress on the corrosion of steel reinforcement bars embedded in cracked concrete.

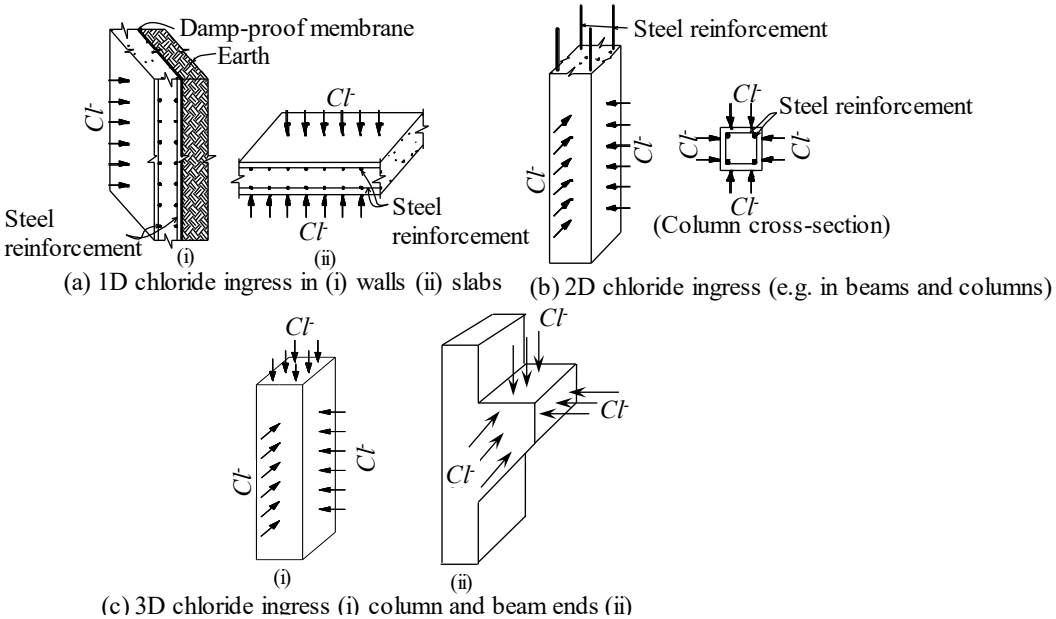

Figure 1: Illustration of (a) 1D, (b) 2D and (c) 3D chloride ingress in RC structures

2 EXPERIMENTAL MATERIALS AND METHODS

2.1 Materials

The plain Portland cement, and slag were obtained from Pretoria Portland Cement Company Limited (PPC) while the fly ash brand used was produced by Dura-Pozz® (Class F Fly Ash). The fine and coarse aggregates used in the concrete mix were obtained from the same source; crushed Andesite rock produced by AfriSam (South Africa) (Pty) (Ltd) in the Eikenhof quarry, Johannesburg.

2.2 Mix proportions, casting, curing, cracking and chloride exposure of specimens

The concrete mix proportions and compressive strengths are presented in Table 1. A water/binder ratio of 0.40 was used in both concrete mixes.

Table 1: Concrete mix material proportions

Concrete type	Material quantity (kg/m^3)						28-day compressive strength (MPa)
	PC	FA	SL	Water	Fine aggregate	Coarse aggregate	
PC(70)/FA(30)	355	155	-	205	745	1115	59
PC(50)/SL(50)	255	-	255	205	780	1135	57

Each of the concrete mix was used to cast 6 beams of size 150 × 150 × 625 mm and six 100 mm concrete cube specimens which were used to obtain the concrete compressive strength. The beams were reinforced with a single 10 mm diameter high yield steel reinforcement bar that is 600 mm long. The steel bars were placed at a cover of 20 mm through the middle (M) or near the orthogonal edge (E) of the beam. Figure 2(a) illustrates the reinforcement position and

chloride ingress directions (1D and 2D) which are modified by epoxy sealing the concrete surfaces.

After casting, all the specimens were cured in water (at 23 ± 2 °C for 28 days), thereafter they were air-dried for 7 days and then epoxy-coated to achieve the desired 1D and 2D chloride exposure (see Figure 2(a)). The beams were then clamped in pairs (back-to-back) using a 3-point loading arrangement (see Figure 2(b)) until a single crack was induced in the beams tensile face. A mean crack width of 0.28 mm (standard deviation = 0.06) was achieved in the beam specimens. To ease the creation of a single crack in each beam, a thin shim (to form a notch) was placed transversely across the middle of the wooden mould before the beam is cast.

The cracked fly ash (F) and ground granulated blast furnace slag (S) beams exposed to 1D chloride ingress were labelled F1D-M (1, 2, and 3) and S1D-M (1, 2, and 3) respectively, while those exposed to 2D chloride ingress were labelled F2D-E (1, 2, and 3) and S2D-E (1, 2, and 3).

The cracked beams were exposed to cyclic regimes of 2-weeks wetting (in 5% NaCl solution) and 2-weeks air-drying (in an ambient laboratory environment) for a total experimental duration of 110 weeks. The steel corrosion rate was measured using the coulostatic technique 24 hours after each wetting cycle.

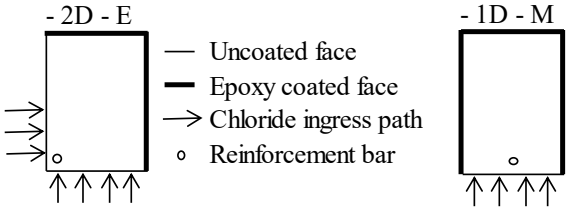

(a)

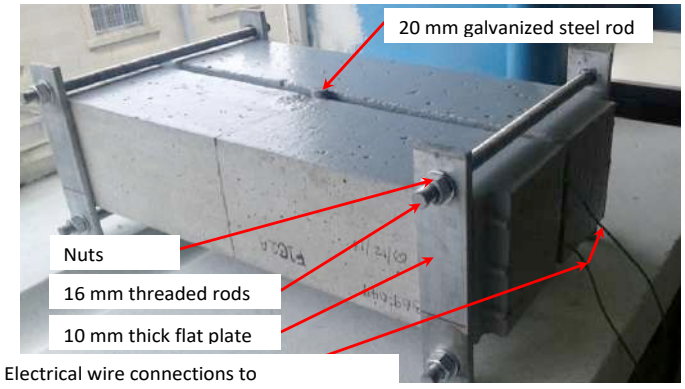

(b)

Figure 2: (a) Cross-section of beam specimens showing 1D and 2D chloride exposure, (b) clamped beams

2.3 Assessment of corroded steel bars

At the end of the experimental duration, the corroded steel bars were extracted from the beam specimens and cleaned before measuring the residual diameter of each corroded steel bar with a Vernier caliper. The ultimate tensile strength of the corroded bars was then measured using a Tinius-Olsen universal testing machine (UTM). The set-up for the tensile strength testing is shown in Figure 3.

Figure 3: Tensile strength testing set-up

The crosshead displacement of the UTM during loading was used to monitor the steel displacement. The load and corresponding displacement of the steel bar were recorded using a data logger; the data was used to plot the stress-strain curve of the steel specimens.

The percentage elongation and percentage reduction in CSA were obtained using the Equations (1) and (2). These parameters give an indication of the ductility of the steel reinforcement bars.

$$Percentage\ elongation = \frac{L_f - L_i}{L_i} \times 100\% \qquad \textbf{Equation 1}$$

$$Percentage\ reduction\ in\ CSA = \frac{D_i - D_f}{D_i} \times 100\% \qquad \textbf{Equation 2}$$

where L_f is the final length of the reinforcement bar (after the tensile test)

L_i is the initial length of the reinforcement bar

D_f is the final diameter of the reinforcement bar at the point of fracture

D_i is the nominal diameter of the reinforcement bar before the tensile test is conducted

A decrease in the percentage elongation of the corroded steel bar will indicate a reduction in its ductility; this should correspond to a reduction in the CSA of the corroded steel bar.

3 RESULTS

3.1 Corrosion rate results

The corrosion rate results are presented in Figure 4. The results show that:

(i) Regardless of the binder type (PC/FA or PC/SL), the corrosion rate of the steel bars in concretes exposed to 2D chloride ingress is significantly higher than that of steel bars in concretes exposed to 1D chloride ingress, and

(ii) In both 1D and 2D exposure, the PC/SL concrete had significantly higher corrosion rate than the PC/FA concrete.

1. The corrosion rate (after 110 weeks) of the PC/FA beams exposed to 2D chloride ingress was higher than that of the beams exposed to 1D chloride ingress by 62% while that of the PC/SL concrete was higher by 77%. These results clearly indicate the severity of steel corrosion in RC elements exposed to 2D chloride ingress. The high corrosion rate is attributed to an increased penetration of corrosion agents (chlorides, oxygen, and moisture) from adjacent surfaces of a RC element [3, 8, 9].

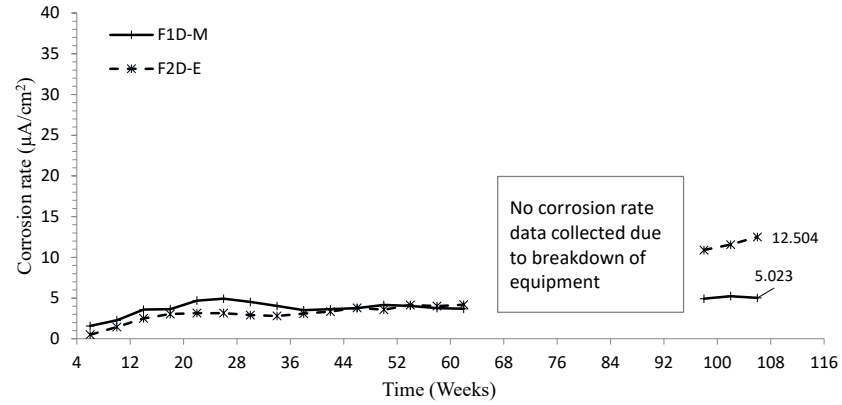

(a)

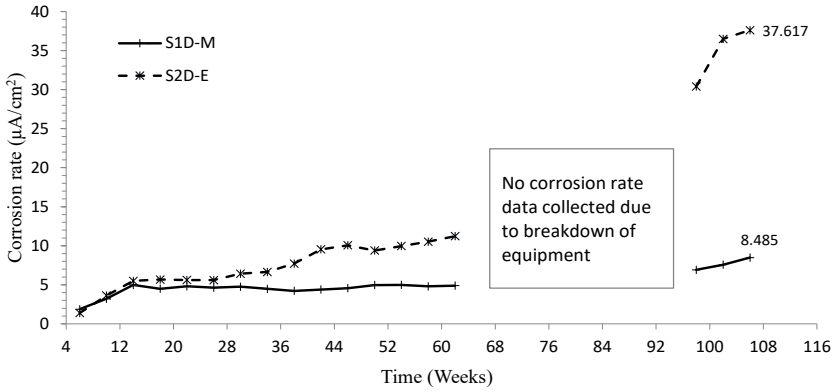

(b)

Figure 4: Steel corrosion rate in (a) PC/FA and (b) PC/SL concretes exposed to 1D and 2D chloride ingress

3.2 Steel corrosion morphology and diameter loss

The corroded steel bars in the cracked beams exposed to 1D chloride ingress had mainly isolated corrosion pits while those exposed to 2D chloride ingress had a combination of isolated pits and uniform corrosion on the steel surface (see Figure 5).

Figure 5: Typical corrosion morphology of steel bars embedded in concrete exposed to (a) 1D and (b) 2D chloride ingress

In general, the corroded sections of the reinforcement bars were in the region where the concrete crack intercepted the steel bar. The length of the corroded section and area of the corroded bar of the specimens exposed to 2D ingress of corrosion agents was about twice that of specimens exposed to 1D ingress of corrosion agents (Figure 6). The error bars in the graphs indicate that there is more variation in both the area and length of the corroded section of the reinforcement bars that are exposed to 2D ingress of corrosion agents.

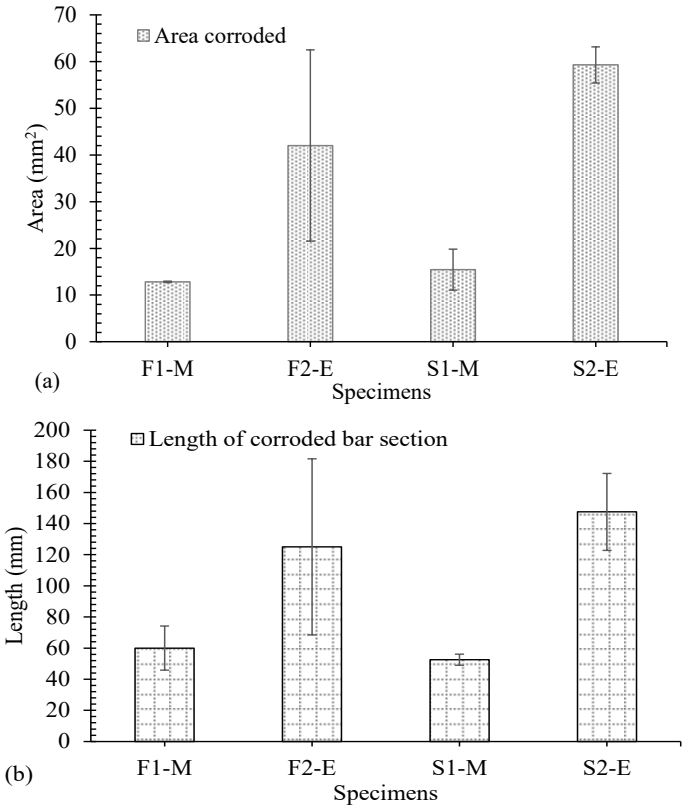

Figure 6: (a) Area of corroded steel bar (b) Length of corroded steel bar in PC/FA and PC/SL specimens exposed to 1D and 2D ingress of corrosion agents.

3.3 Ultimate tensile strength of the corroded steel bars

The stress-strain plots of the corroded steel bars in the PC/FA and PC/SL specimens are shown in **Error! Reference source not found.**.

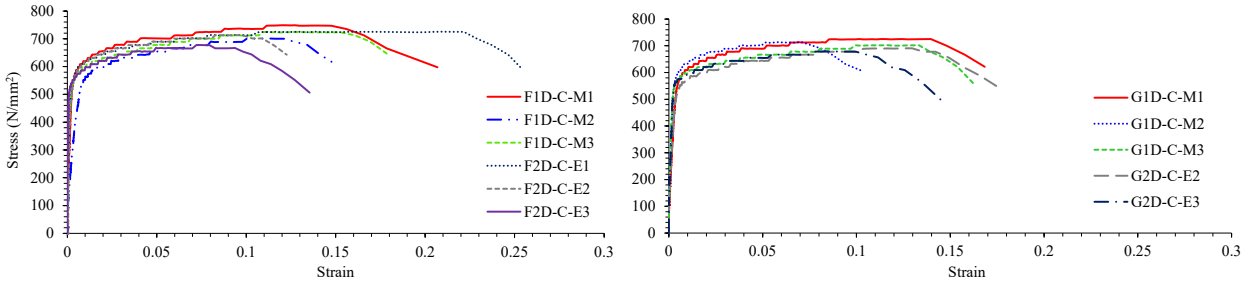

Figure 7: Stress-strain relationship of reinforcement bars placed in PC/FA and PC/SL concrete exposed to1D and 2D chloride ingress

From the results obtained, the yield strength of the corroded reinforcement bars was not significantly affected by the corrosion process; all the reinforcement bars had a yield stress that exceeded 500 N/mm^2. This value exceeds the required minimum yield strength (i.e., 450 N/mm^2) of steel reinforcement bars (SANS 920: 2011). The results however indicate that the region of plastic deformation of the reinforcement bars was affected by the corrosion of the steel bars. A plot of the ultimate tensile strength of the specimens is shown in Figure 8.

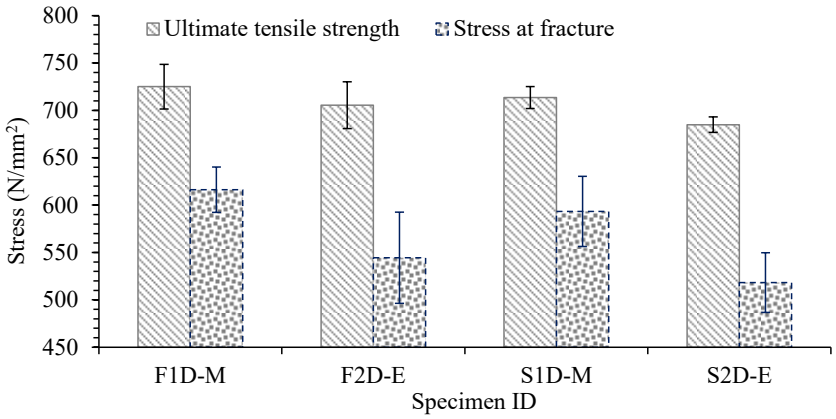

Figure 8: Ultimate tensile strength and fracture stress of the steel bars in concrete exposed to 1D and 2D ingress of corrosion agents.

A statistical analysis to test the significance of the difference between the ultimate tensile strength and failure load of the specimens subjected to 1D and 2D ingress of corrosion agents is summarized in Table 2.

Table 2: Severity of ultimate tensile stress and failure load of the 1D and 2D steel specimens

	PC/FA	PC/SL
Ultimate tensile strength	Significant	Significant
Stress at fracture	Not Significant	Significant

The fracture stress was significantly lower than the ultimate tensile stress, and the ultimate tensile stress and fracture stress of the specimens of the specimens exposed to 2D ingress of corrosion agents was lower than that of specimens exposed to 1D ingress. The lower stress values of the corroded steel bars in concretes exposed to 2D chloride ingress indicates that steel bars located at square edges of concrete elements experienced a higher degree of corrosion compared to those in the concrete that is exposed to 1D chloride ingress.

3.4 Ductility of corroded reinforcement bars

The plot showing the elongation after fracture and reduction in CSA at the point of fracture is shown in Figure 9.

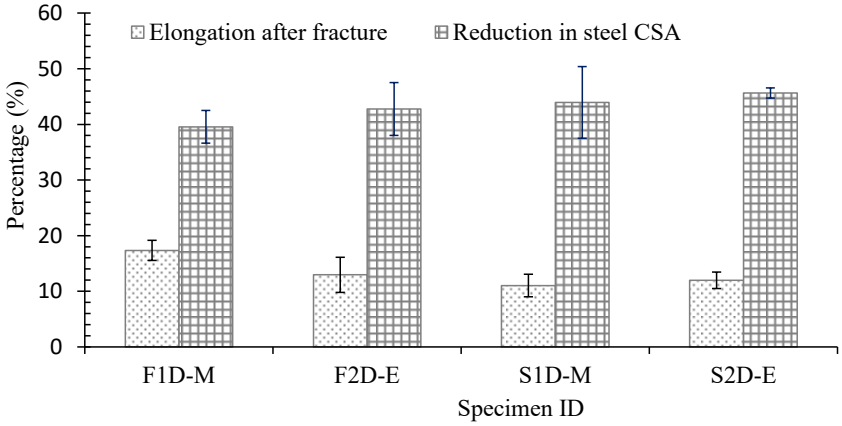

Figure 9: Percentage elongation after fracture and reduction in steel cross-sectional-area

The ductility of the reinforcement bars was affected by the morphology of corrosion pits in the steel bars. The steel bars with a higher CSA resulted in lower ductility (elongation). The specimens with higher corrosion rates (i.e., corner located steel bars) resulted in a lower elongation (or ductility) and CSA at the point of fracture (see Figure 9). In the overall results, the steel bars in the PC/SL concrete had lower ductility, this corroborates with the higher corrosion rate that was attained by these specimens.

4 CONCLUSIONS

The results of this study have shown that the ultimate tensile strength of steel reinforcing bars embedded at orthogonal edges of concrete elements exposed to 2D chloride ingress is significantly less than that of steel bars that are located at the middle of the cracked concrete beam. At loads that cause deformation of the steel bar beyond its elastic region, the steel bars exposed to 2D ingress of corrosion agents have a lower ultimate tensile strength, CSA, and ductility, hence, overloading a structure that has undergone severe corrosion may result in its sudden failure.

Although the sustained load on the specimens was not measured, the crack width opening was used to determine the stress applied. The sustained stress on the specimens may have also increased the penetration of corrosion agents into the concrete, thus aggravating the corrosion rate of the steel bars.

To mitigate rapid corrosion of steel bars that are located at the edge of concrete elements, chemicals that mitigate the penetration of corrosion agents should be applied to concrete edges, or where cost permits, steel bars with higher passivity may be utilized in these locations.

5 ACKNOWLEDGEMENTS

The authors acknowledge the support that was received from the South African National Research Foundation (NRF), PPC Ltd., AfriSam South Africa (Pty) Ltd, Galvaglow (Pty) Ltd., Sika South Africa (Pty) Ltd, and ABE (Pty) Ltd.

REFERENCES

[1] Andrade, C. and Alonso, C. (2001) ‘On-site measurements of corrosion rate of reinforcements’, *Construction and Building Materials*, 15(2–3), pp. 141–145.

[2] Cao, C. and Cheung, M. M. S. (2014) ‘Non-uniform rust expansion for chloride-induced pitting corrosion in RC structures’, *Construction and Building Materials*. Elsevier Ltd, 51, pp. 75–81.

[3] Kang, B. and Shim, H. (2011) ‘Two Dimensional Chloride Ion Diffusion in Reinforced Concrete Structures for Railway’, *International Journal of Railway*, 4(4), pp. 86–92.

[4] Ortega, N. F. and Robles, S. I. (2014) ‘Assessment of Residual Life of concrete structures affected by reinforcement corrosion’, *HBRC Journal*. Housing and Building NationalResearch Center.

[5] SANS 902 (2011), South African National Standard, Steel bars for concrete reinforcement.

[6] Tan, R., Hendriks, M. A. N. and Kanstad, T. (2017) ‘Evaluation of current crack width calculation methods according to Eurocode 2 and fib Model Code 2010’, *High Tech Concrete: Where Technology and Engineering Meet - Proceedings of the 2017 fib Symposium*, (January), pp. 1610–1618.

[7] Yoon, S. *et al.* (2000) ‘Interaction between Loading, Corrosion, and Serviceability of Reinforced Concrete’, *ACI Materials Journal*, 97(6), pp. 637–644.

[8] Zhang, Y., Sun, W., Liu, Z., *et al.* (2011) 'One and two dimensional chloride ion diffusion of fly ash concrete under flexural stress', *Journal of Zhejiang University - SCIENCE A (Applied Physics & Engineering)*, 12(9), pp. 692–701.
[9] Zhang, Y., Sun, W., Chen, S., *et al.* (2011) 'Two- and three-dimensional chloride ingress into fly ash concrete', *Journal of Wuhan University of Technology-Mater. Sci. Ed.*, 26(5), pp. 978–982.